[5mm]312pt761pt
0em0em

UNIVERSITÀ
DEGLI STUDI
DI PADOVA

**DIPARTIMENTO DI ASTRONOMIA**
**SCUOLA DI DOTTORATO IN ASTRONOMIA**
**CICLO XXII**

TESI DI DOTTORATO

# MESS:
# a Monte Carlo simulation tool for the statistical analysis and prediction of survey results for exoplanets


Direttore della Scuola: **Ch.mo Prof. GIAMPAOLO PIOTTO**
Supervisore: **Ch.mo Prof. GIAMPAOLO PIOTTO**
Co-Supervisore: **Prof. RAFFAELE GRATTON**
Co-Supervisore: **Dott. SILVANO DESIDERA**

Candidato: **MARIANGELA BONAVITA**

*Spread our codes to the stars!*
*You must rescue us all!*

*— M. Bellamy*

## ABSTRACT

Since the discovery of the very first planetary mass companion around a pulsar star (Wolszczan & Frail 1992) and shortly after around stars similar to our Sun (51 Peg, Mayor & Queloz 1995), many steps have been done in exoplanet science. This lead to a rapidly growing sample of detected planets: the minimum mass of the companions is decreasing fast, and is now close to the Earth mass.

New and more precise instruments have been built and many other are planned.

The final goal is the discovery of *earth twins* and, ultimately, traces of exosolar life.

As learnt with the discovery of 51 Peg, about fifteen years ago, observations often open new question about how the discovered planets can form and survive, ending in the needs of more sophisticated theories to address these items.

Many statistical studies have been done using information coming from more than a decade of extensive searches for exoplanets, trying to answer questions either related to the distribution of the properties of those objects, such as the mass, orbital period and eccentricity (Lineweaver & Grether 2003; Cumming et al. 2008) as well as about the relevance of the host star characteristics (mass, metallicity) on the final frequency and distribution of planetary systems (see Fischer & Valenti 2005; Santos et al. 2004b; Johnson et al. 2007). Since the most successful techniques (radial velocity and transit) have focused on the inner ($\leq 5AU$) environment of main sequence solar-type stars, most of the available information on the frequency of planets concern this kind of targets.

However, a clear determination of the frequency of giant planets as a function of orbital separation out to hundreds AU is a crucial issue to clarify the relative importance of various models of planet formation and migration. Formation through core accretion is, as example, strongly dependent on the surface density of solid material in the protoplanetary disk. Formation of Jupiter mass planets becomes increasingly less efficient as the density of planetesimals decreases, highly increasing the formation timescales. However even in a scenario in which giant planets form only close to the snow-line in the protoplanetary disk, a significant fraction of

massive planets might be found on stable orbits of tents of AU. This can be possible because of outward migration (see Veras & Armitage 2004), which can be induced both by gravitational interaction between massive objects in multiplanetary systems, and by interactions between the planet and gaseous disks. Alternative models of planet formation (disk instability, disk fragmentation) are efficient mostly at wide separations from the central star.

Direct imaging is currently the most viable technique to probe for planets at large separations, providing clues on their frequency. In fact recent discoveries of young distant planetary mass objects with this technique (see e. g. Kalas et al. 2008; Lagrange et al. 2008) are nowadays giving us a first hint on the potential of the direct detections in the exploration the outer region of the planetary systems.

These partially unexpected new detection also raised many questions about how such objects could form (see Absil & Mawet 2009).

Besides the few detections, there is anyway a wealth of data that can be used to put constraints on the frequency of planets in wide orbits. In addition there are many new instruments planned for the next future specially designed for imaging of exoplanets, like the Gemini Planet Imager (GPI: Macintosh et al. 2007) and VLT/SPHERE (Spectro-Polarimetric High-contrast Exoplanet REsearch: Beuzit et al. 2008). These instruments will likely allow us to extend such systematic characterization at larger scales ($\geq 10AU$).

Due to practical limitations (inner working angle, best contrast achievable), these instrument will focus on warm giant planets, on orbits far away from their stars, preparing the path for the ELTs facilities. It is in fact becoming clear that with 30-40 meter-class telescopes a wide range of planetary masses and separations will be explored, down to the rocky planets (and, in very favorable cases even reaching the habitable zone), finally allowing an overlap between the discovery spaces of direct and indirect techniques.

In this context it is useful and crucial to have a tool which goals are either to learn as much as possible from the available data and to predict the performances of the forthcoming instruments. This tool may be used not only to estimate the number of expected detections, but also to figure out what will be the explored parameter space and even the possible synergies between different discovery techniques. This is crucial to properly design such instruments as well as to plan the most appropriate observing programs.

Kasper et al. (2007), Lafrenière et al. (2007), Nielsen et al. (2008), Nielsen & Close (2009) have initiated a statistical analysis to constrain the physical and orbital properties (mass, period, eccentricity distributions) of a giant planet population. They developed statistical analysis tools to exploit the performances of deep imaging surveys. They tested the consistency of various sets of parametric distributions of planet parameters, using the specific case of a null detection. The first assumption of these tools is that planet mass, eccentricity and period distributions coming from the statistical results of RV studies at short period (see e.g. Lineweaver & Grether 2003; Cumming et al. 2008) can be extrapolated and normalized to obtain informations on more distant planets. Despite the model-dependency on the mass predictions, the approach is attractive for exploiting the complete set of detection performances of the survey and characterizing the outer portions of exo-planetary systems.

With all of this in mind, we tried to go a step further, creating a Multi-purpose Exo-planet Simulation System (hereafter MESS).

The MESS algorithm is based on three fundamental steps: first, a synthetic planet population is produced, either using the results of the statistical analysis of the properties of the discovered planets or the results of the planet formation theories. Then the physical parameters of these planets are determined, and this allow deriving the expected values for the observables (radial velocity signature, astrometric signal, expected separation and contrast. Finally, these expected values for the observables are compared with the predicted capabilities of existing or planned instruments. This last step allows defining a sample of fully characterized *detectable planets*, which characteristics can be easily investigated. This means, in the case of planned instruments, that using MESS it will be possible to tune not only the main instrument parameter, but even the observing strategy.

The main strength of the code is that it's completely independent from the kind of instrument/technique one wants to test and also from any evolutionary model used to estimate the planet intrinsic flux. Neither the detectability relations nor the evolutionary models are directly included into the code, but both are given as inputs. Moreover, the Monte Carlo simulation provide both all orbital elements and all the physical parameters of the planets (radius, temperature, luminosity, etc.), then it's easy to evaluate any kind of observable parameter (Contrast, RV semi-amplitude, transit probability, astrometric signature) and, given a detectability relation, end with a set of planets detectable by the chosen facility. Since the

characteristics of the detectable objects could also be easily investigated, in the case of planned instruments it's possible use MESS to tune not only the main instrument parameter, but even the observing strategy.

In addition to that, the use of a real sample of stars allows us to make a *case by case* analysis, taking into account the properties of each star and how they affect either the characteristics of the planets or the instrument capabilities.

The aim of this thesis is to present the code itself and all the results obtained with its use, and it's organized as follows:

**Part I** includes a brief overview of the current knowledge of exosolar planets and it is divided into two parts:

*Chapter 1* reviews the planet formation mechanisms in different environments and the impact of the host star properties (stellar mass, metallicity, presence of a companion) on the planet formation;

*Chapter 2* analyzes the properties of the planets which are important from a detection point of view (mostly focusing on the imaging technique);

**Part II** presents an update of the work on the frequency of planets in binaries done by (Bonavita & Desidera 2007), which analyzes in detail the differences in the planet frequency due to the presence of a stellar companion.

**Part III** gives a detailed description of the code, of its different operation modes and of all the assumptions on which it is based, together with some examples of the output synthetic planet populations obtained.

**Part IV** includes the description of the application of MESS for the analysis of real data.

Two different cases are discussed: the case of an extended sample of objects coming from the VLT/NACO deep imaging survey of young, nearby austral stars (*Chapter 5*), and the application to a data set that belongs to the deep imaging observation of an individual object with peculiar characteristics: the T-Tauri star LkCa15 (*Chapter 6* )

**Part V** presents the results of the extensive use of MESS for the prediction of the detection capabilities of future instruments, either in construction or proposed for the next future.

It includes *Chapter 7* which focuses on SPHERE, the next generation VLT planet finder, and *Chapter 8* that concerns EPICS, the planned planet finder for the European Extremely Large Telescope.

Then in *Chapter 9*, as an ideal conclusion of this part, we present a discussion based on the comparison of the expected detections of different

direct imaging facilities, both from ground and in space. This allows an analysis of the overlap of the discovery space of the different techniques, in a context where the synergy between them will be the key for a complete characterization of the planetary systems.

**Part VI** finally summarizes the conclusions and future perspectives of the work.

# RIASSUNTO

A partire dalla scoperta del primio compagno di massa planetaria attorno ad una pulsar (Wolszczan & Frail 1992) e quella, poco tempo dopo, attorno ad una stella simile al nostro Sole (51 Peg, Mayor & Queloz 1995), numerosi passi avanti sono stati compiuti nello studio dei pianeti extrasolari. Ciò ha portato alla rapida crescita del campione rapidamente di pianeti rivelati, insieme con la progressiva diminuzione della massa minima dei compagni rivelati, che è ora vicina a quella della Terra.

Nel corso degli anni sono stati costruiti strumenti nuovi e sempre piu' precisi e molti altri sono in previsione.

Lo scopo finale è quello della scoperta di pianeti *gemelli* della Terra e, infine, delle tracce di vita al di fuori del nostro pianeta.

Con la scoperta di 51 Peg, circa quindici anni fa, si è imparato come le osservazioni aprano spesso nuovi dubbi riguardo a come i pianeti scoperti si siano formati e come siano sopravvissuti, concludendosi con la necessità di sviluppare teorie più sofisticate per affrontare tali questioni.

Grazie alle informazioni provenienti da più di un decennio di ricerca di pianeti estrasolari sono stati eseguiti numerosi studi statistici per cercare di rispondere alle domande sia correlate alla distribuzione delle proprietà di questi oggetti, come massa, periodo orbitale ed eccentricità (Lineweaver & Grether 2003; Cumming et al. 2008) come pure quelle riguardanti le caratteristiche delle stelle ospitanti (massa, metallicità) sulla frequenza e distribuzione finale dei sistemi planetari (see Fischer & Valenti 2005; Santos et al. 2004b; Johnson et al. 2007). Poichè le tecniche maggior successo (velocità radiali e transiti) si sono focalizzate sull'ambiente interno ($\leq 5UA$) dei sistemi planetari formati attorno a stelle di tipo solare, gran parte delle informazioni disponibili sulla frequenza di pianeti riguardano questo tipo di target.

In ogni caso una chiara determinazione sulla frequenza dei pianeti giganti in funzione della separazione orbitale maggiore di centinaia di UA è un risultato cruciale per chiarire l'importanza relativa di vari modelli di formazione e migrazione planetaria. La formazione attraverso l'accrescimento del nucleo è, per esempio, fortemente dipendente dalla densità superficiale del materiale solido nel disco protoplanetario. La formazione di pianeti della massa di Giove diventa sempre meno efficiente

con la diminuzione della densità dei planetesimi che aumenta notevolmente i tempi-scala di formazione. In ogni caso perfino in uno scenario in cui i pianeti giganti si formano solo vicini alla snow-line nel disco protoplanetario, si può trovare una frazione significativa di pianeti massivi su orbite stabili di decine di UA. Questo è possibile grazie alla migrazione verso l'esterno (si veda Veras & Armitage 2004), che può essere indotta sia da interazione gravitazionale tra oggetti massicci in sistemi multiplanetari, che dalle interazioni tra pianeta e il gas del disco. Modelli alternativi di formazione planetaria (instabilità del disco, frammentazione del disco) sono efficienti in gran parte ad ampie separazioni dalla stella centrale.

L'imaging diretto è al momento la tecnica più fattibile per indagare pianeti a grandi separazioni, fornendo indizi sulla loro frequenza. Recenti scoperte di oggetti giovani e distanti di massa planetaria eseguite con questa tecnica (si veda ad esempio Kalas et al. 2008; Lagrange et al. 2008) forniscono al giorno d'oggi un primo suggerimento sulle potenzialità della rivelazione diretta nell'esplorazione della regione esterna dei sistemi planetari.

Queste rivelazioni parzialmente inaspettate fanno sorgere anche molte questioni riguardanti a come tali oggetti si possano formare (si veda Absil & Mawet 2009).

Oltre alle poche rivelazioni, c'è comunque una grande quantità di dati che possono essere utilizzati per fissare limiti alla frequenza dei pianeti in orbite larghe. Oltre a questo sono in progetto molti nuovi strumenti per il prossimo futuro specificamente disegnati per l'imaging di pianeti extrasolari, come il Gemini Planet Imager (GPI: Macintosh et al. 2007) e VLT/SPHERE (Spectro-Polarimetric High-contrast Exoplanet REsearch: Beuzit et al. 2008). Questi strumenti ci permetteranno probabilmente di estendere tale caratterizzazione sistematica a grandi scale ($\geq 10UA$).

A causa delle limitazioni pratiche (inner working angle, miglior contrasto ottenibile), questi strumenti si focalizzeranno su pianeti caldi giganti, su orbite molto lontane dalle loro stelle, spianando la strada alle capacità di ELT. Sta diventando chiaro infatti che con telescopi di classe 30-40 metri sarà possibile esplorare un ampio intervallo di masse e separazioni planetarie, fino ai pianeti rocciosi (e, in casi molto favorevoli raggiungere anche la zona abitabile), permettendo infine una sovrapposizione tra i diversi spazi di scoperta delle tecniche dirette ed indirette.

In questo contesto sarà utile e cruciale disporre di uno strumento i cui scopi saranno sia comprendere il più possibile dai dati gi`disponibili che prevedere le prestazioni delle future strumentazioni. Questo strumento

potrebbe essere usato non solo per stimare il numero previsto di rivelazioni, ma anche di capire quale sarà lo spazio dei parametri esplorato e anche le possibili sinergie tra le differenti tecniche di scoperta. Ciò sarà cruciale per permettere di miglioare il disegno delle strumentazioni come pure per pianificare programmi osservativi appropriati.

Kasper et al. (2007), Lafrenière et al. (2007), Nielsen et al. (2008), Nielsen & Close (2009) hanno iniziato un'analisi statistica per vincolare le proprietà fisiche e orbitali (distribuzione di massa, periodo, eccentricità) di una popolazione di pianeti giganti. Essi hanno sviluppato uno strumento di analisi statistica per sfruttare le prestazioni delle survey di imaging profondo. Hanno testato la consistenza di vari set di distribuzioni parametriche di parametri di pianeti, usando il caso specifico di una rivelazione nulla. La prima assunzione di questi strumenti è quella che la massa del pianeta, l'eccentricità e la distribuzioni dei periodi provenienti dai risultati statistici degli studi di velocità radiali a corto periodo (see e.g. Lineweaver & Grether 2003; Cumming et al. 2008) possono essere estrapolate e normaizzate per ottenere informazioni su pianeti più distanti. Nonostante la dipendenza dai modelli delle previsioni sulla massa, l'approccio è interessante grazie all'uso del set completo delle performance di rivelazione delle survey e per la sua caratterizzazione delle parti esterne dei sistemi planetari.

Fissato tutto questo abbiamo provato a fare un passo ulteriore, creando un algoritmo chiamato *MESS*, ovvero *Multi purpose Exoplanet Simulation System*

MESS si basa su tre passi fondamentali: primo, la produzione di una popolazione di pianeti sintetici, sia usando i risultati dell'analisi statistica delle proprietà dei pianeti scoperti che i risultati delle teorie di formazione dei pianeti. Di questi pianeti possono essere determinati tutti i parametri fisici, e questo permette di derivare i valori previsti degli osservabili (semi ampiezza di velocità radiali, segnale astrometrico, separazione prevista e contrasto). Infine questi valori degli osservabili vengono confrontati con i limiti di rivelabilità stimati per strumenti esistenti o in progetto. Quest'ultimo passo permette la definizione di un campione di *pianeti rivelabili* pienamente caratterizzati, le cui caratteristiche possano essere facilmente investigate. Questo significa, nel caso di strumenti in fase di progettazione, che l'uso di MESS permetterà di mettere a punto non solo i principali parametri dello strumento, ma anche la strategia osservativa.

Il punto di forza del codice risiede nel fatto che esso è completamente indipendente dal tipo di strumento o tecnica da testare e anche da qualsiasi modello evolutivo venga usato per stimare il flusso intrinseco del pianeta. Nè le relazioni di rivelabilità nè i modelli evolutivi sono introdotti nel codice ma entrambi vengono dati come input. Inoltre, le simulazioni Monte Carlo forniscono sia tutti gli elementi orbitali che tutti i parametri fisici dei pianeti (raggio, temperatura, luminosità, etc...), quindi è facile valutare qualsiasi tipo di parametro osservativo (contrasto, semi-ampiezza di VR, probabilità del transito, segnale astrometrico) e, data una relazione di rivelabilità, ottenere un set di pianeti rivelabili le cui caratteristiche variano a seconda dello strumento scelto.

Oltre a questo, l'uso di un campione reale di stelle permette di eseguire un'analisi *caso per caso*, tenendo conto le proprietà di ogni stella e di come esse influenzino sia le caratteristiche del pianeta che le capacità dello strumento.

Lo scopo di questa tesi è di presentare tale codice e tutti i risultati ottenuti grazie al suo impiego, ed è organizzata come segue:

La **I Parte** include una breve panoramica della conoscenza odierna sui pianeti extrasolari ed è suddivisa in due parti:

Il *Capitolo 1* passa in rassegna i meccanismi di formazione nei diversi ambienti e l'impatto delle proprietà della stella ospite (massa stellare, metallicità, presenza di un compagno) sulla formazione planetaria;

Il *Capitolo 2* analizza le proprietà dei pianeti che sono importanti dal punto di vista della rivelazione (focalizzandosi in particolare sulla tecnica dell'imaging);

La **II Parte** presenta un aggiornamento sul lavoro sulla frequenza dei pianeti in binarie presentato da Bonavita & Desidera (2007), che analiza in dettaglio le differenze nella frequenza dei pianeti dovute alla presenza di un compagno stellare;

La **III Parte** fornisce una descrizione dettagliata del codice, dei suoi differenti modi di operazione e tutte le assunzioni su cui è basato, insieme ad alcuni esempi delle popolazioni di pianeti sintetici ottenute;

La **IV Parte** include la descrizione delle applicazioni di MESSper l'analisi di dati reali.

Vengono discussi due differenti casi: il caso di un campione esteso di oggetti provenienti dalla survey di imaging, effettuata con VLT/NACO, avente come target stelle giovani e vicine (dell'emisfero australe it Capitolo 5), e l'applicazione ad un set di dati che appartiene a osservazioni di

un oggetto singolo con caratteristiche peculiari: la stella T Tauri LkCa15 (*Capitolo 6*);

La **V Parte** presenta i risultati dell'uso esteso di MESS per la previsione delle capacità di rivelazione di strumenti futuri, sia in costruzione che solo proposti per il futuro;

Include il *Capitolo 7* focalizzato su SPHERE, il planet finder di nuova generazione del VLT, e il *Capitolo 8* che riguarda EPICS, il planet finder programmato per lo European Extremely Large Telescope;

Quindi nel *Capitolo 9*, come ideale conclusione di questa parte, presentiamo una discussione basata sul confronto delle rivelazioni previste di differenti attrezzature di imaging diretto, sia da terra che dallo spazio. Ciò permette un'analisi della sovrapposizione dello spazio di scoperta delle differenti tecniche, in un contesto in cui le sinergie tra di esse saranno la chiave per una completa caratterizzazione dei sistemi planetari.

La **VI Parte** riassume infine le conclusioni e le prospettiva future del lavoro.

# ACKNOWLEDGMENTS

There are so many people that I should thank at the end of these three years, that I will surely forget someone, so I'd like to start these acknowledgements with a big apologize to all of them.

Then the first person I want to thank is my supervisor Prof. G. Piotto, from the University of Padova, who gave me the chance doing this research.

Indeed a special thank goes to the two co-supervisors, R. Gratton and S. Desidera, from the Astronomical Observatory of Padova. With his enormous experience in the field, Prof. Gratton has always been a guiding light for me, during these years. Giving me the first version of the code, Dott. Desidera has been the one that officially started the MESS! Both of them patiently followed all the steps of my work, always providing me new challenges, but at the same time helping me to overcome all the difficulties I found on my path.

Many thanks also to D. Mouillet, Prof. W. Benz and Prof. H.M. Schmid, who accepted to be the external advisers of my work.

Right after that, I want to thank all the people who collaborate with me to the MESS, and with whom I shared successes and failures of the code. I must start with all the people in the SPHERE and EPICS science groups, and especially Markus Kasper, who also helped me to get a post-doc with a wonderful recommendation letter. Then Christophe Mordasini, for his suggestions about the planet populations and for being such a great touring guide in Bern, where I've spent a week at the very beginning of my PhD. Last, but not least, the people of the LAOG in Grenoble, where I spent six wonderful months, enjoying the French *joie de vivre*. Among those, I want to especially thank Jean Luc Beuzit, who accepted to be my supervisor during the time I spent in France, Gael Chauvin, who has been a friend and a landmark in a foreign country and Anne-Marie Lagrange, for the precious help she gave me to find one of the many bugs of MESS. Also, a big thank goes to Stéphanie Renard, Anna Szostek and Federica Scalabrin, who helped me to survive in a french-speaking world.

I want to thank all the friends at the Observatory of Padova. In no particular order: Milena Bufano (for sharing with me the long trips back

home), Mauro Barbieri (for solving me all the bugs and compilation errors, and for the last minute suggestion for the thesis), Riccardo Claudi (for giving me a place where I can always bang my head, if necessary), Marica Valentini (for all the canarian dinners she cooked for us), Marcella Massardi (for showing me how a perfect wife should be) and all the other who have been like a family for me. And, even if it sounds strange, I want to thank the Observatory itself, which has been like a home, hosting me during weeks and wee-ends, and in the cold winter nights, until late, when I was finishing this thesis.

I have been lucky enough to spend many weeks around Europe, for conferences and PhD schools, and I want now to thank all at once the people I met there, with just one special thank to Krzysztof Helminiak, Patricia Cruz, David Anderson and Carla Torres.

I thank my family, all of them, for being such a pillar in my life, even from far away.

I want to thank Francesca Teso, who's always my best friend, and my *Captain*, and Manuel Fasolo, for being always the best fellow traveller ever. I want to hug and thank my flatmates, Serena Benatti, Elena Carolo and, last arrived, Sara Buttiglione, who always took care, helped and tolerated me (and R2).

One of the final thanks goes to Prof. Ray Jayawardhana, who gave me the opportunity to work with him in Toronto, in the next two years.

Then I have to thank someone I haven't met yet: Koraljka Muzic. She deserves these few lines, because even without knowing me at all, she chose to share with me the whole new life that it's going to began for me in Canada.

Close to the end, I want to thank all the people who passed trough my path in these three years, being part of my life even just for a while. I must thank every one of you for participate in making me what I am now.

# PUBLICATIONS

The following publications has been submitted/accepted during this thesis:

## JOURNAL ARTICLES

- Bonavita M., Desidera S.
  2007A&A...468..721B
  **On the frequency of planets in multiple systems**

- Desidera, S.; Gratton, R.; Endl, M.; Martinez Fiorenzano, A. F.; Barbieri, M.; Claudi, R.; Cosentino, R.; Scuderi, S.; Bonavita, M.
  **The SARG planet search**
  Chapter to appear in the book "Planets in Binary Star Systems", ed. Nader Haghighpour (Springer publishing company), 2007

- G. Cauvin, A.M. Lagrange, M. Bonavita, B. Zuckerman, C. Dumas, M.S. Bessel, J.L. Beuzit, M. Bonnefoy, S. Desidera, J. Fahiri, D. Mouillet, P. Lowrance, I. Song
  **Deep imaging survey of young, nearby austral associations - VLT/NACO Near-Infrared Lyot-Coronagraphic Observations**
  2009 A&A Accepted

- Bonavita M., G. Chauvin, A. Boccaletti, V. Pietu, P. Baudoz, J.-L. Beuzit, A. Dutrey, S. Guilloteau, A.-M. Lagrange, D. Mouillet, G. Niccolini
  **Searching for sub-stellar companion in the LkCa15 protoplanetary disk**
  2009 A&A Submitted

## CONFERENCE PROCEEDINGS

- Desidera, S.; Gratton, R.; Claudi, R.; Barbieri, M.; Bonanno, G.; Bonavita, M.; Cosentino, R.; Endl, M.; Lucatello, S.; MartÃNez Fioren-

zano, A. F.; Marzari, F.; Scuderi, S.
**Searching for planets around stars in wide binaries**
Tenth Anniversary of 51 Peg-b: Status of and prospects for hot Jupiter studies.
Colloquium held at Observatoire de Haute Provence, France, August 22-25, 2005.
Edited by L. Arnold, F. Bouchy and C. Moutou.
Published by Frontier Group, Paris (ISBN-2-914601-17.4) p.119-126

- Benatti, S.; Bonavita, M.; Claudi, R. U.; Desidera, S.; Endl, M.; Barbieri, M.
**Search for Massive Earths Around SARG Asteroseismology Targets**
Extreme Solar Systems, ASP Conference Series, Vol. 398
Proceedings of the conference held 25-29 June, 2007, at Santorini Island, Greece.
Edited by D. Fischer, F. A. Rasio, S. E. Thorsett, and A. Wolszczan, p.37

- Desidera, Silvano; Gratton, Raffaele; Claudi, Riccardo; Barbieri, Mauro; Bonannno, Giovanni; Bonavita, Mariangela; Cosentino, Rosario; Endl, Michael; Lucatello, Sara; Martinez Fiorenzano, Aldo F.; Marzari, Francesco; Scuderi, Salvo
**Searching for Planets Around Stars in Wide Binaries**
Multiple Stars Across the H-R Diagram, ESO Astrophysics Symposia
Volume . ISBN 978-3-540-74744-4.
Springer-Verlag Berlin Heidelberg, 2008, p. 193

- Claudi, R. U.; Turatto, M.; Gratton, R. G.; Antichi, J.; Bonavita, M.; Bruno, P.; Cascone, E.; De Caprio, V.; Desidera, S.; Giro, E.; Mesa, D.; Scuderi, S.; Dohlen, K.; Beuzit, J. L.; Puget, P.
**SPHERE IFS: the spectro differential imager of the VLT for exoplanets search**
Ground-based and Airborne Instrumentation for Astronomy II.
Edited by McLean, Ian S.; Casali, Mark M.
Proceedings of the SPIE, Volume 7014, pp. 70143E-70143E-11 (2008)

- M. Bonavita, R. U. Claudi, G. Tinetti, J.L. Beuzit, S. Desidera, R. Gratton, M. Kasper, C. Mordasini

**High contrast imaging: a new frontier for exo-planet search and characterization**
COOL STARS, STELLAR SYSTEMS AND THE SUN
Proceedings of the 15th Cambridge Workshop on Cool Stars, Stellar Systems and the Sun
AIP Conference Proceedings, Volume 1094, pp. 429-432 (2009)

- Claudi, R.; Benatti, S.; Bonanno, A.; Bonavita, M.; Desidera, S.; Gratton, R.; Leccia, S.; Cosentino, R.; Endl, M.; Carolo, E.
**Asteroseismology of solar–type stars with SARG@TNG**
Communications in Asteroseismology, Vol. 159, p. 21-23.
Proceedings of "JENAM 2008 Symposium No 4: Asteroseismology and Stellar Evolution"
September 8-12 2008, edited by Sonja Schuh and Gerald Handler.

- Chauvin, G.; Lagrange, A.-M.; Mouillet, D.; Beuzit, J.-L.; Beust, H.; Ehrenreich, D.; Bonnefoy, M.; Allard, F.; Bessel, M.; Bonavita, M.; Desidera, S.; Dumas, C.; Farihi, J.; Fusco, T.; Gratadour, D.; Lowrance, P.; Mayor, M.; Rouan, D.; Song, I.; Udry, S.; Zuckerman, B.
**The LAOG-Planet Imaging Surveys**
EXOPLANETS AND DISKS: THEIR FORMATION AND DIVERSITY:
Proceedings of the International Conference.
AIP Conference Proceedings, Volume 1158, pp. 183-188 (2009).

- R. Gratton, M. Bonavita, S. Desidera
**Scientific Output of Single Aperture Imaging of Exoplanets**
review to appear in the proceeding of the
PATHWAYS TOWARD HABITABLE PLANETS conference
Barcelona, Spain, 14-18 September 2009

# CONTENTS

# Part I

# SCIENTIFIC BACKGROUND

Since the discovery of the very first planetary mass companion around a pulsar star (Wolszczan & Frail 1992) and ultimately around a star similar to our Sun (51 Peg See Mayor & Queloz 1995), many steps have been done, leading to a sample of detected planets which grows rapidly, as much as the minimum mass of these companion decreases and get closer to the Earth mass.

New and more precise instruments have been built and many other are already planned, all of them looking forward for the discovery of *earth twins* and, ultimately, of traces of life somewhere else than here.

As appended with the discovery of 51 Peg, about fifteen years ago, the observations often open new question about how the discovered planets can form and survive, ending in the needs of more sophisticated theories to address these items.

In this first part of the manuscript we will try to put our work in context, by summarizing the status of the art of the extrasolar planet research, both on the theoretical and observational side.

First we will present an overview of the planet formation theories (mostly focusing on the *Core accretion model*, in Chap. 1.1) with an eye on the effects of the environment characteristics on the final appearance of the planetary systems.

Then in Chap. 2 we'll summarize the properties of the exoplanets as they come from the observational results.

# 1

# PLANETARY FORMATION

## 1.1 CORE ACCRETION PARADIGM

Studies based on observations of the Solar System, of extra-solar planets and young stellar systems have led to the general concept that after the collapse of a dense gas cloud, a proto-star surrounded by a proto-planetary disk was formed. In this disk, solids started to coagulate from fine dust and grew further by mutual collision to form planetesimals, then proto-planets, and ultimately the actual planets. Some of the proto-planets managed to accrete a massive gaseous envelope onto their core, forming the giant planets (see Fig. 1.1).

These are the fundamental assumptions of the so-called *core accretion model* (see Alibert et al. 2005), which is nowadays the most favored scenario to explain the planet formation process.

In this model, the formation of gas giant planets can be thus be seen as a two steps process:

1. The formation of a solid core

2. A runaway gas accretion, which occurs if the core reaches critical mass and leads to a quick build-up of a massive envelope (Perri & Cameron 1974; Mizuno et al. 1978; Bodenheimer & Pollack 1986).

The growth of the core occurs through collisional accretion of background planetesimals, which themselves are formed by collisional coagulation of small dust grains (Wetherill & Stewart 1989) or instability in the dust layer (Johansen et al. 2007).

The formation of the core occurs through the same mechanism as the one generally accepted for the formation of terrestrial planets. When the core has reached roughly the mass of the Moon, it can hold an initially tenuous hydrostatic atmosphere. Its structure is well described by the classical set of 1-D stellar structure equations except for the nuclear energy release term that has to be replaced by heating due to infalling planetesimals. The calculations presented in Pollack et al. (1996) first treated the accretion rates of gas and solids in a self-consistent way. Their

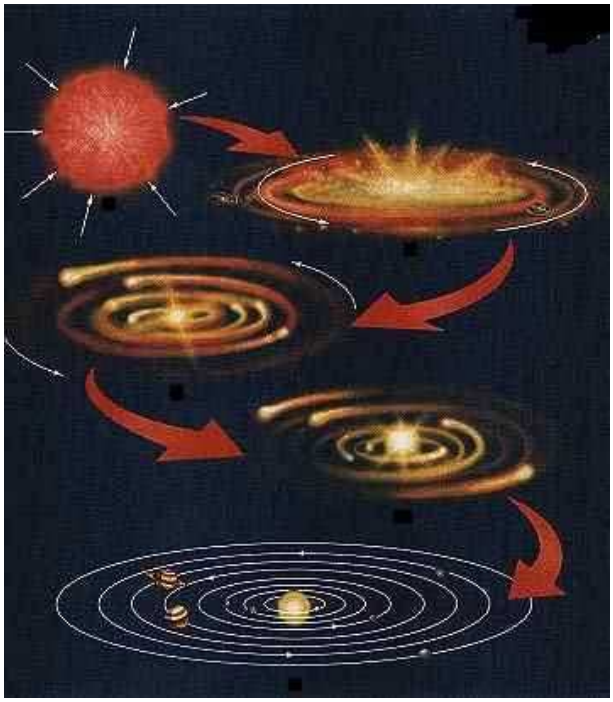

Figure 1.1: The four stages of planet formation

calculations show three distinct phases: phase I ($t < 0.5$ Myr) is characterized by a rapid build-up of the core. It ends when all the planetesimals in the core's initial feeding zone have been accreted. During phase II ($0.5 < t < 7.5$ Myr), the core is capable of extending its feeding zone by slowly accreting some surrounding gas. An increased core mass leads to a deeper potential well which leads to a contraction of the envelope which in turns leads to additional gas accretion from the surrounding disk and so on until the systems runs away and enters phase III ($t > 7.5$ Myr). This phase starts at the critical mass which is reached when the mass of the core and the envelope become roughly equal. Runaway accretion occurs because in this regime the radiative losses from the envelope can no longer be compensated for by the accretion luminosity from the planetesimals.

As a result, there is no equilibrium anymore and the envelope begins to contract on much shorter timescales. This contraction increases the gas accretion rate, which in turn increases the energy losses and the process runs away. The existence of such a critical mass is intrinsic to the core-envelope model and does not depend upon the detail of the input physics

(Stevenson 1982). The critical core mass is usually of the order of 5 to 20 Earth masses (Papaloizou & Terquem 1999). In the runaway phase, the gas accretion rate is limited either by the planet itself (its ability to radiate away the gravitational energy) or by how much gas the disk can supply.

The baseline core-accretion formation model has many appealing features, producing in a nebula with a surface density about four times the *minimum mass* solar nebula a Jupiter like planet with an internal composition compatible to what is inferred from internal structure models (though the uncertainties in these models also allow a Jupiter without solid core: Saumon & Guillot 2004). However, the timescale to form the planet (8 Myr) is uncomfortably long compared to observationally derived lifetimes of protoplanetary disks (Haisch et al. 2001). Higher surface densities lead to significantly shorter formation timescales, which means that the baseline core accretion process is not intrinsically slow, but at the price that the resulting final content of heavy elements is very high (Pollack et al. 1996).

This *timescale problem* finally lead to the hypothesis that another, faster formation mechanism might be needed for giant gaseous planets which suggest their formation trough gravitational instabilities in the protoplanetary disk (*disk instability model*, see Boss 1997).

Since Pollack et al. (1996), the core accretion model has been significantly improved and extended, so that this *formation timescale problem* is no longer a problem. Extended core accretion models have included new physical mechanisms: concurrent calculation of the evolution of the protoplanetary disk, and most importantly, planetary migration. The discovery of numerous Hot Jupiters has forced upon us the necessity of planetary migration as in-situ formation of these objects is beyond the capability of any known formation theory. As planet formation, disk evolution and migration occur all on similar timescales, it is necessary to treat these processes in a self consistent, coupled manner (Alibert et al. 2004). Extending the standard core accretion model by these mechanisms not only leads to a natural explanation of the *Hot planets* (Alibert et al. 2006), but also solves the *timescale problem*: for the same initial conditions that lead to runaway growth in the in situ case after 30 Myr, including concurrent disk evolution and migration leads to the formation of a Jupiter-like planet at 5.5 AU that has an internal composition compatible with internal structure models in just $< 1 Myr$ starting with an embryo of $0.6 M_{Earth}$ at 8 AU (Alibert et al. 2005). The reason for this speed up is that owing to migration, the planet's feeding zone is never as severely depleted and the lengthy

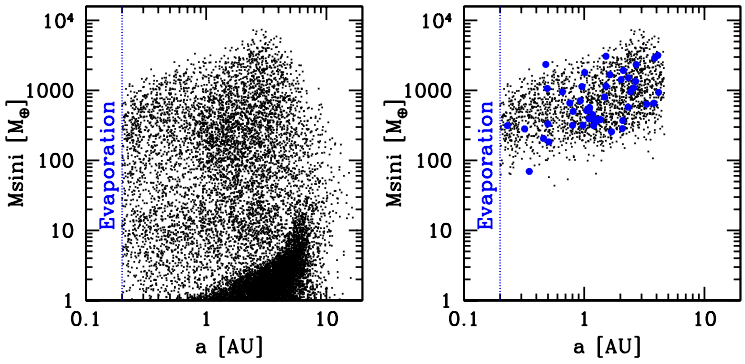


(a) (b)

Figure 1.2: **Left:** Minimum mass versus semi-major axis for all synthetic planets of the nominal population. **Right:** The sub-population of synthetic planets detectable by a radial velocity survey with an instrumental accuracy of 10 m/s and duration of 10 years. Real exo-solar planets are indicated by large dots. Near the star subsequent evaporation of planets could be significant, making a direct comparison with the observations difficult (from Mordasini et al. 2008).

phase II is skipped. Instead, the planet always migrates into regions of the disk where fresh planetesimals are available.

Monte Carlo models have been constructed using this approach (see e.g. Alibert et al. 2005; Mordasini et al. 2009a). Results are shown in Figure 1.2, that show synthetic population of planets let forming through the previous scheme, starting from a population of planetesimals of 0.6 $M_{Earth}$ each. These simulations suggest that planets can be broadly divided into three distinct populations:

- Giant planets ($M_p > 40\ M_{Earth}$)
- Neptune-like planets ($10 < M_p < 40\ M_{Earth}$)
- Rocky planets ($M_p < 10\ M_{Earth}$)[1].

This is more clearly seen examining the expected planet initial mass function (IMF, see Figure 1.3). From the left panel, it is seen that the IMF has a quite complex structure. Starting at the large mass end, we note

[1] In our discussion we will further divide this group in Super-Earths ($1.2 < M_p < 10\ M_{Earth}$) and Earths ($M_p < 1.2\ M_{Earth}$)

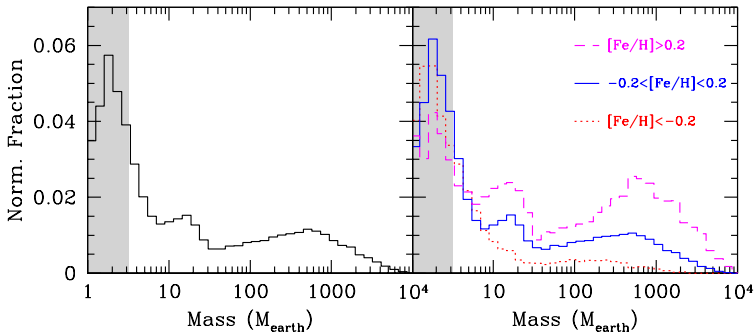


Figure 1.3: Initial mass function of all planets of the synthetic population around G type stars (from Mordasini et al. 2008). In the right panel, the population has been split in a low, medium and high metallicity bin. The region of a few $M_{Earths}$ has been shaded as the model is incomplete there

that core accretion is able to form planets that can, at least if the presence of the core is not important, ignite deuterium burning. However, such planets are rare. At about 500 $M_{Earth}$, the IMF has a local maximum, followed by a local minimum at $\sim$ 40 $M_{Earth}$ (this minimum is even more pronounced in models by Lin and co-workers). A small bump occurs in the Neptune mass domain. At around 6 $M_{Earth}$, the IMF finally starts to rise rapidly. As models are incomplete for these very low masses, quantitative predictions should be regarded with caution here. Qualitatively, a strong raise of the IMF at such masses is however nevertheless expected, as it is simply a consequence of the fact that very often the conditions in the protoplanetary nebula are such that they don't allow the formation of a giant planet. In the right panel, the population was split in a low, medium and high metallicity bin. One can see that the IMF is clearly metallicity dependent, with metal rich systems producing more massive objects, and metal poor small bodies. The distributions cross at around 6 $M_{Earth}$. This metallicity dependent IMF explains why radial velocity technique based planet searches, which are biased towards large masses, have found planets preferentially orbiting metal rich stars.

## 1.2 PLANET-METALLICITY CORRELATION

It is nowadays well known that the frequency of giant planets correlates with the metallicity ([Fe/H]) of the host stars (Fischer & Valenti 2005). One of the most probable explanations of this effect is that high metallicity enhances planet formation because of higher quantity of small particle

condensates which are, according with the core accretion paradigm described above, the building blocks of the planets. Fischer & Valenti (2005) carried out an uniform analysis of the stars in the target lists of the largest Radial Velocity (RV) planet searches, ending with a measurement of the percentage of planet host stars in different metallicity bins.

The result is a dependence of the frequency of giant planets (with orbital periods shorter than 4 years and radial velocity semi-amplitude (K) higher than 40 m/s) from the metallicity of FGK main sequence stars (with $-0.5 < [Fe/H] < 0.5$) which can be expressed as

$$\mathrm{P}(planet) = 0.03 \times 10^{2.0 \times [Fe/H]} \quad (1.1)$$
$$= 0.03\ \mathrm{N}_{Fe} \times N_H \frac{}{(N_{Fe} \times N_H)_\odot}$$

Thus the occurrence of planets is nearly proportional to the number of Iron atoms, as particle collisions are similarly proportional to the number of particles. This suggests a link between the dust particle collision rate in the protoplanetary disk and the formation rate of gas giants, favoring the hypothesis that higher metallicities are inherited from the primordial clouds, rather than the consequence of ingestion of migrating planetary cores. this gives further weight to the core accretion theory.

## 1.3 INFLUENCE OF STELLAR MASS

Besides metallicity, protoplanetary disk masses and surface densities are other important factors suspected to strongly influence the formation of giant planets. They are thought to be dependent on stellar mass, in the sense that more massive stars will have more massive disks and higher surface densities (see Ida & Lin 2005), although this point needs confirmation. The exact impact of this on planet formation is presently poorly known theoretically but such a scaling in the mass distribution of exoplanets is expected in the core-accretion scenario of planet formation since more massive stars probably have more massive disks, which make it possible to accrete larger amounts of rock, ice and gas. However, more quantitative studies are needed. Very recent simulations by Mordasini et al. (2009b) suggest that in more massive disks a larger fraction of planetary cores are able to pass through the bottleneck due to the threshold for gas accretion. This results in a much higher incidence of gas giants at moderate and large distances from the central star.

On the other hand, in the disk-instability paradigm (e.g. Boss 2006b), it is not clear how planet formation depends on stellar mass in general, although Boss (2006b) predicts that this mechanism should not be too sensitive to this parameter.

It also remains to be seen if high luminosities and winds will not prevent the formation of gas giants in the inner regions surrounding intermediate-mass stars. As an example,Ida & Lin (2005) predict that the location of the ice boundary at larger distances is likely to make the formation process of gas giants less efficient.

Kennedy & Kenyon (2008) developed a model for the evolution of the snow line in a planet-forming disk and applied it over a range of stellar masses to derive the probability distribution of gas giant as a function of stellar mass. They found that, given an initial distribution of disk masses, the probability that a star has at least one giant planet increases linearly with stellar mass from 0.4 to 3 $M_{\odot}$. If the frequency of gas giant around solar mass stars is 6%, their model predicts and occurrence rate of 1% and 10% respectively for a $0.4M_{\odot}$ and a $1.5M_{\odot}$ star.

Although sample numbers are small, the observable gas giant frequency seems to confirm this trend. Lovis & Mayor (2007) reported for the first time observational hints suggesting that more massive stars do form more massive planetary systems than lower-mass stars.

The apparently high frequency of massive planets around intermediate-mass stars indeed suggests a rather higher efficiency for the accretion process. Those results, obtained observing a sample of red giant stars in a number of intermediate age open clusters, has been confirmed by Johnson et al. (2007), who obtained fairly similar results combining their sample of M stars from the NASA Keck M Dwarf Survey with the ones from the California and Carnegie Planet Search (CCPS). By measuring the fraction of stars with planets belonging to three stellar bins, they found that the frequency of planets with $M_{*} > 0.8M_{Jup}$ within $a < 2.5AU$ increases with stellar mass (see Fig. 1.4. Thus, the evolved A-type stars in their sample appear to have a probability to harbor a giant planet which is 5 times higher than for the M dwarfs[2].

If confirmed, this mass scaling raises questions on how to classify objects above 13 $M_{Jup}$ the orbit solar-type and intermediate-mass stars.

[2]Note that the high–mass bin is uncorrected for the decreased sensitivity of Doppler measurements of higher–mass sub-giants compared to lower–mass stars. The reported occurrence rate for high–mass stars therefore represents a lower limit unlike the Solar–mass and low–mass bins

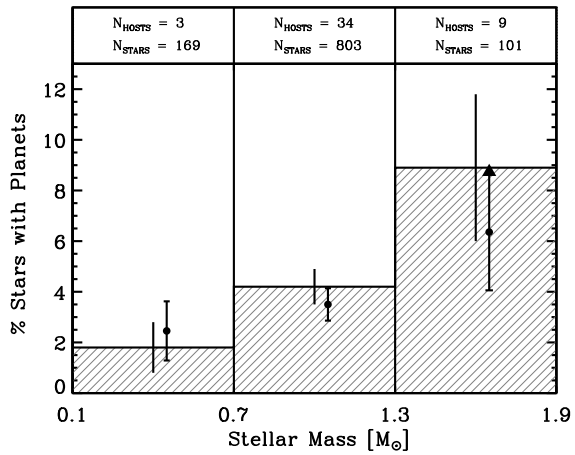


Figure 1.4: Adapted from Johnson et al. (2007). Histogram illustrating the rising percentage of stars with detectable planets as a function of stellar mass. The stars selected for each mass bin have 8 or more observations providing detectability of planets with masses $\geq 0.8$ out to $a = 2.5$ AU. After correcting the measured percentages in each mass bin for the effects of stellar metallicity, the rising trend is slightly diminished (Filled circles). The error bars on each bin are from Poisson statistics and the numbers above each bin compare the number of stars with planets $N_{HOSTS}$ to the total number of stars in each bin $N_{STARS}$

.

An abrupt transition between planets and brown dwarfs would have little meaning if both categories of objects are formed by the same physical process.

## 1.4 PLANET FORMATION IN BINARY SYSTEMS

Although the study of the dynamics of planets in or around binary stars dates back about forty years ago, it remains an unresolved issue. Many attempts have been done to understand whether planets could form in multiple star systems, and whether the notion of habitability, as we know it, could be extended in such environments.

As seen in the previous sections, the current theories of planet formations focus only on single stars and their extension to binary environments are limited to either the Sun–Jupiter system (focusing on the effects of Jupiter on the formation of the inner planets, see e.g Heppenheimer 1974, 1978; Drobyshevski 1978; Diakov & Reznikov 1980; Whitmire et al. 1998; Kortenkamp et al. 2001) or systems in which the stellar companions

belongs to the brown dwarf regime, thus resembling some of extrasolar planets (see Whitmire et al. 1998).

Marzari & Scholl (2000); Nelson (2000); Barbieri et al. (2002); Quintana et al. (2007); Lissauer et al. (2004) and many others attempted to extend these studies to binaries with comparable mass components, but without any constraint or comparison with observations, since there has been no clear evidence of the existence of such binary planet systems until recently.

All these studies lead to the conclusion that, given the core accretion paradigm presented in Sec. 1.1, one must consider that the presence of a stellar companion can significantly alter the various stages of planet formation process, having significant effects on their efficiency, especially in the case of a binary star system with a moderate to small separation.

As shown by Boss (2006b), a binary companion can alter the structure of a planet-forming nebula, and create regions where the densities of the gas and dust are locally enhanced In addition, as shown by Artymowicz & Lubow (1994) and Pichardo et al. (2005) a stellar component on an eccentric orbit can truncate the circumprimary disk of embryos to smaller radii and remove material that may be used in the formation of terrestrial planets. As a result, it used to be believed that circumstellar disks around the stars of a binary may not be massive enough to form planets. However, observations by Mathieu (1994); Akeson et al. (1998); Rodríguez et al. (1998); Mathieu et al. (2000) indicated that potentially planet-forming circumstellar disks can indeed exist around the stars of a binary system, implying that planet formation in binaries may be as common as around single stars. The masses of these disks are comparable to the minimum solar-mass model of the primordial nebula of our solar system (Weidenschilling 1977; Hayashi 1981), implying that, planet formation in dual-star systems can begin and continue in the same fashion as around our Sun.

Despite the observational evidence in support of the existence of planet-forming environments in moderately close binary star systems, the perturbing effect of the binary companion may not always favor planet formation. For instance, as shown by Nelson (2000), giant planet formation cannot proceed through the disk instability mechanism Boss (2000) around the primary of a binary star system with separation of $\sim 50$ AU.

Also, when forming planetary embryos, the perturbation of the secondary star may increase the relative velocities of planetesimals and cause their collisions to result in breakage and fragmentation, as shown by Heppenheimer (1978); Whitmire et al. (1998); Thébault et al. (2004).

Results of the studies by these authors suggest that planetesimals accretion will be efficient only in binaries with large separation: 50 AU as indicated by Heppenheimer (1978), 26 AU as shown by Whitmire et al. (1998), and 100 AU as reported by Mayer et al. (2005). Finally, in a binary star system, the stellar companion may create unstable regions where the building blocks of planets will not maintain their orbits and, as a result, planet formation will be inhibited (Whitmire et al. 1998).

Interestingly, despite all these difficulties, numerical simulations have shown that it may indeed be possible to form giant and/or terrestrial planets in and around a dual-star system. Recent simulations by Boss (2006b), and Mayer et al. (2005) indicate that Jupiter-like planets can form around the primary of a binary star system via gravitational instability in a marginally unstable circumprimary disk. On the other hand, as shown by Thébault et al. (2004), the core accretion mechanism may also be able to form giant planets around the primary of a binary star.

Despite the destructive role of the binary companion in increasing the relative velocities of planetesimals, which causes their collisions to result in erosion, this efficiency of terrestrial planet formation in binary systems may be attributed to the fact that the effect of the binary companion on increasing the relative velocities of planetesimals can be counterbalanced by dissipative forces such as gas-drag and dynamical friction (Marzari et al. 1997; Marzari & Scholl 2000).

The combination of the drag force of the gas and the gravitational force of the secondary star may result in the alignment of the periastron of planetesimals and increases the efficiency of their accretion by reducing their relative velocities. This is a process that is more effective when the sizes of the two colliding planetesimals are comparable and small. For colliding bodies with different sizes, depending on the size distribution of small objects, and the radius of each individual planetesimal, the process of the alignment of periastron may instead increase the relative velocities of the two objects, and cause their collisions to become eroding (see Thébault et al. 2006).

### 1.4.1 *Dynamical evolution and stability*

Once a planetary companion has managed to form in a binary environment, it must end up on a stable orbit to survive. Simulations show that

a planet-size body can have three types of stable orbits in and around a binary star (as described by Dvorak 1982):

- *s-type orbit* where it revolves around one of the stars of the binary
- *p-type orbit* if it's around the entire binary systems
- *l-type orbit* when it librates in a stable orbit around the $L_4$ or $L_5$ Lagrangian points.

Instability occurs when the perturbing effects cause the semi-major axis and orbital eccentricity of a planet change in such a way that either the object leaves the gravitational field of the system, or it collides with another body. For a planet in an S-type orbit, the gravitational force of the secondary star is the source of these perturbations. That implies, a planet at a large distance from the secondary, i.e., in an orbit closer to its host star, may receive less perturbation from the binary companion and may be able to sustain its dynamical state for a longer time (Harrington 1977). Since the perturbing effect of the stellar companion varies with its mass, and the eccentricity and semi-major axis of the binary (which together determine the closest approach of the secondary to the planet), it is possible- to estimate an upper limit for the planet's distance to the star beyond which the orbit of the planet would be unstable.

As shown by Rabl & Dvorak (1988) and Holman & Wiegert (1999), the maximum value that the semi-major axis of a planet in an S-type orbit can attain and still maintain its orbital stability is a function of the mass-ratio and orbital elements of the binary, and is given by:

$$\begin{aligned} a_c/a_b = {} & (0.464 \pm 0.006) + (-0.380 \pm 0.010)\mu \\ & + (-0.631 \pm 0.034)e_b + (0.586 \pm 0.061)\mu e_b \\ & + (0.150 \pm 0.041)e_b^2 + (-0.198 \pm 0.047)\mu e_b^2 \end{aligned} \tag{1.2}$$

In this equation, $a_c$ is *critical* semi-major axis , $\mu = M_1/(M_1 + M_2)$, $a_b$ and $e_b$ are the semi-major axis and eccentricity of the binary, and $M_1$ and $M_2$ are the masses of the primary and secondary stars, respectively. The $\pm$ signs in equation 1.2 define a lower and an upper value for the critical semi-major axis $a_c$, and set a transitional region that consists of a mix of stable and unstable systems. Such a dynamically *grey* area, where the state of a system changes from stability to instability, is known to

exist in multi-body environments, and is a characteristic of any dynamical system.

Similar to S-type orbits, in order for a P-type planet to be stable, it has to be at a safe distance from the two stars so that it would be immune from their perturbing effects. That is, planets at large distances from the center of mass of a binary will have a better chance of begin stable. This distance, however, cannot be too large because at very large distances, other astronomical effects, such as galactic perturbation, and perturbations due to passing stars, can render the orbit of a planet unstable.

Dvorak (1984) showed that planets at distances 2-3 times the separation of the binary have stable orbits. Subsequent studies by Dvorak (1986); Dvorak et al. (1989), and Holman & Wiegert (1999) lately showed that the orbit of a P-type planet will be stable as long as the semi-major axis of the planet stays larger than the critical value given by

$$\begin{aligned} a_c/a_b = (1.60 \pm 0.04) + (5.10 \pm 0.05)e_b \\ +(4.12 \pm 0.09)\mu + (-2.22 \pm 0.11)e_b^2 \\ +(-4.27 \pm 0.17)e_b\mu + (-5.09 \pm 0.11)\mu^2 \\ +(4.61 \pm 0.36)e_b^2\mu^2. \end{aligned} \tag{1.3}$$

Similar to equation 1.2, equation 1.3 represents a transitional region with a lower boundary below which the orbit of a P-type planet will be certainly unstable, and an upper boundary beyond which the orbit of the planet will be stable. The *mixed zone* between these two boundaries represents a region where a planet, depending on its orbital parameters, and the orbital parameters and the mass-ratio of the binary, may or may not be stable.

## 1.5 GIANT PLANET THERMAL EVOLUTION MODELS

Within six years of the Voyager 2 fly-by of Neptune, the encounter that completed our detailed census of the planets in the outer solar system, came the stunning discoveries of the extrasolar giant planet 51 Peg b (Mayor & Queloz 1995) and also the first bona fide brown dwarf, Gliese 229B (Nakajima et al. 1995). We were not yet able to fully understand the structure and evolution of the solar system's planets before we were given a vast array of new planets to study. In particular the close-in orbit of 51 Peg b led to immediate questions regarding its history, structure,

and fate (Guillot et al. 1996; Lin et al. 1996). Four years later, the first transiting planet, HD 209458 (Charbonneau et al. 2000; Henry et al. 2000), was found to have an inflated radius of $\sim$1.3 , confirming that proximity to a parent star can have dramatic effects on planetary evolution (Guillot et al. 1996). The detections of over 50 additional transiting planets (as of August 2009) have conclusively shown that planets with masses greater than that of Saturn are composed predominantly of H/He, as expected. However, a great number of important questions have been raised.

Much further from their parent stars, young luminous gas giant planets are being directly imaged from the ground and from space (Kalas et al. 2008; Marois et al. 2008; Lagrange et al. 2009). For imaged planets, planetary thermal emission is only detected in a few bands, and a planet's mass determination rests entirely on comparisons with thermal evolution models, these aim to predict a planet's luminosity and spectrum with time. However, the luminosity of young planets is not yet confidently understood (Marley et al. 2007; Chabrier et al. 2007)

Giant planet thermal evolution models are being tested at Gyr ages for solar system planets and the transiting planets. It is clear from giant planet formation theories that these planets are hot, luminous, and have larger radii at young ages, and they contract and cool inexorably as they age. However, since the planet formation process is not well understood *in detail*, we understand very little about the initial conditions for the planets' subsequent cooling. Since the Kelvin-Helmholtz time is very short at young ages (when the luminosity is high and radius is large) it is expected that giant planets forget their initial conditions quickly. This idea was established with the initial Jupiter cooling models in the 1970s (Graboske et al. 1975; Bodenheimer 1976).

Since our solar system's giant planets are thought to be 4.5 Gyr old, there is little worry about how thermal evolution models of these planets are affected by the unknown initial conditions. The same may not be true for very young planets, however. Since giant planets are considerably brighter at young ages, searches to directly image planets now focus on young stars. At long last, these searches are now bearing fruit (Chauvin et al. 2005; Marois et al. 2008; Kalas et al. 2008; Lagrange et al. 2009). It is at ages of a few million years where understanding the initial conditions and early evolution history is particularly important. Traditional evolution models, which are applied to both giant planets and brown dwarfs, employ an arbitrary starting point. The initial model is large in radius, luminosity, and usually fully adiabatic. The exact choice of the starting

model is often thought to be unimportant, if one is interested in following the evolution for ages greater than 1 Myr (Chabrier & Baraffe 2000; Burrows et al. 1997).

Thermal evolution models, when coupled to a grid of model atmospheres, aim to predict the luminosity, radius,$T_{Eff}$, thermal emission spectrum, and reflected spectrum, as a function of time. When a planetary candidate is imaged, often only the apparent magnitudes in a few infrared bands are known. If the age of the parent star can be estimated (itself a tricky task) then the observed infrared magnitudes can be compared with calculations of model planets for various masses, to estimate the planet's mass. Recall here that mass is not an observable quantity unless some dynamical information is also known. It is not known if these thermal evolution models are accurate at young ages–they are relatively untested, which has been stressed by Baraffe et al. (2002) for brown dwarfs and Marley et al. (2007) for planets.

Marley et al. (2007) examined the issue of the accuracy of the arbitrary initial conditions (termed a "hot start" by the authors) by using initial conditions for cooling that were not arbitrary, but rather were given by a leading core accretion planet formation model (Hubickyj et al. 2005). The core accretion calculation predicts the planetary structure at the end of formation, when the planet has reached its final mass. The Marley et al. (2007) cooling models used this initial model for time zero, and subsequent cooling was followed as in previously published models. Figure 1.5 shows the resulting evolution. The cooling curves are dramatically different, yielding cooler (and smaller) planets. The initial conditions are not quickly "forgotten," meaning that the cooling curves do not overlap with the arbitrary start models for $10^7$ to $10^9$ years. What this would mean, in principle, is that a mass derived from "hot start" evolutionary tracks would significantly underestimate the true mass of a planet formed by core accretion.

Certainly one must remember that a host of assumptions go into the formation model, so it is unlikely that these new cooling models are quantitatively correct. However, they highlight that much additional work is needed to understand the *energetic* of the planet formation process. The Hubickyj et al. (2005) models yield relatively cold initial models because of an assumption that accreting gas is shocked and readily radiates away this energy during formation. This energy loss directly leads to a low luminosity starting point for subsequent evolution. Significant additional work on multi-dimensional accretion must be done, as well as on radia-

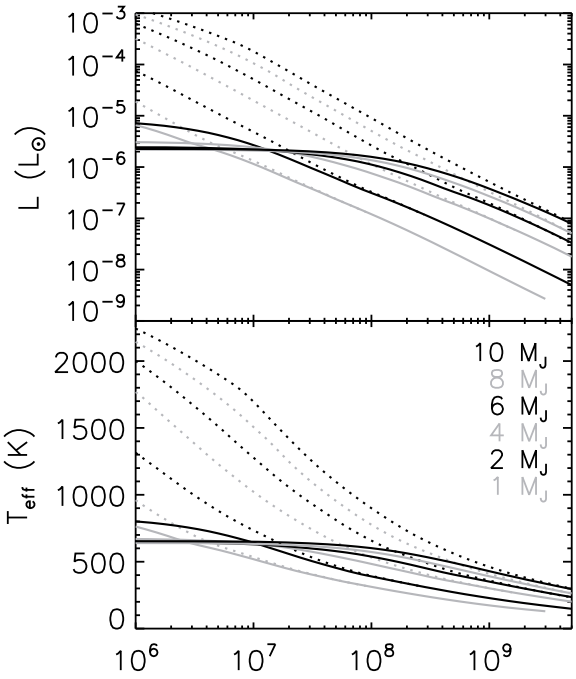


Figure 1.5: Thermal evolution of giant planets from 1 to 10 $M_J$, adapted from Marley et al. (2007). The dotted curves are standard "hot start" models with an arbitrary initial condition, and the solid curves use as an initial condition the core accretion formation models of Hubickyj et al. (2005).

tive transfer during the accretion phase, before we can confidently model the early evolution. Thankfully, it appears that detections of young planets are now beginning to progress quickly, which will help to constrain these models.

## 1.6 PLANET STABILITY AND HABITABILITY

Based on the knowledge of carbon-based life on Earth, which requires water for its chemical reactions, the habitable zone has been defined as the distance range over which liquid water is likely present on a planet surface, and the continuously habitable zones are those regions in which liquid water is expected to be present over a significant fraction of the main-sequence lifetime of the star. For this reason the search for habitable planets will focus on rocky planets in low-eccentricity orbits around Sun-like stars at about 1 AU distance. For planets without atmospheres, the habitable zone is determined by the equilibrium condition between the flux coming from its parent star impinging on the planet surface and emission by the planet surface itself. The cooler the star, the closer to the star is the habitable zone. In the M star case the planet in the HZ is in a synchronous orbit, generally considered not suitable for life.

The position and extent of the habitable zone depends mainly on the stellar luminosity and age, but also on the planetary atmosphere and on possible internal heat sources. If the planet has an atmosphere, the definition of habitable zone is complicated by the presence of negative feedback processes that stabilizes the climate. This process is driven by the greenhouse effect. Inner and outer limits of HZ are where these negative feedback loops begin to fail to stabilize climate and planets become inhospitable for life. This was the fate of Venus (high irradiation and thick atmosphere gave rise to a runaway greenhouse effect which evaporated all the water in the planet) and Mars (where the solar radiance and a thin atmosphere were not able to produce a sufficient greenhouse effect in order to warm the surface). Various mechanisms are relevant to define the efficiency of the greenhouse effect, and among these the most important is the presence/absence of plate tectonic activity, which may help stabilizing the $CO_2$ content in the atmosphere.

# 2

# EXOPLANETS PROPERTIES

In the previous chapter we reviewed the basics of the planet formation and the expected properties of the planetary systems as comes from the theories, depending on the different initial conditions.

In the following section we will then see what are the characteristics of the planets that are important from the observational point of view, thus focusing on the observable quantities for the various detection techniques which aim is to find and (in case of direct measurement of the planet spectra) characterize the planetary objects, thus providing important constraint to be fulfilled by the theories.

## 2.1 CHARACTERISTICS OF DIFFERENT PLANET CLASSES

### 2.1.1 *Giant planets*

Theoretical models of planet formation following the core accretion scenario predicts that the peak of formation of giant planets is found close to the snowline, thanks to the availability of a larger amount of condensates in the protoplanetary disk. In outer regions the longer timescales involved should make planet formation a less efficient process. Migration mechanisms will alter the original distribution. We expect then to observe a roughly bell-type distribution, which shape is a function of the efficiency of the migration mechanisms (that may also create asymmetric distributions or secondary peaks). Furthermore, current models of planet migration within a disk predict smaller migration rates for the most massive giant planets. Therefore, a significant population of massive EGP can be expected not too far from their birth zone (3-10 AU for solar-type stars).

According to Ida & Lin (2004) core accretion mechanism is able to form giant planets up to 30 AU from the central star while outward migration might push some of them up to 50-100 AU from the central star. Outward migration within the disk has been studied by Veras & Armitage (2004) and Martin et al. (2007). Depletion of outer disk by photo-

evaporation should also favour outward migration. Formation of planets or brown dwarfs in-situ at very wide separation might be instead possible for thew disk instability mechanisms (Boss 2006a).

A further mechanism potentially able to populate the outer regions of a planetary system is gravitational scattering between planets (the *Jumping Jupiter* scenario, see Marzari & Weidenschilling 2002). It predicts the presence of giant planets in very wide orbits (e.g. 100 AU) beyond the limit where standard planet formation is thought to be possible. Therefore, determination of the frequency of giant planets in wide orbits ($> 5 - 10$ AU) will allow testing several aspects of the planet formation models.

Beside frequency it would also be interesting to derive the distributions of planet parameters such as mass, semi-major axis and eccentricities and any difference with respect to those observed for planets orbiting close to their central star. Very massive planets are expected to be found mostly at a separation close to the snowline. On the other hand, planets at very wide separations might have typically smaller mass, somewhat resembling the run of mass vs. separation in the Solar System Benz et al. (2006). However, some models show that also massive planets can have large outward migration Veras & Armitage (2004). Larger eccentricities are expected if planets arrived at their location through the Jumping Jupiter mechanism. The details of the mass functions of sub-stellar companions, including brown dwarfs, at wide separation and the study of the brown dwarf desert will put constraints on their formation mechanisms and the actual mass separation between the two classes of objects.

### 2.1.2 *Neptune-like planets*

In the last few years, improvements in instrumental precision and observing strategies techniques allowed the start of a new era in RV planet searches, extending the area of investigation to masses well below the gas giant mass range, down to masses $\sim 5 - 25\ M_{Earth}$. This new era will likely revolutionize our understanding of the physics of formation and evolution of rocky/icy planets, in a similar way the first detections of giant planets did for the field of gas giant planets. The first discoveries of the so-called Hot Neptunes ($M_{Neptune} = 17 M_{Earth}$) occurred thanks to densely sampled observations of two planet hosts for Asteroseismology

(Santos et al. 2004a) or improved characterization of the orbital properties of known planets (McArthur et al. 2004).

After these serendipitous discoveries, some systematic searches were started, leading to the identification of about fifty Neptune mass planets. These represent only a minor fraction of the planets known today, because of the excellent instrument performances and large amount of telescope time needed for the detection. Instead, their frequency is probably larger than giant planets with masses larger than Jupiter and Saturn, possibly as much as 10% of the stars host Neptune mass planets in close orbits, and an even larger fraction in wider orbits. The limited number of detected Neptune-mass planets allows some very preliminary analysis of their properties (Udry & Santos 2007). There are some hints of differences with respect to Jupiter mass planets, in terms of period and eccentricity distributions and properties of host stars (mass, metallicity) . However they need confirmation with significantly enlarged sample of objects.

From the theoretical point of view, Neptune-mass planets have a specific role in constraining the scenarios of planet formation, and in particular to quantify the migration and disk dissipation timescales. Determination of mass and radius of the planet are of special relevance for Neptune-mass or massive Earth-like planets, which should have different composition and mean density according to their formation mechanisms (failed cores of giant planets with small amount of gas, massive rocky planets, evaporated close-in giant planets).

### 2.1.3 *Rocky planets (Earths and super-Earths)*

The ultimate goal of planet searches is the direct detection and characterization of earth like planets in habitable zones of Solar â type stars. This is an almost unknown territory up to now, as current instrumentation have very limited capabilities of detecting such planets. The goal for the coming decades is to detect Earth-like planets around other stars, to estimate the frequency of their occurrence and possibility to obtain direct images of some of these with an ELT or a space interferometer. This may allow a future spectroscopic characterization for the search for exo-solar life. Current radial velocity and transit search programs are limited to planets larger than the Earth, the so called super-Earths (i.e. planets with masses in the range 1.2 to 10 $M_{Earth}$, and likely radii from 1 to 2.5 $R_{Earth}$). Some of them, such as Gliese 581c ($\sim 5M_{Earth}$) are presumably made of rock

(Udry et al. 2007), while others may be volatile-rich, such as the $5.5 M_{Earth}$ OGLE-2005-BLG- 390Lb (Beaulieu et al. 2006).

Few super-Earths have recently been discovered around main sequence stars, 3 in the same planetary system (Mayor et al. 2009). In the near future, Kepler will provide an enormous enhancement in our capabilities of detecting planets via transits. This will allow determining the frequency of occurrence of super-Earths at small distances from a variety of stars. Otherwise, both observational evidence and theoretical simulations indicate that small planets are more numerous than giant ones, in particular: the observed mass histogram rises towards small masses.

## 2.2 MASS-RADIUS RELATION

The mass-radius relationship for planets, and more generally for substellar/stellar objects, contains essential information about their main composition and the state of matter in their interior. The fundamental work by Zapolsky & Salpeter (1969) is a perfect illustration of this statement. The analysis of cold (zero-temperature) spherical bodies of a given chemical composition and in hydrostatic equilibrium shows the existence of a unique mass-radius relation and of a maximum radius $R_{\max}$ at a critical mass $M_{\rm crit}$. The very existence of a maximum radius stems from two competing physical effects characteristic of the state of matter under planetary conditions. The first effect is due to electron degeneracy, which dominates at large masses and yields a mass-radius relationship $R \propto M^{-1/3}$ characteristic of fully degenerate bodies (Chandrasekhar 1939). The second effect stems from the classical electrostatic contribution from ions (Coulomb effects) which yields a mass radius relation $R \propto M^{1/3}$, characteristic of incompressible Earth-like planets. Zapolsky & Salpeter (1969) find a critical mass of 2.6 where the radius reaches a maximum value $R_{\max} \sim 1$ for a gaseous H/He planet. The critical mass increases as the heavy element content increases, while $R_{\max}$ decreases.

The true mass-radius relationship, derived from models taking into account a realistic equation of state yields a smoother dependence of radius with mass, as displayed in Fig. 2.1. The transition between stars and brown dwarfs marks the onset of electron degeneracy, which inhibits the stabilizing generation of nuclear energy by hydrogen burning. The typical transition mass is $\sim 0.07$ (Burrows et al. 2001; Chabrier & Baraffe 2000). Above this transition mass, the nearly classical ideal gas yields a

mass-radius relationship $R \propto M$. In the brown dwarf regime the dominant contribution of partially degenerate electrons, balanced by the contribution from ion interactions yields $R \propto M^{-1/8}$ instead of the steeper relationship for fully degenerate objects. The increasing contribution of Coulomb effects as mass decreases competes with electron degeneracy effects and renders the radius almost constant with mass around the critical mass. The full calculation yields, for gaseous H/He planets, $M_{\rm crit} \sim 3$, amazingly close to the results based on the simplified approach of Zapolsky & Salpeter (1969). Below the critical mass, Coulomb effects slightly dominates over partially degenerate effects, yielding a smooth variation of radius with mass close to the relation $R \propto M^{1/10}$.

The determination of mass-radius relationships of exoplanets, using photometric transit and Doppler follow-up techniques, provides an unprecedented opportunity to extend our knowledge on planetary structure and composition.

Two benchmark discoveries illustrate the surprises planet hunters were faced with. The very first transiting planet ever discovered, HD 209458b (Charbonneau et al. 2000; Henry et al. 2000) was found with an abnormally large radius, a puzzling property now shared by a growing fraction of transiting exoplanets. At the other extreme, a Saturn mass planet, HD 149026b (Sato et al. 2005) was discovered with such a small radius that more than 70  of heavy elements is required to explain its compact structure. This discovery raised in particular new questions on the formation process of planets with such a large amount of heavy material. The diversity in mean density of transiting planets yet discovered is illustrated in Fig. 2.1.

### 2.2.1 *Irradiation effects*

The discovery of HD 209458b and of many other additional transiting exoplanets has opened a new era in giant planet modeling. The modern theory of exoplanet radii starts with models including irradiation effects from the parent star. These effects on planet evolution are accounted for through the coupling between inner structure models and irradiated atmosphere models, following the same method described in §2.3. Current treatments are based on simplified treatments of the atmosphere, using 1D plane parallel atmosphere codes. They however allow understanding the main effects on planetary evolution. In reality the impinging stellar

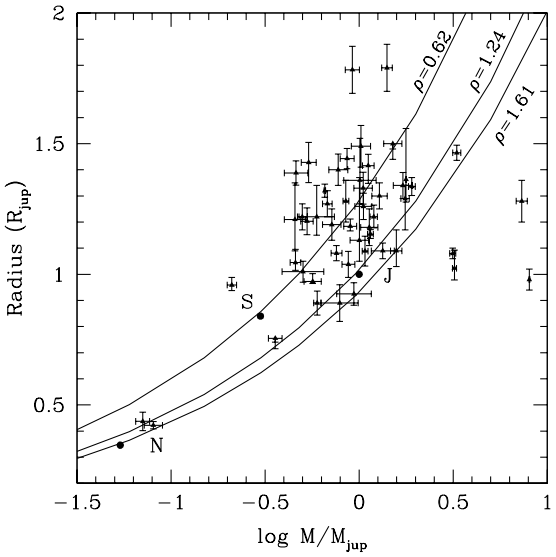


Figure 2.1: Mass-radius diagram for the known transiting planets, adapted from Fortney et al. (2009) (data from: www.inscience.ch/transits). Three iso-density curves are shown for the mean densities of Saturn ($\bar{\rho} = 0.62$), Jupiter ($\bar{\rho} = 1.24$) and Neptune ($\bar{\rho} = 1.61$). These three solar system giant planets are also indicated by solid points.

flux has an angle of incidence which is a function of the latitude and longitude, but in 1D one attempts to compute a planet-wide or day-side average atmosphere profile, using a parameter $f$ which represents the redistribution factor of the stellar flux over the planet surface (Baraffe et al. 2003; Burrows et al. 2003; Fortney et al. 2006). The incident stellar flux $F_{\rm inc}$ is explicitly included in the solution of the radiative transfer equation and in the computation of the atmospheric structure and is defined by:

$$F_{\rm inc} = \frac{f}{4} \left( \frac{R_*}{a} \right)^2 F_*, \tag{2.1}$$

where $R_*$ and $F_*$ are the stellar radius and flux respectively, and $a$ the orbital separation. The current generation of models often use $f = 1$, corresponding to a stellar flux redistributed over the entire planet's surface or $f = 2$ if heat is redistributed only over the day side. Heat redistribution is a complex problem of atmospheric dynamics, depending in particular on the efficiency of winds to redistribute energy from the day side to the night side. This question is a challenge for atmospheric circulation modelers (Showman et al. 2008). This nascent field is growing rapidly

with observational constraints provided by infrared light curves obtained with *Spitzer*, which are starting to provide information on the temperature structure, composition and dynamics of exoplanet atmospheres.

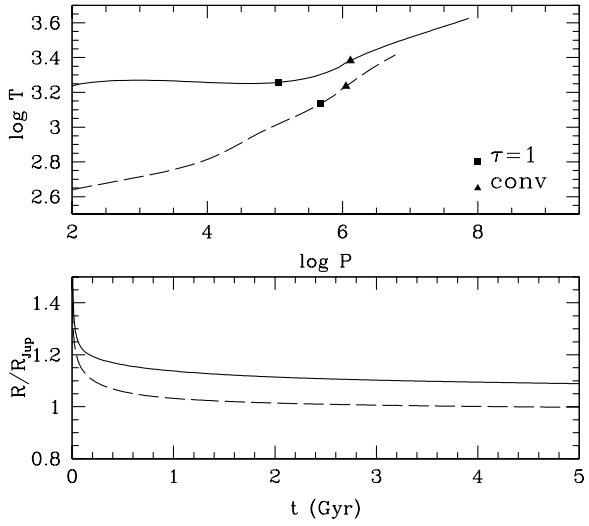


Figure 2.2: Adapted from Fortney et al. (2009). Effect of irradiation for a planet at 0.05 AU from the Sun (adapted from Fortney et al. 2009). *Upper panel:* $T - P$ profiles of atmosphere models with intrinsic =1000 K (a high value representative of giant planets at young ages) and surface gravity $\log g$=3 (cgs). The solid line corresponds to the irradiated model and the dashed line to the non-irradiated model. The locations of the photosphere ($\tau \sim 1$) and of the top of the convective zone are indicated by symbols (Barman et al. 2001, Models after). *Lower panel:* evolution of the radius with time of a 1 giant planet. Irradiated case: solid line; Non irradiated case: dashed line (Models after Baraffe et al. 2003).

Although treatments of irradiation effects can differ in the details, with possible refinements accounting for phase and angle dependence of the incident flux (Barman et al. 2005; Fortney & Marley 2007), different models converge toward the same effect on the planet atmosphere and evolutionary properties. Atmospheric thermal profiles are strongly modified by irradiation effects (see Barman et al. 2001; Sudarsky et al. 2003) as illustrated in Fig. 2.2 (upper panel). The heating of the outer layers by the incident stellar flux yields to an isothermal layer between the top of the convective zone and the region where the stellar flux is absorbed. The top of the convective zone is displaced toward larger depths, compared to the non-irradiated case. The main effect of the shallower atmospheric

pressure-temperature profile is to drastically reduce the heat loss from the planet's interior, which can maintain higher entropy for a longer time (Guillot et al. 1996). Consequently, the gravitational contraction of an irradiated planet is slowed down compared to the non-irradiated counterpart and the upshot is a larger radius at a given age (see Fig. 2.2, lower panel)

The quantitative effect on the planet's radius depends on the planetary mass, parent star properties and orbital distance. Typical effects on the radius of irradiated Saturn mass or Jupiter mass planet located at orbital distances ranging between 0.02 AU and 0.05 AU around a solar-type star are of the order of 10%-20% (Baraffe et al. 2003; Burrows et al. 2003; Chabrier et al. 2004; Fortney & Marley 2007). A consistent comparison between the theoretical radius and the observed transit radius requires an additional effect due to the thickness of the planet atmosphere (Baraffe et al. 2003; Burrows et al. 2003, 2007). The measured radius is a transit radius at a given wavelength, usually in the optical, where the *slant* optical depth reaches $\sim$1. This is at atmospheric layers above the photosphere (Hubbard et al. 2001; Burrows et al. 2003). The latter region is defined by an averaged normal optical depth $\tau \sim 1$, where the bulk of the flux is emitted outward and which corresponds to the location of the theoretical radius. The atmospheric extension due to the heating of the incident stellar flux can be significant, yielding a measured radius larger than the simple theoretical radius. This effect can add a few % (up to 10%) to the measured radius (Baraffe et al. 2003; Burrows et al. 2003). Effects of irradiation on both the thermal atmosphere profile and the measured radius must be included for a detailed comparison with observations and can explain some of the less inflated exoplanets. They are however insufficient to explain the largest radii of currently known transiting exoplanets, such as TrES-4 with a radius $R = 1.78$ (Sozzetti et al. 2009). This fact points to other mechanisms to inflate close-in planets.

## 2.3 PLANETARY SPECTRA: TEMPERATURE AND ALBEDO

Both the reflected flux and the thermal flux depend on the size of the planet, on the distance between the observer and the planet, and on the planetâs phase angle. They also depend on the composition and structure of the planetâs atmosphere, the properties of the surface (if applicable). More specifically, clouds, aerosols and surface types can highly influence the planetary reflectivity (albedo). Spectroscopy will provide very rich

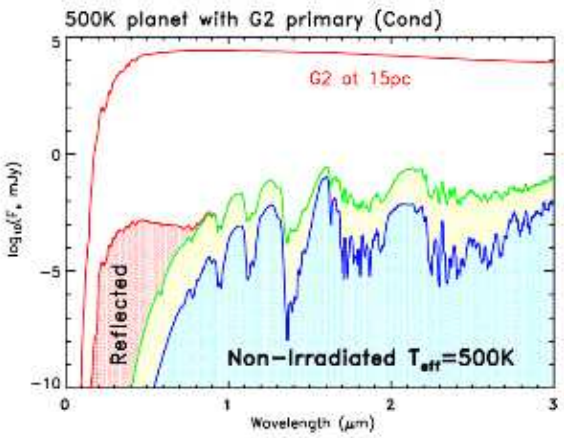


Figure 2.3: Spectrum of a 500 K planet around a G2V star is shown: the planet is modelled located at orbital distance less than $\sim AU$ (middle-green) and then, at larger distance (few AUs), where the planet is not irradiated anymore by the star (bottom-blue) and shines uniquely in the near-IR, in between broad absorption bands (Allard et al. 2000).

information, such as the species present in the atmosphere, the cloud coverage and, if applicable, the surface properties.

Models of the intrinsic emission of sub-stellar objects of different masses and ages, down to the masses of giant planets, have been presented by e.g. Burrows et al. (2003) and Baraffe et al. (2003). Figures 2.3 and 2.4 show examples of such spectra.

At temperatures below about 1300 K, the near infrared spectra are dominated by methane and water absorption. Rather broad and strong spectral features are available in J and H bands. These are ideal for

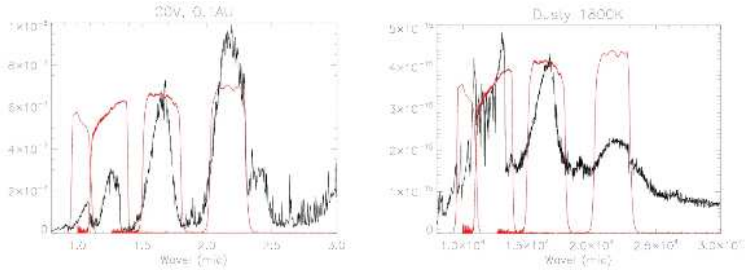

Figure 2.4: Spectra ($F\nu$ vs $\lambda$) of two objects for which the flux in the Ks band is important. Left: an irradiated Jupiter-like planet in short orbit of a solar-type star (Sudarsky et al. 2003)Right: a massive and hot planet or T dwarf with dust in its atmosphere (Allard et al. 2000).

speckle noise suppression using differential imaging techniques, either using narrow-band filters or integral field spectroscopy. Significant flux at optical wavelengths is present only in case of irradiation by the central star. The red edge of the K band is strongly depressed by methane absorption. Note that planets at temperatures larger than 1300 K are brighter in K than at shorter wavelengths (e.g. Fig. 2.4). Such temperatures can be achieved only for massive planets at very young ages (or BDs at older ages).

Water and ammonia clouds appear at temperature lower than about 400 and 150 K respectively. The locations and characteristics of cloud layers affect the observed spectrum significantly. As discussed by Baraffe et al. (2002); , models should not be considered reliable for very young planets (¡10 Myr), due to the strong dependence on the (unknown) initial conditions. Most recent models (Marley et al. 2007) claim that the initial luminosity of giant planets is lower (up to a factor of 100) when initial conditions of a spherical shock accretion are included. Then, the young planets would take up to 20 Myr (resp. 1 Gyr) to get to normally adopted luminosities for an initial mass of 1 (respectively 10) Jupiter mass(es). However, the core-accretion model is not the only model for forming giant planets, and the simple hypothesis describing the critical shock accretion (e.g. spherical instead of disk-like) may still affect the final result by a large factor. Mass estimates of young sub-stellar objects in clusters have also shown that, oppositely, the young planets could be less massive than expected, at a given luminosity (Mohanty et al. 2004). This controversy illustrates the critical need for observational constraints of forming giant planets. Future detection of the luminosities and colours of giant planets in their first billion years lifetime will definitely validate the models of their formation and evolution.

The albedo of the giant planets (Sudarsky et al. 2003) are generally expected to be higher in the optical range ($\sim$ 0.7) than in the near infrared (0.4-0.5), where absorption bands of methane, ammonia, and water are present. The sequence of albedo spectra is roughly similar to that expected for thermal emission spectra in the near-IR, and the same absorption bands are present. The rough subdivision in spectral classes should therefore also apply in this case. For old planets (brightness dominated by reflected light), the temperature sequence corresponds to a sequence of decreasing orbital separations of the planets. Since stellar irradiation affects the atmospheric structure, it is not correct to apply theoretical albedo's computed for the atmospheric structure of an object of the same

mass and age in isolation. Instead, a self-consistent computation is required (Burrows et al. 2004, see e.g.) Arguments made insofar are based on models; they may be tested against observations. The most important test for the models described above is represented by the observed reflection spectra of giant planets in the Solar System (Karkoschka & Tomasko 1998). The good fit of the Jupiter spectrum thus supports the use of Sudarsky et al. models, in spite of their preliminary nature. Additional benchmark for the test/calibration of models of sub-stellar objects is represented by brown dwarfs (BDs) and transiting hot Jupiters. BDs have been discovered in large numbers during past years. The few cases for which dynamical masses and system ages are available are very useful targets for the calibration of the models. Recent observations of the AB Dor C low-mass object (Close et al. 2005; Luhman & Potter 2006; Janson et al. 2007, $\sim 100 Myr$, 90 $M_{Jup}$) are in agreement with the models of Baraffe et al. (2003).

Of particular interest is the study of cool ($T_{Eff} < 1300K$¡1300 K) T dwarfs, whose spectra are dominated by methane absorption. Figure 2.3 shows the spectra of GL 570D, one of the coolest BDs known ($T_{eff} \sim 800K$ Geballe et al. 2001), and of Saturn. This plot shows how the near infrared spectra of cool sub-stellar objects are typically characterized by three 'peaks' (actually the spectral ranges outside the methane and water absorption bands) whose shape and relative intensity depend on the properties of the sub-stellar object (mass, age, etc) and on the amount of stellar irradiation. Very young EFP are expected to have temperatures comparable to the T dwarfs discovered recently in significant numbers (see e.g. Testi et al. 2001). In spite of the gravity differences, their spectra are expected to be qualitatively similar to those of cool BDs as GL 570D.

## 2.4 CHEMICAL SPECIES

Water ($H_2O$) is made from the two most abundant chemically reactive elements in the universe, and it is the necessary ingredient for the type of life found on Earth. The importance of water as a condensable and chemically active specie in protoplanetary disks has long been emphasized in planetary literature. The time-varying location at which water is saturated in a formal thermodynamic sense (*the snow line*) can be considered the dividing line between the inner and outer Solar System (Lunine et al. 2000). For planets at orbital distances $\leq 1AU$, $H_2O$ is expected to be one of the

most abundant atmospheric components. Indeed, water vapour was detected to be present in more than one Exoplanet atmosphere Tinetti et al. (2007); Burrows et al. (2007); Swain et al. (2008). Liquid water has played an intimate, if not fully understood, role in the origin and development of life on Earth.

Water contributes to the dynamic properties of a terrestrial planet, permitting convection within the planetary crust that might be essential to support Earth-like life by creating local chemical disequilibrium that provide energy. Water absorbs electromagnetic-magnetic radiation over a broad wavelength range, covering part of the visible and most of the near-IR, and has a very distinctive spectral signature.

The greatest anomaly in the composition of the planets in our solar system is the large amount of oxygen ($O_2$) in the terrestrial atmosphere. This molecule is so reactive chemically that it must be continuously produced at enormous rates to persist. Thus the Earthâs atmosphere can only be the result of a large input from the biosphere (Lovelock & Watson 1982). The challenge of remotely detecting life on a planet that has not developed a biogenic source of oxygen is fraught with unknowns. $O_2$ shows a spectral signature only in the VIS-NIR wavelength range.

The major carbon-bearing gases in a solar composition gas of any given metallicity are generally methane, carbon monoxide, and/or carbon dioxide, depending on temperature and total pressure Lodders & Fegley (2002). Hot and less dense atmospheres are more likely to show abundant CO (and carbon dioxide $CO_2$ at lower temperature), while in cooler and denser objects methane is the abundant gas. In addition to water, the search for carbon-dioxide for terrestrial planets is of special interest. Its presence would indicate

1. that carbon is available for the biosphere

2. a (natural) greenhouse effect

3. a possible regulation by the hydro- and geosphere.

The major features of nitrogen chemistry are similar to those of carbon. The distribution of nitrogen between the major gases $NH_3$ and $N_2$ is described by equilibrium chemistry, which depends on temperature and total pressure. At high pressures, ammonia gas dominates, and at low pressures, $N_2$ gas dominates, but the $NH_3$ to $N_2$ transition is favored by higher temperatures (Lodders & Fegley 2002).

Because the chemistry of sulphur and hence the abundance of its principal volatile molecular form, hydrogen sulphide ($H_2S$), is greatly affected by the oxygen abundance. $H_2S$ is the dominant sulphur species throughout most of the nebula when the oxygen abundance is solar (Pasek et al. 2005). $SO_2$ appears to be present and sometimes quite abundant in the atmospheres of terrestrial planets where volcanic activity occurs (Venus, Io, Earth, and Mars).

## 2.5 OBSERVABLE PARAMETERS

Given the properties of planets listed above, one can derive several observable quantities that can lead both to the detection and the characterization of planets. Those properties can be roughly divided into two categories:

- Dynamical signatures, which signal the presence of a companion by the orbital motion of the host stars among the barycenter of the star-planet system (variation in radial velocities, astrometric signature)

- Information coming from the direct measurement of the light of the stat-planet system (transits) or of the planet itself (direct imaging)

Figure 2.5 summarizes the detection methods considered to date, also giving an indication of the lower mass limits which foresee in the near future.

### 2.5.1 *Dynamical signatures*

The motion of a single planet in a circular orbit around a star causes the star to undergo a reflex circular motion about the star-planet barycentre, with orbital semi-major axis $a_* = a \cdot (M_p / M_*)$ and period $P$. This results in the periodic perturbation of three observables, all of which have been detected (albeit in different systems): in radial velocity, in angular (or astrometric) position, and in time of arrival of some periodic reference signal.

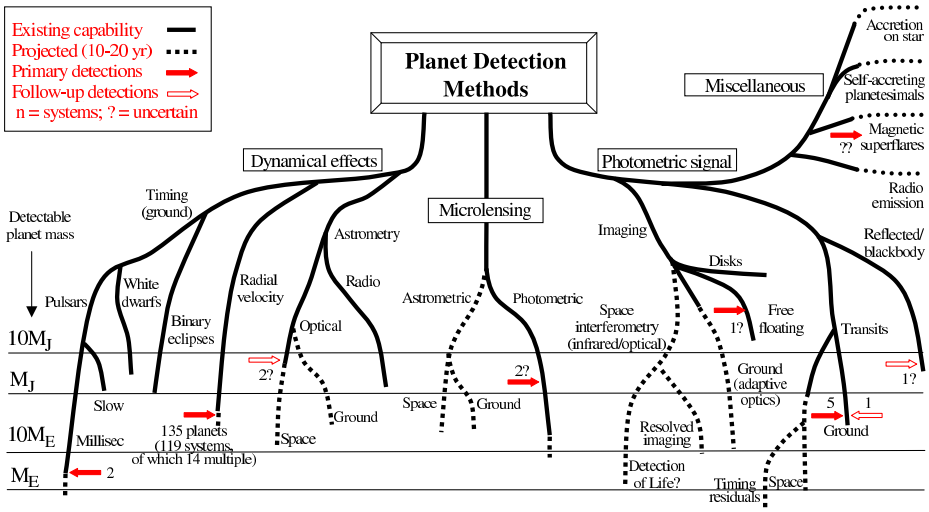


Figure 2.5: Detection methods for extra-solar planets, adapted from Perryman et al. (2005). The lower extent of the lines indicates, roughly, the detectable masses that are in principle within reach of present measurements (solid lines), and those that might be expected within the next 10 years (dashed). The (logarithmic) mass scale is shown at left. The miscellaneous signatures to the upper right are less well quantified in mass terms. Solid arrows indicate (original) detections according to approximate mass, while open arrows indicate further measurements of previously-detected systems. '?' indicates uncertain or unconfirmed detections. The figure takes no account of the numbers of planets that may be detectable by each method.

#### 2.5.1.1 *Radial velocity signal*

The velocity amplitude $K$ of a star of mass $M_*$ due to a companion with mass $M_p \sin i$ with orbital period $P$ and eccentricity $e$ is (e.g. Cumming et al. (1999)):

$$K = \left(\frac{2\pi G}{P}\right)^{1/3} \frac{M_p \sin i}{(M_p + M_*)^{2/3}} \frac{1}{(1-e^2)^{1/2}} \tag{2.2}$$

In a circular orbit the velocity variations are sinusoidal, and for $M_p \ll M_*$ the amplitude reduces to:

$$K = 28.4 \left(\frac{P}{1 \text{ year}}\right)^{-1/3} \left(\frac{M_p \sin i}{M}\right) \left(\frac{M_*}{M_\odot}\right)^{-2/3} \text{ m s}^{-1} \tag{2.3}$$

where $P$ and $a$ are related by Kepler's Third Law:

$$P = \left(\frac{a}{1 \text{ AU}}\right)^{3/2} \left(\frac{M_*}{M_\odot}\right)^{-1/2} \text{ year} \tag{2.4}$$

The semi amplitude of this radial velocity curve is about $K = 12.5$ m s$^{-1}$ with a period of 11.9 yr in the case of Jupiter orbiting the Sun, and about 0.1 m s$^{-1}$ for the Earth. The $\sin i$ dependence means that orbital systems seen face on ($i = 0$ if seen by an observer on the ecliptic) result in no measurable radial velocity perturbation and that, conversely, radial velocity measurements can determine only $M_p \sin i$ rather than $M_p$, and hence provide only a lower limit to the planet mass since the orbital inclination is generally unknown. Although the radial velocity amplitude is independent of the distance to the star, signal-to-noise considerations limit observations to the brighter stars (typically $V < 8$ mag, $10 - 12$ for lower accuracy data). Equation 2.2 indicates that radial velocity measurements favour the detection of systems with massive planets, and with small $a$ (and hence small $P$).

#### 2.5.1.2 *Astrometric signal*

The principle of planet detection with astrometry is similar to that underlying the Doppler technique: the presence of a planet is inferred from the motion of its parent star around the common centre of gravity. In the case of astrometry the two components of this motion are observed in the plane of the sky; this gives sufficient information to solve for the orbital elements without the $\sin i$ ambiguity. The path of a star orbiting the star-planet barycentre appears projected on the plane of the sky as an ellipse with angular semi-major axis $\alpha$ given by:

$$\alpha = \frac{M_p}{M_*} \cdot \frac{a}{d} \tag{2.5}$$

where $\alpha$ is in arcsec when $a$ is in AU and $d$ is in pc (and $M_p$ and $M_*$ are in common units). This 'astrometric signature' is therefore proportional

to both the planet mass and the orbital radius, and inversely proportional to the distance to the star.

Astrometry also has the advantage of being applicable to all types of stars. It is more sensitive to planets with larger orbital semi-major axes and hence complements radial velocity measurements. However, planets with large orbits have very large periods, this limiting the usefulness of this technique to separation of few AU.

For multi-planet systems astrometric measurements can determine their relative orbital inclinations (i.e., whether the planets are co-planar), an important ingredient for formation theories and dynamical stability analyses.

#### 2.5.1.3 *Pulsar timing*

Although all orbital systems are affected by changes in light travel time across the orbit, in general there is no timing reference on which to base such measurements. A notable exception are radio pulsars[1], rapidly spinning highly-magnetised neutron stars, formed during the core collapse of massive stars (8–20 $M_\odot$) in a supernova explosion. Pulsars emit narrow beams of radio emission parallel to their magnetic dipole axis, seen as intense pulses at the object's spin frequency due to a misalignment of the magnetic and spin axes. There are two broad classes: 'normal' pulsars, with spin periods around 1 s, and of which several hundred are known; and the millisecond pulsars, 'recycled' old ($\sim 10^9$ yr) neutron stars that have been spun-up to very short spin periods during mass and angular momentum transfer from a binary companion, with most of the 30 known objects still having (non-accreting) binary companions, either white dwarfs or neutron stars. The latter are extremely accurate frequency standards, with periods changing only through a tiny spin-down at a rate $\sim 10^{-19}\,\mathrm{s\,s^{-1}}$ presumed due to their low magnetic field strength (Bailes 1996).

For a circular, edge-on orbit, and a canonical pulsar mass of 1.35 $M_\odot$, the amplitude of timing residuals due to planetary motion is (Wolszczan (1997)):

$$\tau_p = 1.2 \left(\frac{M_p}{M_\oplus}\right) \left(\frac{P}{1\ \mathrm{yr}}\right)^{2/3} \ \mathrm{ms} \tag{2.6}$$

[1] pulsating white dwarfs can also be considered (see Mullally 2009)

The extremely high accuracy of pulsar timing allows the detection of lower mass bodies orbiting the pulsar to be inferred from changes in pulse arrival times due to orbital motion.

It's not surprising, then that the first planetary system discovered around an object other than our Sun was found around the 6.2-ms pulsar PSR 1257+12 ($d \sim 500$ pc), with at least two plausible terrestrial-mass companions (Wolszczan & Frail (1992)) having masses of 2.8 and 3.4 $M_\oplus$, and almost circular orbits with $a = 0.47$ and 0.36 AU, and $P = 98.22$ and 66.54 days respectively, close to a 3:2 orbital resonance.

### 2.5.2 *Direct measures*

#### 2.5.2.1 *Transit depth and probability*

The transit method aims at detecting the dimming of the stellar light by occultation due to an orbiting planet.

Transit experiments offer a relatively easy way to investigate the planet atmosphere, doing spectroscopy during the planet transit. Massive planets with short orbits (*Hot Jupiters*) can be observed from the ground, while planets down to Earth-mass or below can be detected from space.

The probability of viewing a planet to transit over the stellar disk at the right angle, depends on the distance of the planet to the central star. For close-in orbits it is about 10%, decreasing for more distant planets (See eq. 2.7). The transit amplitude depends primarily on the relative angle of the planets and stellar disk.

$$\frac{\Delta L}{L_*} \simeq \left(\frac{R_p}{R_*}\right)^2 \tag{2.7}$$

If the radius of the star can be estimated from, say, spectral classification, then $R_p$ can be estimated from equation 2.7. With knowledge of $P$ and an estimate of $M_*$ (also from spectral classification or via evolutionary models), the semi major axis of the orbit, $a$, can be derived from Kepler's law. Usually transiting planet orbit have very low eccentricities. With the approximation of circular orbit, other observational parameters are given, to first order, by simple geometry (Deeg (1998)). Thus the duration of the transit is:

$$\tau = \frac{P}{\pi}\left(\frac{R_* \cos\delta + R_p}{a}\right) \simeq 13 \left(\frac{M_*}{M_\odot}\right)^{-1/2} \left(\frac{1}{1\text{ AU}}\right)^{1/2} \left(\frac{R_*}{R_\odot}\right) \text{ hours} \tag{2.8}$$

where $\delta$ is the latitude of the transit on the stellar disk.

With the other parameters estimated as above, $\delta$ can be derived from equation 2.8, and hence the orbital inclination from $\cos i = (R_* \sin \delta)/a$. The minimum inclination where transits can occur is given by $i_{\min} = \cos^{-1}(R_*/a)$, with the probability of observing transits for a randomly oriented system of $p = R_*/a = \cos i_{\min}$. Evaluation of $i$ and $p$ for realistic cases demonstrates that $i$ must be very close to $90^\circ$, while $p$ is very small, implying that only a small fraction of planets can ever be detected or monitored using this technique.

#### 2.5.2.2 *Direct Imaging*

The main parameter determining detectability of planets from direct imaging are the apparent separation and the luminosity contrast between the star and the planet.

From the detection point of view, in the case of direct imaging, the planets can be roughly divided into two classes, depending on the dominant source of planet luminosity:

- **Warm planets**, for which the intrinsic (thermal) flux dominates
- **Cold planets** that shines mainly thanks to the reflected light from the parent star

The separation between these two classes cannot be rigorously defined, since it depends on several factors: wavelength, age of the system, mass of the planet, albedo, orbital separation and luminosity of the parent star. Similarly there cannot be a rigorous distinction between intrinsic and reflected light, since stellar irradiation alters the atmospheric structure and models must consider the two contributions self-consistently.

Planets at young ages are mostly self luminous, their luminosity depending on age, mass and atmosphere composition. Therefore planet/star contrast does not depend on the planet distance to the star. These planets are cool, and then much more luminous in the near infrared than in the visible domain, with peaks of emission around wavelengths 1.05, 1.25, 1.6 and 2.1 micron depending on their effective temperature (i.e. mass/age). After a bright and short accretion phase, contraction and differentiation are the remaining energy sources of the planet. Initially, the planet is still quite warm ($T \sim 1500K$) and bright (about 100 times brighter than Jupiter).

At old ages, the intrinsic flux of planets becomes small (for stars older than the sun, it remains dominant only for super-Jupiters/brown dwarfs companions) and thus their contrast strongly depends on the distance, and on reflective properties of the atmosphere: albedo and polarization level. The radius is weakly dependent on mass for old objects in the sub-stellar regime. Therefore, similar brightness values are expected for planets of different masses. The spectra should also look similar because temperature and the location and physical characteristics of clouds in the upper atmosphere (which deeply affect the emergent spectrum) are also not strongly mass dependent. Therefore, for these objects determination of mass requires detection of the reflex motion of the star. The reflected light is smaller in the near infrared (because the star flux and planetary albedo drop) and thus the optimal wavelength domain for such systems is the I-J band.

#### 2.5.2.3 *Planet Polarization*

Integrated over the stellar disc, the direct light of a solar type star is essentially unpolarized. However, scattering by molecules and other constituents in planetary atmospheres introduces polarization that can be detected when the planet is seen at suitable angles. Space-based observations of Jupiter performed by the Photopolarimeter/Radiometer (PPR) instrument on-board the Galileo Orbiter show degrees of polarization up to 50° latitudes (Braak et al. 2002). Polarization is expected to be large for planets dominated by reflected light (old planets). The intrinsic emission of young planets and brown dwarfs is expected to show little if any polarization (Ménard et al. 2002).

Multiple scattering and scattering by other particles (clouds) within the extrasolar planet atmospheres will decrease the observed degree of polarization. Because of this effect, polarization measurements provide diagnostics about atmosphere structure and composition. For giant planet models, there is a large difference (a factor of two) in the degree of polarization between the 'clear' and 'cloudy' model atmospheres described. Furthermore, the degree of polarization is expected to be wavelength dependent, being maximal within the methane band spectral regions, and larger in I than in the J-band: this is confirmed by observation of solar system planets. Therefore, planet detection probability is enhanced by a suitable choice of the band passes used, and appropriate filters can be used to study the heights of atmospheric clouds. Because the degree of

polarization of a planet is measured relative to the local background light (from the central star), it can in principle be obtained with very high accuracy without the need for an absolute instrument calibration.

In addition to detection, the degree of polarization of starlight reflected by an EGP can also be used for characterizing the planetary atmospheres. For example, observations of Solar System planetary atmospheres have shown that the degree of polarization of the reflected sunlight is very sensitive to the atmospheric composition and vertical structure (for an overview see Sinton 1974; Mishchenko et al. 1997a,b).

# BIBLIOGRAPHY


Absil, O. & Mawet, D. 2009, A&Ar, 16

Akeson, R. L., Koerner, D. W., & Jensen, E. L. N. 1998, in Bulletin of the American Astronomical Society, Vol. 30, Bulletin of the American Astronomical Society, 1362–+

Alibert, Y., Baraffe, I., Benz, W., et al. 2006, A&A, 455, L25

Alibert, Y., Mordasini, C., & Benz, W. 2004, A&A, 417, L25

Alibert, Y., Mordasini, C., Benz, W., & Winisdoerffer, C. 2005, A&A, 434, 343

Allard, F., Hauschildt, P. H., & Schweitzer, A. 2000, ApJ, 539, 366

Artymowicz, P. & Lubow, S. H. 1994, ApJ, 421, 651

Bailes, M. 1996, in Astronomical Society of the Pacific Conference Series, Vol. 105, IAU Colloq. 160: Pulsars: Problems and Progress, ed. S. Johnston, M. A. Walker, & M. Bailes, 3–+

Baraffe, I., Chabrier, G., Allard, F., & Hauschildt, P. H. 2002, A&A, 382, 563

Baraffe, I., Chabrier, G., Barman, T. S., Allard, F., & Hauschildt, P. H. 2003, A&A, 402, 701

Barbieri, M., Marzari, F., & Scholl, H. 2002, A&A, 396, 219

Barman, T. S., Hauschildt, P. H., & Allard, F. 2001, ApJ, 556, 885

Barman, T. S., Hauschildt, P. H., & Allard, F. 2005, ApJ, 632, 1132

Beaulieu, J., Bennett, D. P., Fouqué, P., et al. 2006, Nature, 439, 437

Benz, W., Mordasini, C., Alibert, Y., & Naef, D. 2006, in Tenth Anniversary of 51 Peg-b: Status of and prospects for hot Jupiter studies, ed. L. Arnold, F. Bouchy, & C. Moutou, 24–34

Beuzit, J., Feldt, M., Dohlen, K., et al. 2008, in Society of Photo-Optical Instrumentation Engineers (SPIE) Conference Series, Vol. 7014, Society of Photo-Optical Instrumentation Engineers (SPIE) Conference Series

Bodenheimer, P. 1976, Icarus, 29, 165

Bodenheimer, P. & Pollack, J. B. 1986, Icarus, 67, 391

Bonavita, M. & Desidera, S. 2007, A&A, 468, 721

Boss, A. P. 1997, Science, 276, 1836

Boss, A. P. 2000, ApJl, 536, L101

Boss, A. P. 2006a, ApJl, 637, L137

Boss, A. P. 2006b, ApJ, 643, 501

Braak, C. J., de Haan, J. F., Hovenier, J. W., & Travis, L. D. 2002, Icarus, 157, 401

Burrows, A., Hubbard, W. B., Lunine, J. I., & Liebert, J. 2001, Reviews of Modern Physics, 73, 719

Burrows, A., Hubeny, I., Budaj, J., & Hubbard, W. B. 2007, ApJ, 661, 502

Burrows, A., Hubeny, I., Hubbard, W. B., Sudarsky, D., & Fortney, J. J. 2004, ApJl, 610, L53

Burrows, A., Marley, M., Hubbard, W. B., et al. 1997, ApJ, 491, 856

Burrows, A., Sudarsky, D., & Hubbard, W. B. 2003, ApJ, 594, 545

Chabrier, G. & Baraffe, I. 2000, , 38, 337

Chabrier, G., Baraffe, I., Selsis, F., et al. 2007, Protostars and Planets V, 623

Chabrier, G., Barman, T., Baraffe, I., Allard, F., & Hauschildt, P. H. 2004, ApJl, 603, L53

Chandrasekhar, S. 1939, An introduction to the study of stellar structure

Charbonneau, D., Brown, T. M., Latham, D. W., & Mayor, M. 2000, ApJl, 529, L45

Chauvin, G., Lagrange, A., Dumas, C., et al. 2005, A&A, 438, L25

Close, L. M., Lenzen, R., Guirado, J. C., et al. 2005, Nature, 433, 286

Cumming, A., Butler, R. P., Marcy, G. W., et al. 2008, PASP, 120, 531

Cumming, A., Marcy, G. W., & Butler, R. P. 1999, ApJ, 526, 890

Deeg, H. 1998, in Astronomical Society of the Pacific Conference Series, Vol. 134, Brown Dwarfs and Extrasolar Planets, ed. R. Rebolo, E. L. Martin, & M. R. Zapatero Osorio, 216–+

Diakov, B. B. & Reznikov, B. I. 1980, Moon and Planets, 23, 429

Drobyshevski, E. M. 1978, Moon and Planets, 18, 145

Dvorak, R. 1982, Sitzungsber., Österr. Akad. Wiss., Math.-Naturwiss. Kl. Abt. II, 191. Band, 10. Heft, p. 423 - 437, 191, 423

Dvorak, R. 1984, Celestial Mechanics, 34, 369

Dvorak, R. 1986, A&A, 167, 379

Dvorak, R., Froeschle, C., & Froeschle, C. 1989, A&A, 226, 335

Fischer, D. A. & Valenti, J. 2005, ApJ, 622, 1102

Fortney, J. J., Baraffe, I., & Militzer, B. 2009, ArXiv e-prints

Fortney, J. J. & Marley, M. S. 2007, ApJl, 666, L45

Fortney, J. J., Saumon, D., Marley, M. S., Lodders, K., & Freedman, R. S. 2006, ApJ, 642, 495

Geballe, T. R., Knapp, G. R., Leggett, S. K., Fan, X., & Golimowski, D. A. 2001, ArXiv Astrophysics e-prints

Graboske, Jr., H. C., Olness, R. J., Pollack, J. B., & Grossman, A. S. 1975, ApJ, 199, 265

Guillot, T., Burrows, A., Hubbard, W. B., Lunine, J. I., & Saumon, D. 1996, ApJl, 459, L35+

Haisch, Jr., K. E., Lada, E. A., & Lada, C. J. 2001, ApJL, 553, L153

Harrington, R. S. 1977, , 82, 753

Hayashi, C. 1981, Progress of Theoretical Physics Supplement, 70, 35

Henry, G. W., Marcy, G. W., Butler, R. P., & Vogt, S. S. 2000, ApJl, 529, L41

Heppenheimer, T. A. 1974, Icarus, 22, 436

Heppenheimer, T. A. 1978, A&A, 65, 421

Holman, M. J. & Wiegert, P. A. 1999, , 117, 621

Hubbard, W. B., Fortney, J. J., Lunine, J. I., et al. 2001, ApJ, 560, 413

Hubickyj, O., Bodenheimer, P., & Lissauer, J. J. 2005, Icarus, 179, 415

Ida, S. & Lin, D. N. C. 2004, ApJ, 616, 567

Ida, S. & Lin, D. N. C. 2005, ApJ, 626, 1045

Janson, M., Brandner, W., Lenzen, R., et al. 2007, A&A, 462, 615

Johansen, A., Oishi, J. S., Low, M., et al. 2007, Nature, 448, 1022

Johnson, J. A., Butler, R. P., Marcy, G. W., et al. 2007, ApJ, 670, 833

Kalas, P., Graham, J. R., Chiang, E., et al. 2008, Science, 322, 1345

Karkoschka, E. & Tomasko, M. G. 1998, in Bulletin of the American Astronomical Society, Vol. 30, Bulletin of the American Astronomical Society, 1097–+

Kasper, M., Apai, D., Janson, M., & Brandner, W. 2007, A&A, 472, 321

Kennedy, G. M. & Kenyon, S. J. 2008, ApJ, 673, 502

Kortenkamp, S. J., Wetherill, G. W., & Inaba, S. 2001, Science, 293, 1127

Lafrenière, D., Doyon, R., Marois, C., et al. 2007, ApJ, 670, 1367

Lagrange, A. ., Gratadour, D., Chauvin, G., et al. 2008, ArXiv e-prints

Lagrange, A., Gratadour, D., Chauvin, G., et al. 2009, A&A, 493, L21

Lin, D. N. C., Bodenheimer, P., & Richardson, D. C. 1996, Nature, 380, 606

Lineweaver, C. H. & Grether, D. 2003, ApJ, 598, 1350

Lissauer, J. J., Quintana, E. V., Chambers, J. E., Duncan, M. J., & Adams, F. C. 2004, in Revista Mexicana de Astronomia y Astrofisica Conference Series, Vol. 22, Revista Mexicana de Astronomia y Astrofisica Conference Series, ed. G. Garcia-Segura, G. Tenorio-Tagle, J. Franco, & H. W. Yorke , 99–103

Lodders, K. & Fegley, B. 2002, Icarus, 155, 393

Lovelock, J. E. & Watson, A. J. 1982, , 30, 795

Lovis, C. & Mayor, M. 2007, A&A, 472, 657

Luhman, K. L. & Potter, D. 2006, ApJ, 638, 887

Lunine, J. I., Owen, T. C., & Brown, R. H. 2000, Protostars and Planets IV, 1055

Macintosh, B., Graham, J. R., Palmer, D., et al. 2007, in Bulletin of the American Astronomical Society, Vol. 38, Bulletin of the American Astronomical Society, 782–+

Marley, M. S., Fortney, J. J., Hubickyj, O., Bodenheimer, P., & Lissauer, J. J. 2007, ApJ, 655, 541

Marois, C., Macintosh, B., Barman, T., et al. 2008, Science, 322, 1348

Martin, R. G., Lubow, S. H., Pringle, J. E., & Wyatt, M. C. 2007, , 378, 1589

Marzari, F. & Scholl, H. 2000, ApJ, 543, 328

Marzari, F., Scholl, H., Tomasella, L., & Vanzani, V. 1997, , 45, 337

Marzari, F. & Weidenschilling, S. J. 2002, Icarus, 156, 570

Mathieu, R. D. 1994, , 32, 465

Mathieu, R. D., Ghez, A. M., Jensen, E. L. N., & Simon, M. 2000, Protostars and Planets IV, 703

Mayer, L., Wadsley, J., Quinn, T., & Stadel, J. 2005, , 363, 641

Mayor, M. & Queloz, D. 1995, Nature, 378, 355

Mayor, M., Udry, S., Lovis, C., et al. 2009, A&A, 493, 639

McArthur, B. E., Endl, M., Cochran, W. D., et al. 2004, ApJl, 614, L81

Ménard, F., Delfosse, X., & Monin, J. 2002, A&A, 396, L35

Mishchenko, M. I., Travis, L. D., Kahn, R. A., & West, R. A. 1997a, , 102, 13543

Mishchenko, M. I., Travis, L. D., Kahn, R. A., & West, R. A. 1997b, , 102, 16831

Mizuno, H., Nakazawa, K., & Hayashi, C. 1978, Progress of Theoretical Physics, 60, 699

Mohanty, S., Jayawardhana, R., & Basri, G. 2004, ApJ, 609, 885

Mordasini, C., Alibert, Y., & Benz, W. 2009a, A&A, 501, 1139

Mordasini, C., Alibert, Y., Benz, W., & Naef, D. 2008, in Astronomical Society of the Pacific Conference Series, Vol. 398, Astronomical Society of the Pacific Conference Series, ed. D. Fischer, F. A. Rasio, S. E. Thorsett, & A. Wolszczan, 235–+

Mordasini, C., Alibert, Y., Benz, W., & Naef, D. 2009b, A&A, 501, 1161

Mullally, F. 2009, Journal of Physics Conference Series, 172, 012056

Nakajima, T., Oppenheimer, B. R., Kulkarni, S. R., et al. 1995, Nature, 378, 463

Nelson, A. F. 2000, ApJl, 537, L65

Nielsen, E. L. & Close, L. M. 2009, ArXiv e-prints

Nielsen, E. L., Close, L. M., Biller, B. A., Masciadri, E., & Lenzen, R. 2008, ApJ, 674, 466

Papaloizou, J. C. B. & Terquem, C. 1999, ApJ, 521, 823

Pasek, M. A., Milsom, J. A., Ciesla, F. J., et al. 2005, Icarus, 175, 1

Perri, F. & Cameron, A. G. W. 1974, Icarus, 22, 416

Perryman, M., Hainaut, O., Dravins, D., et al. 2005, ArXiv Astrophysics e-prints

Pichardo, B., Sparke, L. S., & Aguilar, L. A. 2005, , 359, 521

Pollack, J. B., Hubickyj, O., Bodenheimer, P., et al. 1996, Icarus, 124, 62

Quintana, E. V., Adams, F. C., Lissauer, J. J., & Chambers, J. E. 2007, ApJ, 660, 807

Rabl, G. & Dvorak, R. 1988, A&A, 191, 385

Rodríguez, L. F., D'Alessio, P., Wilner, D. J., et al. 1998, Nature, 395, 355

Santos, N. C., Bouchy, F., Mayor, M., et al. 2004a, A&A, 426, L19

Santos, N. C., Israelian, G., & Mayor, M. 2004b, A&A, 415, 1153

Sato, B., Fischer, D. A., Henry, G. W., et al. 2005, ApJ, 633, 465

Saumon, D. & Guillot, T. 2004, ApJ, 609, 1170

Showman, A. P., Menou, K., & Cho, J. 2008, in Astronomical Society of the Pacific Conference Series, Vol. 398, Astronomical Society of the Pacific Conference Series, ed. D. Fischer, F. A. Rasio, S. E. Thorsett, & A. Wolszczan, 419–+

Sinton, W. M. 1974, Science, 186, 627

Sozzetti, A., Torres, G., Charbonneau, D., et al. 2009, ApJ, 691, 1145

Stevenson, D. J. 1982, Planss, 30, 755

Sudarsky, D., Burrows, A., & Hubeny, I. 2003, ApJ, 588, 1121

Swain, M. R., Vasisht, G., & Tinetti, G. 2008, Nature, 452, 329

Testi, L., Natta, A., Shepherd, D. S., & Wilner, D. J. 2001, ApJ, 554, 1087

Thébault, P., Marzari, F., & Scholl, H. 2006, Icarus, 183, 193

Thébault, P., Marzari, F., Scholl, H., Turrini, D., & Barbieri, M. 2004, A&A, 427, 1097

Tinetti, G., Vidal-Madjar, A., Liang, M., et al. 2007, Nature, 448, 169

Udry, S., Bonfils, X., Delfosse, X., et al. 2007, A&A, 469, L43

Udry, S. & Santos, N. C. 2007, , 45, 397

Veras, D. & Armitage, P. J. 2004, , 347, 613

Weidenschilling, S. J. 1977, , 51, 153

Wetherill, G. W. & Stewart, G. R. 1989, Icarus, 77, 330

Whitmire, D. P., Matese, J. J., Criswell, L., & Mikkola, S. 1998, Icarus, 132, 196

Wolszczan, A. 1997, in Astronomical Society of the Pacific Conference Series, Vol. 119, Planets Beyond the Solar System and the Next Generation of Space Missions, ed. D. Soderblom, 135–+

Wolszczan, A. & Frail, D. A. 1992, Nature, 355, 145

Zapolsky, H. S. & Salpeter, E. E. 1969, ApJ, 158, 809

# Part II

# PLANETS IN MULTIPLE STELLAR SYSTEMS

# 3

# FREQUENCY OF PLANETS IN BINARY STELLAR SYSTEMS

*adapted from "The frequency of planets in multiple systems" (Bonavita & Desidera 2007 A&A...468..721B) and its update (Bonavita et al. 2009, to appear in Extrasolar Planets in Multi-Body Systems: Theory and Observations, ed. K. Gozdziewski, A. Niedzielski, and J. Schneider, EAS Publications Series)*

The determination of the frequency of planets in binaries is an important issue in the field of extrasolar planets studies, because of its relevance for an estimate of the global planet population of our Galaxy (more than half of solar type stars are in binary or multiple systems as reported in Duquennoy & Mayor 1991) and the clues it can give to our understanding of planet formation and evolution. The study of the properties of planets in binaries, and any difference to those of the planets orbiting single stars, would shed light on the effects caused by the presence of the companions.

A recent study by Desidera & Barbieri (2007) showed that the mass distribution of short period planets in relatively tight binaries (separation $\leq 150 - 200$ AU) is significantly different to that of planets orbiting the components of wide binaries and single stars. There are also other possible peculiar features of planets in tight binaries with respect to planets orbiting single stars, such as a lack of long-period planets and multiple planets, that need confirmation. The properties of exoplanets orbiting the components of wide binaries are instead compatible with those of planets orbiting single stars, except for a possible larger abundance of high-eccentricity planets.

The determination of the planet frequency in binaries is made difficult by the occurrence of biases against binaries in most of the on-going planet search surveys (topically binaries with $\rho < 2''$ and spectroscopic binaries are excluded) and by incompleteness of binary and planet detections in these samples.

A first step in this direction was made by Eggenberger et al. (2006), performing an adaptive-optics search for companions around stars with and without planets and without previously known stellar companions from the Coralie survey. This guarantees a fairly homogeneous binary detectability in their sample. However, the small number of objects (and the lack of confirmation of the physical association in a few cases) did not allow them up to now to make clear inferences on the planet frequency and in particular on possible differences as a function of the binary separations.

A much wider sample (850 stars vs the 110 stars studied by Eggenberger et al. (2006)) that might be used for a study of planet frequency is the 'Uniform Detectability' (hereafter UD) sample collected by Fischer & Valenti (2005) (hereafter FV05). This sample is complete for detection of planets with radial velocity (hereafter RV) semi–amplitude $> 30$ m/s and period $< 4$ yr. However, the binarity of stars in the UD sample does not have been considered up to now.

Despite some incompleteness and biases concerning binarity, this sample can be considered valid to draw an independent measure of the frequency of planets in binary stars, thanks to the completeness of planet detection and the large sample size. So, the binarity of the stars within the Uniform Detectability sample was investigated in this work by searching some stellar catalogs listing stellar companions (Sec. 3.2). The result is a sub-sample of UD binaries, separated according with their different values of periastron and critical semi-axis for dynamical stability of planetary orbits (see Holman & Wiegert 1999) (Sec. 3.2.2). In this way it has been possible to compare the values of the frequency of planets in the two sub-samples (single stars and binary stars), and to verify a possible dependence of the frequency from critical semi-axis and periastron (Sec. 6.4). As the comparison of the frequency is performed for stars in the UD sample, the occurrence of biases against binaries in the sample is not relevant for our purpose. The results were discussed in Sec. 3.4 and in Sec. 3.5 we summarize our conclusions and future perspectives.

## 3.1 THE UNIFORM DETECTABILITY SAMPLE

The Uniform Detectability sample has been built by considering that, despite the detectability of the planets changes from a star to the other and from a Survey to the other because of the different time span of the observations and different levels of RV errors, we can consider it complete for companions with velocity amplitudes K>30 m/s and orbital periods shorter than 4 years. Then, beginning from the initial target list, that included 1330 stars observed by Lick, Keck and Anglo Australian Surveys, FV05 selected a sub-sample of 850 stars that satisfy these entries and provided that at least 10 observation spanning four years. Stars that were added after a planet was discovered by other groups were not included in the sample. However, stars independently present in one of these surveys were considered even if a planet was detected first by another group.

Only planets with K> 30 m/s and orbital periods shorter than 4 years were considered for the study of planet frequency. This corresponds to Saturn-mass planets for the shortest periods and Jupiter-mass planets for 4 year orbits.

### 3.1.1 *Changes in th Uniform Detectability sample*

During the analysis made for our work, we made some changes to the original UD sample, such as:

- we excluded 51 Peg because it was added to the considered target lists after the planet detection by Mayor & Queloz (1995) (Marcy et al. (1997); Fischer 2005 private communication);

- $\tau$ Boo e $\upsilon$ And were marked as "without planets", but the known small companions fulfill all the selection criteria for the UD sample (Fischer 2005, private communication), so we included these stars as "with planets";

- HD 20782 hosts a planet revealed after the compilation of the UD sample (Jones et al. 2006), but it is coherent with the UD requirements, so that this star has been considered as "with planets". The lack of this planet in the original UD sample confirms the hypothesis that high eccentricity (e=0.93 in this case) acts to make detection more difficult, as suggested by Cumming (2004);

- HD 18445 is flagged as "with planets" in the UD sample, probably because of a typo (it is not listed in the tables of stars with planets). The RV companion ($M \sin i = 44 M_J$) has a mass outside the giant planet range and it was shown to be a 0.18 $M_\odot$ star orbiting nearly pole-on by both astrometry (Halbwachs et al. 2000) and direct imaging (Beuzit et al. 2004). So we considered it as "without planets" (see Appendix A.2 for details);

The modified UD sample that is the result of those changes was then searched for companions, in order to build a sample of UD binaries.

## 3.2 SEARCHING FOR BINARIES IN THE UNIFORM DETECTABILITY SAMPLE

In order to identify known or claimed companions for the stars included in the UD sample, we checked available sources listing stellar companions. Some of the most important sources are listed below:

- *The Hipparcos and Thyco Catalogues* (Perryman & ESA 1997);
- *The Catalogue of the Components of Double and Multiple Stars (CCDM)* (Dommanget & Nys 2002);
- *The Washington Visual Double Star Catalog (WDS)*(Worley & Douglass 1997);
- *Sixth Catalog of Orbits of Visual Binary Stars*(Hartkopf & Mason 2006);
- *The Catalogue of Nearby Stars, Preliminary 3rd Version (C3)* (Gliese & Jahreiß 1991);
- Gould & Chanamé (2004): *New HIPPARCOS-based parallaxes for 424 faint stars*;
- Nidever et al. (2002): *Radial Velocities for 889 late-type stars*;
- Allen et al. (2000): *Wide binaries among high-velocity and metal-poor stars*;
- Makarov & Kaplan (2005): *Proper motion derivatives of binaries*;
- Tokovinin (1997): *MSC - a catalogue of physical multiple stars*[1]
- Latham et al. (2002) *Orbits of 171 single-lined spectroscopic binaries*;
- Halbwachs (1986) *Common proper motions stars in AGK3*;
- *The revised NLTT catalogue* (Salim & Gould 2003);
- Valenti & Fischer (2005) *Spectroscopic properties of cool stars. I.*;
- *The Tycho Double Star Catalogue (TDSC)* (Fabricius et al. 2002);

[1]Updated version available at www.ctio.noao.edu/ atokovin/stars/

- *A Catalog of Northern Stars with Annual Proper Motions Larger than 0.15" (LSPM-NORTH Catalog)*" (Lépine & Bongiorno 2006)

- *SB9: The ninth catalogue of spectroscopic binary orbits* (Pourbaix et al. 2004)

- *The 2MASS All Sky Catalog of point sources* (Cutri et al. 2003) has been used only for deriving JHK photometry (used for mass determination) and for common proper motion confirmation, not for a search for further companions.

We also consider additional references for individual objects (see Table A.1 and Appendix A.2).

### 3.2.1 *Selection criteria*

After this search, we excluded from our UD binary sample, and considered those stars as singles, the stars with non confirmed companions and with companions listed in CCDM but with inconsistent proper motions (and without other indication of binarity found in literature). Stars with long term RV and/or astrometric trends were included in the binary sample, on the basis of the dynamical evidence for the presence of a companion. The RV trends we included (from Nidever et al. 2002) that cause an overall RMS of RV larger than 100 m/s cannot be due to planetary companions. We included in the sample of binaries also stars with brown dwarf companions. At small separation, the existence of the brown dwarf desert (see Butler et al. 2006) guarantees little ambiguity in the classification of an object as a massive planet or a brown dwarf (a couple of individual cases are listed in Appendix A.2). At large separations, where brown dwarfs companions are probably more frequent (Gizis et al. 2001) this ambiguity should be taken into account but is again limited to few individual cases e.g. HD 206860, that has a T dwarf companion of mass $0.021 \pm 0.09\ M_{\odot}$ according to Luhman et al. (2006), smaller than the mass limit for planetary companions adopted by Butler et al. (2006). The small number of brown dwarfs companions makes anyway this issue not relevant for the global results.

### 3.2.2 *The sub-sample of UD binaries*

The properties of the UD binaries, selected from the modified UD sample, are listed in Table 5. The stars with both components included in the UD sample are listed twice, otherwise only the star under planet scrutiny is listed. If more than one companion is known, we report only the closest one, because of its stronger influence on planetary formation/stability. For hierarchical triple (or higher order multiplicity) systems, for which the isolated star is included in the UD sample, we sum the mass of the closest pair to consider its effective dynamical influence. For single-lined spectroscopic binaries the minimum mass is listed.

For each object we report:

- the HD number;
- the projected separation;
- the eccentricity, if available[2];
- the semi major axis in AU [3];
- the mass of the objects, from Valenti e Fischer (2005) (hereafter VF05)[4];
- the companion mass:
  a) from VF05 if both components are included in the UD sample;
  b) calculated with the mass-luminosity relation derived by Reid & Gizis (1997); Delfosse et al. (2000);
  c) from other literature sources (listed in the Table caption).
- the critical semi-major axis calculated using equation 1.2 reported in Sec. 1.4.

[2]Otherwise we assume e=0.36 (mean eccentricity for a binary system, from Duquennoy & Mayor (1991))

[3]if not available from literature, the reported value is estimated using a(AU)=1.31$\rho$(arcsec)d(pc) Fischer et al. (2002); Duquennoy & Mayor (1991)

[4]the exceptions are listed in Appendix A.2

The result of the search for stellar companions for the UD stars is a sub-sample of 210 objects; of those 17 have planets, so the global frequency of planets in the UD binary sample is 8.0%. If we consider the singles sub-sample, we found that 5.0% of UD singles have planets (see Table 3.3.1). The two frequencies are compatible within their errors[5], the slightly higher value of the global frequency in the binary sub-sample is probably due to some incompleteness in the sample, which is discussed in Sect. 3.3.1.

The rather large sample size allows us to make some binning with different values of critical semi-axis ($a_{crit}$). We choose $a_{crit}$ as a reference value because, as already pointed out in § 1.4, it is a physical quantity that better represents the dynamical effects due to a companion on planet formation and stability, including both the orbital parameters and mass ratio. All the stars with RV and/or astrometric trend were included in the closest bin, as it is likely that the companion responsible of the trend is at small separation. We also bin the UD binary sample according with the periastron because this allow us to make a direct comparison with theoretical expectations, such as those of Pfahl & Muterspaugh (2006).

The resulting values of the frequency are listed in Tables **??** and 3.3.1 together with the characteristics of each sample. In Table 3.3.1 we also showed the values of frequency for the complete UD binary sample and for the UD single sub-sample.

### 3.3.1 *Completeness and selection effects*

The completeness of binarity in this sample is probably a function of the separation. Very wide binaries ($\rho > 5$ - 10 arcsec) are more easily discovered and then included in CCDM and WDS. Intermediate values of separation are probably the most incomplete ones, as the detection of low mass companion requires dedicated high-resolution imaging, not available for all the stars, and the companions are not expected to produce detectable RV or astrometric signatures. At small separations, the inclusion of stars with RV and astrometric trend in the sample probably allows

[5]The errors reported in Tables 1 and 2 are calculated trough the equation: $\sigma_f = \left(N_{planets}^{-1/2} + N_{star}^{-1/2}\right) * \left(\frac{N_{star}}{N_{planets}}\right)$ They do not include the additional error due to incompleteness of binary detection.

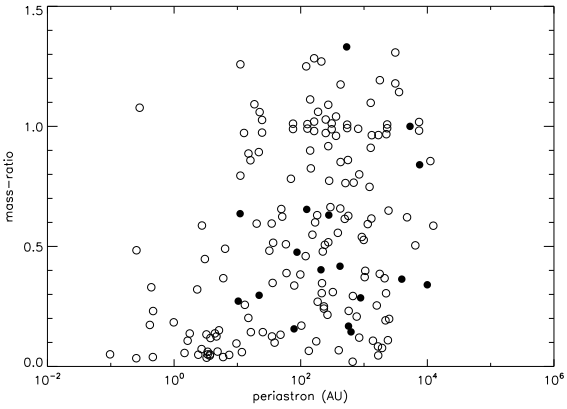


Figure 3.1: Periastron vs mass-ratio for the binaries with planets (filled circles) and without planets (open circles) in the UD sample.

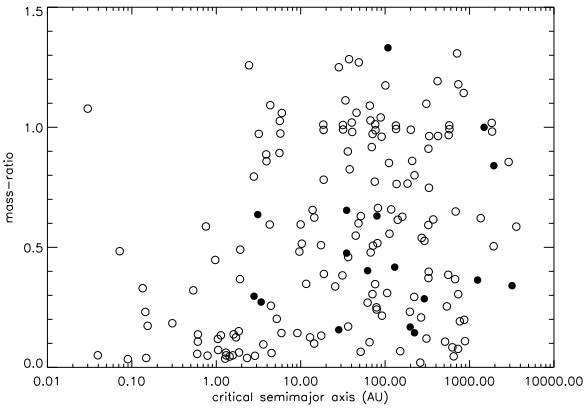


Figure 3.2: Critical semi-axis (from Holman & Wiegert (1999)) vs mass-ratio for the binaries with planets (filled circles) and without planets (open circles) in the UD sample.

| Periastron | $N_{star}$ | $N_{planets}$ | $\frac{N_{star}}{N_{planets}}$ |
|---|---|---|---|
| 50 AU | 91 | 3 | 0.033±0.022 |
| 50 - 200 AU | 29 | 3 | 0.103±0.079 |
| 200 - 500 AU | 29 | 3 | 0.103±0.079 |
| 500 - 1000 AU | 22 | 4 | 0.181±0.130 |
| $>$ 1000 AU | 39 | 4 | 0.102±0.068 |

Table 3.1: Frequency of planets in binaries with different values of periastron.

a fairly high completeness level. In fact, most of the binaries recently discovered by mean of deep adaptive optics imaging (e.g. HD 13445; HD 161797, HD 190406, HD 196885) would have been included as binaries in this study thanks to their dynamical signatures, even without the direct imaging identification.

Another important selection effect is that the completeness of the binarity of planet hosts is certainly larger than that of stars without planets, because these stars are systematically searched for companions after planet discoveries. This likely explains the slightly larger planet frequency of planets in binaries.

Finally, the UD sample has a selection bias against the binarity, because the input target lists exclude spectroscopic binaries and binaries with separation less than 2" (see Jones et al. 2002; Marcy et al. 2005; Wright et al. 2004). This last limit means that, for distances of e.g. 10, 50, and 100 pc, binaries with separation between 20, 100 and 200 AU respectively are excluded (if known at the time of the target selection). Therefore we expect that the distribution of the orbital parameters and mass ratio of the binaries in the UD sample are different with respect to unbiased samples (Duquennoy & Mayor 1991).

Finally, in spite of most of the biases in the UD sample are against the binarity, we can argue that there also could be some inclusions in the input target lists that favour the presence of certain types of systems. In fact a few binary systems were probably included in the sample after dedicated studies on chemical abundances differences between the components (Gratton et al. 2001; Martín et al. 2002), but this should have only a marginal role in the global binary statistics.

| $a_{crit}$ | $N_{star}$ | $N_{planets}$ | $\frac{N_{planets}}{N_{stars}}$ |
|---|---|---|---|
| $<$ 20 AU | 97 | 3 | 0.030±0.020 |
| 20 - 50 AU | 20 | 3 | 0.150±0.120 |
| 50 - 100 AU | 25 | 2 | 0.080±0.072 |
| 100 - 250 AU | 23 | 4 | 0.173±0.123 |
| $>$ 250 AU | 45 | 5 | 0.111±0.066 |
| UD Singles sub-sample | 639 | 32 | 0.050±0.011 |
| Entire UD binary sub-sample | 210 | 17 | 0.080±0.024 |

Table 3.2: Frequency of planets in binaries with different values of $a_{crit}$.

| Periastron | $N_{star}$ | $N_{planets}$ | $\frac{N_{star}}{N_{planets}}$ |
|---|---|---|---|
| $<$ 50 AU | 20 | 3 | 0.150±0.120 |
| $>$ 50 AU | 25 | 2 | 0.080±0.073 |

Table 3.3: Frequency of planets in binaries with different values of periastron for the volume limited sample.

### 3.3.2 *The volume limited sample*

In analogy with FV05 we define a volume-limited sample with a radius of 18 pc, that can be used as a control. In fact, within this radius the number of FGK stars per unit volume on the planet search programs is nearly constant as a function of distance while the number density of intrinsically faint stars starts to decline rapidly. The census of companions of stars in this sample is expected to be more complete from that of the global sample because at close distance the 2 arcsec limit correspond to a smaller physical separation (36 AU at 18 pc) and the closest stars were in general more carefully searched for stellar companions. The Volume Limited UD sample (hereafter VLUD) includes 129 stars, of these 45 are binaries. We find that 8.9% of the binaries in the VLUD sample have planets.

We select some bins in $a_{crit}$ and periastron also for the VLUD sample but, because of the small number of stars included in this sample, we consider only 2 ranges of values. Tables 3.3.2 and 3.3.2 show the frequency values obtained for the VLUD sub-samples.

| $a_{crit}$ | $N_{star}$ | $N_{planets}$ | $\frac{N_{star}}{N_{planets}}$ |
|---|---|---|---|
| $<$ 20 AU | 22 | 3 | 0.136±0.107 |
| $>$ 20 AU | 23 | 2 | 0.087±0.080 |
| VLUD Singles sub-sample | 84 | 8 | 0.095±0.044 |
| Entire VLUD binary sub-sample | 45 | 5 | 0.111±0.066 |

Table 3.4: Frequency of planets in binaries with different values of $a_{crit}$ for the volume-limited sample.

The similar frequency of planets in single stars and in binaries is probably due to the better completeness of binarity. It is also worth of mention that the frequency of planets in tight binaries is not lower than in wide binaries and probably this is also an effect of better completeness. This result seems to odds with that obtained with the full sample analysis, even if the small number of objects make statistical error bars quite large.

## 3.4 DISCUSSION

### 3.4.1 *Global estimate of frequency of planets in binary stars.*

Using a sample made of binaries with uniform planet detectability, we try to evidentiate possible differences between frequency of planets in binaries and planets orbiting single stars.

Looking at the whole binary sample we can conclude that the frequency of planets in binaries is not statistically different with respect to that of planets orbiting single stars. However, incompleteness in binary detection probably causes a spurious increase of planet frequency in binaries. Therefore we investigate the effect of binary incompleteness as follows.

We can derive an upper limit on this binarity incompleteness assuming that the stars in the UD sample have the same binary frequency of Duquennoy & Mayor (1991) (57%). The number of missing binaries in the sample would be then $\sim$ 285 [6] We stress that this is an upper limit because we know that the UD sample must have a lower binary fraction

[6]For the estimate of the number of lost binaries we exclude (and than consider them as single stars) the stars with brown dwarfs companions, because the sub stellar companions are not included in the statistical analysis by Duquennoy & Mayor (1991).

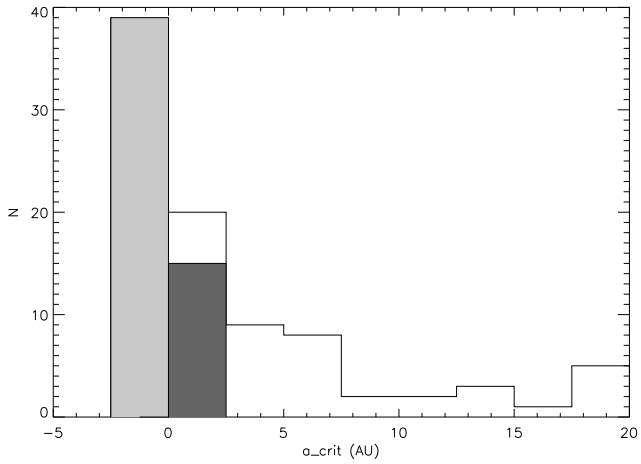


(a)

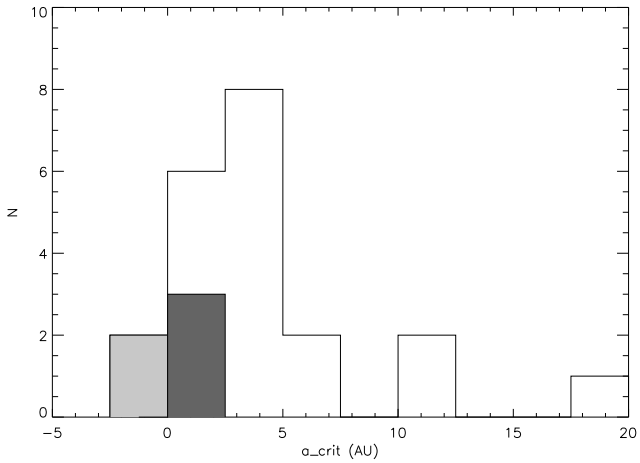


(b)

Figure 3.3: Distribution of $a_{crit} < 20$ AU for the complete UD binary sample (a) and for the VLUD sample (b). The first column contain the stars with long term RV or astrometric trends (for which $a_{crit} = 0.0$). In both panels is evidenced the contribute of spectroscopic binaries.

than Duquennoy & Mayor (1991), because of the exclusion of visual binaries with separation less than 2" and spectroscopic binaries known at the time of the sample selection. The median of distance of the stars in the UD sample is $\sim$ 33 pc. At this distance, the 2 arcsec limit corresponds to a projected semi-axis of $\sim$ 66 AU, larger than the peak of semi-major axis distribution of Duquennoy & Mayor (1991) ($\sim$ 35 AU). Therefore we expect that the 2 arcsec selection bias makes the frequency of binaries in the UD sample significantly lower than the value proposed by Duquennoy & Mayor (1991). With the further conservative assumption that all the "missing binaries" are without planets, we would then obtain $f_{bin}$ = 3.1% and $f_{sin}$ = 9.4%. We then conclude that the global frequency of planets in binaries is not lower by more than a factor of three compared to that of single stars. This result is quantitatively consistent with the preliminary results by Eggenberger et al. (2006), that found a frequency of planets in binaries that is within a factor of two with respect to that of planets orbiting single stars.

### 3.4.2 *Dependence on the binary separation*

The size of our sample allow us to divide it in some sub-groups according with the value of the critical semi-axis for the dynamical stability. In this way we can argue that there is no significant dependence of the frequency on $a_{crit}$ (and on the periastron) except for companion with $a_{crit}$ less than 20 AU (that corresponds to a separation $<$ 50-100 AU, depending on the mass-ratio of the components). This result is in good agreement with Desidera & Barbieri (2007) who concluded that the presence of distant companions (separation $>$ 300-500 AU) does not affect significantly the process of planet formation, as the mass and period distribution of planets in such wide binaries are similar to those of planets orbiting single stars. The addition of a similar planet frequency for wide binaries we have shown here makes this conclusion stronger.

On the other hand, the lower value of frequency found for tight binaries ($a_{crit} < 20$ AU) also supports the finding by Desidera & Barbieri (2007)[7] that the properties of planets in close binaries, in particular the mass distribution, are different to those orbiting single stars and components of wide binaries.

[7]Note that the definition of tight binaries used by Desidera & Barbieri (2007) ($a_{crit} <$ 75 AU) is different with respect that adopted here.

These results then suggest a relevant role of the presence of the companion on the formation and/or migration and/or dynamical evolution processes. The frequency of planets in close binaries can be used to further investigate how these planets formed and the origin of their anomalous properties.

Indeed, Pfahl & Muterspaugh (2006) showed that the knowledge of the value of the frequency of planets in close binaries[8] should allow to disentangle between two alternative formation scenario's. A low frequency (about 0.1% but with an uncertainty of about one order of magnitude, so we can consider 1% as a limit-value) would be compatible with dynamical interactions that cause the formation of the tight binary after planet formation. Our result for the frequency of planets in binaries with periastron less than 50 AU is $0.033 \pm 0.022$ that is marginally compatible only with the Pfahl & Muterspaugh (2006) upper limit. This result, if confirmed, would allow one to conclude that instead planets do form in tight binaries in spite of the seemingly unfavourable conditions and leave open the alternative hypothesis, i.e. giant planets formed in binaries with small separation at the time of planet formation, possibly in a different way with respect to planets around single stars (and around wider systems).

Finally, if we consider a volume limited sample, the results seems to be different for the lowest $a_{crit}$ bin. In fact, the frequency of planets in binaries with $a_{crit}$ less than 20 AU appear higher for the stars in the VLUD sample with respect to those in the complete UD sample. These differences might be explained looking at Figure 3.3. The panels show the distribution of $a_{crit}$ for the lowest bin in $a_{crit}$ for the complete UD sample (upper panel) and for the VLUD sample (lower panel). In both panels, the first column on the left contains the stars included as binaries only because the occurrence long term RV or astrometric trends (i.e. mass and separation of the companions not known). From those histograms we can easily see on one hand that the percentage of the stars without definite orbital characteristics (thus included only on the basis of dynamical signatures) is greater in the complete UD sample ($\sim$ 45 %) with respect to the VLUD sample (where is $\sim$ 10%). This confirms that the VLUD sample is less affected by incompleteness effects. At the same time, the distribution of the $a_{crit}$ values for the VLUD sample is centered on the second bin ($2.5 < a_{crit} < 5.0$ AU) while in the complete sample there are a few binaries (at least 20, excluding those with only RV or astrometric trends) for which

[8]Defined as those binaries with semi major axis less than 50 AU

$a_{crit}$ is smaller than $\sim$ 2.5 AU, the separation limit corresponding to $P$=4 yr for solar-type systems. Therefore a lower frequency of planet for such systems is expected in any case as only a part of the separation range considered here can host planets on stable orbits.

We also note that the closest bin ($a_{crit} < 20$ AU or periastron $< 50AU$) contain several stars for which a direct detection of the companion is missing and that are included only on the basis of the occurrence of astrometric acceleration detected by Hipparcos or evidenced as a difference between historical and Hipparcos proper motions (Makarov & Kaplan 2005). This makes the determination of the detail of the run of planet frequency at small separations not possible from available data.

Both the confirmation of the binarity of these stars (with a determination of the physical parameters of these companions) and the completion of on-going surveys focused on binaries (Desidera et al. 2006; Eggenberger et al. 2006; Konacki 2005) would be useful to explain in more details the run of frequency of planets at small separation.

## 3.5 CONCLUSIONS

After a detailed search for binarity of all stars in the 'Uniform Detectability' sample collected by Fischer & Valenti (2005), we make a comparison the frequency of planets in binaries and single stars. It results that the frequencies of planets in these two stellar population are not statistically different. Even taking into account in a very conservative way possible incompleteness in the binary detection, the frequency of planets in the binaries of the sample can not be more than a factor of three lower than that of planets orbiting single stars.

On the other hand, if we look at some sub-samples made according with the separation and effective gravitational influence of the binaries, we found that the frequency seems to be fairly independent from these features, at least for moderately wide binary separation. Considering also the similitude of the mass and period distribution of planets orbiting single stars and components of wide binaries, we then conclude that a wide companion plays a marginal role on the formation and evolution of giant planets.

For the planets in tight binaries, the results are more intriguing. On one hand, there are indication that the properties of planets in tight binaries are significantly different from those of exoplanets orbiting wide

binaries or single stars, as discussed in Desidera & Barbieri (2007). On the other hand, the frequency of planets in close binaries appears to be lower than single stars and components of wide binaries, but probably not as low as required to explain their presence only as the results of modifications of the binary orbit after the planet formation.

Therefore, it seems that planets do form in tight binaries in spite of the unfavourable (according to theoretical models) conditions, possibly in a different way with respect to planets around single stars (and around wider systems).

However, crucial issues still need clarification. In fact, it is still not clear if the run of the planet frequency when moving to smaller separations is characterized by a continuous decrease, by a sharp cut-off at which the differences on planet frequency characteristics suddenly onset, or by a bimodal distribution, with a minimum between $10 < a_{crit} < 30$ AU, a relative maximum at $a_{crit} \sim 3 - 5$ AU, a further decrease to zero at extremely small separations, as the zone for dynamical stability of planets vanishes.

These open points might be clarified by a detailed characterization of the binaries in current samples of RV surveys (completeness of binary detection and, when possible, full determination of the orbital elements) and by the completion of dedicated surveys searching for planets in binaries. The availability of a larger and more complete sample will allow us to better understand the behaviour of the planet frequency in binaries and, at the same time, to disentangle the questions about the formation of planets in these peculiar environments and especially about the formation mechanisms and the different characteristics of the planets in tight binaries.

# BIBLIOGRAPHY


Allen, C., Poveda, A., & Herrera, M. A. 2000, A&A, 356, 529

Beuzit, J.-L., Ségransan, D., Forveille, T., et al. 2004, A&A, 425, 997

Butler, R. P., Wright, J. T., Marcy, G. W., et al. 2006, ApJ, 646, 505

Cumming, A. 2004, MNRAS, 354, 1165

Cutri, R. M., Skrutskie, M. F., van Dyk, S., et al. 2003, 2MASS All Sky Catalog of point sources. (The IRSA 2MASS All-Sky Point Source Catalog, NASA/IPAC Infrared Science Archive. http://irsa.ipac.caltech.edu/applications/Gator/)

Delfosse, X., Forveille, T., Ségransan, D., et al. 2000, A&A, 364, 217

Desidera, S. & Barbieri, M. 2007, A&A, 462, 345

Desidera, S., Gratton, R., Claudi, R., et al. 2006, in Tenth Anniversary of 51 Peg-b: Status of and prospects for hot Jupiter studies, ed. L. Arnold, F. Bouchy, & C. Moutou, 119–126

Dommanget, J. & Nys, O. 2002, VizieR Online Data Catalog, 1274, 0

Duquennoy, A. & Mayor, M. 1991, A&A, 248, 485

Eggenberger, A., Udry, S., Mayor, M., et al. 2006, in Proc. of ESO Workshop Multiple Stars Across HR Diagram

Fabricius, C., Høg, E., Makarov, V. V., et al. 2002, A&A, 384, 180

Fischer, D. A., Marcy, G. W., Butler, R. P., et al. 2002, , 114, 529

Fischer, D. A. & Valenti, J. 2005, ApJ, 622, 1102

Gizis, J. E., Kirkpatrick, J. D., Burgasser, A., et al. 2001, ApJl, 551, L163

Gliese, W. & Jahreiß, H. 1991, Preliminary Version of the Third Catalogue of Nearby Stars, Tech. rep.

Gould, A. & Chanamé, J. 2004, ApJs, 150, 455

Gratton, R. G., Bonanno, G., Claudi, R. U., et al. 2001, A&A, 377, 123

Halbwachs, J. L. 1986, Bulletin d'Information du Centre de Donnees Stellaires, 30, 129

Halbwachs, J. L., Arenou, F., Mayor, M., Udry, S., & Queloz, D. 2000, A&A, 355, 581

Hartkopf, W. I. & Mason, B. D. 2006, Sixth Catalog of Orbits of Visual Binary Stars, http://ad.usno.navy.mil/wds/orb6.html

Holman, M. J. & Wiegert, P. A. 1999, , 117, 621

Jones, H. R. A., Butler, P., Marcy, G. W., et al. 2002, MNRAS, 337, 1170

Jones, H. R. A., Butler, R. P., Tinney, C. G., et al. 2006, MNRAS, 369, 249

Konacki, M. 2005, ApJ, 626, 431

Latham, D. W., Stefanik, R. P., Torres, G., et al. 2002, , 124, 1144

Lépine, S. & Bongiorno, B. 2006

Luhman, K. L., Patten, B. M., Marengo, M., et al. 2006

Makarov, V. V. & Kaplan, G. H. 2005, , 129, 2420

Marcy, G., Butler, R. P., Fischer, D., et al. 2005, Progress of Theoretical Physics Supplement, 158, 24

Marcy, G. W., Butler, R. P., Williams, E., et al. 1997, ApJ, 481, 926

Martín, E. L., Basri, G., Pavlenko, Y., & Lyubchik, Y. 2002, ApJ, 579, 437

Mayor, M. & Queloz, D. 1995, , 378, 355

Nidever, D. L., Marcy, G. W., Butler, R. P., Fischer, D. A., & Vogt, S. S. 2002, ApJs, 141, 503

Perryman, M. A. C. & ESA. 1997, The HIPPARCOS and TYCHO catalogues. Astrometric and photometric star catalogues derived from the ESA HIPPARCOS Space Astrometry Mission (The Hipparcos and Tycho catalogues. Astrometric and photometric star catalogues derived from the ESA Hipparcos Space Astrometry Mission, Publisher: Noordwijk, Netherlands: ESA Publications Division, 1997, Series: ESA SP Series vol no: 1200, ISBN: 9290923997 (set))

Pfahl, E. & Muterspaugh, M. 2006, ApJ, 652, 1694

Pourbaix, D., Tokovinin, A. A., Batten, A. H., et al. 2004, A&A, 424, 727

Reid, I. N. & Gizis, J. E. 1997, , 113, 2246

Salim, S. & Gould, A. 2003, ApJ, 582, 1011

Tokovinin, A. A. 1997, A&As, 124, 75

Valenti, J. A. & Fischer, D. A. 2005, ApJs, 159, 141

Worley, C. E. & Douglass, G. G. 1997, A&As, 125, 523

Wright, J. T., Marcy, G. W., Butler, R. P., & Vogt, S. S. 2004, VizieR Online Data Catalog, 215, 20261

Part III

# A MONTE CARLO TOOL FOR THE STATISTICAL ANALYSIS AND PREDICTION OF EXO-PLANETS SEARCH RESULTS

# 4

# MESS (MULTI-PURPOSE EXOPLANET SIMULATION SYSTEM)

*Adapted from "MESS (Multi-purpose Exoplanet Simulation System) a Monte Carlo tool for the statistical analysis of extrasolar planet search surveys" Bonavita et al. 2010 In preparation*

## 4.1 CONTEXT

Indirect detection methods met a great success in finding planets in small orbits. However the sample of detected planets with these techniques up to now is not giving any constraint on the distributions of planets in wide orbits (more than 5-10 AU). As a result, information on the population of such distant planets is missing.

A clear determination of the frequency of giant planets as a function of orbital separation out to hundreds AU is a crucial issue to clarify the relative importance of various models of planet formation and migration. Formation through core accretion is, as example, strongly dependent on the surface density of solid material in the protoplanetary disk. Formation of Jupiter mass planets becomes increasingly less efficient as the density of planetesimals decreases, highly increasing the formation timescales. However even in a scenario in which giant planets form only close to the snow-line in the protoplanetary disk, a significant fraction of massive planets might be found on stable orbits of tents of AU. This can be possible because of outward migration (see Veras & Armitage 2004), which can be induced both by gravitational interaction between massive objects in multiplanetary systems, and by interactions between the planet and gaseous disks. Alternative models of planet formation (disk instability, disk fragmentation) are efficient mostly at wide separations from the central star.

Direct imaging is currently the most viable technique to probe for planets at large separations, providing clues on their frequency. Various deep imaging surveys of young, nearby stars have recently been completed (see Tab. 4.1) using different high contrast imaging techniques such as coronagraphy, differential imaging or *L*-band imaging.
A significant number have anyway reported a null-detection result of substellar companions, but recent detections are now finally showing the reliability of this method (Kalas et al. 2008; Marois et al. 2008b; Lagrange et al. 2008, see e.g.). These partially unexpected observations also raised

Table 4.1: Deep imaging surveys of young ($< 100$ Myr), nearby ($< 100$ pc) stars dedicated to the search for planetary mass companions and published in the literature. The telescope and the instrument (Tel/Instr.), the imaging mode (CI: coronagraphic imaging; Sat-DI; saturated direct imaging; DI direct imaging; SDI: simultaneous differential imaging; ADI: angular differential imaging) and filters, the field of view (FoV) and the number of stars observed (#) are given. The typical survey sensitivity in terms of mass is also reported with the survey reference.

| Tel/Instr. | Mode & Filter | FoV (arcsec) | # | Mass () | Ref. |
|---|---|---|---|---|---|
| 3.6m/ADONIS | CI, $H-K$ | $13 \times 13$ | 29 | 5 | (1) |
| NTT/Sharp | Sat-DI, $K$ | $11 \times 11$ | 23 | 5 | (2) |
| NTT/Sofi | Sat-DI, $H$ | $13 \times 13$ | 10 | 5 | (2) |
| HST/NICMOS | DI, H | $19 \times 19$ | 45 | 1 | (3) |
| VLT/NaCo | Sat-DI, $H-K$ | $14 \times 14$ | 28 | 5 | (4) |
| VLT/NaCo | SDI, $H$ | $5 \times 5$ | 45 | 1 | (5) |
| VLT/NaCo | DI, $L'$ | $28 \times 28$ | 22 | 1 | (6) |
| Gemini/NIRI | ADI, $H$ | $22 \times 22$ | $85^*$ | 1 | (7) |

- REFERENCES: (1) Chauvin et al. (2003), (2) Neuhäuser et al. (2003), (3) Lowrance et al. (2005), (4) Masciadri et al. (2005), (5) Biller et al. (2007), (6) Kasper et al. (2007), Marois et al. (2008a)

- (*): half have age estimates younger than 200 Myr (see Fig. 1, Marois et al. 2008a)

many questions about how such objects could form (see Absil & Mawet 2009).

Besides the few detections, there is anyway a wealth of data that can be used to put constraints on the frequency of planets in wide orbits. In addition there are many new instruments planned for the next future specially designed for imaging of exoplanets. These facilities will likely allow extending such systematic characterization at larger scales. They will prepare the path for the 30-40 meter-class telescopes that will allow exploring a wide range of planetary masses and separations. With these instruments an overlap between the discovery spaces of direct and indirect techniques will be finally achieved.

In this context it is useful and crucial to have a tool which goals are either to learn as much as possible from the available data and to predict the performances of the forthcoming instruments. This tool may be used not only to estimate the number of expected detections, but also to figure out what will be the explored parameter space and even the possible synergies between different discovery techniques. This is crucial to properly design such instruments as well as to plan the most appropriate observing programs.

Kasper et al. (2007), Lafrenière et al. (2007), Nielsen et al. (2008), Nielsen & Close (2009) have initiated a statistical analysis to constrain the physical and orbital properties (mass, period, eccentricity distributions) of a giant planet population. They developed statistical analysis tools to exploit the performances of deep imaging surveys. They tested the consistency of various sets of parametric distributions of planet parameters, using the specific case of a null detection. The first assumption of these tools is that planet mass, eccentricity and period distributions coming from the statistical results of RV studies at short period (see e.g. Lineweaver & Grether 2003; Cumming et al. 2008) can be extrapolated and normalized to obtain informations on more distant planets. Despite the model-dependency on the mass predictions, the approach is attractive for exploiting the complete set of detection performances of the survey and characterizing the outer portions of exo-planetary systems.

Starting from these works, we tried to go a step further, creating a Multi-purpose Exo-planet Simulation System (hereafter MESS) that is meant to be independent from the kind of instrument/technique under test. This code has been used not only to analyze the outcomes of the observations (see Chap. 5 and 6, but also to predict the behaviour of the discovery space of the future facilities (as showed in Chap. 7, 8 and 9).

The MESS algorithm is based on three fundamental steps: first, a synthetic planet population is produced, either using the results of the statistical analysis of the properties of the discovered planets or the results of the planet formation theories (Sec. 4.2) Then the physical parameters of these planets are determined. This allow deriving the expected values for the observables (radial velocity signature, astrometric signal, expected separation and contrast, as described in Sec. 4.6 ) Finally, these expected values for the observables are compared with the predicted capabilities of existing or planned instruments (Sec. 4.7).

This last step allows defining a sample of fully characterized *detectable planets*, which characteristics can be easily investigated. This means, in the case of planned instruments, that using MESS it will be possible to tune not only the main instrument parameter, but even the observing strategy.

In the forthcoming section we will present this our Monte Carlo code for the statistical analysis and prediction of exoplanets search results, from the inputs needed as a starting point (Sec. 4.2 and 4.3) to the synthetic planet populations produced as output (Sec. 4.6) and finally describes the different setups and operation modes (Sec. 4.7).

## 4.2 RANDOM GENERATION OF MASSES AND PERIODS

The very first step of the MESS code is the generation of a given number of planetary masses and periods. Together with the stellar sample, providing the characteristics of the host stars, this constitute the basis of the construction of the synthetic planet population.
Two possible approaches are possible:

1. **Empirical approach:**
   A fixed number (hereafter $N_{gen}$) of values of $M \sin i$ and $p$ are randomly generated following power-law distribution, as in Eq.4.1:

$$\frac{dN}{d\left(M_p \sin i\right)} \propto \left(M_p \sin i\right)^{\alpha} \qquad \frac{dN}{dP} \propto p^{\beta} \tag{4.1}$$

Both the planetary mass and period range can be given as inputs, together with the power-law exponents. Another free parameter is the semi major axis cut-off, corresponding at the maximum period at which the distribution must be extrapolated.

In a typical setup the power-law exponents are assumed to be $\alpha = -1.31$ and $\beta = -0.74$ respectively, from Cumming et al. (2008), the planetary mass spans the range between 0.6 $M_{Earth}$ and 15 $M_{Jup}$ and the period ($p$) is chosen between 2.5 days and 350 years (corresponding to 50 AUcut off for $1M_{\odot}$ star).

To remove the degeneracy with the orbital inclination, $N_{gen}$ values of $i$ are randomly generated, following an uniform distribution on the solid angle, ending with the real mass of the planets.

A scaling of the planetary mass, and even of the period, with the stellar mass can be also introduced, according the recent results (e.g. Lovis & Mayor 2007), in addition a dependence of the planet frequency on the stellar metallicity may also be considered (see Fischer & Valenti 2005).

2. **Theoretical approach:**
   $N_{gen}$ values of $M_p$ and $p$ are randomly chosen between the values provided by the output of planetary formation models (e.g. the ones developed by the Bern Group, see Benz et al. 2008). In this case the planet mass is directly given as an output of the models, together with the minimum mass ($M \sin i$) which lead to the value of the inclination, without any need for a random generation.

   Different populations of planets, obtained assuming different stellar masses and metallicity values, can be selected according with the characteristics of the real star in the sample, to take into account the effect of the stellar characteristics on the planet formation processes.

## 4.3 STELLAR SAMPLE

As anticipated in Sec. 4.2, MESS requires as input a list of real stars, that can be selected on the basis of the kind of analysis one needs to perform. As an example we will show the results obtained using a group of about 600 nearby ($d < 20$ pc) stars, with magnitude $I > 10.0$, selected from the Hipparcos Catalogue. Apparent magnitude, distance, age and mass are the the basic simulations parameters (see Fig. 4.1).

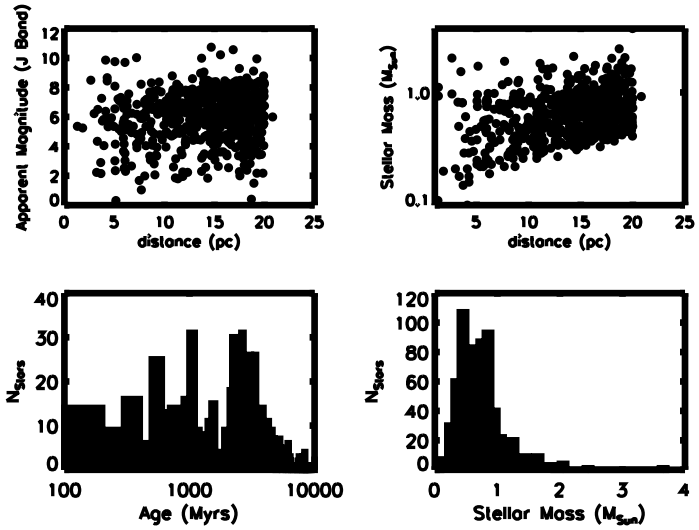


Figure 4.1: Principal characteristics of the sample of nearby stars used by MESS. **Upper Left:** Apparent Magnitude in J Band vs distance in pc. **Upper Right:** Stellar Mass ($M_{\odot}$) vs distance in pc. **Lower Left:** Histogram of stellar ages (Myrs). **Lower Right:** Histogram of stellar masses ($M_{\odot}$).

Depending on the scope of the analysis to be performed, these informations can be used to obtain

- a **Full Population:** for each one of the $N_{Star}$ stars in the sample the whole set of $N_{Gen}$ mass-period pairs (generated as described in Sec. 4.2) is used, ending with a synthetic population of $N_{Gen} * N_{Star}$ planets. This approach is useful for the statistical analysis of existing data, since in this case MESS provides the fraction of detectable planets per star, that can be used to derive the global probability of finding a planet over the whole target list, that can be compared with the real results.

- a **Reduced Population:** We associate to each star in the sample, a *planetary system*[1]. This system is built randomly picking, a fixed number ($n$)of mass-period pairs from the initial generation, ending with a population of $n * N_{Star}$ planets. Then the predicted detection performances of a certain instrument can be used, to derive the population of objects that can be detected around each star.

[1]Note that no discussion on the dynamical stability is made, each star-planet pair being treated individually Modification of the code to treat dynamical stability are planned in the next future

In both case every star is analyzed individually, its characteristics affecting not only the final appearance of the planetary orbits, but also the detection limits used to select the detectable planets.

## 4.4 SEMI-MAJOR AXIS AND ORBITAL ELEMENTS

Given the generated values of masses and period obtained with one of the approaches described below, the semi-major axis is computed using the Kepler's third law, using the real mass of each star in the sample, and neglecting the star of the planet. Eccentricity, $e$, inclination, $i$, longitude of periastron, $\omega$, longitude of ascending node, $\Omega$, and time of periastron passage, $T_0$, are then randomly generated, with uniform distributions. Finally, the circumstance of observation can be also defined.

In practice, the coordinates, $x$ and $y$, of the projected orbit on the plane perpendicular to the line of sight, are computed using the ephemeris formulae of Heintz (1978), reported in Eq. 4.2 to 4.4.

$$\begin{aligned} x &= AX + FY && (4.2)\\ y &= BX + GY \\ X &= \cos E - e && (4.3)\\ Y &= \sqrt[2]{1-e^2}\sin E \\ \rho &= \sqrt{x^2+y^2} && (4.4) \end{aligned}$$

where $X$ and $Y$ are the coordinates on the true orbit (Eq. 4.3), and $A, B, F, G$ the Thiele-Innes elements, which can be obtained from the classical ones $(a, \omega, \Omega, i)$ using Eq. 4.5.

$$\begin{aligned} A &= a\left(\cos\omega\cos\Omega - \sin\omega\sin\Omega\cos i\right) \\ B &= a\left(\cos\omega\sin\Omega + \sin\omega\cos\Omega\cos i\right) \\ F &= a\left(-\sin\omega\cos\Omega - \cos\omega\sin\Omega\cos i\right) \\ G &= a\left(-\sin\omega\sin\Omega + \cos\omega\cos\Omega\cos i\right) \end{aligned} \qquad (4.5)$$

$E$ is the the eccentric anomaly (obtained from the mean anomaly $M$ ( Eq. 4.6) using Eq. 4.7) and $\nu$ the true anomaly (Eq. 4.8).

$$M = \left(\frac{t_{obs} - T_0}{p}\right) 2\pi \qquad (4.6)$$

$$
\begin{aligned}
E_0 &= M + e\sin M + \frac{e^2}{2}\sin 2M \\
M_0 &= E_0 - e\sin E_0 \\
E &= E_0 + (M - M_0)) \,/\, (1 - e\cos E_0) \qquad (4.7) \\
\tan \nu/2 &= \sqrt{(1+e) \,/\, (1-e)}\tan E/2 \qquad (4.8)
\end{aligned}
$$

If not available from the real data, an epoch of observation, $t_{obs}$, is also generated over a time-span chosen according with the considered instrument.
The projected separation, $\rho$ (in arcsecs), can be obtained either using Eq. 4.4 or Eq. 4.9 (which gives also an estimate of the radius vector: $r$), and then dividing for the star distance.

$$
\begin{aligned}
\rho &= r\cos(\nu + \omega)\sec(\theta - \Omega) \qquad (4.9) \\
r &= a\left(1 - e^2\right) \,/\, (1 + e\cos\nu)
\end{aligned}
$$

## 4.5 EVALUATION OF PLANET PHYSICAL CHARACTERISTICS

Given the mass, period and location along the orbit derived as described in Sec. 4.2 and 4.4, MESS can calculate other key parameters, such as radius, temperature, etc. for each planet in the synthetic population. The following sections will summarize all the assumption on which the calculation of planetary physical characteristics are based.

### 4.5.1 *Planet Temperature*

Since we aim to consider both the thermal and reflected flux of the planets, we need two different estimates of the temperature, one which is the internal temperature, $T_{Int}$, coming from the evolutionary models (see Baraffe et al. 2003, and Sec. 1.5) and another which is the equilibrium temperature, $T_{Eq}$ obtained trough Eq. 4.10 (from Sudarsky et al. 2003)

$$
T_{eq} = \left[\frac{(1 - A_B)\, L_*}{16\pi\sigma a^2}\right] \qquad (4.10)
$$

here the bond albedo $A_B$ is assumed to be 0.35 in the J band (Jupiter value, see ) and it's randomly generated between 0.3 and 0.52 in the visible (the latter being the Jupiter albedo in V band, see Sudarsky et al. 2003)

Then our final assumed value for the temperature is given by Eq. 4.11.

$$T_{\rm eff}^4 = T_{\rm int}^4 + T_{\rm eq}^4. \tag{4.11}$$

### 4.5.2 *Planet radius*

To evaluate the planetary radius, MESS uses the approach developed by Fortney et al. (2007). Practically the radius is assumed to depend on the planet mass:

1. For Jupiter-like planets ($M \geq 100 M_{earth}$ ) interpolation is performed within the published values given by Fortney et al. (2007). Values of age and distance of each star are entered, yielding a value for $R_{Gas}$. A core mass of $10 M_{earth}$ is assumed.

2. For the lighter planets ($M \leq 10 M_{earth}$ ) Equations 4.12 and 4.13 from Fortney et al. (2007) are used, respectively for ice/rock and rock/iron planets.

$$\begin{aligned} R = (0.0912 \quad & imf + 0.1603)(\log M)^2 \\ & + (0.3330 \quad imf + 0.7387) \log M \\ & + (0.4639 \quad imf + 1.1193) \end{aligned} \tag{4.12}$$

$$\begin{aligned} R = (0.0592 \quad & rmf + 0.0975)(\log M)^2 \\ & + (0.2337 \quad rmf + 0.4938) \log M \\ & + (0.3102 \quad rmf + 0.7932) \end{aligned} \tag{4.13}$$

   Here $R$ is in $R_{earth}$ and $M$ is in $M_{earth}$, while $imf$ is the ice mass fraction (1.0 for pure ice and 0.0 for pure rock) and $rmf$ is the rock mass fraction (1.0 for pure rock and 0.0 for pure iron).

   In the typical setup, the ice/rocky or rocky/iron fraction is set to 0.3 (50% of chance for a planet of being mainly icy or rocky).

3. Finally prediction are uncertain for the Neptune-like planets, where transition between the two relations described above should occurs. The most reasonable approach seems to fit the mass-radius relation of the Solar System in the same mass-range ($10 - 40 M_{earth}$ ). This

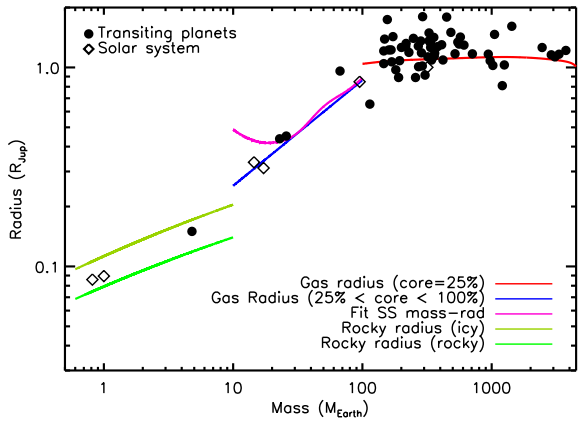


Figure 4.2: Summary of the planetary Mass - Radius relations adopted for the different mass ranges. All the model computation are made assuming an host star of 1 $M_{\odot}$ and the semi-major axis value is fixed to 5 AU.

procedure provides a good agreement with the radii for the few transiting Neptunes found so far (see Fig. 4.2).

The resulting mass-radius relations are showed in Fig. 4.2, with over-plotted the data corresponding to the planets discovered with the transit technique and the planets from our Solar System, for comparison.

## 4.6 CHARACTERISTICS OF THE PRODUCED SYNTHETIC PLANET POPULATIONS

As an example of a possible synthetic population generated by MESS, we will consider here the *reduced population* (see Sec. 4.3) obtained considering the *Nearby Sample* already mentioned in Sec.4.3.

In order to compare physical properties of the planets with observed data, we need to define observable quantities. These includes masses and distance from the star(see Fig. 4.3), from which the indirect effect of the presence of the planet, such as radial velocity (RV) semi-amplitude and astrometric signal (Fig. 4.4) can be computed, as well as the planet luminosity contrast, needed for the direct observations (see Fig. 4.5).

### 4.6.1 *Masses and semi-major axes*

Fig. 4.3 shows the distribution of planets of the synthetic population in the mass vs semi-major axis plane, obtained using both the approaches described in Sec. 4.2. The upper panel shows the results obtained using the power-law distributions from Cumming et al. (2008), with the *typical setup* defined in Sec. 4.2. In the lower panel, we plotted mass vs semi-major axis of the planets obtained using the outputs of the extended core accretion model (Alibert et al. 2005) as described in Sec. 4.2.

The planets are separated in the three classes defined in Sec. 1.1, using different colors:

- **Giant (or Jupiter-like)** planets ($M_{planet} > 40 M_{Earth}$). A distinction between *Cold Jupiters* (orange dots) and *Warm Jupiters* (red dots) is also made, where the definition of cold and warm planets is the same as in Sec. 4.6.3.
- **Neptune-like** planets ($10 M_{Earth} \leq M_{planet} \leq 40 M_{Earth}$ blue dots)
- **Rocky** planets ($M_{planet} < 10 M_{Earth}$ green dots)

### 4.6.2 *RV and astrometric signal*

Given the characteristics of the planetary orbit, one can also derive the observable effects of the planet on the motion of the stars, as discussed in Sec. 2.5.

Fig. 4.4 shows run of the the Radial velocity (upper panel) and astrometric signatures (lower panel) vs period of the synthetic planets populations. These were evaluated using Eq. 2.2 and 2.5 from Sec. 2.5.1.

### 4.6.3 *Planet/star Contrast*

For each planet, MESS gives an estimate of both the intrinsic and reflected flux, in the chosen band. Both contributions are considered in the evaluation of the final planet/star contrast.

- The intrinsic emission is estimated using the prediction of evolutionary models at the age of the star (assumed to be also the age of the system). To this purpose two classes of models can be considered,

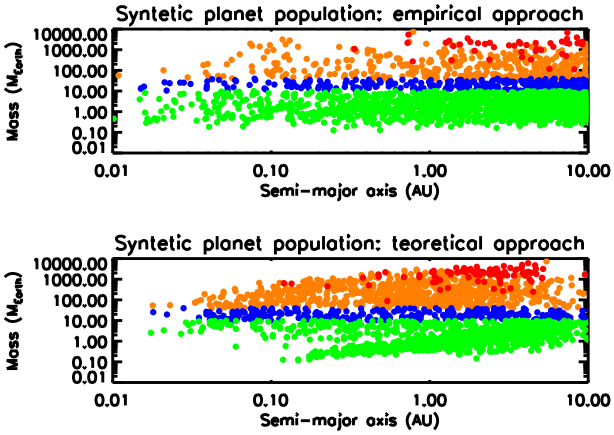


Figure 4.3: Mass semi-major axis distribution of the synthetic planets in the populations generated by MESS. Results obtained using both the empirical (upper panel) and theoretical (lower pane) approaches described in Sec. 4.2 are shown. The different classes of planets are plotted using different colors: red/orange for the warm/cold Jupiters, blue for the Neptune like planets, green for the rocky planets.

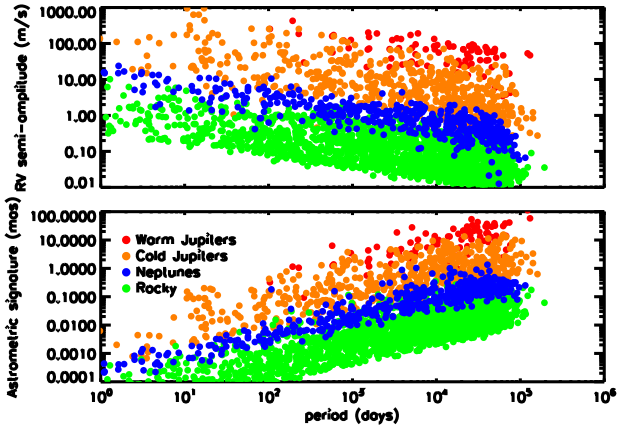


Figure 4.4: Distribution of radial velocity (upper panel) and astrometric signatures (lower panel) vs period of the synthetic planets in the populations generated by MESS using the empirical approach described in Sec. 4.2. The color code is the same as in Fig. 4.3.

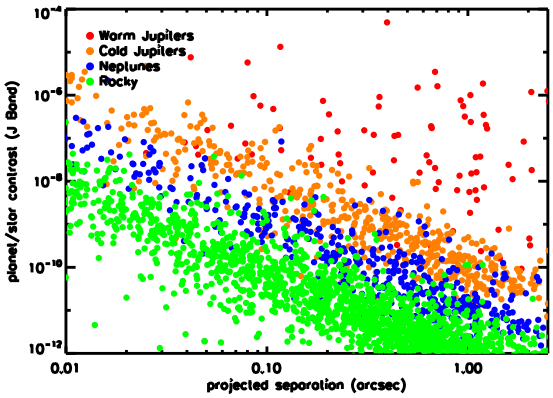


Figure 4.5: Distribution of planet/star contrast vs projected separation of the synthetic planets for the populations generated by MESS using the empirical approach described in Sec. 4.2. The color code is the same as in Fig. 4.3.

based on different assumptions on the initial conditions: Hot Start models (Chabrier et al. 2000; Baraffe et al. 2003; Saumon & Marley 2008) which consider an initial spherical contracting state and Core Accretion models (Marley et al. 2007; Fortney et al. 2008), which couple planetary thermal evolution to the predicted core mass and thermal structure of a core-accretion planet formation model.

We choose to show only the results obtained using the hot start models for the nearby sample that is presented here (which is not such young, see lower left panel of Fig. 4.1), because the differences between the two approach become more important at ages less than few million years (see Sec. 1.5).

However the problem of the initial condition, together with the errors coming from the uncertainties on the stellar ages, is one of the main limitation of the approach in case of young stellar samples and will be discussed in detail when presenting the results of the application of MESS in Part III and IV.

- For the evaluation of the reflected light, we scaled the Jupiter/Sun value in J-Band, according with planet radius (expressed in Jupiter radii), semi-major axis, albedo and illuminated fraction of the planet. This last contribution is computed through a phase dependent term, $\Phi(\beta)$, which is given by Eq. 4.14 (see Brown 2004), where $\beta$ is the

phase angle (angle at companion between star and the observer) and $z = r \sin(\nu + \omega)$ is the radial coordinate of the radius vector.

$$\Phi(\beta) = [\sin\beta + (\pi + \beta)\cos\beta] / \pi \tag{4.14}$$

The Jupiter/Sun contrast in J-Band is obtained using Eq. 4.15 which gives an estimate of the fraction of stellar light captured by a planet, depending on the values of the planet radius, semi-major axis and geometrical albedo (which is assumed to be 0.35 in J-Band, see ), being $\Phi(\beta) = 1$ (at opposition).

$$(L_{Jup}/L_*)_{Ref} = A(\lambda)\frac{R_{Jup}^2}{a_{Jup}^2} = 2.5 \times 10^{-9} \tag{4.15}$$

Then we end with a final value of the contrast in reflected light given by Eq.4.16.

$$(L_p/L_*)_{Ref} = \left(L_{Jup}/L_*\right)_{Ref} \Phi(\beta)\frac{(R_p/R_{Jup})^2}{(a/a_{Jup})^2} \tag{4.16}$$

### 4.6.4 *Degree of polarization*

The degree of polarization is assumed to be of the form:

$$P = Pmax \times (1 - cos(\beta)^2)/(1 + cos(\beta)^2) \tag{4.17}$$

where Pmax is randomly generated between 0.1 and 0.3 and $\beta$ is the same as in Eq. 4.14

Then the contrast due to the polarized light of the planets is $P$ times the contribute in reflected light evaluated with Eq. 4.16

## 4.7 OPERATION MODES

Once the synthetic population of planets has been created, the next step is to compare the characteristics of the generated planets with the detection limits appropriate for the instrument under consideration.

Two different operation modes (OM) can be used, depending on which kind of analysis needs to be performed.

1. the **Statistical Analysis Mode (SAM)**, which is built for the analysis of real data and uses the *full population* defined in Sec. 4.3. The properties of the planets are then compared with the information on the detection performances of an existing instrument.

2. the **Prediction mode**, which starts from the *reduced population* (see Sec. 4.3), and given the predicted performances of a planned instruments, select the sub-sample of detectable planets.

For both OMs it is possible to choose between:

- The *1D mode* which extracts the detectable planets using a threshold or a curve which sets the lower limit for the detection with the chosen technique, defined by the instrumental capabilities

- The *2D mode*, which is especially built for the analysis of the performances of the Deep Imaging instruments. This mode take advantage from the knowledge of all the orbital elements of the planets, to place them on a two dimensional detection map. This mode allow using all the spatial information that comes with it.

The two OMs are described in detail in Sec. 4.7.1 and 4.7.2; the results of their application will be presented in Part III and IV respectively.

### 4.7.1 *Statistical Analysis Mode*

A first approach is to test the consistency of various sets of (mass, eccentricity, semi-major axes) parametric distributions of a planet population. Only the Empirical approach described in Sec. 4.2 is used, the underlying assumption being that is reasonable to extrapolate and normalize planet mass, period and eccentricity distributions using statistical results of RV studies at short periods.

Given the detection performances of a survey, the frequency of detected simulated planets (over the complete sample) enables derivation of the probability of non-detection of a given planet population associated with a normalized distribution set. Then the comparison with the survey results tests directly the statistical significance of each distribution.

A second more general approach aims at actually constraining the exoplanet fraction $f$ within the physical separation and mass probed by the survey, in the case of null or positive detections. Contrary to what was assumed before, $f$ becomes an output of the simulation, which actually

depends on the assumed (mass, period, eccentricity) distributions of the giant planet population. This statistical analysis aims at determining $f$ within a confidence interval as a function of mass and semi-major axis, given a set of individual detection probabilities $p_j$ directly linked to the detection limits of each star observed during the survey and the considered giant planet distributions.

The probability of planet detection for a survey of $N$ stars can be in fact described by a binomial distribution, given a success probability $fp_j$, with $f$ the fraction of stars with planets and $p_j$ the individual detection probabilities of detecting a planet if present around the star j. Each individual $p_j$ can be replaced by $\langle p_j \rangle$, the mean survey detection probability of detecting a planet if present. Finally, assuming that the number of expected detected planets is small compared to the number of stars observed ($f\langle p_j \rangle << 1$), the binomial distribution can be approximated by a Poisson distribution to derive a simple analytical solution for the exoplanet fraction upper limit $f_{\max}$ for a given level of confidence CL:

$$f_{\max} = \frac{-\ln(1 - \mathrm{CL})}{N\langle p_j \rangle} \tag{4.18}$$

### 4.7.2 *Prediction mode*

As already pointed out before, beside the analysis of the real data, MESS can be also used to predict the output of the forthcoming searches. In this case the *reduced planet population* is used as input, without any preference for the empirical or theoretical approach (see Sec. 4.2), the goal being also to compare the outcomes of the two methods.

This approach allows predicting the number of detections expected from a future facility. This provides information on:

1. the expected frequency of planets
2. the properties of these objects
3. on the kind of constraints that their observation can put on the planet formation theories.

Moreover, it provides a tool to tune the instrument characteristics in order to fulfill the requirements needed to access a certain domain in the parameter space.

## 4.8 CONCLUSIONS

In this Chapter we presented our Monte Carlo simulation tool for the statistical analysis and prediction of survey results for exoplanets. What we created is then a Multi-purpose Exoplanet Simulation System (MESS). The main strength of the code is that it is meant to be independent from the kind of instrument or techniques under test.

Moreover, for the synthetic planet population it creates, the code provides all the orbital elements, together with all the physical characteristics of the planets (temperature, radii, luminosity, etc.). Then all the observables can be easily evaluated, for a comparison with the detection limits.

The approach still has several limitations, due principally to the assumptions about the planetary distribution and to the choice of the evolutionary models used to evaluate the planet luminosity.

Beside that, being these given as inputs of the code, they can be easily changed, and this also allows testing several hypothesis and initial conditions.

Having in hands such a tool, we used it for several studies. Both the *Statistical Analysis Mode* and the *Prediction Mode* have been extensively used, and the results will be presented in the forthcoming chapters.

# BIBLIOGRAPHY


Absil, O. & Mawet, D. 2009, A&Ar, 16

Alibert, Y., Mordasini, C., Benz, W., & Winisdoerffer, C. 2005, A&A, 434, 343

Baraffe, I., Chabrier, G., Barman, T. S., Allard, F., & Hauschildt, P. H. 2003, A&A, 402, 701

Benz, W., Mordasini, C., Alibert, Y., & Naef, D. 2008, Physica Scripta Volume T, 130, 014022

Biller, B. A., Close, L. M., Masciadri, E., et al. 2007, ApJs, 173, 143

Brown, R. A. 2004, ApJ, 610, 1079

Chabrier, G., Baraffe, I., Allard, F., & Hauschildt, P. 2000, ApJ, 542, 464

Chauvin, G., Thomson, M., Dumas, C., et al. 2003, A&A, 404, 157

Cumming, A., Butler, R. P., Marcy, G. W., et al. 2008, PASP, 120, 531

Fischer, D. A. & Valenti, J. 2005, ApJ, 622, 1102

Fortney, J. J., Marley, M. S., & Barnes, J. W. 2007, ApJ, 659, 1661

Fortney, J. J., Marley, M. S., Saumon, D., & Lodders, K. 2008, ApJ, 683, 1104

Heintz, W. D. 1978, Geophysics and Astrophysics Monographs, 15

Kalas, P., Graham, J. R., Chiang, E., et al. 2008, Science, 322, 1345

Kasper, M., Apai, D., Janson, M., & Brandner, W. 2007, A&A, 472, 321

Lafrenière, D., Doyon, R., Marois, C., et al. 2007, ApJ, 670, 1367

Lagrange, A. ., Gratadour, D., Chauvin, G., et al. 2008, ArXiv e-prints

Lineweaver, C. H. & Grether, D. 2003, ApJ, 598, 1350

Lovis, C. & Mayor, M. 2007, A&A, 472, 657

Lowrance, P. J., Becklin, E. E., Schneider, G., et al. 2005, , 130, 1845

Marley, M. S., Fortney, J. J., Hubickyj, O., Bodenheimer, P., & Lissauer, J. J. 2007, ApJ, 655, 541

Marois, C., Lafrenière, D., Macintosh, B., & Doyon, R. 2008a, ApJ, 673, 647

Marois, C., Macintosh, B., Barman, T., et al. 2008b, Science, 322, 1348

Masciadri, E., Mundt, R., Henning, T., Alvarez, C., & Barrado y Navascués, D. 2005, ApJ, 625, 1004

Neuhäuser, R., Guenther, E. W., Alves, J., et al. 2003, Astronomische Nachrichten, 324, 535

Nielsen, E. L. & Close, L. M. 2009, ArXiv e-prints

Nielsen, E. L., Close, L. M., Biller, B. A., Masciadri, E., & Lenzen, R. 2008, ApJ, 674, 466

Saumon, D. & Marley, M. S. 2008, ApJ, 689, 1327

Sudarsky, D., Burrows, A., & Hubeny, I. 2003, ApJ, 588, 1121

Veras, D. & Armitage, P. J. 2004, MNRAS, 347, 613

Part IV

# APPLICATIONS I : ANALYSIS OF REAL DATA

Having in mind the the informations about the current state of the art of the planet searches given in Part I and having a tool as versatile as the one described in Part II, many different statistical analysis can be done, to address different items.

In this part we will start the review of the results of MESS, describing the application of its *statistical analysis mode* (SAM, see Sec. 4.7.1).

First we will present the analysis of data coming from a deep imaging survey (Chap. 5) using the resulting null detection to put constraint on the frequency of planets in wide orbits.

Then we'll use a slightly modified 2D MESS (see Sec. 4.7), focusing on a single object, the T-Tauri star LkCa15 (Chap. 6), trying putting constraint on the orbital parameters of an unseen companion.

# 5

# ANALYSIS OF A DEEP IMAGING SURVEY OF YOUNG, NEARBY AUSTRAL STARS

*adapted from 'Deep imaging survey of young, nearby austral stars' Chauvin, G., Lagrange, A.-M., Bonavita, M. et al. 2009*

## 5.1 INTRODUCTION

In this chapter we report results of use of MESS for the statistical analysis of the results of a deep coronagraphic imaging survey of several young, nearby austral stars, aimed at discovering sub-stellar companions. In Section 5.2, the sample definition and properties are presented. In Section 5.3, we describe the characteristics of the VLT/NACO instrument and the different observing set-up and modes that we used. The dedicated data reduction and analysis are reported in Section5.4. In Section 5.5, we finally consider the detection sensitivity of our complete survey to statistically constrain the physical and orbital properties of the population of giant planets with $20 - 150$ AU physical separations.

## 5.2 SAMPLE SELECTION

We built up our target sample by combining an exhaustive list of young, nearby stars which selection criteria (age, distance, binarity and observability) are defined in order to optimize the detection of close-in planetary mass companions using NACO at VLT. Youth indicators generally rely on the use of photometry compared to pre-main sequence isochrones and spectroscopy (Lithium and $H_\alpha$ lines) and studies of X-ray activity and IR excess. Membership to associations is inferred from coordinates, proper motion, radial velocity and distance estimation. Since the beginning of the present survey, the number of known young, nearby stars more than doubled and newly identified members were regularly included in our target sample. Known binaries (see Tables B.1 and B.2) with $1.0 - 12.0''$ separation were excluded to avoid degrading the NACO AO and/or coronagraphic detection performances. Our initial complete sample was composed of 88 stars; 51 of them are members of young, nearby comoving groups, 32 are young, nearby stars currently not identified as members

of any currently known association and 5 have been reclassified by us as older (>100 Myr) systems.

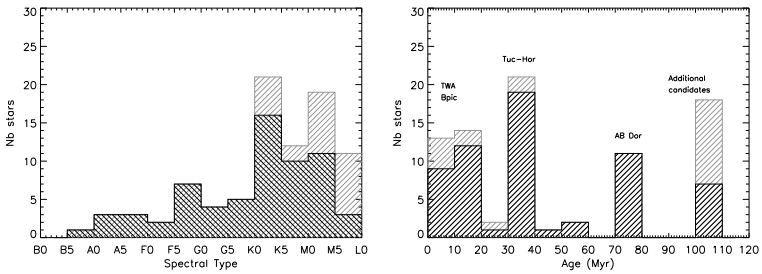


Figure 5.1: Histograms summarizing the main properties of the sample of young, nearby stars observed with NACO at VLT. *Left:* Histogram of spectral types for the stars observed in coronagraphic imaging (*crossed lines*) and in direct imaging (*simple lines*). *Right* Histogram of ages for members of known young, nearby associations (TWA, $\beta$ Pic, Tuc-Hor, AB Dor) and additional young candidates

For those stars not belonging to a known moving group (Table B.2), we employed as many as possible techniques for age dating, exploiting existing data.

The properties of our sample are summarized in Tables **??** (in Appendix B) and illustrated in Fig. 5.1. 93% of the selected stars are younger than about 100 Myr and 94% closer than 100 pc. The spectral types cover the sequence from B to M spectral types with 19% BAF stars, 48% GK stars and 33% M dwarfs.

## 5.3 OBSERVATIONS

### 5.3.1 *Telescope and instrument*

NACO[1] is the first Adaptive Optics instrument that was mounted at the ESO Paranal Observatory near the end of 2001 (Rousset et al. 2000). NACO provides diffraction limited images in the near infrared (nIR). The observing camera CONICA Lenzen et al. (1998) is equipped with a $1024 \times 1024$ pixel Aladdin InSb array. NACO offers both a Shack-Hartmann visible wavefront sensor and a nIR wavefront sensor for red cool (M5 or later spectral type) sources. nIR wavefront sensing was only used on 8% of our sample. Note that in May 2004, the CONICA detector was changed. The new detector was more efficient thanks to an im-

[1] http://www.eso.org/instruments/naos/

proved dynamic range, a lower readout noise and cleaner arrays. Among NACO's numerous observing modes, only the direct and coronagraphic imaging modes were used. The two occulting masks offered for Lyot-coronagraphy have a diameter of $\oslash = 0.7''$. and $\oslash = 1.4''$. According to the atmospheric conditions, we used the $H$ and $K_s$ broad band filters, the narrow band filters, NB1.64, NB1.75 and Br$\gamma$ [2] and a neutral density filter (providing a transmissivity factor of 0.014). In order to correctly sample the NACO PSF (better than Nyquist), the S13 and S27 objectives were used, offering mean plate scales of 13.25 and 27.01 mas per pixel and fields of view of $14'' \times 14''$ and $28'' \times 28''$ respectively.

### 5.3.2 *Image quality*

For ground-based telescopes, atmospheric conditions have always been critical to ensure astronomical observations of good quality. Although AO instruments aim at compensating the distortion induced by atmospheric turbulence, the correction quality (generally measured by the *Strehl Ratio (SR)* and *Full Width Half Maximum (FWHM)* parameters) is still related to the turbulence speed and strength. For bright targets, the NACO AO system can correct for turbulence when the coherent time ($\tau_0$) is longer than 2 ms. For faster ($\tau_0 \leq 2$ ms) turbulence, the system is always late and the image quality and the precision of astrometric and photometric measurements are consequently degraded.

During our NACO observing runs, the averaged $\tau_0$ was about 5 ms and it was larger than 2 ms 80% of the time. The average value of the seeing conditions over all runs was equal to $0.8''$ (which happens to be the median seeing value measured in Paranal over the last decade[3]). Fig. 5.2 shows the (*Strehl Ratio*) performances of the NACO AO system with the visible wavefront sensor as a function of the correlation time of the atmosphere $\tau_0$, the seeing and the primary visible magnitude. As expected, the degradation of the performances is seen with a decrease of $\tau_0$, the Fried radius ($r_0$, inversely proportional to the seeing) and the primary flux. Still, the results clearly demonstrate the good NACO performances and capabilities over a wide range of observing conditions.

[2] see filters description: http://www.eso.org/instruments/naco/inst/filters.html

[3] http://www.eso.org/gen-fac/pubs/astclim/paranal/seeing/adaptive-optics/statfwhm.html

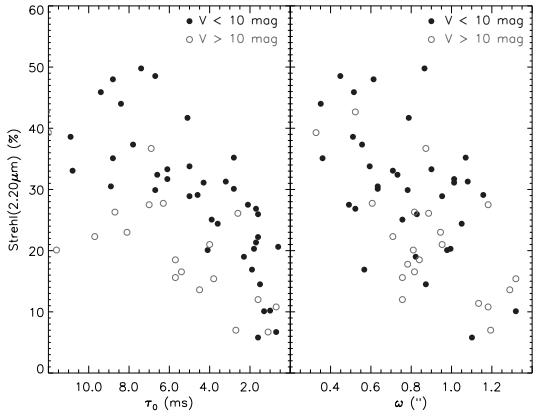


Figure 5.2: VLT/NACO adaptive optics system performances. Strehl ratio at 2.20 $\mu$m is plotted as a function of the correlation time $\tau_0$ and the seeing $\omega$ of the atmospheric turbulence for two regimes of $V$-band magnitude of the primary star (AO reference target). Only those targets observed with the visible WFS are plotted. Close binaries have also been rejected. The results demonstrate the good behavior of NACO over a wide range of stellar magnitudes and under different turbulent conditions. A clear degradation of the performances is seen for decreasing $\tau_0$, increasing $\omega$, and for fainter ($V \geq 10$) targets. A clear drop is seen when $\tau_0$ is faster than 2 ms, the limit of the NACO wavefront sensor sampling frequency.

### 5.3.3 *Observing strategy*

The VLT/NACO survey was conducted as a continuation of the earlier coronagraphic survey performed with the ADONIS/SHARPII instrument at the ESO 3.6 m telescope at La Silla Observatory (Chauvin et al. 2003). A similar observing strategy was adopted to optimize the detection of faint close sub-stellar companions. Most of our stars are relatively bright ($K_s \leq 10$) in nIR. To improve our detection performances, we have adopted the Lyot coronagraph. High contrast imaging techniques, such as Lyot and phase mask coronagraphy, $L$-band saturated imaging and simultaneous differential imaging, enable achievement of contrasts down to $10^{-5}$ to $10^{-6}$. Main differences between these techniques are inherent in the nature of the sub-stellar companions searched and the domain of separations explored. Broad-band nIR Lyot coronagraphy and thermal ($L'$-band or 4 $\mu$m) saturated imaging are among the most sensitive techniques at typical separations between 1.0 to 10.0″. The contrast performances are currently mandatory to access the planetary mass regime when searching for faint close companions.

A dedicated observing block was executed to measure precisely the positions of the faint sources detected in the coronagraphic field relative to the primary star. This block was composed of three successive observing sequences and lasted in total $\sim$ 45 min (including pointing). After the centering of the star behind the coronagraphic mask, a deep coronagraphic observing sequence on source was started. Several exposures of less than one minute each were accumulated to monitor the star centering and the AO correction stability. An effective exposure time of 300 sec was generally spent on target. During the second sequence, either a neutral density or a narrow band filter were inserted in the optical path and the occulting mask and Lyot stop removed. The goal was to precisely measure the star position behind the coronagraphic mask (once corrected for filter shifts). An effective exposure time of 60 sec was spent on source. Counts were adjusted to stay within the 1% linearity range of the detector. The image was also used to estimate the quality of the AO correction. Finally, the last sequence was the coronagraphic sky. This measure was obtained by pointing at $\sim 45''$ from the star using a jittering pattern made of several offset positions to avoid any contaminants in the final median sky. In case of positive detections, whenever possible, the companion candidates (CCs) were re-observed to check whether a faint object shared common proper motion with the primary star. The time span between successive epochs was about 1-2 years depending on each object's proper motion (see Fig. 5.1). When comoving companions were identified, images were recorded with additional nIR filters to directly compare the spectral energy distribution with that predicted by (sub)stellar evolutionary models.

## 5.4 DATA REDUCTION AND ANALYSIS

### 5.4.1 *Cosmetic and image processing*

Classical cosmetic reduction including bad pixels removal, flat-fielding, sky subtraction and shift-and-add, was made with the *Eclipse*[4] reduction software developed by Devillard (1997) for both direct and coronagraphic imaging observations. Median filtering by a kernel of $3 \times 3$ pixels was applied to correct for remaining hot pixels. To remove the central part of the PSF in our reduced coronagraphic images, two methods were ap-

[4]http://www.eso.org/projects/aot/eclipse/

plied. The first method considered different angular sectors uncontaminated by the diffraction spikes and by the coronagraphic mask support. For each sector, the PSF azimuthal average is calculated, circularised and subtracted from the coronagraphic image. The alternative method was to apply directly a high-pass filter with a kernel of $3 \times FWHM$ (assuming the theoretical *FWHM* at each observing set-up). As a result, low spatial frequencies, including the coronagraphic PSF wings, were removed from the reduced image. Finally, each resulting image was inspected by eye for the close companion identification. Fig. 5.3 is an illustration of the data processing applied to the coronagraphic images of HIP 95270, in the case of the second method.

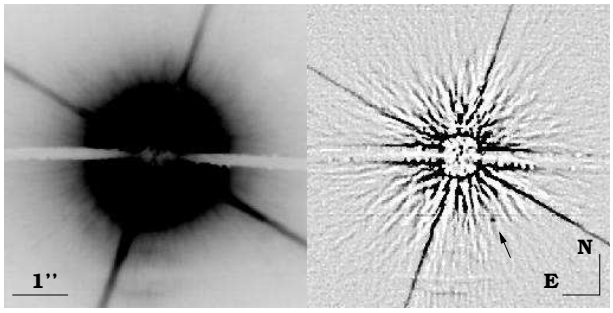


Figure 5.3: *Left*: VLT/NACO coronagraphic image of HIP 95270 obtained in *H*-band with the S13 camera. The small ($\oslash = 0.7''$) coronagraphic mask was used. *Right*: Coronagraphic image after high-pass filtering. A kernel of $3 \times FWHM$ is used to remove the low spatial frequencies of the coronagraphic PSF wings. A fake $\Delta H = 12$ companion has been inserted at $1.2''$ from the star to test the detection performances. Minimum and maximum thresholds of the filtered image were divided by a factor of 15 to show the fake companion and the PSF residuals.

### 5.4.2 *Detection limits*

The coronagraphic detection limits were obtained using combined direct and coronagraphic images. On the final coronagraphic image, the pixel-to-pixel noise was estimated within a box of $5 \times 5$ pixels sliding from the star to the limit of the NACO field of view. Angular directions free of any spike or coronagraphic support contamination were selected. Additionally, the noise estimation was calculated within rings of increasing radii, a method which is more pessimistic at close angular separation due to the presence of coronagraphic PSF non-axisymmetric residuals. Final detection limits at $6\sigma$ were obtained after division by the primary star

maximum flux and multiplication by a factor which takes into account the ratio between the direct imaging and coronagraphic integration times and the difference of filter transmissions and bandwidths. Spectral type correction due to the use of different filters has been simulated and is smaller than 0.04 mag. The variation of the image quality (*Strehl Ratio*) over the observed field remains within 10% and should not impact our contrast estimation by more than 0.1 mag. The median detection limits, using the sliding box method, are reported in Fig. 5.4. They are given for observations obtained in $H$- and $K_s$-bands, with the $\oslash = 0.7''$ and $\oslash = 1.4''$ coronagraphic masks, and for different target spectral types (BAF, GK and M stars). They will be used for the following statistical analysis of the survey.

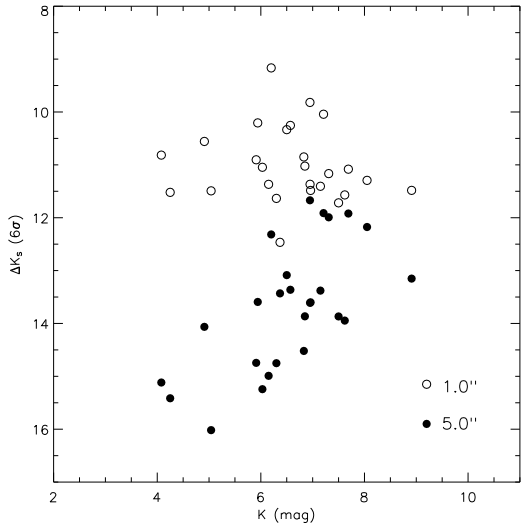


Figure 5.4: VLT/NACO coronagraphic detection limits in $K_s$-band as a function of the primary star brightness for two angular separations ($1.0''$ and $5.0''$). Two regimes can be seen; one at large separations (shown here at $5.0''$) when the detection is limited by detector read-out noise or background noise. The contrast varies then linearly with the primary $K_s$ apparent magnitude due to the flux normalization; a second regime at shorter separations (shown here at $1.0''$) when the detection is speckle noise limited. Instrumental quasi-static speckles are expected to dominate random, short-lived atmospheric speckles and the contrast remains relatively constant over a wide range of primary $K_s$ apparent magnitudes.

At large separations ($\geq 1.0 - 2.0''$) from the star where observations are limited by detector read-out noise or background noise, the contrast

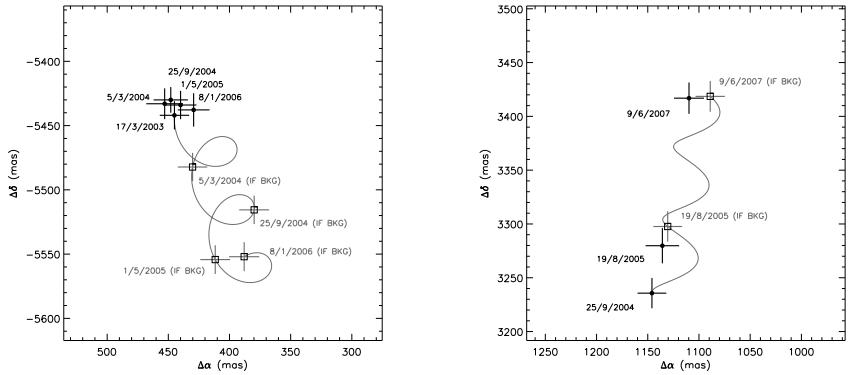


Figure 5.5: VLT/NACO Measurements (*full circles* with uncertainties) of the offset positions of the comoving companion AB Pic b to A (*left*) and of the CC relative to 0ES1847 (*right*). For each diagram, the expected variation of offset positions, if the candidate is a background object, is shown (*solid line*). The variation is estimated based on the parallactic and proper motions of the primary star, as well as the initial offset position of the CC from A. The *empty boxes* give the corresponding expected offset positions of a background object for the different epochs of observations (with uncertainties). In the case of AB Pic b, the relative positions do not change with time confirming that AB Pic b is comoving. On the contrary, the relative position of the CC to 0ES1847 varies in time as predicted for a background stationary contaminant. For our sample, astrometric follow-up over 1-2 years enabled a rapid identification.

variation with the primary spectral type is actually related to the primary nIR brightness. In Fig. 5.4 we shows the case of $K_s$-band detection limits at 5.0″ as a function of the primary $K_s$ apparent magnitude. The contrast varies linearly due to the flux normalization. At shorter separations, the situation is more complex as AO deep images are actually limited by the speckle noise. In this region our detection limits remain constant over a wide range of primary $K_s$ apparent magnitudes.

All published deep imaging surveys dedicated to planet search (Masciadri et al. 2005; Kasper et al. 2007; Lafrenière et al. 2007; Biller et al. 2007), including this one, derived detection threshold assuming that the residual noise in the final processed image follows a Gaussian intensity distribution. A typical detection threshold at 5 or 6 $\sigma$ is then usually assumed over the complete angular range. The approximation of a Gaussian distribution for the residual noise is valid within the detector read-out noise or background noise regime, however the careful analysis by Marois et al. (2009) shows that this is not adequate at small separations when speckle

noise dominate (typically $\leq 1.0 - 2.0''$ in our survey; see Fig. 5.5). In this regime, AO deep images are actually not limited by random, short-lived atmospheric speckles, but by instrumental quasi-static speckles. A non-Gaussian distribution of the residual noise must be taken into account to specify a detection threshold at a given confidence level. Therefore, our current 6 $\sigma$ detection threshold at small separations is probably too optimistic. However, the systematic error induced in our sensitivity limits is probably of lower significance than uncertainties in planet age and use of uncalibrated planet evolutionary models as described below.

## 5.5 STATISTICAL ANALYSIS

For the statistical analysis of our survey results we'll use the *statistical analysis mode* (SAM, see Sec. 4.7.1). of MESS, considering the specific case of a null detection.

The star sample used in the statistical analysis is composed of 65 stars observed in coronagraphic imaging mode (see Table B and B.2). Binaries that could impact the presence of a planet within a range of projected separation of $a = [5 - 150]$ AU were removed. Apparent magnitude, distance, age and mass are the prime simulation parameters. Due to the large spectral type dispersion of our sample, we have included in addition a planet mass dependency on primary mass.

We started converting the detection magnitude limits to masses using COND03 and DUSTY evolutionary models of Chabrier et al. (2000) and Baraffe et al. (2003). COND03 models are most adequate to predict properties of cool ($\leq$ 1700 K) subsets objects, whereas DUSTY model predictions were considered for hotter temperatures. Based on our (6$\sigma$) individual detection limits and target (distance, age, $H$ or $K_s$-band magnitude) properties, we derived the space of predicted masses and projected physical separation explored around each star of the sample (see histogram in Fig. 5.6).



Figure 5.6: Histogram of projected physical separations explored, for various planetary masses (1, 3, 5, 7, 10 and 13) $M_{Jup}$, in the close vicinity of the 65 young, nearby stars observed with NACO at VLT in coronagraphy. Contrast performances have been converted into masses based on the nIR photometry, age and distance of the primary stars.

### 5.5.1 *Extrapolating radial velocity distributions*

As a starting point, we used the mass and period distributions derived by Cumming et al. (2008) with $\alpha = -1.31$ and $\beta = -0.74$. We considered a giant planet frequency of 8.5% in the range $0.3 - 15$ for periods less than 1986 days ($\leq$ 3 AU for a 1 host star). The resulting value is consistent with RV studies of Marcy et al. (2005). Running several sets of simulations, we explored independently the influence of period, planet mass and primary mass distributions on the non-detection probability determined as a function of the period cut-off. The period cut-off was chosen to correspond to a semi-major axis cut-off between 20 and 150 AU. The results are reported in Fig. 5.7, where we show the impact of the variation of planet mass power law index $\alpha$ (fixing $\beta = -0.74$ and $\gamma = 0.0$, *Top* panel), of the period power law index $\beta$ (with $\alpha = -1.31$ and $\gamma = 0.0$ *Middle panel*), and the evolution implied by a planet mass dependency with the primary mass when $\gamma$ varies (and $\alpha = -1.31$ and $\beta = -0.74$ *Bottom* panel). As reference, extrapolated distributions by **??** are reported in *thick solid* lines in all panels of Fig. 5.7. This figure shows that the non-detection probability of our survey as a function of the period cut-off is more sensitive to the variation of $\beta$, the period power law index. Some values of $\beta$ can be excluded with high confidence level for large semi-major axis cut-off. In comparison, the influence of $\alpha$ and $\gamma$ remains limited under the current assumptions.

### 5.5.2 *Exoplanet fraction upper limit*

In this section we use MESS to determine $\langle p_j \rangle$, the survey mean probability of detecting a planet if present around each star of our sample and $f_{\max}$, the maximum value of the frequency of giant planet expected for a given confidence level. We consider the period and mass power law indexes from Cumming et al. (2008) $\alpha = -1.31$, $\beta = -0.74$ and $\gamma = 1.25$ for the period and mass distribution of giant planet. Then, we set the confidence level CL $= 0.95$.

The survey mean detection probability and $f_{\max}$ are reported in Fig. 5.8. It is important to note that both results depend on the assumed (mass, period, eccentricity) distributions of the giant planet population. Similar to other deep imaging surveys, our study begins to constrain the fraction of stars with giant planets to less than 10% for semi-major axes larger than

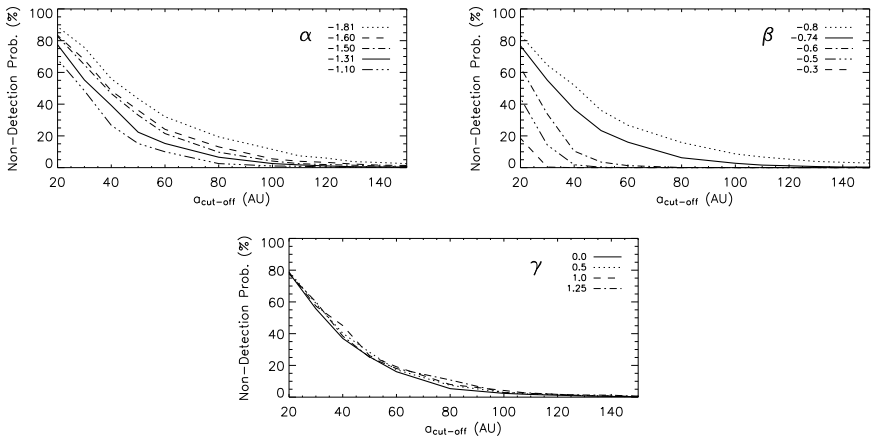


Figure 5.7: Non-detection probability for our survey, based on various sets of period and mass distributions as a function of the semi-major axis cut-off of the period distribution. Mass and period distributions are extrapolated and normalized from RV studies. *Top:* Variation of the non-detection probability with $\alpha$ and fixing $\beta = -0.74$ and $\gamma = 0.0$. *Middle:* Variation of the non-detection probability with $\beta$ and fixing $\alpha = -1.31$ and $\gamma = 0.0$. *Bottom:* Variation with $\gamma$ a planet mass scaling with the primary mass and fixing $\alpha = -1.31$ and $\beta = -0.74$.

typically 40 AU for this specific set of period, mass and eccentricity distributions. We also see that we barely constrain the fraction of 1 planets potentially detectable for 24% of our targets (67% for the 3 planets). Increasing the sample size will enable refinement of the statistical constraints on the upper limits of the fraction of stars with giant planets as a function of their mass and semi-major axis. However, a number of intrinsic limitations (detection threshold, age determination and model calibration) prevent to draw more robust conclusions. We plan to gather detection performances from multiple surveys in order to refine our knowledge of the occurrence of giant planets at wide orbits ($>$ 10 AU) and thus complement RV survey results.

## 5.6 LIMITATIONS

As mentioned above, several issues limit the reliability of our conclusions. The age determination of the young, nearby stars and the use of uncalibrated evolutionary models are the main limitations that directly impact the estimation of the explored planetary masses from observed luminosities.

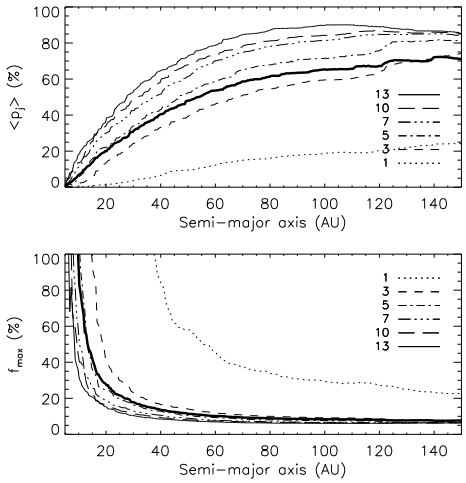


Figure 5.8: *Top:* Survey mean detection probability derived as a function of semi-major axis assuming parametric mass and period distributions derived by Cumming et al. (2008), i.e with $\alpha = -1.31$, $\beta = -0.74$ and $\gamma = 1.25$. The results are reported for individual masses: 1, 3, 5, 7, 10 and 13 . The integrated probability for the planetary mass regime is shown with the *thick solid* line. *Bottom:* Planet fraction upper limit derived as a function of semi-major axis, given the same mass and period distributions.

### 5.6.1 *Age determination*

Ages of young stars near the Sun may be determined trough photometric, spectroscopic and kinematics studies; various diagnostics are commonly used, depending on the spectral type and age of a given star. In general, the most reliable ages are obtained for stars that can be placed reliably into a moving group or association.

Our sample is composed of 88 stars, including 51 members of known young, nearby associations (TWA, $\beta$ Pic, Tuc-Hor and AB Dor). Ages for the TWA and $\beta$ Pic associations are reasonably well constrained by various and independent (stellar properties characterization and dynamical trace-back) studies to: $8^{+4}_{-3}$ Myr (TWA de la Reza et al. 2006; Barrado Y Navascués 2006; Scholz et al. 2007) and $12^{+8}_{-4}$ Myr ($\beta$ Pic Zuckerman et al. 2001a; Ortega et al. 2004) respectively. Isochrones, lithium depletion and X-ray luminosities indicate an age of 30 Myr for Tuc-Hor (Zuckerman et al. 2001b). The age of the AB Dor association is in some dispute (see Zuckerman et al. 2004; Luhman et al. 2005; Luhman & Potter 2006; López-Santiago et al. 2006; Janson et al. 2007; Ortega et al. 2007; Close

et al. 2007; Boccaletti et al. 2008; Torres et al. 2008). In our simulations, we have assumed an age of 70 Myr for stars of this association.

Our statistical analysis is focused on 65 stars observed in coronagraphic imaging mode. Of these 45 are confirmed members of known associations while 17 are young star candidates, currently not identified as members of any kinematic group which makes an age estimate particularly difficult. An excellent example of a young star not known to be a member of the above listed moving groups is HR 8799, identified by Marois et al (2008b) as orbited by 3 giant planets, but with an age uncertain between 30 and 160 Myr. In our analysis, age is directly used to convert the detection limits to mass using evolutionary models. Therefore, age determination remains a main limitation in this work and for similar works aimed to constrain reliably the properties of a putative population of giant planets around young, nearby stars.

### 5.6.2 *Evolutionary models*

Evolutionary model predictions are commonly used to infer subsets masses from observed luminosities We used this approach to convert our survey detection performances into planetary mass limits. Models consider the idealized description of non-accreting systems contracting at large initial radii for stars and brown dwarfs formed by gravitational collapse and fragmentation. Assumption about the amount of remaining circumstellar material, accretion and initial conditions imply that comparisons between observations and models are quite uncertain at young ages ($\leq$ 100 Myr Baraffe et al. 2002). This could be even worse for young giant planets. The implementation of the core-accretion mechanism as initial conditions for evolutionary calculation could substantially modify the model predictions (Marley et al. 2007). Massive giant planets might be significantly fainter than equal-mass objects formed in isolation via gravitational collapse. However, a critical issue is the treatment of the accretion shock through which most of the giant planet mass is processed and which remains highly uncertain. In previous analyses of survey detection performances, only predictions from Chabrier et al. (2000) and Baraffe et al. (2003) models were used. Use of Burrows et al. (2003) , assuming the same initial conditions, does not change significantly the results Nielsen et al. (2008)

## 5.7 CONCLUSIONS

We presented here the results of the statistical analysis of the results a deep adaptive optics imaging survey with NACO at the VLT of 88 nearby stars of the southern hemisphere, as a result of the use of the *statistical analysis mode* of MESS (see Sec. 4.7.1). The sample was selected favouring youth ($\leq$ 100 Myr) and proximity to Earth ($\leq$ 100 pc) to optimize the detection of close planetary mass companions. Known visual binaries were excluded to avoid degrading the NACO AO and/or coronagraphic detection performances. Within our sample, 51 stars are members of young, nearby comoving groups. 32 stars are young and nearby objects currently not identified as members of any known association, and 5 stars have been reclassified as older ($\geq$ 100 Myr) systems. The spectral types cover the sequence from B to M spectral types with 19% BAF stars, 48% GK stars and 33% M dwarfs. The separation investigated typically ranges between 0.1″ to 10″, i.e. between approximately 10 to 500 AU. We selected 65 stars of our sample that were observed in deep coronagraphic imaging, with contrast performances to $10^{-6}$ and thus sensitive to planetary mass companions down to 1 $M_{Jup}$ (at 24% of our sample) and 3 $M_{jup}$ (at 67%). For those objects, the use of the complete set of detection limits enabled us to constrain various mass, period and eccentricity distributions of giant planets extrapolated and normalized from RV surveys at large semi-major axes, from 20 to a few 100 AU,. This allowed us deriving limits on the occurrence of giant planets for a given set of physical and orbital distributions. The survey constrain significantly the population of giant planet for masses $\geq 3$ $_{Jup}$.

In the first few years following the discovery of the companion to 2M1207 (Chauvin et al. 2004), all planetary mass companions discovered by direct imaging technique were at relatively wide separations or with small mass ratio with their primaries. However, the recent discoveries of planetary mass objects around the star Fomalhaut (Kalas et al. 2008), HR 8799 Marois et al. (2009) and $\beta$ Pictoris Lagrange et al. (2008), now open a new era for the deep imaging study of giant planets that probably formed like those of our solar system. In the perspective of ongoing and future deep imaging instruments either from the ground (Gemini/NICI, Subaru/HiCIAO, SPHERE, GPI, EPICS) or from space (JWST, TPF/Darwin), this work represents a pioneer successful study, providing, with other surveys, precise information (stellar and sub stellar multiplicity, non-detections and background contaminants) to better characterize

the overall environment of young, nearby stars, that will be prime targets for future exoplanets search.

# 6

# 2D ANALYSIS OF SINGLE OBJECTS

*adapted from "Searching for sub stellar companions into the LkCa 15 proto-planetary disk " Bonavita et al. 2009 A&A submitted*

The following sections will present the use of MESS to analyze the outcomes of NACO observations of the young star LkCa 15 (Piétu et al. 2006, see). These data were taken using a four quadrant phase mask coronagraph, which aims at offering enhanced detection performances at small angular separations. The goal of this program was to constraint the characteristic of the companion responsible for the large gap in the disk that surrounds LkCa 15, that was observed at mm wavelengths.

## 6.1 LKCA15

LkCa 15 ($V = 12.09$, $K = 8.16$, K5 and $d \sim 140$ pc) is a T Tauri star with an age of $\sim 3 - 5$ Myr (see Simon et al. 2000), located in a hole of the Taurus molecular cloud. Piétu et al. (2006) performed sub-mm observations of the protoplanetary disk of LkCa 15, using the Plateau de Bure interferometer with an angular resolution of about $0.4''$. The observations were made in "track-sharing", observing LkCa 15 and the Herbig star MWC 480 with a common calibration curve. Any morphological difference between the two targets was thus considered to be genuine. They found a clear inner hole around LkCa 15 while the interferogram of MWC 480 is centrally peaked. This is consistent with that produced by an appropriate modeling of the data, which suggests a inner hole with radius $\sim 46$ AU (i.e. the size of our own Solar System). A multi isotopes analysis of CO rotational lines allowed Piétu et al. (2007) deriving the physical properties of the outer circumstellar disk surrounding the star. Contrary to the other system studied in a similar way, no clear vertical temperature gradient was found in the disk structure, possibly due to the peculiar geometry of the LkCa 15 disk.

Piétu et al. (2006) discussed the possible mechanisms that could explain the inner hole structure (which is not completely empty, as some IR excess is present above the stellar black body, see Bergin et al. 2004). The presence of a low-mass companion seems to be a plausible explanation since the LkCa15 disk is quite massive. In fact Simon et al. (2000)

Table 6.1: Physical parameters for the LkCa15 proto-planetary disk reported by Piétu et al. (2007)

| | |
|---|---|
| Orientation, PA (deg) | $151 \pm 3$ |
| Inclination, i (deg) | $49 \pm 3$ |
| $R_{Int}$ (AU) | $46 \pm 3$ |
| $R_{Out}$ (AU) | $177 \pm 12$ |
| Surface density at 100 AU (g.cm$^{-2}$) | $3.1 \pm 0.4$ |
| $M_{Disk}$ $(M_{\odot})$ | 0.029 |
| Temperature at 100 AU (K) | $22 \pm 1$ |

estimated, from the kinematics, a total mass for the system of $M_{\rm dyn} = 1.0 \pm 0.1 M_{\odot}$. This set the maximal mass of the putative companion to 0.2 $M_{\odot}$, since the mass of LkCa 15 could hardly be less than 0.8 $M_{\odot}$, due to its spectral type. Additional results obtained by Alexander et al. (2006) also suggest that alternative mechanisms such as photo-evaporation are unlikely to be effective. In fact the disk density is significantly higher than that expected if the photo-evaporation starts propagating beyond 20-30 AU. Piétu et al. (2006) suggested that a $\sim 5 - 10 M_{\rm Jup}$ planet orbiting at 30 AU would be sufficient to evacuate the inner 50 AU of the LkCa 15 disk. Similar conclusions were reached by Espaillat et al. (2007) from the modeling of the SED of LkCa 15 obtained from Spitzer observations. Their analysis suggests that a gap is present in the disk of LkCa 15, with an inner disk going from 0.12-0.15 AU to 4-5 AU, and an outer disk of inner radius 46 AU, in perfect agreement with the findings of Piétu et al. (2006). They also concluded that planetary formation or the presence of a close-in stellar or sub-stellar companion are the most probable explanations for the circumstellar material shape around LkCa15.

In the following, we will discuss NACO observations aiming to constrain the mass of this putative sub-stellar companion.

## 6.2 OBSERVATIONS

### 6.2.1 *Telescope and instrument*

The observations were performed on December 26th, 2007 at ESO/Paranal, using NACO, the AO-assisted near-IR camera NAOS-CONICA (Rous-

set et al. 2003) mounted on one of the Nasmyth focus of the UT4 8m-telescope. Among the numerous NACO observing modes (Lenzen et al. 2003), both the classical and coronagraphic imaging were used.

Coronagraphic observations were performed with the four-quadrant phase mask (4QPM) optimized for $K_S$ band observations. The S13 objective (FoV of $14'' \times 14''$ and plate-scale of 13.25 mas/pixel) was chosen for a more precise centering with the 4QPM and a better sampling of the PSF. The 4QPM splits the focal plane into four equal areas, two of these being phase-shifted by $\pi$. As a consequence, a destructive interference occurs in the relayed pupil, where the on-axis starlight rejected at the edge of the geometric pupil is filtered by a Lyot stop (being a circular hole 90% of the pupil size). The advantage over the classical Lyot mask is the possibility to access inner angular separations smaller than $0.35''$ (the smallest NaCo occulting mask) at relatively large contrast (see Boccaletti et al. 2004, 2008).

However, a significant part of the starlight is left in the focal plane due to uncorrected aberrations composed with a dynamical halo averaging over time plus a quasi-static halo corresponding to optical aberrations along the optical train (from telescope to detector). To mitigate this last problem, a coronagraphic image of a reference star was taken just after our science target observations, with the same instrumental settings, to serve for speckle calibration in an image-subtraction process. This reference star (BD + 22 729, $V = 11.5$, $K = 7.9$) has similar visible and NIR magnitudes to ensure similar AO correction and signal-to-noise at the detector. Moreover, observations of this reference star were performed at suitable time to match the parallactic angle with LkCa15 observations. In this way the the two observations have the same instrumental pupil configuration. This allows to optimize the overlap of the speckle pattern and diffraction spikes position in the two images, resulting in a better final subtracted image of the halo around LkCa15.

### 6.2.2 *Observing strategy*

The coronagraphic observations were preceded by a classical imaging sequence that provides a photometric reference. A neutral density was used to avoid detector saturation. Table 6.2 summarizes the observing parameters. During the coronagraphic observing sequence, the precise centering of the science target behind the focal plane mask was critical

Table 6.2: Observing parameters used for each source, observed in classical and coronagraphic imaging. The individual integration time ($t_{\rm int}$), the number of frames (Nframes) averaged by the detector and the number of repeated exposures ($N_{\rm exp}$) are reported on source and on sky. At the end, $N_{\rm exp}$ give the number of images available for the data reduction and analysis.

| Object | LkCa15 (Classical) | LkCa 15 (Coronagr.) | BD +22 729 (Coronagr.) |
|---|---|---|---|
| Filter | $ND + NB_{2.17}$ | $K_s$ | $K_s$ |
| Objective | S13 | S13 | S13 |
| $t_{\rm int}$ (s) | 30 | 24 | 24 |
| $N_{frame} \times N_{exp}$ | $2 \times 1$ | $4 \times 8$ | $4 \times 8$ |
| $t_{\rm int}$[sky](s) | 30 | 24 | 24 |
| $N_{frame} \times N_{exp}$[sky] | $2 \times 1$ | $4 \times 1$ | $4 \times 1$ |

to maximize the central star attenuation. To allow applying the angular differential imaging, the coronagraphic observations were acquired at two instrument positions rotated by 33°. Sky images were observed for LkCa15 and its reference immediately after each coronagraphic sequence.

## 6.3 DATA REDUCTION AND ANALYSIS

### 6.3.1 *Image processing and selection*

The data were processed using the Eclipse [1] reduction software (Devillard 1997) for bad pixel correction, flat fielding and sky subtraction. Individual frames were inspected by eye to remove all low-quality images degraded by waffle aberrations or variable AO corrections. Finally, only the images of LkCa15 and BD + 22 729 with similar parallactic angles were selected to optimize our PSF-subtraction. The upper panel of Fig. 6.1 shows the parallactic angle variations as a function of UT time during our observations for each source and each rotator position. The lower panel of the same Figure shows the time dependence of the coherent energy, which depends on air-mass, seeing, and turbulence correlation time. Among the initial data set of 8 images per source and per rotator position, only 3 were kept after the selection process totaling an integration time of 288 seconds (filled symbols in Fig. 6.1).

[1] http://www.eso.org/projects/aot/eclipse/

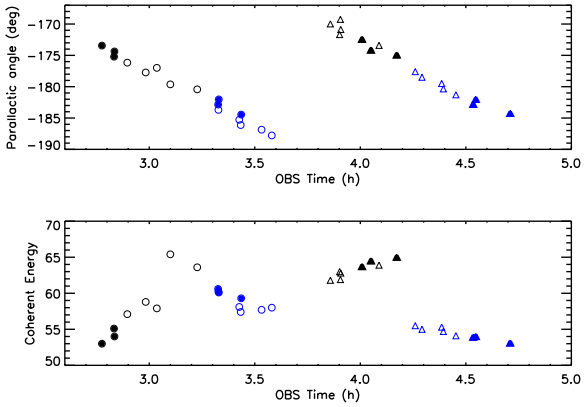


Figure 6.1: Summary of the variation of the observing parameters from LkCa 15 (circles) and the reference (triangles), both for $PA = 0°$ (black symbols) and $PA = 33°$ (blue symbols). The values of the images chosen for the scientific analysis are plotted with filled symbols.

### 6.3.2 *Subtraction of the diffraction residuals*

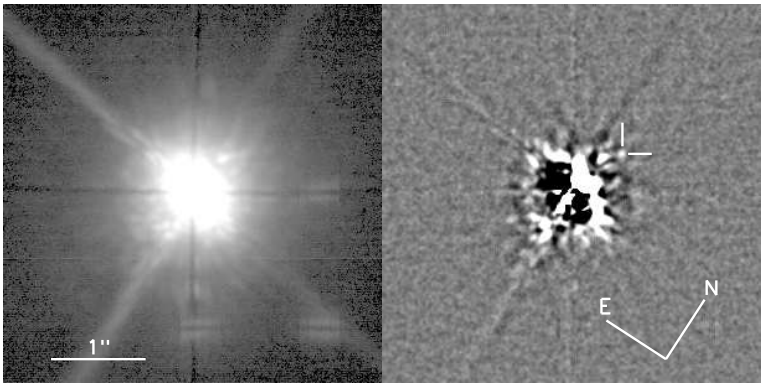


Figure 6.2: LkCa15 coronagraphic image at a rotator position of 33° before (left panel) and after (right panel) the reference image subtraction. Field of view is 4″ and the display is not linear.

Next step was to properly subtract the stellar contribution from the LkCa15 images. For each rotator and parallactic angle position, the reference star was shifted at a 0.1-pixel accuracy, scaled and subtracted to minimize the residuals. An IDL custom-made tool was used to rapidly converge to an acceptable shift and scaling solution. Alternatively, a resid-

ual minimization using the AMOEBA[2] function was applied giving consistent results. The right panel of Fig. 6.2 shows the result of the single image-subtraction image of LkCa15 at a rotator position of 33° corresponding to the set that provides the best contrast.

Additionally, we took advantage of the observations taken at two rotator positions to :

1. explore dead zones hidden by the secondary spikes and the coronagraphic mask transition;
2. derotate and sum to average speckles and increase the final signal-to-noise;
3. subtract images taken at different angles to remove the non rotating aberrations (related to static optics in NACO) and possibly reveal a positive-negative signature expected for a true companion (and not for instrumental residuals).

All sets of single, double-subtracted and derotated-averaged images were finally compared to identify the most performing ones at different angular separations.

### 6.3.3 *Detection limit*

pixel-to-pixel 2D noise maps were estimated, on our single, double subtracted and derotated averaged images of LkCa15, using a sliding box of $5 \times 5$ pixels over the whole NACO FoV, as in Lagrange et al. (2008). The 6 $\sigma$ detection limit maps were obtained after renormalization by the LkCa15 images acquired in classical imaging. This renormalization took into account all corrections related to the use of different optical set-ups: exposure times (see Table 6.2), neutral density and Lyot-stop transmissions (a factor of 89 and 0.808 respectively,according to Boccaletti et al. 2008) and $NB_{2.17}$ to $K_s$ filter transformation.

The great advantage offered by a 2D-detection limit map is to use all available spatial information to better constrain the region around LkCa15. Fig. 6.3 (top) gives the 1D-detection limits estimated at four angular directions to illustrate the azimuthal variation. Fig. 6.3 (bottom) shows the 1D-detection limits estimated for the single subtracted images at 0° and 33°, the double-subtracted and the derotated-averaged

[2] *http : //www.physics.nyu.edu/grierlab/idl_html_help/A8.htmlwp992475*

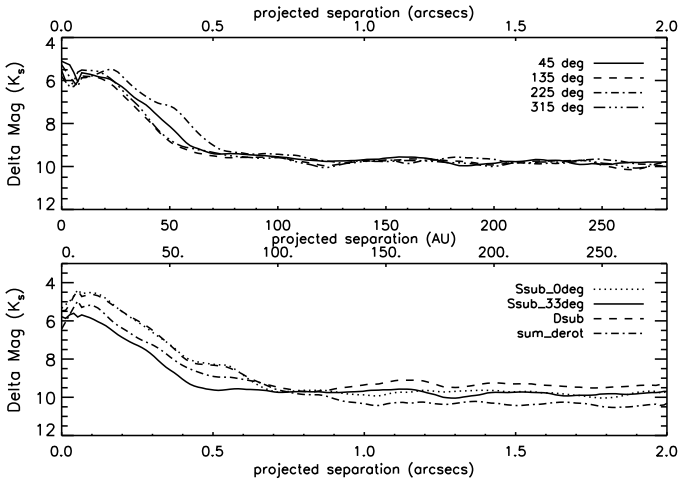


Figure 6.3: **Upper panel:** Comparison of different 1D detection limits extracted at 4 different directions from the 2D map (the single subtracted image at 33° is used as example). **Lower panel:** Comparison between 1D-limits estimated from images obtained with different subtraction and derotated methods.

images of LkCa15. It comes out that the single- subtracted image at 33° (Ssub_33deg: solid line) assures the best detection limit at close angular separations (up to $\rho \sim 0.7''$), due to the excellent and stable atmospheric conditions over the whole sequence (see Fig. 6.1). At larger distances, that are background-noise limited, the derotated-averaged image (sum_derot: dashed-dotted line) appears naturally as the most performing one. Our final choice was therefore to use a composite map (see Fig. 6.4) of both 2D-detection limit maps to optimize the detection performances over the complete NaCo field of view.

Finally, we also took into account that the presence of the four-quadrant mask causes an attenuation of the off-axis objects due to the 4QPM transition, decreasing our sensitivity close to the axis (Boccaletti et al. 2004).

## 6.4 RESULTS

### 6.4.1 *Null-detection in the central hole*

As it is shown in Fig. 6.3, the best contrast is achieved with the single subtracted image at a position angle of 33° for angular separation closer than 0.7″ (corresponding to a projected distance 98 AU).

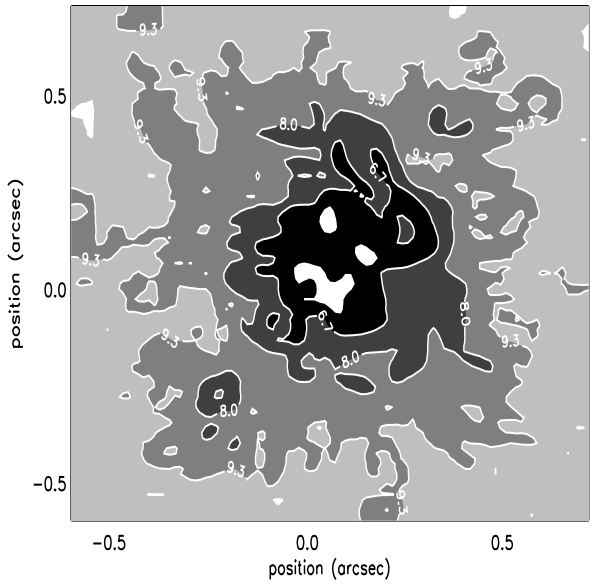


Figure 6.4: $K_s$ Composite $\Delta Mag$ ($K_S$ Band) 2D-Map obtained using the single-subtracted image at 33° (up to 0.6″) and the derotated-averaged image (at larger distances).

No evidence of a point-like object was found in any of our image-subtracted sets at separations corresponding to the central hole ($\rho < 0.33''$). The azimuthal averaged contrast places a limit of $\Delta K_s = 7$mag equivalent to about $12 M_J$ for a hypothetical projected distance of 30 AU. A statistical approach of this detection limit is analyzed thoroughly in section 6.4.2.

We also searched for point-like objects at separations that are not compatible with the presence of the central hole. We found a low significant point-source at a separation of $\rho = (0.67 \pm 0.02)''$ at a position angle of $PA = (340.7 \pm 0.3)^\circ$. Although close to the detection limit, this point-source lies at the boundary between the speckle and the background noise regimes and is then visible in the subtracted image of Fig. 6.2. We coarsely estimated a contrast of $\Delta K_s = 10.2$mag in a 5 pixels aperture. Error bars were not estimated as the point-source is quite close to the noise level (less than $6\sigma$ if we refer to Fig. 6.3), so that the previous contrast value should be taken with caution.

There are a number of artifacts that may produce such patterns like waffle and spiders. The nearest spider spike of which the trace is still

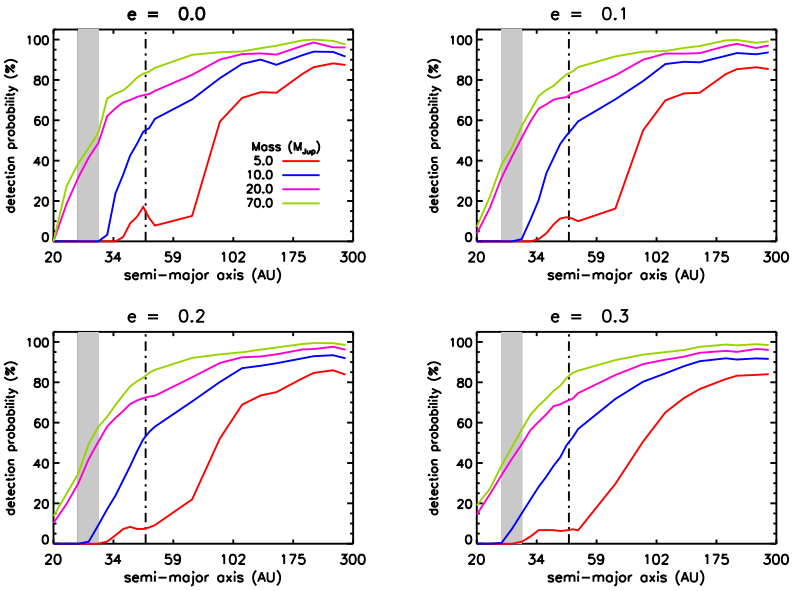


Figure 6.5: Detection probability as a function of the semi-major axis $a$, for different values of planetary mass, and fixing inclination $i = 49^o$ and the longitude of the ascending node $\Omega = 151 \pm 90^o$ according with the disk properties.

visible in Fig. 6.2 is offset by 25° while the waffle mode appears in a 45° direction at a position of 0.49″ therefore not compatible with the location of this point-source. However, the point source is not visible in the subtracted image obtained for the 0° rotator position while at such separation the detection limit is almost similar for both rotator positions (see Fig. 6.3). In the image, the point-source would be at about 0.2″ from the vertical 4QPM transition and slightly attenuated. As it is difficult to rule out such a structure as due to the speckle pattern, additional observations are mandatory to test the presence of this potentially low-mass object.

### 6.4.2 *Companion mass and orbital parameters*

In this section we discuss the implication of our null detection on the mass of the putative planet around LkCa15. To this purpose, we compared our observations with simulations performed with MESS.

#### 6.4.2.1 *Simulation description*

A first step is to convert our 6 $\sigma$ detection limit map in terms of minimum mass map. This is usually done considering the star apparent magnitude in the $K_s$-band and its distance, and use the evolutionary model predictions at the age of the system to convert the absolute magnitude limits derived in the NACO filters in masses. We have considered here an age of 4 Myr and a distance of 140 pc for LkCa15. We then considered two classes of evolutionary models based on different assumptions on the initial conditions: Hot Start models considering an initial spherical contracting state (Chabrier et al. 2000; Baraffe et al. 2003; Saumon & Marley 2008) and core accretion models coupling planetary thermal evolution to the predicted core mass and thermal structure of a core-accretion planet formation model (Marley et al. 2007; Fortney et al. 2008). In the case of the core-accretion model predictions, our detection performances do not allow to access the planetary mass regime at all. Massive hot Jupiters are indeed predicted to be much fainter at young ages (Marley et al. 2007). Therefore, detectable mass maps were determined using Hot Start model predictions over the planetary and brown dwarf mass regime.

In a second step we used our minimum detectable mass maps to calculate the detection probability ($P_{\rm D}$) of companions of various masses and orbital parameters (semi-major axis $a$, eccentricities $e$, inclination $i$, longitude of the ascending node $\Omega$, longitude of periastron $\omega$ and time of periastron passage $T_p$). Considering the disk properties (inclination, position angle and inner radius), different assumptions can be made to fix partially the companion orbital properties. The rest of the orbital parameters can be randomly generated. The projected position of the simulated companion on the sky is compared to our minimum detectable mass map to test its detectability. Running the simulation 10.000 times for a given set of mass and orbital parameters enables to derive a detection probability.

The smallest projected physical separation probed around LkCa15 is limited by the 4QPM coronagraph attenuation inside 0.15" (equivalent to 3 times the angular resolution), setting the minimum semi-major axis considered in our simulations to 20 AU. Projected physical separations as large as 1000 AU are explored, but we decided to restrain our study to the close circumstellar environment considering semi-major axis a = [20,280] AU. Additionally, we limited the parameters space explored to $M = [3, 100]$ $M_{\rm Jup}$ and eccentricity $e = [0., 0.3]$.

#### 6.4.2.2 *Results*

In Fig. 6.5, we have reported the most constraining case of an inclination and a longitude of the ascending node fixed by the disk properties: $i_{Disk} = 49^o$ and $\Omega = PA_{Disk} \pm 90^o (= 151 \pm 90)$. In each panel the results for different values of eccentricity are shown , spanning from 0 (upper-left panel) to 0.3 (lower-right panel). The shaded area gives the range of semi-major axis estimated for the predicted planetary companion (25-30 AU, see Piétu et al. 2006), the dashed-dotted line indicates the inner radius of the disk (46 AU).

Following the results showed in Fig. 6.5, any low stellar mass companion with masses larger than $M \geq 70\ M_{Jup}$ should have been detected with $P_{\rm D} = 55\%$ and 85% for semi-major axis $a = 30$ and 46 AU. The probability goes up to 90% at more than 60 AU. In the case of a (brown dwarf) companion more massive than 20 $M_{Jup}$, we find $P_{\rm D} = 50\%$ and 70% at respectively $a = 30$ and 46 AU. Thus, in spite of the high angular resolution and sensitivity, our observations are not deep enough to provide strong constraints on the presence of planetary mass companions in the region appropriate to create the cavity (30 to 45 AU). Even companions more massive than 20 $M_{Jup}$ or above, cannot be excluded with high confidence level, although they are more unlikely than lower mass objects. At larger distances ($a > 100\ AU$) companions of any mass above 7 $M_{Jup}$ can be excluded with 70% probability.

Although we only explored low eccentricity solutions in a systematic way, the above results also provide lower limits on the detection probabilities for larger eccentricity values, as the time spent far from the star becomes progressively larger.

#### 6.4.2.3 *Limitations*

The main limitations of our analysis come from the conversion of our detection limits in terms of minimum detectable masses. They are related to the uncertainty in the age determination of LkCa15 and the use of non-calibrated evolutionary models for young ages and very low masses. By comparison, uncertainties on the system distance and $K_s$ apparent brightness are negligible. Age and model predictions are discussed below:

1. LkCa15 is a confirmed member of the Taurus-Auriga association, for which an age of 3–5 Myr is estimated (Simon et al. 2000). To explore how the age uncertainty affects our results, we ran similar

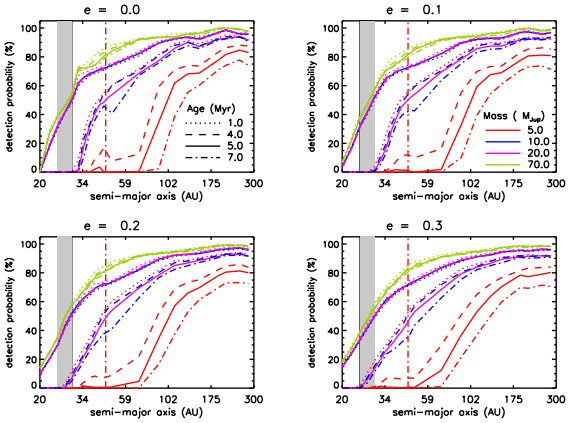


Figure 6.6: Results of the simulations (detection probability vs semi-major axis in AU) made assuming different ages for the mass-limit conversion. Only the cases of 5 $M_{Jup}$ (red curves), 10 $M_{Jup}$ (blue curves), 20 $M_{Jup}$ (purple curves) and 70 $M_{Jup}$ (light green curves), are showed.

simulations for ages of 1, 4 and 7 Myr. Fig. 6.6 shows the results of these runs for different companion masses: 5, 10, 20 and 70 $M_{Jup}$.

The impact of the age uncertainty is much more important in the planetary mass domain than in the brown dwarf regime of interest here. Consequently, it does not significantly affect our conclusions relative to the presence of a brown dwarf or low stellar mass companion in the inner disk cavity of LkCa15.

2. The applicability of evolution tracks of brown dwarfs at ages less than a few million years have been already cautioned by Baraffe et al. (2003). The role of the initial conditions has been also questioned by Marley et al. (2007), specifically for young giant planets where a connection between giant planet formation and evolution models seems mandatory. At the location of the LkCa15 inner disk cavity (between 20 and 46 AU), our 4QPM observations are not sensitive at all to apparent magnitudes predicted for planetary mass companions described by the core accretion start models. They are marginally sensitive to high planetary masses range with fluxes predicted by the Hot Start models. The strongest constraints are actually set in the brown dwarf regime for masses $M \geq 20$ $M_{Jup}$, where the Hot Start evolutionary models are more appropriate. Although these models still need to be more extensively calibrated for this range of masses and ages. Preliminary data using young calibrator

(Mohanty et al. 2004; Close et al. 2005; Stassun et al. 2006) suggests that their prediction are adequate at the level of accuracy obtained with this study. Our conclusions related to the probable presence of a brown dwarf or low mass star companion responsible for the inner hole detected in the LkCa15 disk remain then meaningful.

## 6.5 CONCLUSIONS

The T-Tauri star LkCa 15 was observed with VLT/NACO using the 4QPM coronagraph, reaching a contrast lower than 9.5 in $K_s$ band, at separations higher than $0.5''$. Our goal was the detection of a low-mass companion, with a mass spanning from 0.2 $M_\odot$ down to 5 $M_{Jup}$, which presence has been suggested as an explanation for the large cavity, evidenced by sub-millimeter observations, in the disk surrounding the star.

We do not report any positive detection of a close companion to the star LkCa15. Based on our detection limits and Hot Start evolutionary model predictions, we ran simulations to take into account that the presence of a putative companion enable us to constrain its mass and semi-major axis given reasonable assumptions from the disk geometry. We can exclude the existence of a low mass star and brown dwarf companion with a probability of 85% and 70% resp. at more than 46 AU. The confidence level goes down 50% in both cases at 30 AU. The planetary mass regime is only explored at larger semi-major axis where the existence of massive ($M \geq 5\ M_{Jup}$) planetary mass companions can be excluded with $P_{\rm D} = 70\%$ detection probability.

Limitations of our study are discussed. The LkCa15 age uncertainty does not affect much our conclusions in the case of low mass star and brown dwarf companions. Also and of the uncertainty related to the initial conditions adopted for the evolutionary model is particularly critical only in the planetary mass regime. Finally, in case of a true companion orbiting LkCa15 in the inner disk cavity, our observations would favor a planetary mass or low-mass brown dwarf companion, although more massive companions cannot be completely excluded with high detection probability.

Further deep imaging studies at the $5 - 50\ AU$ scale at a new epoch should provide complementary information to completely reject the existence of close stellar or brown dwarf companion to LkCa15 and pursue

the search for the putative companion that would be responsible for the disk geometry and inner cavity within 46 $AU$.

# BIBLIOGRAPHY


Alexander, R. D., Clarke, C. J., & Pringle, J. E. 2006, , 369, 229

Baraffe, I., Chabrier, G., Allard, F., & Hauschildt, P. H. 2002, A&A, 382, 563

Baraffe, I., Chabrier, G., Barman, T. S., Allard, F., & Hauschildt, P. H. 2003, A&A, 402, 701

Barrado Y Navascués, D. 2006, A&A, 459, 511

Bergin, E., Calvet, N., Sitko, M. L., et al. 2004, ApJL, 614, L133

Biller, B. A., Close, L. M., Masciadri, E., et al. 2007, ApJS, 173, 143

Boccaletti, A., Chauvin, G., Baudoz, P., & Beuzit, J.-L. 2008, A&A, 482, 939

Boccaletti, A., Riaud, P., Baudoz, P., et al. 2004, PASP, 116, 1061

Burrows, A., Sudarsky, D., & Lunine, J. I. 2003, ApJ, 596, 587

Chabrier, G., Baraffe, I., Allard, F., & Hauschildt, P. 2000, ApJ, 542, 464

Chauvin, G., Lagrange, A., Dumas, C., et al. 2004, A&A, 425, L29

Chauvin, G., Thomson, M., Dumas, C., et al. 2003, A&A, 404, 157

Close, L. M., Lenzen, R., Guirado, J. C., et al. 2005, Nature, 433, 286

Close, L. M., Thatte, N., Nielsen, E. L., et al. 2007, ApJ, 665, 736

de la Reza, R., Jilinski, E., & Ortega, V. G. 2006, , 131, 2609

Devillard, N. 1997, The Messenger, 87, 19

Espaillat, C., Calvet, N., D'Alessio, P., et al. 2007, ApJL, 670, L135

Fortney, J. J., Marley, M. S., Saumon, D., & Lodders, K. 2008, ApJ, 683, 1104

Janson, M., Brandner, W., Lenzen, R., et al. 2007, A&A, 462, 615

Kalas, P., Graham, J. R., Chiang, E., et al. 2008, Science, 322, 1345

Kasper, M., Apai, D., Janson, M., & Brandner, W. 2007, A&A, 472, 321

Lafrenière, D., Doyon, R., Marois, C., et al. 2007, ApJ, 670, 1367

Lagrange, A. ., Gratadour, D., Chauvin, G., et al. 2008, ArXiv e-prints

Lenzen, R., Hartung, M., Brandner, W., et al. 2003, in Presented at the Society of Photo-Optical Instrumentation Engineers (SPIE) Conference, Vol. 4841, Society of Photo-Optical Instrumentation Engineers (SPIE) Conference Series, ed. M. Iye & A. F. M. Moorwood, 944–952

Lenzen, R., Hofmann, R., Bizenberger, P., & Tusche, A. 1998, in Society of Photo-Optical Instrumentation Engineers (SPIE) Conference Series, Vol. 3354, Society of Photo-Optical Instrumentation Engineers (SPIE) Conference Series, ed. A. M. Fowler, 606–614

López-Santiago, J., Montes, D., Crespo-Chacón, I., & Fernández-Figueroa, M. J. 2006, ApJ, 643, 1160

Luhman, K. L. & Potter, D. 2006, ApJ, 638, 887

Luhman, K. L., Stauffer, J. R., & Mamajek, E. E. 2005, ApJl, 628, L69

Marley, M. S., Fortney, J. J., Hubickyj, O., Bodenheimer, P., & Lissauer, J. J. 2007, ApJ, 655, 541

Marois, C., Macintosh, B., Barman, T., et al. 2009, in American Astronomical Society Meeting Abstracts, Vol. 213, American Astronomical Society Meeting Abstracts, 319.07–+

Masciadri, E., Mundt, R., Henning, T., Alvarez, C., & Barrado y Navascués, D. 2005, ApJ, 625, 1004

Mohanty, S., Jayawardhana, R., Natta, A., et al. 2004, ApJL, 609, L33

Nielsen, E. L., Close, L. M., Biller, B. A., Masciadri, E., & Lenzen, R. 2008, ApJ, 674, 466

Ortega, V. G., de la Reza, R., Jilinski, E., & Bazzanella, B. 2004, ApJ, 609, 243

Ortega, V. G., Jilinski, E., de La Reza, R., & Bazzanella, B. 2007, , 377, 441

Piétu, V., Dutrey, A., & Guilloteau, S. 2007, A&A, 467, 163

Piétu, V., Dutrey, A., Guilloteau, S., Chapillon, E., & Pety, J. 2006, A&A, 460, L43

Rousset, G., Lacombe, F., Puget, P., et al. 2000, in Society of Photo-Optical Instrumentation Engineers (SPIE) Conference Series, Vol. 4007, Society of Photo-Optical Instrumentation Engineers (SPIE) Conference Series, ed. P. L. Wizinowich, 72–81

Rousset, G., Lacombe, F., Puget, P., et al. 2003, in Presented at the Society of Photo-Optical Instrumentation Engineers (SPIE) Conference, Vol. 4839, Society of Photo-Optical Instrumentation Engineers (SPIE) Conference Series, ed. P. L. Wizinowich & D. Bonaccini, 140–149

Saumon, D. & Marley, M. S. 2008, ApJ, 689, 1327

Scholz, A., Coffey, J., Brandeker, A., & Jayawardhana, R. 2007, ApJ, 662, 1254

Simon, M., Dutrey, A., & Guilloteau, S. 2000, ApJ, 545, 1034

Stassun, K. G., James, D. J., Montalban, J., & Jeffries, R. 2006, in NOAO Proposal ID #2006B-0099, 99–+

Torres, C. A. O., Quast, G. R., Melo, C. H. F., & Sterzik, M. F. 2008, Young Nearby Loose Associations, ed. B. Reipurth, 757–+

Zuckerman, B., Song, I., & Bessell, M. S. 2004, ApJL, 613, L65

Zuckerman, B., Song, I., Bessell, M. S., & Webb, R. A. 2001a, ApJl, 562, L87

Zuckerman, B., Song, I., & Webb, R. A. 2001b, ApJ, 559, 388

Part V

# APPLICATIONS II : PREDICTION OF FUTURE INSTRUMENT PERFORMANCES

In the previous part we showed the outcomes of the application of the *Statistical Analysis Mode* of MESS. These studies aimed starting to constrain the frequency of giant planets in wide orbits, their main limitation being the lack of informations on the behaviour of the distributions at high distances.

It is now becoming clear that the future High contrast imaging instrument have the potential to provide us the key to open us a door to an unexplored region of star planet separation and to shed light on these unknown far away worlds.

But it's not just a matter of detections. In fact coupling integral field spectrographs to extreme adaptive optic modules at the focus of 8m class telescopes (SPHERE for VLT and GPI for South Gemini), and in the future to ELTs (EPICS), would allow us to perform a first order characterization of the exoplanets themselves.

In this part we report the results of the application of the *Prediction Mode* of MESS to these future direct imaging facilities. The aim of the work is first of all to figure out what will be the contribute of these instruments to the sample of detected planets, which is growing fast, feed by the increasingly precise radial velocity instruments. Moreover, having a tool as versatile as MESS is, one can also try to define the requirements that these facilities have to fit, in order to reach their science goals, the ultimate of them being the detection and characterization of habitable earths.

# 7

# EVALUATION OF THE SPHERE-IFS DETECTION CAPABILITY

SPHERE, the ESO extra-solar planet imager for the VLT is aimed at the direct detection and spectral characterization of extra-solar planets. Its whole design is optimized towards reaching the highest contrast in a limited field of view and at short distances from the central star. SPHERE has passed its Final Design Review (FDR) in December 2008 and it is now in the manufacturing and integration phase.

Here we will present the results of the application of the 1D version of the *prediction mode* of MESS to evaluate the capabilities of the Integral Field Spectrograph (IFS) that will be one of the three science channels of SPHERE.

First we will briefly summarize the principal characteristics of SPHERE (Sec. 7.1), and its science goals (Sec. 7.2). Then we will focus on the IFS, describing its concept in detail (Sec. 7.3). In Sec. 7.4 we will finally show our results.

## 7.1 SPHERE: THE EXOSOLAR PLANET IMAGER FOR THE VLT

SPHERE (Spectro-Polarimetric High-contrast Exoplanets Research) is a second generation instrument for VLT optimized for high contrast imaging to be mounted at the Nasmyth focus of one of the VLT units (Fig. 7.1). Its prime objective is the discovery and study of new extra-solar giant planets orbiting nearby stars by direct imaging of their circumstellar environment. The challenge consists in the very high contrast between the host star and the planet ($> 12.5$ *mag*), at very small angular separations. The whole design of SPHERE is therefore optimized towards reaching the highest contrast in a limited field of view and at short distances from the central star.

SPHERE is constituted by a common path optics and three science channels (see Fig. 7.1):

1. The differential imaging camera (IRDIS),
2. The Integral Field Spectrograph (IFS)

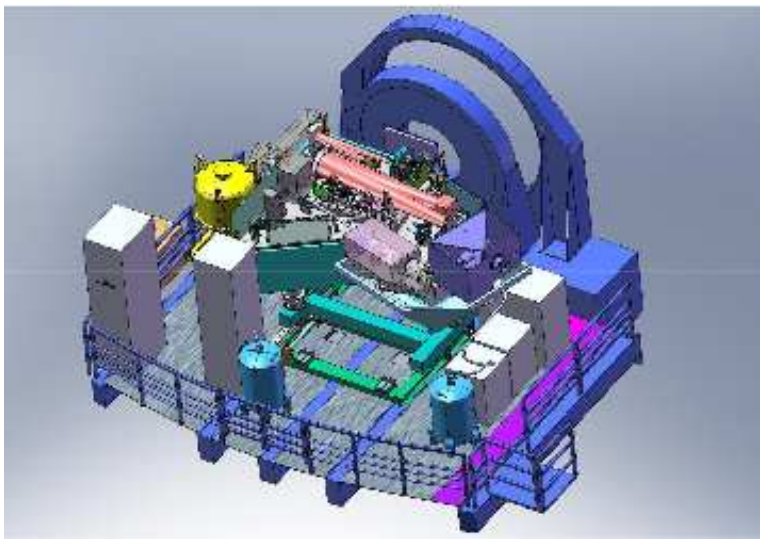

Figure 7.1: SPHERE implementation on the Nasmyth platform of the VLT

3. The visible imaging polarimetry (ZIMPOL)

The Common Path includes pupil stabilizing fore optics (tip-tilt and derotator) , calibration units, the SAXO extreme adaptive optics system, and NIR and visible coronagraphic devices. ZIMPOL shares the visible channel with the wavefront sensor through a beam splitter, which can be a grey (80% to ZIMPOL) beam splitter, a dichroic beam splitter, or a mirror (no ZIMPOL observations). IRDIS is the main science channel responsible for wide-field imaging in one or two simultaneous spectral bands or two orthogonal polarizations and low and medium resolution long slit spectroscopy. The IFS, working from 0.95 to 1.65 $\mu m$, provides low spectral resolution ($R \sim 30$) over a limited, 1.8x1.8 arcsecs, field-of-view. A photon sharing scheme has been agreed between IRDIS and IFS, allowing IFS to exploit the NIR range up to the J band ($R \sim 30$ in this case), leaving the H-band, judged optimal for the DBI mode, for IRDIS for the main observation mode. This multiplexing optimizes the observational efficiency. This global concept is illustrated in Fig. 7.1.

The key high level requirements derived from the science analysis and driving the design of the instrument are:

- High contrast capability to detect giant planets 15 magnitudes fainter than their host star at 0.5 arcsecs (for host stars with $J < 6$).

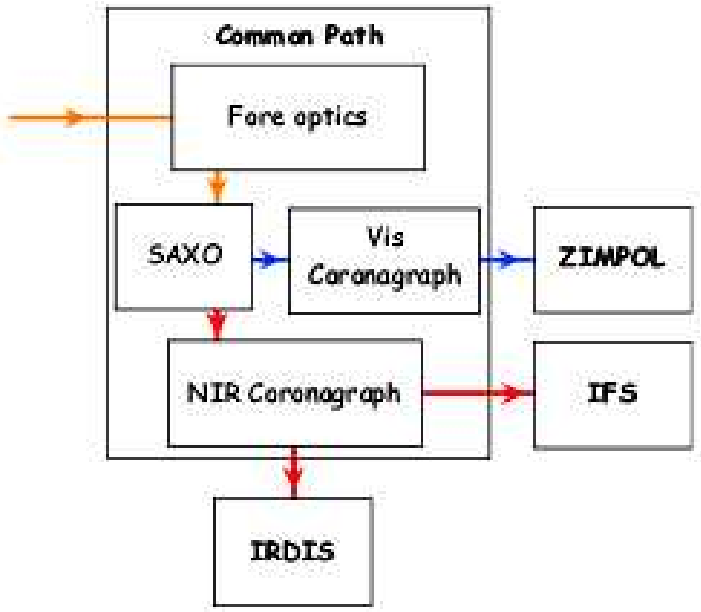


Figure 7.2: The four sub-systems of SPHERE. Optical beams are indicated in red for NIR, blue for visible and orange for CPI

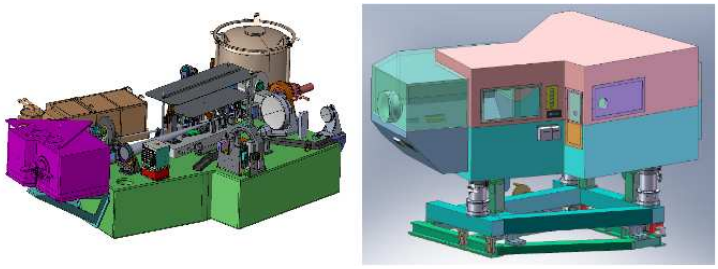

Figure 7.3: The view on the left shows the complete SPHERE opto-mechanical assembly. The view on the right shows how SPHERE will look like in operation, when the opto-mechanical assembly is mounted onto the vibration damping system and into the thermal-vacuum enclosure. To facilitate integration and operations, this enclosure has separate modules for the IFS and ZIMPOL mount, so that this instrument can be mounted and dismounted with limited impact.

- Access to very small angular separations, 0.1″ to 3″ from the host star.

- Optimal performance for targets up to visible magnitude $\sim 9$, for building a large enough target list (several hundred targets).

- Access to an extended spectral domain at low resolution, for the characterization of the detected objects, at a resolving power $\sim 30$.

- Sensitivity to extended sources down to $\sim 17$ magnitudes per arcsecond squared at less than 0.2″ from the host star.

## 7.2 SCIENCE GOALS

The main scientific goal of SPHERE will be the description of the properties of young planets in the expected peak region of gas giant formation and in the outer regions of the systems. Imaging of planets already detected by RV and/or astrometry would additionally represent a major breakthrough thanks to the availability of dynamical constraints (or even full orbit determinations) on the planet masses and on the orbital elements. Therefore, these objects will represent the ideal benchmarks for the calibration of models for sub stellar objects. Furthermore, a direct imager like SPHERE provides the only way of obtaining spectral characteristics for outer planets.

While radial velocity spectroscopy remains the best technique currently available to study the inner side of the planet distribution with semi-major axis ($< 5AU$), high-resolution, high contrast imaging like that provided by SPHERE is expected to be the most efficient technique to discover planets in the outer regions of planetary systems (Fig. 7.2).

Current results from direct imaging surveys allow excluding only planet distributions with a large population of massive planets in outer orbits (see Chap. 5). With its enhanced capabilities (a gain of two orders of magnitudes in contrast with respect to existing instruments) and a list of potential targets including several hundred stars, SPHERE will provide a clear view of the frequency of giant planets in wide orbits. With the number of expected detections (several tens), the level of the large separation wing of the distribution with semi-major axis can probably be estimated with an accuracy of about 20-30%, good enough for a first statistical discussion of the properties of planetary systems. Beside frequency, it would

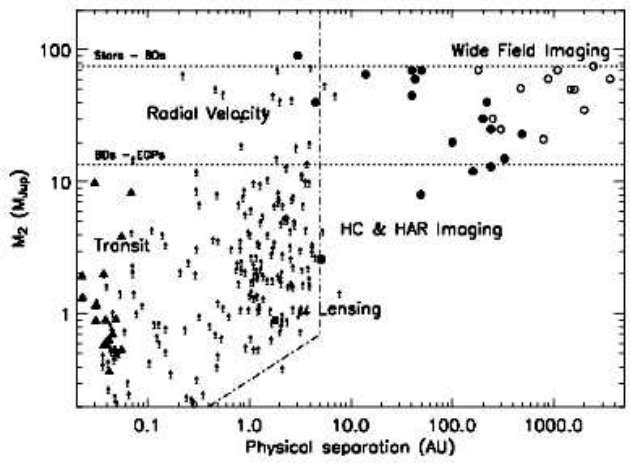


Figure 7.4: SPHERE extra-solar planets discovery space compared to other techniques: radial velocity (arrows), transit (filled triangles), micro lensing (filled boxes), wide field imaging (open circles) and high contrast and high dynamic range imaging (filled circles)

also be interesting to derive the distributions of planets parameters such as mass, semi-major axis and eccentricities.

Finally, a few planets shining by reflecting stellar light might be detected by the SPHERE polarimetric channel (ZIMPOL). SPHERE will be then highly complementary to current and contemporaneous studies of extrasolar planets.

### 7.2.1 *Target Classes*

These science objectives fully justify a large effort in an extended observational survey of several hundred nights concentrating on the following classes of targets:

- Nearby young associations (10-100 Myr, 30-100pc) will offer the best chance of detecting low mass planets, since they will have brighter sub-stellar companions.
- Young active F-K dwarfs of the Solar neighbourhood (ages less than 1 Gyr, $d < 50pc$).
- Nearest stars (all ages within 20 pc of the Sun) will allow probe the smallest orbits and will also be the only opportunities for detecting planets directly by reflected light.

- Stars with known planets, especially any that exhibit long-term residuals in their radial velocity curves, indicating the possible presence of a more distant planet (F-G-K stars within 50-100pc).
- Young early type stars.
- Planet candidates from astrometric surveys.

### 7.2.2 *SPHERE in the context of other contemporary high contrast imaging projects*

With respect to already existing or upcoming high contrast imaging projects, the goal of SPHERE is to offer a dramatic performance improvement in terms of achievable contrast at very short angular separation ($< 0.5''$, $< 25AU$ for a star at 50 pc; see Figure 7.2.2 ). Such an improvement will allow to characterize systematically the outer part of planetary systems and to probe the content and the physical and chemical properties of EGPs around a large sample of stars. SPHERE will then bring unique observational constraints for planetary formation mechanisms, which are currently barely restricted to a combination of relatively large separations ($> 50AU$) around young, nearby stars and/or very faint stars or BDs. Existing HAR projects include VLT/NACO, GEMINI/Altair, Keck, HST (in visible or NIR), AEOS/Lyot, Gemini/NICI (July 2007), and the upgraded HAR imager HiCIAO on Subaru (Sep 2007). While a few detections have been already obtained with these experiments, SPHERE will realize a very significant break through in performance, while still providing high robustness and efficiency needed for large and homogeneous surveys dedicated to a large community and keeping a tight schedule .

On this horizon of 2011, Gemini Planet Imager (GPI) shares the same main goals as SPHERE. This competition and the corresponding emulation definitely remind any actor, if needed, of the world-wide scientific motivation for this approach of planetary system studies, and of the need to keep the foreseen system performance level and schedule. On this basis, some slight differences in the projects can be underlined and may lead to some specific choices to maximize the return of each system:

- Some high level system choices differ concerning the main subsystem definitions and technological choices. This primarily reduces the overall risk associated with any single system development. The eventual on-sky tests will reveal the final exact capabil-

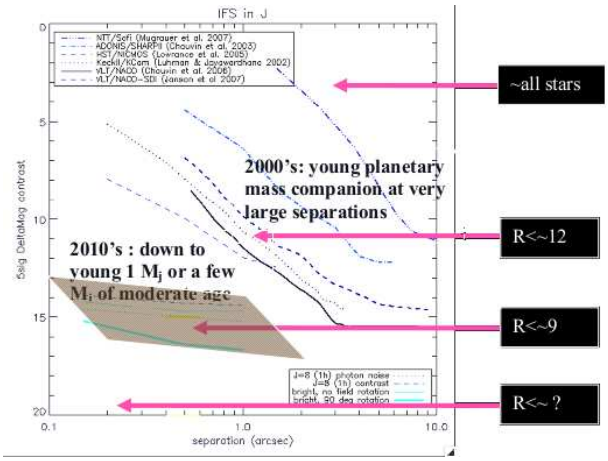


Figure 7.5: Contrast versus angular separation in the case of the IFS, compared with the performances of the current instruments.

ities of each system in a comparable manner and in various conditions (in terms of observing wavelength, targets classes and magnitudes etc...).

- With 3 scientific sub-systems, SPHERE will offer several observing modes not covered by GPI

- Installed at the focus of one of the 4 VLTs, SPHERE may benefit from a larger number of observing nights. The ability to handle such large observing programs is definitely a goal to be taken into account in the system definition, and the efficiency of SPHERE in a large detection survey (with in particular some wide spectral range obtained simultaneously) also contributes to this goal. It may favor in particular the inclusion of a variety of target classes down to fainter targets (whereas some very ambitious performance goal of GPI may be more appropriate to a sample optimized on the brightest targets).

## 7.3 SPHERE IFS

The main goal of the Integral Field Spectrograph of SPHERE is to explore the innermost part of the field. This instrument has in fact a field of view of 1.8 x 1.8 arcsecs and can resolve the image spectrally with a resolution

of 50 in the $0.95 - 1.35\ \mu m$ band, or with a resolution of 30 in the $0.95 - 1.7\ \mu m$ band.

### 7.3.1 *Concept*

IFS are very versatile instruments, well adapted for spectroscopic differential imaging as needed for detection of planets around nearby stars. The basic characteristic of an IFS is to image the array of slits generated by an Integral Field Unit (IFU) and chromatically separated by a suitable device on the final image plane. The main advantage of this approach is that differential aberrations can be kept at a very low level; this is true in particular for lenslet based systems, where the optical paths of light of different wavelength within the IFS itself can be extremely close to each other. Additionally, IFS provide wide flexibility in the selection of the wavelength channels for differential imaging, and the possibility to perform spectral subtraction, which in principle allows recovering full information on the planet spectra, and not simply the residual of channel subtraction, as in classical differential imagers.

The main drawback is that the IFS requires a large number of detector pixels, resulting in a limitation in the field of view, which is more severe for lenslet-based systems. Classical differential imagers and IFS are then clearly complementary in their properties, and an instrument where both these science modules are available may be extremely powerful for planet search.

In the case of SPHERE, a BIGRE (Antichi et al. 2009) concept has been selected for the IFU. (Fig. 7.3.1).

This is a design based on lenslet system in which a second lenslet array allows formation of pseudo-slit images corresponding to a very small portion of the field, which are then imaged on the detector after being dispersed (Fig. 7.3.1). The main advantage of the BIGRE concept is that the pseudo-slit images are only very mildly dependent on wavelength and have a quasi-top-hat profile. This allows to better controlling the diffraction effects and a much lower level of cross-talk.

In addition to the micro-lens system at the entrance of the spectrograph, the opto-mechanical concept includes collimation optics, an Amici Prism providing zero beam deviation and almost constant resolution within the entire wavelength range, camera optics, and the detector cryostat (Fig. 7.3.1). Thermal background is controlled by extending the cryo-

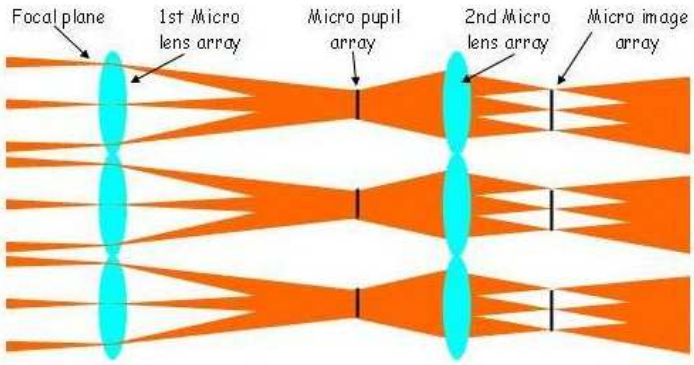


Figure 7.6: Optical concept of a BIGRE IFU: the IFS Slits Plane is filled with an array of micro-images of the telescope Focal Plane.

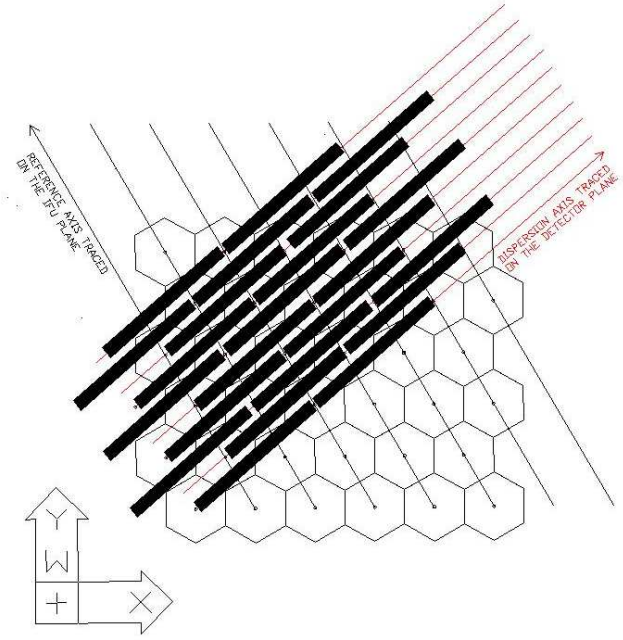


Figure 7.7: Sketch of the spectra Hexagonal-C configuration. The black axis is the reference on the IFU plane (filled with hexagons representing a portion of the spaxels); the red axis traces the dispersion direction and the black rectangles the final spectra imaged onto the IFS Detector plane. The angle between these two axes should be 79.11 deg

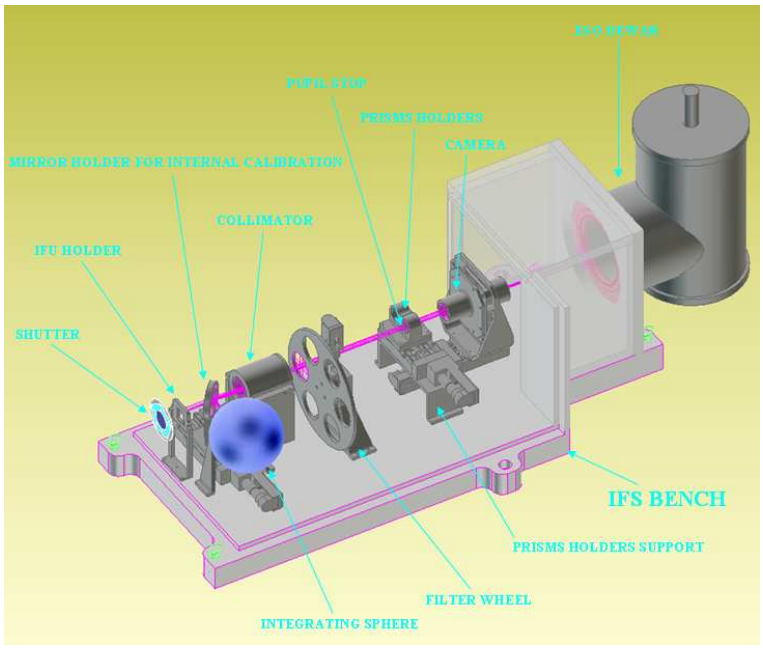


Figure 7.8: Mechanical sketch of IFS

stat $>$ 150 *mm* in front of the detector, thus limiting the solid angular view of the warm environment, and by including a cold short-pass filter. Detector dithering (in order to improve flat-field precision) is achieved by small movements of the camera optics, realized by commercial piezos.

### 7.3.2 *Foreseen contrast performances*

The main aim of IFS is to gather spectra in order to perform high contrast imaging exploiting the S-SDI technique. This enhances the high contrast capacity of the instrument itself. In order to take under control this peculiar characteristic of the instrument many simulations for the SPHERE-IFS were performed, using different codes available inside the SPHERE consortium. These codes provide a very detailed description of IFS itself, including details about its geometry, adequate derivation of wavelength calibration and of the impact of related uncertainties on the handling of speckle chromatism, and a full description of the incoherent cross talk, together with a data reduction packet and a cross talk estimator. Further, also the SPHERE common path is simulated with full description of phase screens (that are treated as complex matrices using a Fraunhofer

approach). Beyond the instrument model, there are also different effects limiting the contrast that can be achieved when using the SPHERE IFS, that can be ordered according to the following classes:

1. Calibration of the stellar coronagraphic halo
2. Instrumental effects, like spurious effects associated with cross-talk between the various IFU sub-pupils
3. Photon noise
4. Detector issues (noise associated with detector read-out noise and limited accuracy on detector Flat-field; detector persistence)
5. Noise possibly introduced in the operations of data reduction and analysis (interpolations, etc.)

Noise introduced in the data reduction is difficult to estimate and obviously depends on the exact final coding of the data reduction recipes as provided in the pipeline.

In Figure 7.3.2 we plotted the $5\sigma$ contrast limit as a function of separations for stars of different magnitude (J=2, 6, and 8). In this figure, we considered the case of 1 hr observations and 30 degree field rotation. The contrast at 5 $\sigma$ achieved by the IFS at 0.5 arcsecs is between $10^{-6}$ and $10^{-7}$, depending on star and observing conditions.

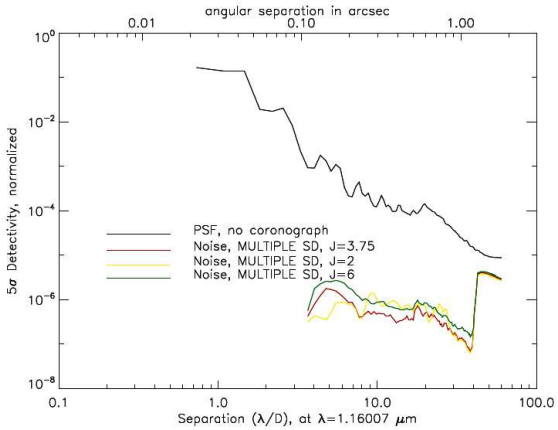


Figure 7.9: Run of the $5\sigma$ calibration limit with separation for stars with J=2, 3.75 and 6. All cases are for 1 hr exposure time and rotation by 30 degrees. The mask subtraction method and the azimuth filtering were applied.

## 7.4 RESULTS

We used the 1D *prediction mode* of MESS, using a reduced population created with the empirical approach, and the following setup:

- mass and period power-law distribution from Cumming et al. (2008)
- planet masses between $0.3 - 1.5\ M_{Jup}$ and scaled according with the stellar mass
- period between 2.5 days and 250 years, corresponding to a cut-off of 40 AU for a 1 $M_{Sun}$ star

The expected fraction of planets is normalized to the value reported by Cumming et al. (2008), that is 8.5% for RV planets with $p < 3$ *years*, in the same mass range. Extrapolating the period distribution up to 250 years lead to an expected frequency of planets of about 26%.

The stellar samples are the one selected for the SPHERE GTO survey, according with the target classes listed in Sec. 7.2.1. We then end with a sample of 1237 stars belonging from nearby associations and young field stars[1].

We finally selected the sub sample of planets detectable with SPHERE-IFS, on the basis of the contrast limits evaluated as in Sec. 7.3.2.

The results are summarized in Fig. 7.4, which shows the behaviour of the detectable planets in the mass-semi axis plane, and Fig. 7.4, in which the contrast in J band is shown for the planets detectable around the stars in the sample.

These plots show that SPHERE-IFS is expected to detect a few tens of planets, almost all of them in the range of contrast between $10^{-4}$ to $10^{-6}$, as it is clear also from Fig. 7.4. This figure shows the fraction of detected planets per bins of contrast (log scale), for the whole sample.

### 7.4.1 *Frequency of planets and distribution with planet mass*

As already pointed out in Sec. 7.2.2, SPHERE is expected to achieve better contrast that presently available instruments by about two orders of magnitude. This would imply a large improvement in mass limits. The

[1] From this preliminary sample, a final sample of 300-500 stars, will be then selected for the GTO survey

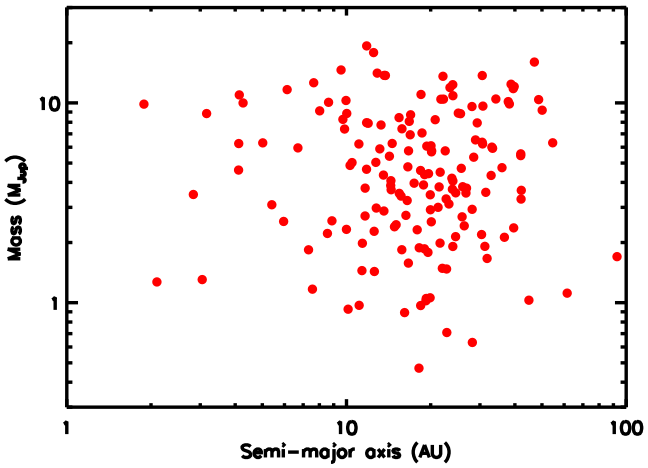


Figure 7.10: Mass and Semi-major axis values of the planets detectable with SPHERE-IFS around the stars in the preliminary GTO sample.

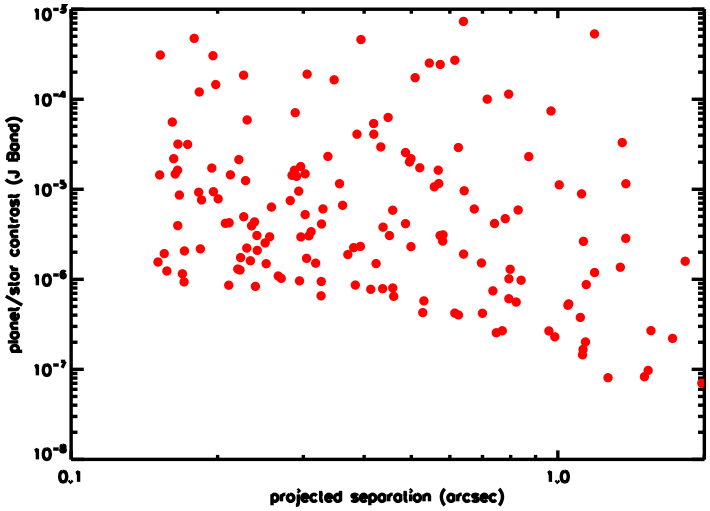


Figure 7.11: Star/Planet Contrast in J Band versus projected separation in arcsecs for the planets detectable in the sample used for the simulations.

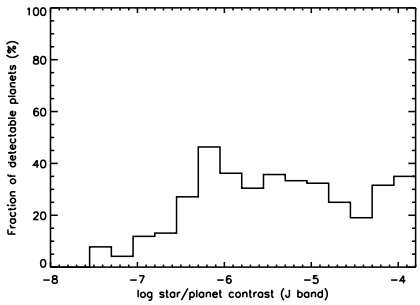


Figure 7.12: Histogram of the fraction of planets detectable per bin of contrast (log scale) for the whole target list

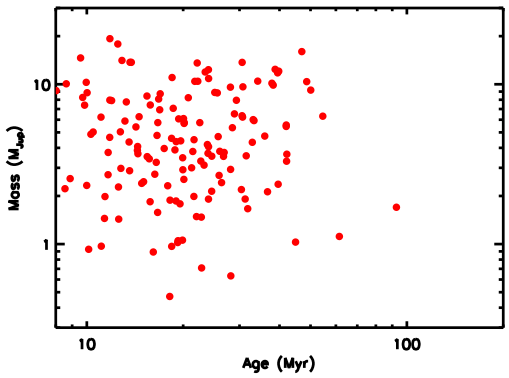


Figure 7.13: Mass of the planets detectable with IFS as a function of the age of the targets.

detectability limits achieved by SPHERE clearly allow detecting planets over a broad range of stellar masses.

The right panel of Figure 7.4.2 shows the histogram of the masses of detectable planets, for the whole target list. The smallest planets detectable with SPHERE have masses below 1 $M_{Jup}$, which represents an order of magnitude improvement over current detections or upper limits. Not only SPHERE will detect planets over a wide range of masses, but it will also be able to provide an unbiased distribution with masses over a reasonably wide mass range. This is possible exploiting young targets.

When considering this target list, the fraction of planets detected among those generated (M=0.3-15 $M_{Jup}$, P¡250 Yr) is $\sim$ 13%. This fraction rises to more than 15% for stars of beta Pic and TW Hydrae moving groups (younger than 12 Myrs).

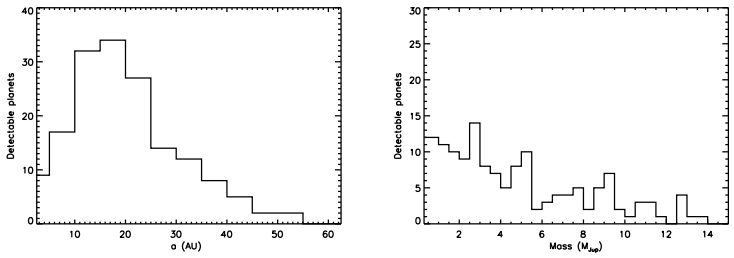


Figure 7.14: Distribution of semi-major axis (left) and masses (right) of planets expected to be detected by IFS, for the whole GTO preliminary target list

The impact on mass distribution of the observation of young targets, is summarized also by Figure 7.4.1, which shows the mass vs age of planets expected to be discovered with the SPHERE-IFS for the young sample.

### 7.4.2 *Distribution with semi-major axis*

One of the most powerful features of SPHERE is the possibility to explore a wide range of separations from the central star, which is allowed by combining IFS (very deep observations in the central region) and IRDIS (wide sky coverage). This allows a nearly constant limiting contrast over a wide area, strongly enhancing the capability to derive useful information on the distribution of planets with semi-major axis, a crucial issue in models for formation of planetary systems. The left panel of Figure 7.4.2 shows the distribution of semi-major axis of planets expected to be detected by IFS .

The number of planets expected to be detected is a very strong function of the (assumed) distribution of planet separation. Extending the semi-major axis distribution up to P=250 yr (about 40 AU 8) yield a number of planet detections about 3.5 larger than for the same distribution truncated at P=70 yr (about 17 AU). Several tens of planet detection (details depend on target number and selection criteria) are then expected between 20 and 40 AU if planets are there. SPHERE has clearly the potential for an accurate determination of the frequency of planets in wide orbits.

### 7.4.3 *Stars with known planets*

Figure 7.4.3 shows the contrast limit in J band of the planets discovered up to now with the radial velocity technique, as a function of the projected separation. The contrast limit of SPHERE-IFS for a G2V star is plotted for comparison.

Even if the result of this plot seems to be really pessimistic (none of the planets already discovered is expected to be re-observed with IFS), some detections could be expected in case of favourable orbital characteristics of the planets (high eccentricity and/or inclination). Moreover, the orbital elements of these candidates are known, then some dedicated observing strategies can be planned enhance the chance of detection. Nevertheless, IFS has also good chances to discover further companions responsible for long-term RV trends observed in several cases.

Therefore, there are good perspectives that the synergy between ongoing RV surveys and SPHERE (and also astrometry) will allow a full derivation of the separation distribution of giant planets, from the very close-in planets with period of a few days to planets at separation of several tens of AU.

In addition, direct observations of planets (and hence luminosity determination) with dynamical masses around stars of known age allows to calibrate models. Furthermore, their spectra allows detailed study of the atmospheres. This will open a wide space for planet characterization, actually limited to the warm Jupiters observable in transit. So even if likely a few such planets will be detectable with SPHERE, they may have a large impact on the understanding of extrasolar planets.

## 7.5 CONCLUSIONS

In this chapter we started reviewing the results of the use of the *Prediction Mode* of MESS, presenting its application aimed to evaluating the performances of the SPHERE IFS.

This analysis confirmed the potential of SPHERE IFS in the discovery of young giant planets orbiting far away from theyr host stars. This makes SPHERE, as the other next generation imagers, complementary to the traditional indirect methods, allowing us to explore a nearly undiscovered mass-period domain. Moreover, being the young stars the most favourable targets for SPHERE IFS, it will provide informations on the

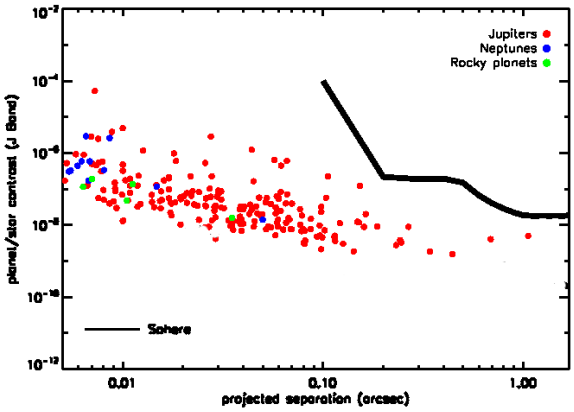


Figure 7.15: SPHERE IFS contrast limit in J band (solid curve) as function of the orbital separation. The planets detected up to now with the radial velocity technique are shown for comparison

first stages of the planet evolution, helping in clarifying the uncertainties on the evolutionary models at such young ages. Furthermore, coupling integral field spectrographs to extreme adaptive optic modules, would allow us to perform a first order characterization of the exoplanets themselves, giving informations on their atmosphere and composition. Finally, even if only in some favourable cases, SPHERE will also allow the characterization of planets already detected by radial velocity searches.

Such an instrument is then an indispensable intermediate step that will allow us to gather informations on the behaviour of the external part of the planetary systems, preparing the path of ELT instruments that will give us a wide view on planetary systems at different stages of their evolution.

# 8

# EVALUATION OF EPICS CAPABILITIES

In this chapter we discuss the application of MESS to evaluate the performances of the Exo-Planet Imaging Camera and Spectrograph (EPICS, see Kasper et al. 2008). EPICS is an instrument project for the direct imaging and characterization of extrasolar planets with the E-ELT. EPICS will have photometric, spectroscopic and polarimetric capabilities and will be optimized for observations in the visible and near-IR.

### 8.0.1 *Epics concept*

The EPICS baseline concept includes:

- A calibration Unit, providing all needed calibrations
- An XAO module, able to provide high Strehl ($>$ 90% in H) down to 600 nm (Strehl $>$ 60% in R for bright sources), and ideally down to 350 nm. The reference source should have $I < 9$ (goal $I < 13$).
- A Diffraction Suppression module. This will allow efficient suppression of the central diffraction peak, as well as efficient observations ($>$ 50%) down to an inner Field of View of 0.03 arcsec (goal =0.02 arcsec), over the working wavelength range.
- A set of scientific instruments, able to exploit simultaneous Image Differential Imaging techniques. During Phase A, three different scientific instruments were studied:
  - An Integral Field Spectrograph. This might be based on either a lenslet (BIGRE) scheme or an Image Slicer one. The Integral Field Spectrograph should cover at least a square field of view with a side of 0.79 arcsec, well sampling (at Nyquist limit) the diffraction image; the spectra should cover the wavelength region $0.95 - 1.7\mu m$ at a spectral resolution of $R \sim 120$. It will also allow a pseudo-long slit (0.79x0.012 arcsec) mode providing intermediate ($R \sim 4000$) and high ($R \sim 20.000$) spectral resolution for follow up observations of bright planets.

- A Polarization analyzer (E-POL), based on a concept similar to the ZIMPOL one under development for SPHERE. E-POL should yield high precision ($\sim 10-5$) differential polarimetry over the whole Field of View, Nyquist sampled at diffraction limit. E-POL should work in the wavelength range 600-900 nm (goal 350-900 nm).
- Not included in the baseline design, EPICS might also include in the future a Self-Coherent Camera exploiting interference fringes within speckles for the wavelength range $0.6-1\mu m$, as well as a Visible Integral Field Spectrograph for the same wavelength range.

#### 8.0.2 *Observing modes*

##### 8.0.2.1 *Spectroscopic modes*

There are three main spectroscopic modes for the near IR:

1. **NIR-LR mode:** this is the full IFS mode, providing the highest contrast, to be used for planet detection in survey mode. It allows to get spectra at a resolution of R=125 of the spectral range 0.95-1.70 micron, over the whole FoV (square, side 0.799 arcsec), at a resolution of 2.33 mas/pixel.

2. **NIR-MR mode:** this is a pseudo-long slit mode (with a mask covering the lenslet array, save for a strip 6 lenslet wide crossing the whole FoV), providing medium resolution spectra at R=1500 of the whole spectral range 0.95-1.70 micron, to be used for characterization of planets down to super-Earth mass around bright stars.

3. **NIR-HR mode:** this is a pseudo-long slit mode (using the same lenslet configuration of the previous mode), providing high resolution spectra at R=21000 covering one possible choice among the following three ranges: 0.95-1.15, 1.15-1.40, 1.40-1.70 micron. It can be used for characterization of young, bright planets. The FoV is 0.014x0.799 arcsec.

##### 8.0.2.2 *Polarimetric modes*

A mode for differential polarimetry with E-POL (600-900 nm)

1. **VIS-P mode:** this is the high-sensitivity polarization mode of EPOL to be used for the detection of reflected and therefore polarized light from planets. EPOL will provide broad and narrow band polarimetry in the range 600-900nm with a polarimetric precision of $10^{-5}$ for point sources. If possible the wavelength range should be extended towards shorter wavelength (say 500nm if possible) because the expected polarization signal from exoplanets is expected to by higher in the blue (Rayleigh scattering). The diffraction limited resolution is 3 mas at 600 nm. Accordingly the resolution will be 1.5 mas per spatial resolution element and the field of view 1.37x1.37 arcsec. The mode is limited by the stellar background. The highest contrast (better than $10^{-9}$) will be possible for bright stars (¡ 5 mag) for which the full sensitivity of the high precision polarimeter can be exploited within a reasonable observing time.

A mode for classical imaging with EPOL:

1. **VIS-I mode:** this is a high-resolution imaging mode using EPOL without polarimetric components. This provide filter imaging with the available EPOL filters including differential imaging using two different filters in the two EPOL arms. This mode allows coronagraphic and non-coronagraphic (using neutral density filters) imaging. Field of view, spatial resolution, filter and coronagraph configurations are identical to VIS-P.

### 8.0.3 *Science Goals*

EPICS will be a very powerful instrument for detection and characterization of extra-solar planets. Its design will be optimized in order to reach very significant goals in a number of areas. The main science goal of EPICS are the following:

1. Determine frequency and mass distribution of self-luminous gas giants within star forming regions or young associations.

2. Detection and characterization of mature gas giants at orbital distances between 5 and 15 AU in the solar neighbourhood ($< 20pc$) and detection and 1st order characterization of warm Neptunes and massive rocky planets and super-Earths around very nearby stars ($\leq 10pc$) with the ultimate goal of detecting such planets located in the HZ (for M-dwarfs and very close systems $< 4pc$).

3. Imaging and characterization of warm or young Jupiters that have been previously discovered by radial velocity searches or direct imaging with smaller telescopes. Understand giant planetsâ atmospheric composition and structure.

The importance of these objectives is briefly reviewed in the following sections.

#### 8.0.3.1 *Self-luminous gas giants in star forming regions and young associations*

Detection of young self-luminous giants in star forming regions and young associations is basic in order to determine the initial frequency and distribution with mass and separation of giant planets. This will allow extensive comparisons with models of planetary system formation and evolution. This is crucial, because these mechanisms are still far from being properly understood, mainly because available data are strongly biased toward old/short period systems. In particular the peak of the distribution of giant planets with separation is expected to lie slightly out of the so-called snow-line, where ices can survive, providing a wealth of material for the formation of large planetary cores: for solar type stars, the snow-line is expected to be at $\sim 3-5$ AU. Explorations of regions even further out ($> 10$ AU) is also crucial in order to understand the possible impact of neighbours on the dynamical evolution of the orbits of already formed planets. These regions are difficult to explore or even inaccessible with indirect methods like radial velocities and transits. While astrometric signal from such systems would be detectable with PRIMA or GAIA, the typical long periods involved would require long time coverage in order to provide enough data. Finally, microlensing data, while statistically very useful, provide only a photograph of the planet orbits, so that important parameters like stellar age, real separation or orbital eccentricity cannot be determined. Direct detection may be very helpful for several reasons:

- A single image is enough for describing main characteristics of the whole system
- Repeated visits may allow determination or at least constraints on the main orbital parameters (semi-major axis, eccentricity, inclination)

- Possibly coupled with indirect methods, planetary masses can be derived, fully constraining system parameters

#### 8.0.3.2 *Mature planets in the solar neighbourhood*

Observation of samples of giant planets in the solar neighbourhood is very important for various reasons:

- Frequency and mass distribution of giant planets at old ages, once dynamic evolution have cleaned systems from planets in unstable orbits, can be compared with the results obtained in star forming regions and young associations.
- These systems may be studied in more detail, even in regions much closer to the central star with respect to the snowline, allowing exploring the HZ and even inner regions.
- These observations are important forerunner for Darwin and TPF, clarifying which systems are most likely to host rocky planets in the HZ.

Even more interesting would be detection of small mass planets (Neptunes and Super-Earths). As mentioned in Section2.1, this is the current frontier of exo-solar planet studies. Detection of a statistical significant number of Neptune-like and Super Earths would be crucial for various reasons:

- The expected frequency of low-mass planets at various separations from the central star is a basic parameter for models of planet formation.

- Even low resolution and low S/N spectra of such objects would allow a first characterization of their atmosphere. This is extremely important because little is known about the range of possible variations for the atmospheres of low-mass planets, and moreover about the incidence of Earth-like ($O_2$-dominated) atmospheres.

#### 8.0.3.3 *Planets discovered by RV, astrometry and transit searches*

In most cases masses for planets detected by EPICS cannot be determined independently of ages. Imaging of EGP already detected by RV, transits and/or astrometry would represent a major breakthrough thanks to the

availability of dynamical constraints (or even full orbit determination) on the planet masses and on the orbital elements. In most cases, stellar ages are or can be determined rather well exploiting suitable indicators (isochrones, magnetic activity and rotation, kinematics, etc.). Therefore, these objects will represent the ideal benchmarks for the calibration of models for sub-stellar objects. They would represent the bridge between the rather different detection space of direct imaging, astrometry and radial velocity techniques. This is relevant for a proper interpretation of the statistical results on planet frequency resulting from the various techniques in their different separation ranges. Spectroscopic and polarimetric observation of these planets (for which most important parameters are known) is also crucial for testing models of their atmospheres.

#### 8.0.3.4 *Planet Characterization*

The core science program of EPICS consists of the direct detection and characterization of exo-planets, ranging in size from gas giants down to Super-Earth and Earth-size objects. EPICS will be used both in survey mode to search for and detect a large number of planets, and in characterization mode to probe the atmospheric composition and structure of a limited number of planets. To guarantee the accomplishment of both these observation strategies, EPICS performances need to be flexible. Once EPICS has detected an interesting planet, follow-up spectroscopic observations will be planned to improve S/N of the spectra, or to acquire spectra at higher resolution.

The emergent spectra of Extrasolar Giant Planets (EGPs) are determined mainly by the chemical composition of their outer atmospheric layers. Cool atmospheres generate complex spectra that are rich in molecular features, especially at near - infrared (NIR) wavelengths, where rotovibrational transition of many molecules dominate. Most EGPs contain in fact condensed species that contribute substantially to the opacities. Some condensates, such as water ice or iron grains, are formed homogeneously (i.e., from a single species), while the formation of others such as forsterite or gehlenite (Sudarsky et al. 2003) is heterogeneous, resulting in the depletion of several gas-phase species. For solar metallicity, the dominant equilibrium form of Carbon near and above BD/EGP photospheres is $CH_4$ or CO, that of oxygen is $H_2O$, and that of nitrogen is either $N_2$ or $NH_3$ depending upon $T_{Eff}$ (Fegley & Lodders 1996). Hydrogen is predominantly in the form of $H_2$, Silicates most metals, TiO and VO are

found at temperatures above 1600-2000 K. Neutral alkali metals and lines of Al I, Fe I, Mn I, and Ti I, are found at temperatures above $\sim$ 1000 K. Clouds of $NH_3$ and $H_2O$ can form for $T_{Eff}$ below $\sim 200 - 300$ K. Observations with significantly higher spectral resolution are potentially very important because line blending from molecular transitions is reduced and weak features are resolved. Higher resolution spectra are more useful for constraining models of the complex molecular chemistry of brown dwarfs (cool atmosphere benchmarks) and EGPs atmospheres and for characterizing properties such as gravity and metallicity (Mohanty et al. 2004). For example, less massive EGPs and younger giant planets have smaller surface gravities, which results in less pressure broadening and a different line shape. Furthermore, spectra with $R \geq 20.000$ ($\leq 15 kms^{-1}$) are required for the measurement of radial and rotational velocities, and to search for radial velocity variability associated with faint companion (EGPs and/or BDs) spectroscopic binaries.

Super-Earths, having thin gaseous envelopes, should exhibit a large variety of spectra, depending on atmosphere temperature and composition, and on presence of clouds. While very few super-Earths are expected to be detectable by EPICS, additional targets might likely be given by observations with other instruments (e.g. CODEX). Given the enormous interest of these observations, a considerable investment of observing time in follow-up observation of these objects can be considered Table 8.0.3.4 lists the most important molecular bands in the Earth shine and Venus spectra in the wavelength range $0.6 - 1.7 \mu m$. For each band, we list the wavelength, the band width (FWHM), the equivalent width of the band, and the S/N that spectra at a spectral resolution of R=120 should have for a $3\sigma$ detection of the band. Band strength values actually depends on the extent of the region of the atmosphere above the cloud top or surface, and on the atmospheric composition; so these values are only vaguely indicative of what can be expected in rocky planets. The bands might of course be detected on higher resolution spectra, insofar the product R (S/N) is larger than the value given in the Table; however band detection is not expected to be easier, because of the impact of detector read out noise. We also notice that all bands listed are resolved in spectra with a resolution $R > 200$.

| Specie | $\lambda$ | FWHM | Earth | | Venus | |
|---|---|---|---|---|---|---|
| | ($\mu m$) | (nm) | Eq. Width (nm) (nm) | S/N for $3\sigma$ det. at R=120 | Eq. Width (nm) | S/N for $3\sigma$ det. at R=120 |
| $O_2$ | 0.76 | 4 | 1.4 | 14 | weak | |
| | 1.27 | 10 | 2.7 | 12 | weak | |
| $CO_2$ | 1.21 | 14 | weak | | 8 | 5 |
| | 1.57 | 14 | 2.4 | 17 | 13.2 | 3 |

Table 8.1: Most important molecular bands in the Earth shine and Venus spectrum in the 0.6-1.7 $\mu m$ wavelength range

## 8.1 SIMULATIONS OF EPICS DETECTION PERFORMANCES

The estimation of EPICS performances is made using the PESCA (see Verinaud et al. in prep) code. This code is based on a semi-analytical method to estimate the signal to noise ratio (SNR) similar to the one developed by Soummer et al. (2007).

The SNR can be defined by Eq. 8.1

$$SNR = \frac{C(x,y)\, f(x,y)}{\sqrt{\Sigma_i \sigma_i^2 (x,y)}} \tag{8.1}$$

where $C(x,y)$ is the contrast in a given SNR range and $f(x,y)$ is a weighting function for the signal, describing the coronagraphic transmission and/or signal processing impact on the field of view (FOV). The $\sigma_i^2$ terms represent the different uncorrelated noise variance terms.

There are two main quantities of the scientific image (coronagraphic or direct image) that need to be evaluate to compute the noise, as the variance of the intensity in the long exposure image (see Fig. 8.1):

- **The deterministic term, $I_c$:** obtained by computing the PSF with a wave optic end-to-end code, including all the static aberrations and weighting it with the value of the Strehl Ratio.
- **The random term, $I_s$:** which is the average of the speckle halo due to dynamic wave-front evolution. This term is estimated using the analytical model of the AO system by Jolissaint et al. (2006)

Separating the two components both system optical errors ($I_c$) and AO residuals ($I_S$) can be taken into account, depending on the observing conditions (seeing, star magnitude). The variance obtained in this way will

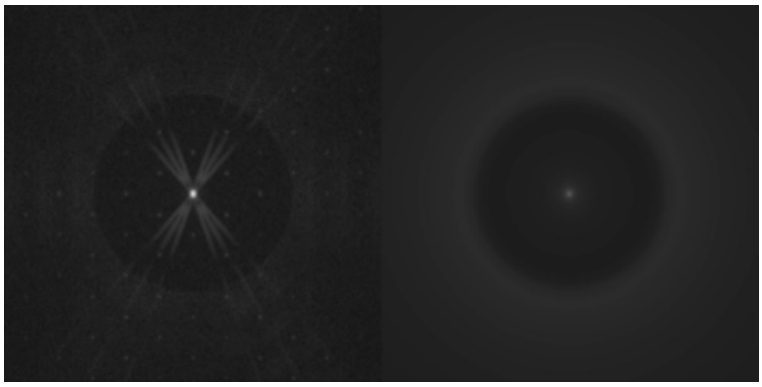

Figure 8.1: The 2 components used to determine the long exposure PSF of EPICS in the NIR. Left: deterministic term: static aberrations and diffraction suppression system obtained from end-to-end simulation. Right: average random term, AO halo obtained from analytical model. Baseline NIR concept, bright star , $\lambda = 1\mu m$

includes both the speckle noise (dominated by $I_c$, following a Rician statistic) and the photon noise (dominated by $I_s$, following a Poisson statistic).

As in Soummer et al. (2007), the total variance is given by Eq. 8.2[1]:

$$\sigma^2 = (I_c + I_s) + \left(I_s^2 + 2I_c I_s\right) \tag{8.2}$$

Including as main noise terms:

1. photon noise: $\sigma^2_{ph}(x,y)$
2. instrumental system noise: $\sigma^2_{sys}(x,y)$
3. flat field (FF) noise: $\sigma^2_{FF}(x,y)$

Eq.8.1 can be used to obtain the contrast $C(x,y)$ as follows:

$$C(x,y) = \frac{SNR}{f(x,y)}\sqrt{\sigma^2_{ph}(x,y) + \sigma^2_{sys}(x,y) + \sigma^2_{FF}(x,y)} \tag{8.3}$$

$$= \sqrt{C^2_{ph}(x,y) + C^2_{sys}(x,y) + C^2_{FF}(x,y)} \tag{8.4}$$

[1]Note that Eq. 8.2 is only valid for the evaluation of the SNR in a single image, but in the case of EPICS, which is based on differential method, one has to take into account the differential techniques. Using an IFS, a large number of different wavelenght spanning over a large spectral bandwidth can be used. This property, together with the very high spatial resolution of the E-ELT, allow to use the spectral deconvolution method described by Sparks & Ford (2002), and successfully tested on sky by Thatte et al. (2007), to evaluate the noise on the deterministic term $I_c$.

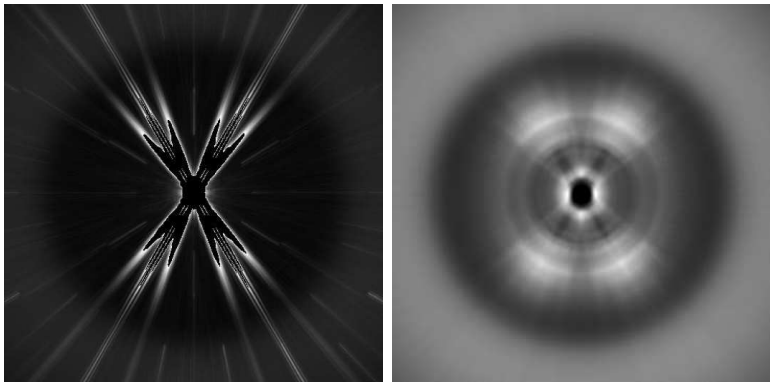

Figure 8.2: Left: Long exposure PSF with exclusion of data. Right: same PSF but rotated and integrated to simulate the field rotation during a typical observation.

where we introduced the contrast limits $C_{ph}$, $C_{sys}$ and $C_{FF}$ that allow to individually evaluate the contrast limits due to the main error sources.

The last thing that might be taken into account is that in the focal plane, the diffraction spikes due to the spiders are particularly bright. Even tough light diffracted by spiders should not saturate the detector, the photon noise will be very high, thus the instantaneous contrast in these region is lower. In this context, the rotation of the field could be an advantage and a disadvantage at the same time:

- A source embedded in a spider diffraction pattern at a given time, can came out in a different exposure
- If the field rotation is high, a large fraction of the FOV will be polluted by photon noise

A simple solution to this issue is to exclude data that exceed a given brightness threshold in individual long exposure frames when the rotation is negligible. Fig. 8.1 shows the PSF with excluded data ($10^5$ contrast threshold) and the equivalent PSF in case of field rotation.

### 8.1.1 *Final contrast maps*

All the informations coming from the PESCA code described above are used to compute the final 5 sigma detection limit maps, taking into account the observation definition:

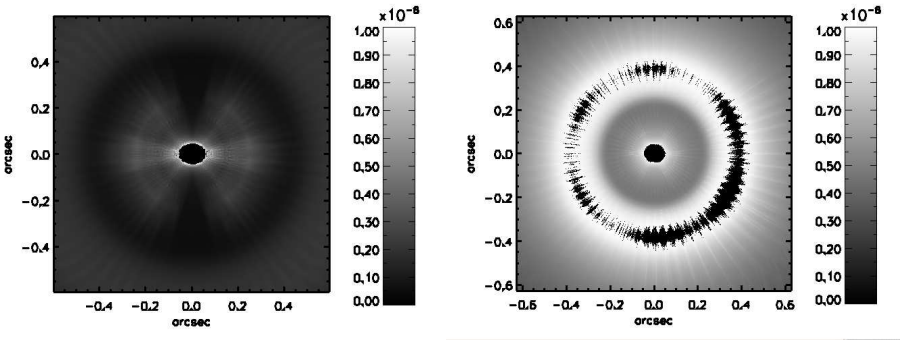


Figure 8.3: Simulation of IFS (left panel) and EPOL (right panel) 5 sigma detection limit for a G2 star at 30pc. DEC=-35. Observation: over 10 night of 1.0 hours (10 H total integration time).

- Observing time (randomly generated, in a time-span of 1 year, starting from 1st Jan. 2018)
- Exposure time
- Hour angles
- Target declination and I magnitude (from the target sample described in Sec. 8.2)
- Target flux in science wavelenght

We used PESCA to evaluate performances of both IFS and EPOL, in order to obtain the 2D contrast maps to be used as inputs for the MESS code. An example of the output contrast maps is given in Fig. 8.1.1 for IFS (left panel) and EPOL (right panel) respectively. A G2V star at 30 pc is used, then assuming I=4.9, J=3.26, V=4.7, R=5.23.

## 8.2 RESULTS

To examine the potentialities of EPICS for the scientific goals listed in Sec 8.0.3, we used MESS to derive the properties of the planet expected to be detected around the stars in three lists of potentially interesting targets for high contrast imaging, compiled within the preparation work for SPHERE GTO:

1. Young stars: 1200 stars with ages $< 5 \times 10^8$ yr, southern of declination +20, with magnitude $I < 10$

2. Nearby stars: 600 stars within 20 pc, southern of declination +20, with magnitude $I < 10$

3. Stars with planets discovered in RV surveys: stars with planets[2] having projected semi-major axis ¿0.02 arcsec, southern of declination +20, with magnitude $I < 10$

The method used is the *Prediction Mode* of MESS described in Sec. 4.7.2, which uses a *reduced population* built randomly choosing 5 planets generated using the distribution by Cumming et al. (2008).Luminosity of each planet is estimated taking into account both intrinsic luminosity and reflected light contribution, as described in Sec. 4.6.3. We then compared the expected contrasts with the 2D maps for limiting detections obtained with the PESCA code (see Sec. 8.1) for different observing conditions.

We distinguished four different planet mass ranges:

all the objects with $M_P \geq 40 M_{Earth}$ are considered as Jupiter-like planets (red/orange filled dots)

those with $10 M_{Earth} < M_P < 40 M_{Earth}$ are the Neptune-like planets (blue filled dots)

those with $1.2 M_{Earth} < M_P < 10 M_{Earth}$ are the Super Earths (green dots)

and finally the ones with $M_P \leq 1.2 M_{Earth}$ are marked as Earth-like planets (cyan filled dots)

Several runs has been performed, considering separately IFS and EPOL performances, aiming to:

- Evaluate the number of detectable planets by the two channels
- Estimate the number of target needed to reach the science goals
- Identify the instrumental requirement (minum contrast, inner working angle, field of view, etc.) to be fulfilled in order to address the science goals.
- Underline dependencies, if any, of the number of planets detected by the stellar characteristics (age, distance, magnitude).

[2]data from http://exoplanet.eu/

### 8.2.1 *Number of detectable planets*

The first purpose of our simulations was to evaluate the number of planets in the various mass bins, detected by the two channels of EPICS. Given the shape of the E-ELT pupil, limiting contrast for planet detection depends not only on separation from the central star, but also on the azimuth angle. For this reason, different observing strategies might lead to different levels of completeness in search for planets. In this section, we will examine the productivity of different observing strategies when observing with EPICS in survey mode. In this discussion we consider that due to the effects of the spiders supporting M2, limiting contrast achievable with EPICS depends on the azimuth angle of the planet with respect to the star. Spiders are expected to rotate with the pupil; since E-ELT has an alt-azimuth mounting, the field rotate during exposure with respect to the pupil. Location of the planets on the images provided by EPICS is then expected to rotate with respect to the pupil. For this reason, faint planets near detection limit might be visible only if they happen to be projected toward a region where better contrast is achievable. Figure 8.2.1 displays the location of rocky and Neptune-like planets detected by EPICS in a simulation with MESS. This is a simulation of 10x1 hr observations of the whole sample of stars in the nearby sample ($\sim$ 600 stars); in this simulation, we assumed all observations are taken when the target was close to meridian. While the details of this simulation are not realistic (we assumed a total of 50 planets around each star), it shows the impact of the spider on detection. There is actually indeed a shortage of these faint planets when projected toward the spiders, although the effect is not very pronounced. However, this azimuth dependence of the planet detections suggest that appropriate observing strategies might result in a larger number of detections.

In order to evaluate the impact of different strategies on planet detection with EPICS, we considered the following ones:

A: 1 visit of 1 hr at meridian (from HA=-30 min to +30 min)

B: 10 visits of 1 hr at meridian (from HA=-30 min to +30 min)

C: 5 visits of 1 hr before meridian (from HA=-1 hr to 0) + 5 visits of 1 hr after meridian (from HA=0 hr to 1). Data are analyzed separately for the two series; planets are detected if visible in at least one series of observations.

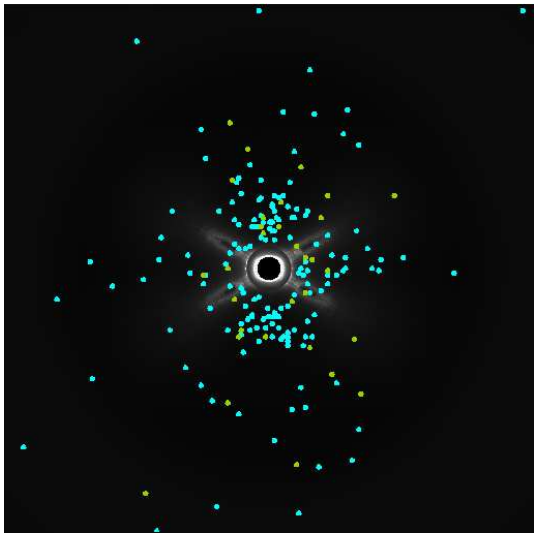

Figure 8.4: Position relative to the EPICS IFU of small planets (Neptune-like and rocky planets) detected in a simulation of observation of the whole nearby sample ($\sim$ 600 stars with $d < 20$ pc). In this simulation, we assumed that each target is observed 1hr while passing at meridian, and that this observation is repeated 10 times. To enhance statistics, we assumed that each star hosts 50 planets.

D: 5 visits of 1 hr before meridian (from HA=-2 hr to -1) + 5 visits of 1 hr after meridian (from HA=1 hr to 2). Data are analyzed separately; planets are detected if visible in at least one series of observations.

E: 5 visits of 1 hr (from HA=-2 hr to -1) + 5 visits of 1 hr from HA=-1 hr to 0) + 5 visits of 1 hr from HA=0 to 1) + 5 visits of 1 hr from HA=1 hr to 2. Data are analyzed separately; planets are detected if visible in at least one series of observations.

F: 5 visits of 1 hr (from HA=-2 hr to -1) + 5 visits of 1 hr from HA=-1 hr to 0) + 5 visits of 1 hr from HA=0 to 1) + 5 visits of 1 hr from HA=1 hr to 2. Data are analyzed either separately, or combining series of observations; planets are detected if visible in at least one such combination.

For each of these strategies we run the MESS code, using detection maps appropriate for each star both in the nearby and young samples, computed according to the recipes for each strategy. The procedure was repeated ten times to reduce impact of statistical errors.

Table 8.2.1 and 8.2.1 give the number of planets of different masses expected to be detected with IFS observing the whole samples. Table

| $M_{Earth}$ | IFS: Young Sample ($\sim$ 1200 stars) | | | | | |
|---|---|---|---|---|---|---|
| Strategy | A | B | C | D | E | F |
| Tot hr | 1 | 10 | 10 | 10 | 20 | 20 |
| $> 300$ | 230.3 | 251.0 | 256.5 | 256.0 | 262.1 | 276.6 |
| 300-100 | 42.3 | 62.6 | 65.4 | 69.3 | 72.5 | 88.7 |
| 100-40 | 17.1 | 29.0 | 31.2 | 32.4 | 35.8 | 50.2 |
| 40-10 | 1.9 | 3.2 | 4.6 | 4.6 | 5.8 | 9.6 |
| $< 10$ | | | | | | |

Table 8.2: IFS detection for the young sample, according with planet distribution from Cumming et al. (2008)

| $M_{Earth}$ | IFS: Nearby Sample ($\sim$ 600 stars) | | | | | |
|---|---|---|---|---|---|---|
| Strategy | A | B | C | D | E | F |
| Tot hr | 1 | 10 | 10 | 10 | 20 | 20 |
| $> 300$ | 51.5 | 68.7 | 68.9 | 71.2 | 73.5 | 85.2 |
| 300-100 | 24.1 | 41.6 | 42.4 | 42.4 | 46.7 | 58.4 |
| 100-40 | 22.8 | 37.6 | 39.2 | 40.5 | 40.5 | 43.5 |
| 40-10 | 6.3 | 17.5 | 18.5 | 21.4 | 24.1 | 40.5 |
| $< 10$ | 1.5 | 3.3 | 3.2 | 4.0 | 4.6 | 7.9 |

Table 8.3: IFS detection for the nearby sample, according with planet distribution from Cumming et al. (2008)

8.2.1 shows the same results for EPOL, using the nearby sample only. The analysis was done using planet distribution from Cumming et al. (2008).

Inspection of these tables reveals the following results:

- Massive planets are discovered efficiently even with short exposures (1 hr)

- The number of small planets (Neptune-like and Rocky) detected increases very significantly when more observations are added up to about 10 hr; the gain with a further increase to 20 hr is significant if data are fully exploited (that is, the whole set of combinations of single 1 hr visits is considered).

- The details of the observing strategy are not critical: different strategies lead to similar amount of detections.

| $M_{Earth}$ | EPOL: Nearby Sample ($\sim$ 600 stars) | | | | | |
|---|---|---|---|---|---|---|
| Strategy | A | B | C | D | E | F |
| Tot hr | 1 | 10 | 10 | 10 | 20 | 20 |
| $> 300$ | 52.7 | 70.1 | 65.2 | 65.5 | 65.5 | 80.5 |
| 300-100 | 27.5 | 40.3 | 35.9 | 36.1 | 36.2 | 50.5 |
| 100-40 | 30.3 | 45.4 | 41.0 | 40.8 | 41.0 | 36.5 |
| 40-10 | 14.7 | 32.8 | 26.5 | 26.5 | 27.1 | 48.9 |
| $< 10$ | 3.2 | 10.2 | 7.7 | 7.3 | 8.0 | 23.5 |

Table 8.4: EPOL detection for the nearby sample, according with planet distribution from Cumming et al. (2008)

### 8.2.2 *Estimation of the number of targets needed to reach the science goals*

In Figure 8.2.2 we plotted the number of targets that should to be observed to obtain a given fraction of the planets of each type. Targets are sorted according to the probability that they have planets. This is evaluated trough a merit function, that takes into account the characteristics of the stars, and of the planets that to be detected around it. The details of the calculation of the merit functions are given in App. C.

This figure shows that small planets are detectable only among the top ranked targets: for instance, all detectable rocky planets ($M < 10 M_{Earth}$) are in orbit around the $\sim$ 10% top ranked nearby stars (that is, only stars within 6-7 pc from the Sun), while $\sim$ 50% of the young Neptune-like planets ($10 < M < 40 M_{Earth}$) may be detected if we limit our survey to $\sim$ 12% of the young star sample. Most massive planets existing around the EPICS targets we considered in this analysis will be detected, so that their number increases roughly proportionally to the sample size. However, to properly normalize the results we should also consider how many planets of the various mass ranges are expected to be detected. They are some 4 rocky planets, 14 Neptune-like planets, and about 150 Giant Planets from observation of the full sample of nearby stars; and no rocky planets, 4 Neptune-like planets, and 340 Giant Planets from the young star sample, if 10 hr are devoted to each single target. Hence, while the number of small planets we expect to detect is very small, while those of massive planets is so large that even observation of a fraction of the whole sample may provide very useful information.

Based on these considerations, different strategies may be considered to reach the EPICS science goals:

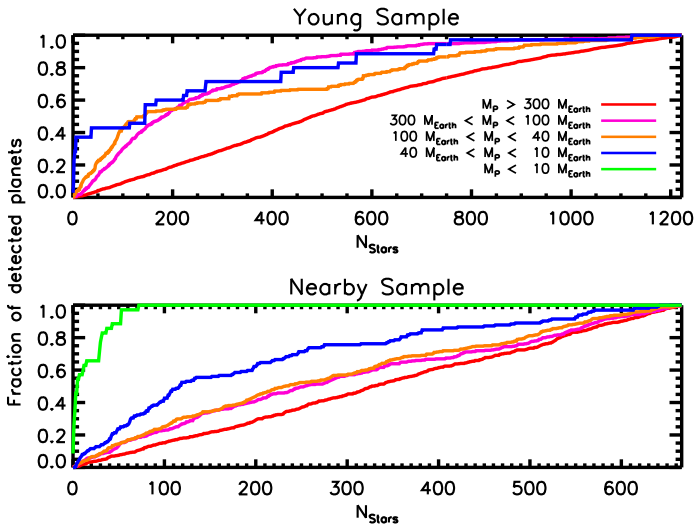


Figure 8.5: cumulative distributions of stars with detected planets. Stars have been sorted according to descending value of a merit function, evaluated as described in appendix C. Lines of different colors are for planets with different mass ranges.

1. Science goal 1: We may detect 100 Giant Planets from the Young star sample from a shallow survey, dedicating some 1 hr each to about 500 targets (a total of 500 hr). Such a survey will likely be limited to planets with masses $> 40 M_{Earth}$. Observation of Neptune-like planets (down to $10 M_{Earth}$) is in principle possible, but it requires both a larger sample ($\sim 700 targets$) and deeper observations ($\sim 10 hr$). This is very time consuming (a total of 7000 hr requested).

2. Science goal 2: Detection of $>$ 50 mature giant planets around nearby stars may be obtained by a shallow survey of about 500 targets, each with 1 hr observation. However, reaching the 100 detection limit requires deeper observations and/or a larger sample, and might be time consuming. Possibly a large fraction of the targets for this science goal may be stars previously identified either from radial velocities or from astrometry (GAIA). To get 100% of the detectable rocky planets, we need to observe between 50 and 70 stars from the nearby sample (that is a total of 500-700 hr). To get about 10 Neptune-like planets, we need to observe 200 stars (from the nearby sample). They include those with detectable rocky planets. In total, we need some 2000 hr (such a survey will also discover

some 85 giant planets, essentially covering the needs of Science goal 2).

EPICS will be clearly limited by available observing time rather than by the number of targets. All science goals require a considerable investment of observing time, but all of them (including follow-up observations) can be reached within 1.5 yr dedicated to EPICS, which is reasonable within the first decade of E-ELT.

### 8.2.3 *Evaluation of the requirements related to monochromatic contrast*

Achievement of scientific goals listed in Section 8.0.3 sets a requirement on monochromatic contrast, because the number of detected planets is a function of the contrast given by the instrument, as well as of the number of surveyed targets (provided that the best targets are indeed included in the sample: see below). On the other hand, a higher contrast requires a more effective extreme adaptive optic module (XAO), that includes either a larger number of actuators or a shorter timescale for instrument response, or (likely) both. This results in a brighter limiting magnitude. In order to better achieve science goals, some compromise between sample size (limiting magnitude, discussed in the next subsection) and contrast should be found. Details depend on many parameters including expected instrument performances, the assumed planet distributions, and target sample characteristics, because in general, detection probability is expected to change largely from target to target. However, considering a reasonably optimized target sample like that described in Section , we may consider the data of Table 4 as rough order of magnitude estimates of the expected number of detections. Limiting contrast is mainly determined by:

1. Photon noise, which depends on many parameters, including e.g. instrument efficiency, XAO performances etc.

2. Calibration errors, which also depend on many parameters, like residual post-coronagraphic wavefront errors, flat field accuracy, etc.

Figure 8.2.3 and 8.2.3 illustrate the dependency of the number of planets detected in the nearby star sample considered in Sec. 8.2 while changing the instrument efficiency (which directly impacts on photon noise) and at different contrast limits (which is related to calibration errors). While

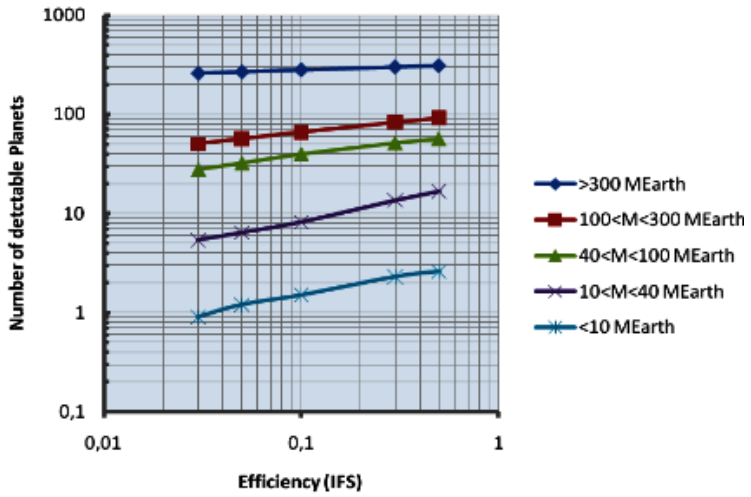


Figure 8.6: Detected planets in the nearby sample as a function of instrument efficiency (1 hr exposure time; average of ten simulations).

detection of warm giant planet is not sensitive to these limits (essentially because all such planets are detected at rather high SNR), the number of detected cold giant planets and Neptunes changes significantly: by a factor of $\sim 3-4$ for a variation of a factor of 17 of the efficiency (from 0.03 to 0.5; this approximate square root dependence is expected for photon noise limited cases); and by factors of $\sim 3-4$ for a change in limiting contrast between $10^-8$ to $10^-9$. Even more sensitive to variations in limiting contrast is detection of rocky planets; in this case essentially no detection is expected if the efficiency is $< 0.05$ and limiting contrast is not better than $10^{-8}$ at a separation of $\sim 0.1$ arcsec.

### 8.2.4 *Evaluation of the requirements on the magnitude limit of adaptive optics*

A fainter magnitude limit of XAO allows more planet detections (see Figure 8.2.4). However, the magnitude limit of EPICS is critical in particular for observation of young, self luminous planets in star forming regions: members of young clusters/groups (e.g. $\eta$Cha, US, UCL, LCC, etc, at distances of $\eta$ Cha, US, UCL, LCC, etc, at distances of 100-150 pc) of spectral types G have $I \sim 9$. The magnitude limit of the instrument is typically set by XAO working conditions. For the EPICS XAO a requirement of I=9 was established. These XAO magnitude limit corresponds to different horizons for main sequence stars of different spectral types, as listed

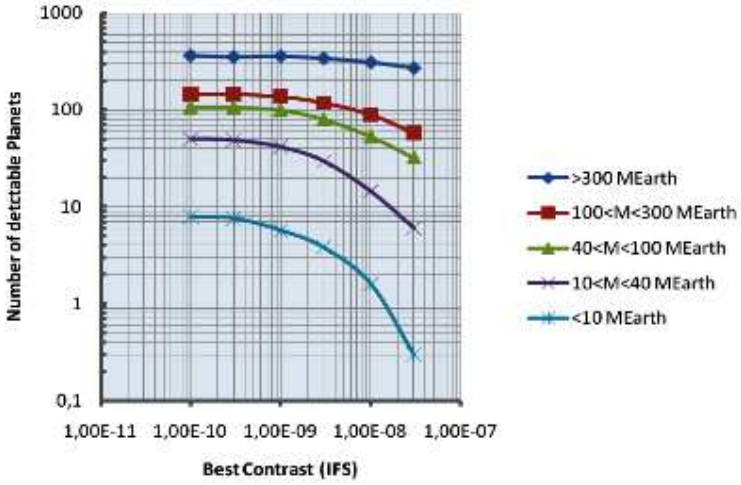


Figure 8.7: Detected planets in the nearby sample as a function of limiting contrast (20 hr observations; average of ten simulations).

| Spectral Type | Mass $M_\odot$ | $M_I$ | Dist TLR | Snowline (AU) | Snowline at 1/2 dist TLR (arcsec) |
|---|---|---|---|---|---|
| AoV | 2.40 | 0.7 | 457 | 15.6 | 0.068 |
| GoV | 1.12 | 3.6 | 120 | 3.4 | 0.057 |
| MoV | 0.52 | 6.3 | 35 | 0.7 | 0.040 |

Table 8.5: Approximate maximum distance at which main sequence stars of different spectral types can be observed with EPICS (XAO mag limit). Interstellar absorption in neglected. The last two columns list the location of the snowline in AU and in arcsec at a distance of half of the limiting distance for full AO performances

in Table 8.2.4. This table also lists the location of the snowline in the protoplanetary disks in AU and in arcsec at one half the horizon distances (for TLR conditions).

#### 8.2.4.1 *Operation at faint magnitudes*

For stars with magnitude close to the XAO limits, photon noise is expected to overcome the residual speckle calibration noise for typical integration time of a few hours but in the very inner regions of the FoV. In general we can expect that stars with J and H $> 8$ might become high priority targets only when the planet/star contrast is highly favourable (intrinsically faint stars such as nearby M dwarfs or white dwarfs and very young stars at moderate distance). In any case, the dominance of

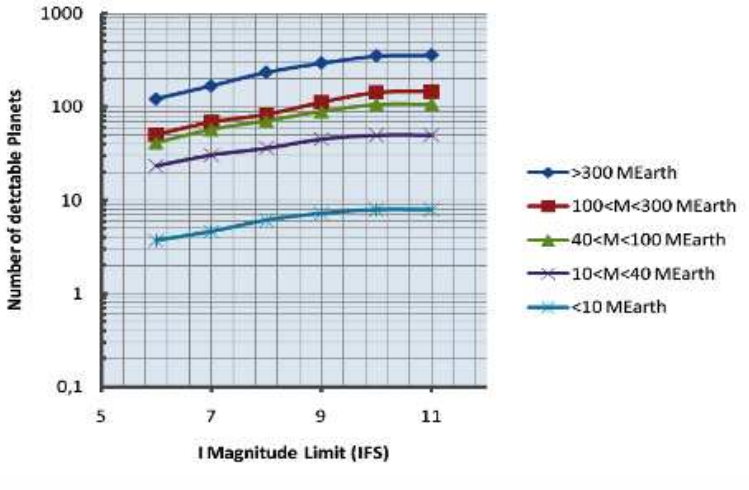


Figure 8.8: Number of detected planets as a function of the limiting I magnitude (20 hr exposures, average of 10 simulations)

photon noise suggests the usefulness of an appropriate observing strategy in these cases, which allows increasing observational efficiency.

#### 8.2.4.2 *Very bright targets*

Some of the brightest stars in the sky ($\alpha$ Cen, Sirius, Aldebaran) are interesting targets for EPICS. The brightest star in J and H bands is Betelgeuse (J=â3.0, H=â4.0), possible target for secondary science. It is useful that EPICS has the capabilities to observe all the brightest stars in the sky. In case of saturation in the shortest possible DIT, suitable neutral density filters should be included.

### 8.2.5 *The Poor-Man AO Case*

Performance of XAO on the E-ELT might be limited by technological achievements, at least in the short term. For this reason we considered in our study also performances obtained with a less challenging XAO system, that we call Poor-Man AO. In Table 8.2.5, we compare the number of planets expected to be detected with EPICS if either the default AO performances are achieved, or those relevant for the Poor-Man case. Of course, a smaller number of planets are expected to be detected in this last case. However, the limitation is severe only for rocky planets; hence,

| | Young Sample | | Nearby Sample | |
|---|---|---|---|---|
| $M_P(M_{Earth}$ | Default | Poor Man | Default | Poor Man |
| $> 300$ | 276.6 | 244.8 | 85.2 | 58.0 |
| 300-100 | 88.7 | 53.4 | 58.4 | 30.8 |
| 100-40 | 50.2 | 22.2 | 56.8 | 29.7 |
| 40-10 | 9.6 | 2.6 | 40.5 | 10.9 |
| $< 10$ | | | 7.9 | 1.5 |

Table 8.6: Comparison between numbers of planets expected to be detected with default and Poor-Man AO (IFS alone).

EPICS would be a very competitive instrument even if only Poor-Man XAO would be available.

### 8.2.6 *Requirements related to spatial information*

#### 8.2.6.1 *Inner working angle*

Extra solar planets are expected at small angular separations from the stars, so that a small Inner Working Angle (IWA) is generally required. The constraint from the total number of detected planets is not very significant (see Figure 8.2.6.1). The most stringent constraints are those given by:

- Observation of the snow-line region around solar type stars (G2V) in star forming regions and young associations. From inspection of data given in , IWA should be as small as possible: a value of 0.03 arcsec is required to explore the snow-line region in the TW Hya associations, while an even smaller value of 0.02 arcsec is required to get close to that region in the remaining star forming regions listed in that table.

- Observation of those planets for which the reflex motion of the star is detected by RV. indicates that several tens of planets discovered by radial velocities are detectable with EPICS if the IWA is as small as 0.05 arcsec; however, this number would be twice as large for an IWA=0.02 arcsec. Furthermore, detection of (giant) planets in the HZ requires an IWA as small as 0.02 arcsec.

- observation of rocky planet shining by reflected light

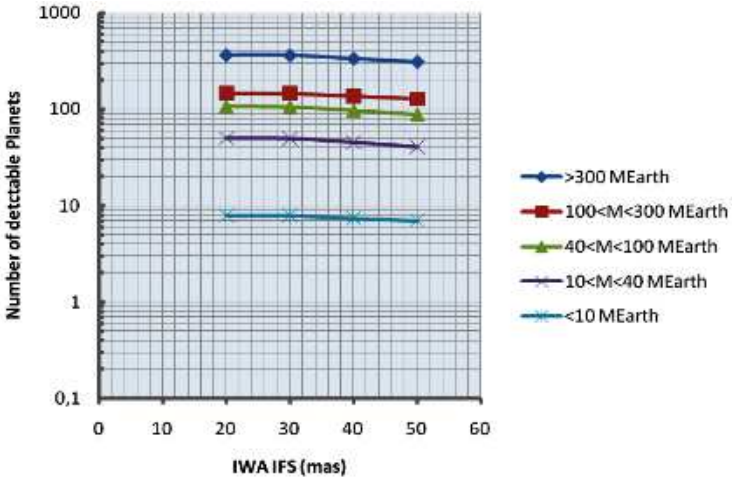


Figure 8.9: Number of detected planets with EPICS IFS as a function of the IWA (20 hr exposure; average of 10 simulations)

These are very important observations, essentially driving the whole design of EPICS and of the same E-ELT. These considerations set the minimum working angle of IFS at 0.03 arcsec, with a goal at 0.02 arcsec. Incidentally, we note that a peculiar characteristic of IFS is the possibility to derive accurate spectra using the spectrum deconvolution technique (Thatte et al. 2007). The method works best outside the so-called bifurcation point, which depends on spectral coverage and minimum wavelength: the bifurcation point is closer to the stars if the spectral coverage is larger, and if the minimum wavelength is shorter; in an IFS design, spectrum length is generally weighted against field of view, so that some compromise should be considered. Ideally, the bifurcation point should coincide with the IWA: however somewhat less accurate spectra can be obtained even closer to the star than the bifurcation limit, using a suitable iterative procedure (see Thatte et al. 2007). The bifurcation point is at $\sim$ 0.03 arcsec for the current design of the IFS; this coincides with the minimum working angle.

#### 8.2.6.2 *Field of view*

The field of view should be as large as possible in order to image most of the planetary systems. Practically however, planets are not expected at angular separations larger than a few arcsec. Even if a larger FoV will allow a significant science potential (planets at extremely large separa-

tion, better astrometry if suitable background objects are included in the FoV) performances of AO are expected to degrade significantly at large distances from the reference star. XAO is not expected to be much superior to other AO techniques at separations larger than the control radius (about 0.4-0.6 arcsec from the reference star, depending on wavelength). A FoV of 0.8 arcsec square is adequate. Our simulation indeed suggests that less than 1% of the planets detected on a 1 arcsec FoV (radius) are expected to be lost for an even smaller FoV (radius) of 0.4 arcsec.

## 8.3 CONCLUSIONS

The extensive use of the prediction mode of MESS, applied to the two science channels of EPICS, IFS and EPOL, allowed a detailed analysis of both the expected performances of these two instruments and the evaluation of the requirements to be fulfilled, in order to achieve the science goals listed in Sec. 8.0.3.

The results of all these studies can be summarized as follows:

*Young self-luminous giants*

While instruments on 8-10 m class telescope (SPHERE and GPI) should allow detection of a few tens planets (essentially Giant Planets) around a few of the closest young objects (see Sec. 7.4), the much higher sensitivity of EPICS should allow to observe much fainter planets, that is both less massive and/or older, and moreover to explore with high sensitivity much inner regions, close to the snowline. Figure **??** suggests in fact that Neptune-like planets should be detectable by EPICS down to a few (2-3) AU even if the limiting contrast is only $10^{-6}$. EPICS should then allow a complete census of the gaseous planets that form outer of the snowline. This is very important in order to better constrain the mechanism of formation of giant planets in the outer parts of the system. As discussed in Sec. 8.2.4 and 8.2.6.1, the most critical requirements for this science goal concern EPICS limiting magnitude (I=9 and possibly even fainter) and inner working angle (0.03 arcsec, and possibly 0.02 arcsec), while limiting contrast is less critical (see Sec. 8.2.3); very useful data could be obtained even if only a rather conservative value of $10^{-6}$ is achieved (although of course this program will gain significantly from achievement of a better contrast). It should be noticed that young massive planets will be de-

tected at quite high S/N with EPICS. This means that they can be targets of follow-up observations with higher spectral resolution.

*Mature planets in the solar neighborhood*

Figure 8.3 shows the behaviour of the detected simulated planets in the plane contrast vs projected separation, while Figure 8.3 shows the detected planets in the semi-major axis vs mass plane.

It comes out that essentially all giant planets at projected separation beyond the EPICS IWA will be detected, making up a sample of several hundred objects.

A similar survey will also be quite effective in detecting Neptune like planets, with several tens of them detected, in the range of projected separation from the IWA up to about 0.1 arcsec. This will be fully adequate for a statistical discussion of their properties.

On the other hand, in our simulations only a few Earths and super-Earth are detected (around very close and bright stars), making the success rate heavily dependent on random fluctuations. Inspection of Figure 8.3 indicates that the most critical parameter for detection of Super-Earths in this sample of stars is the best limiting contrast that could be achieved by EPICS for very bright stars: out of the EPICS IWA (0.02 arcsec at best), all mature Super-Earths have a contrast worst than $10^{-9.5}$, making them difficult objects at these small separations.

*Planets discovered with other techniques*

Given the distribution of separations for planets known from radial velocities (see e.g. Figure 8.3), imaging of planets detected by RVs put constrains on both the Inner Working Angle and on the contrast at very small separations. While planets at larger distances from the star are expected from RV surveys in the next years (stars that have clear trends of radial velocities being obvious candidates), it is clear that accessibility to planets at angular separations of $< 0.05$ arcsec and with monochromatic contrasts of at least $10^{-8}$ is required in order to obtain images of a large sample of planets already discovered by radial velocities.

In addition, minimum semi-major axis decrease from $\sim 1.5AU$ for IWA=0.05 arcsec to $\sim 0.8AU$ for IWA=0.02 arcsec: this should allow obtaining spectra of objects in the Habitable Zone, where significant variations of atmospheric composition are expected. On this respect, EPICS

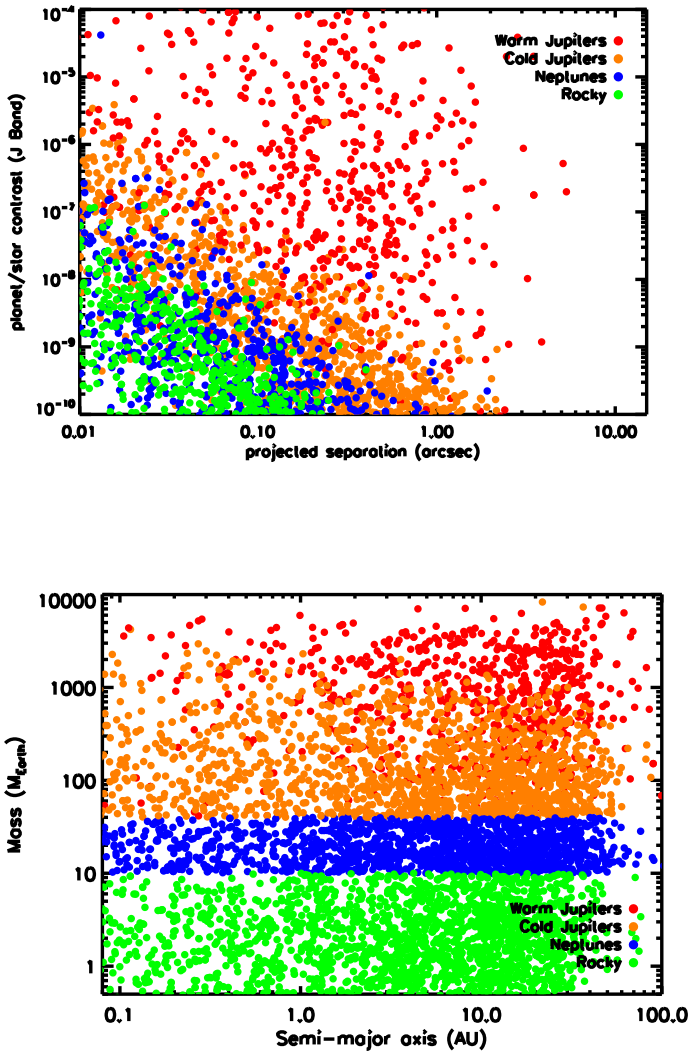


Figure 8.10: Expected simulated planets for the combination of young ($Age < 200$ Myr, $\sim 1200$ stars) and nearby ($d < 20pc$, $\sim 600$ stars) samples in the plane contrast versus projected separation (left) and in the semi-major axis versus mass plane (right). Different mass ranges are plotted with different colors.

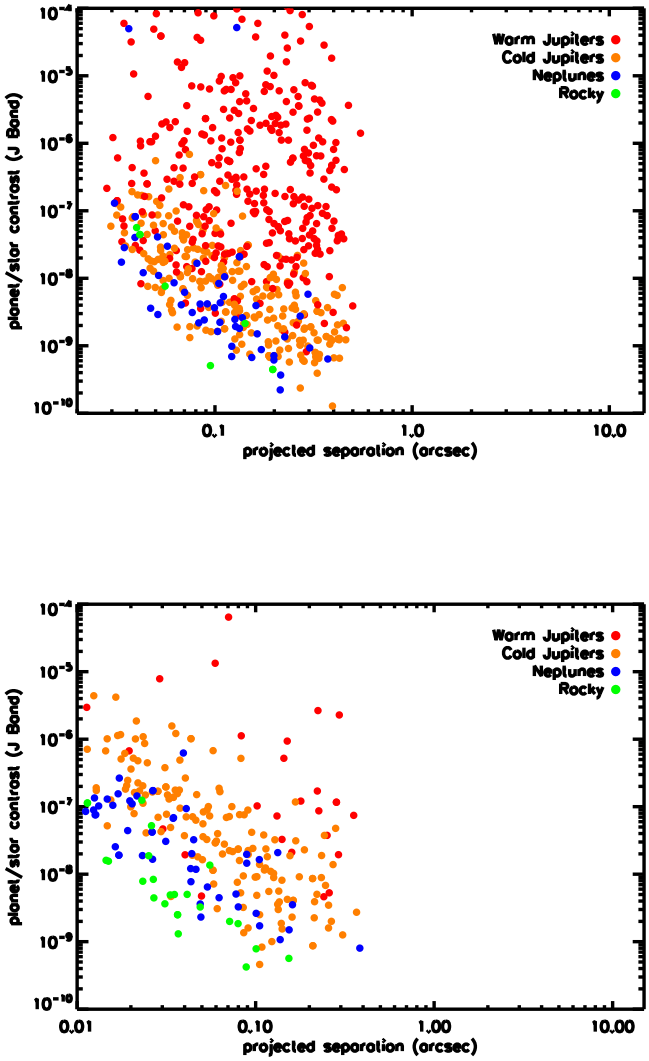


Figure 8.11: Detected (top: IFS; bottom: E-POL) simulated planets for the combination of young ($Age < 200$ Myr, $\sim 1200$ stars) and nearby ($d < 20pc$, $\sim 600$ stars) samples in the plane contrast versus projected separation. Only the results of the simulation for the observing strategy F (20 poses of 1 hour, see Sec. 8.2.1) are showed.

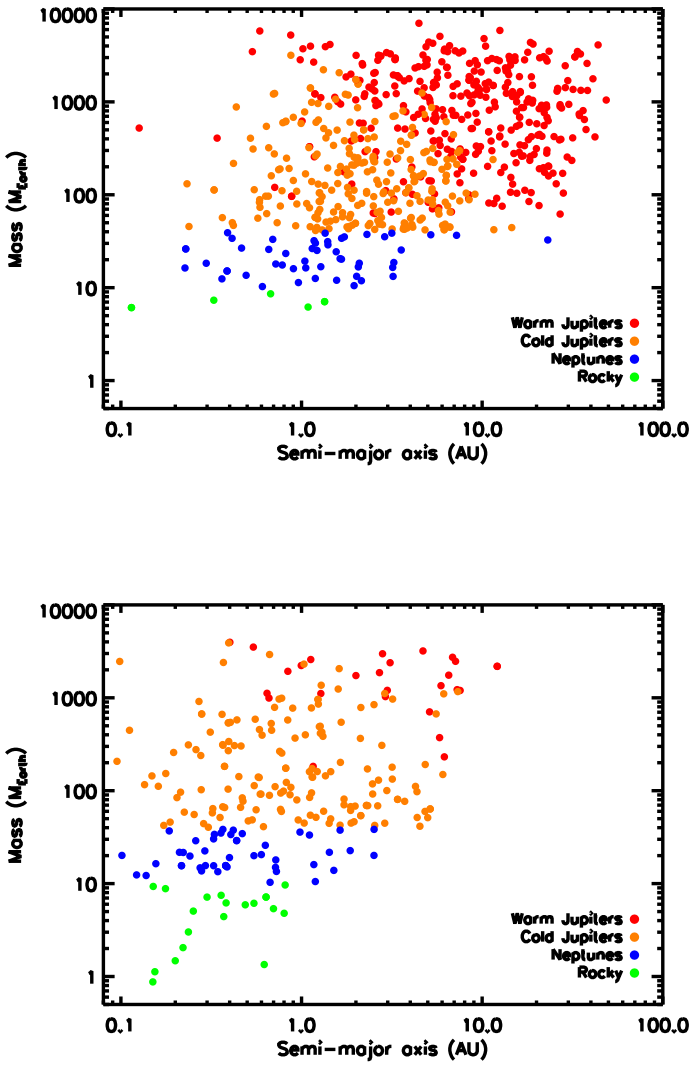


Figure 8.12: Planets detectable by IFS (top) and E-POL (bottom) plotted in the semi-major axis versus mass plane

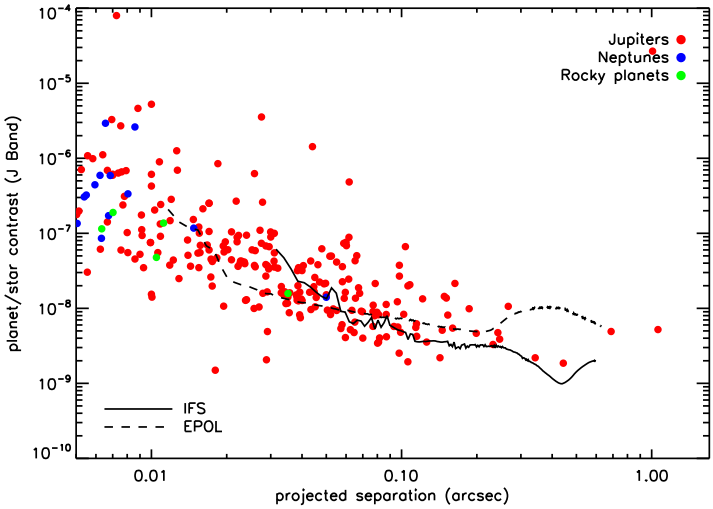


Figure 8.13: Exosolar planets already discovered with radial velocities in the separation-contrast plane. The solid line represents the approximate detection limit for IFS and the dashed line for E-POL for a G2V star at 30 pc (10x1 hr exposures). EPICS should be able to detect several tens of these planets.

should represent a major step forward with respect to SPHERE, GPI, and JWST, that should be able to detect only very few if any of these planets. It should also be noticed that a few of these planets are several order of magnitude above the EPICS limiting contrast: very accurate characterization should be possible for such objects.

An interesting overlap region also exists with the planets that might be discovered by the PLATO transit mission, proposed within the ESA Cosmic Vision program and currently approved for a definitive phase A. Planets down to about 10 Earth masses around M dwarfs with magnitude about V=8.5-10 (the bright end of PLATO) can be detected also with EPICS (see Figure 8.3). For K dwarfs, planets in the habitable zone are detectable. The availability of planet spectra from EPICS and planet radii from PLATO will be extremely relevant for the physical study of the planets. For G and F stars (and K and M dwarfs as well) planets at separation larger than that accessible to PLATO can be detected, allowing to study the outer planetary system of PLATO targets.

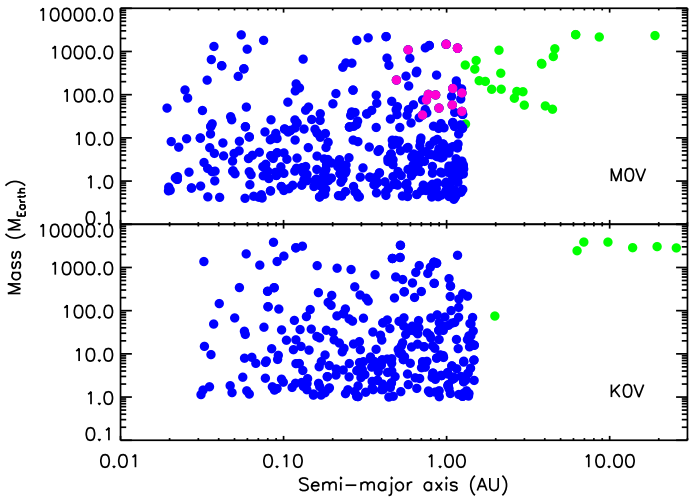


Figure 8.14: Expected overlap of detections with EPICS and PLATO; only K and M stars are shown because only for these stars there is overlap.

*Planet characterization*

A large number of planets can be observed with EPICS at resolution R=3,000, and even a few at high spectral resolution of R=20,000 (see Figure 8.3 and 8.3, respectively). Observable objects include warm and cold Jupiters, Neptunes, and even a few Rocky Planets.

Expected observable planets cover a wide range of expected parameters (mass, temperature, atmospheric composition, etc.). Figure 8.3 shows the mass- temperature relation for the planets expected to be detected by IFS (top) and EPOL (bottom). These planets span a large range in temperature, from over 2000 K for the most massive young planets, down to much less than 100 K for the old gaseous giants far from the central star. Neptunes and Super-Earths are detectable only if they are not too far from the star; they are then expected to be warmer, with (equilibrium) temperatures up to $\sim 200 - 300K$. Spectra of Giant and Neptune-like planets are expected to be dominated by methane bands; these are resolved at a resolution $R > 15$. Spectra with resolution $R > 30$ are then not required in order to detect the Planets, at least insofar the band contrast is considered.

Summarizing, the most critical requirement for the first science goal concerns the limiting contrast achievable with EPICS, which is determined by photon and calibration noise. Limiting contrast should be $10^{-9}$ (Nep-

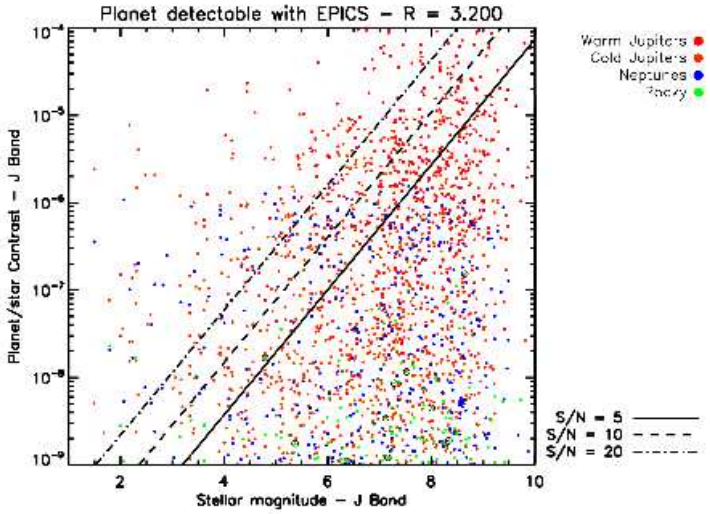


Figure 8.15: Planet-star contrasts as a function of stellar magnitude for the whole sample from our Monte Carlo simulations. Over-imposed are lines representing S/N achievable at a resolution of 3.000 (4 hr observing time). Circles are planets in the habitable zone.

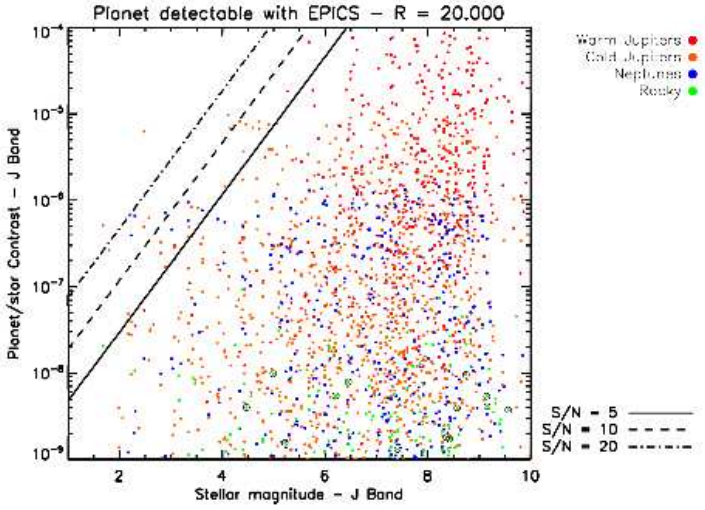


Figure 8.16: Same as Figure 8.3, but this time for a spectral resolution of 20.000.

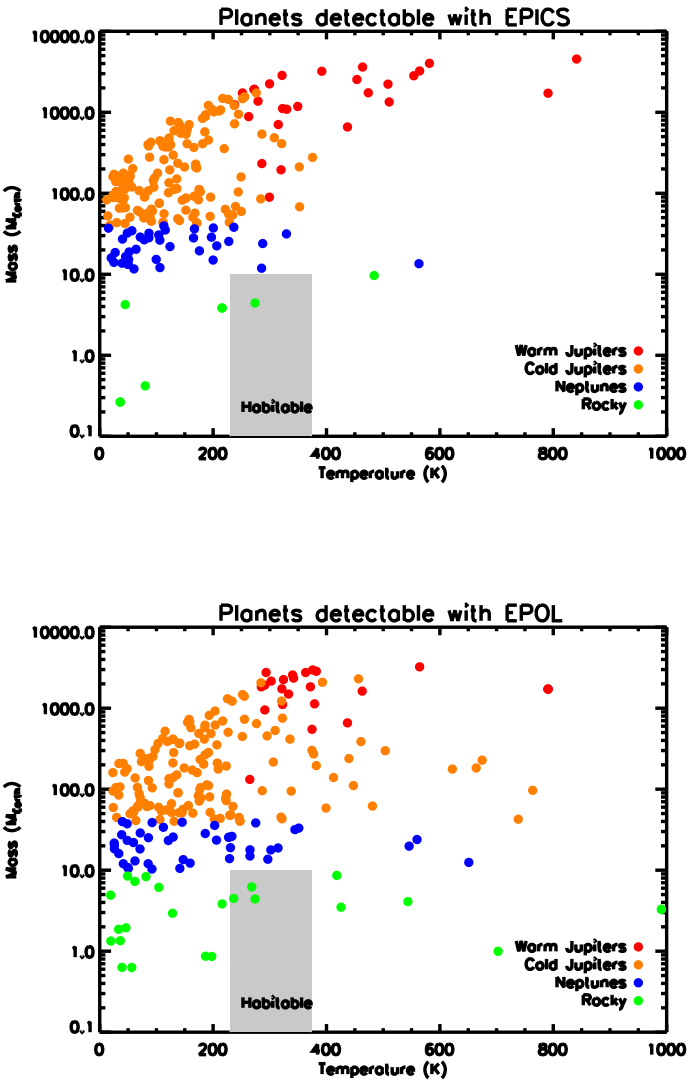


Figure 8.17: Mass-temperature relation for the planets expected to be detected by EPICS (top: IFS, bottom: EPOL), including samples of young as well as nearby stars. For reflecting planets, the equilibrium temperature was computed neglecting greenhouse effect. The habitable zone is marked in gray.

tunes), ideally $10^{-10}$ (Super-Earths), at a separation of 0.1 arcsec. Longer exposure times can be considered, but of course high instrument efficiency and small calibration errors are critical. For science goal 2, the Inner Working Angle is critical (0.03 arcsec, and possibly 0.02 arcsec) together with the contrast at small separation (a contrast better than $10^{-8}$ and as good as $10^{-9}$ at separation in the range 0.05-0.1 arcsec is required). With expected contrasts in the range $10^{-7} - 10^{-8}$, spectra at reasonable high S/N ($> 30$) can be obtained for several tens of these planets in a few hour of observations each with the IFS; higher resolution observations will be possible for a few of them. Coupled with the polarization information that can be derived using E-POL, a detailed characterization of the planetary atmospheres at different position angles will be possible with EPICS.

# 9

# TOWARD OTHER EARTHS

*adapted from " Scientific Output of Single Aperture Imaging of Exoplanets" R. Gratton, M. Bonavita, et al. 2009 to appear in the proceeding of the Pathways Towards Habitable Planets Conference*

In this chapter we discuss the results of the evaluation, done with MESS, of the scientific output expected from single aperture imaging of exoplanets. This has been done by comparing expected detections from different ground-based and space instruments, either in construction or proposed for the next future. Images of a few young giant planets have been already obtained, and many more are expected with planet finders on 8 meter class telescopes or JWST. Direct detections of Neptune-like and rocky planets require a new generation of instruments, either specialized satellites or extremely large telescopes from ground. We underline that ELTs, and in particular the E-ELT, may allow to characterize planets detectable with indirect techniques, like RV and astrometry, allowing an important step forward in planetary science.

## 9.1 CONTEXT

Direct imaging is not only the technique that captures more easily the attention of the general public, but it also provides a wealth of information about exoplanets. First, it might be the fastest way to detect them: a single image is in principle enough, although practically confirmation of candidates might be not easy. Even multiple systems, which require a huge number of observations from indirect techniques, can be solved at once by imaging. Second, images taken at various epochs might provide the planet orbit, if short enough. Finally and more important, detailed characterization of the planets is possible, using photometric, spectroscopic or polarimetric techniques.

However, direct imaging of exoplanets is very difficult, due to the very large contrast between the star and the planet, and the very small apparent separation: it was then for a long time a dream. However, this is not anymore true. Table v lists the planets already discovered by direct imaging (source is the Extrasolar Encyclopedia[1]), along with some of their

[1] http://exoplanet.eu/

| Planet | Planet Mass ($M_J$) | Star Mass ($M_\odot$) | Separation (AU) | Separation (arcsec) | Age (Myr) |
|---|---|---|---|---|---|
| 2M1207 b | 4 | 0.025 | 46 | 0.88 | 8 |
| CT Cha b | 17 | | 440 | 2.67 | |
| USco CTIO 108 b | 14 | 0.057 | 670 | 4.62 | 5.5 |
| AB Pic b | 13.5 | | 275 | 6.03 | 30 |
| GQ Lup b | 21.5 | 0.7 | 103 | 0.74 | 1 |
| $\beta$ Pic b | 8 | 1.8 | 8 | 0.41 | 12 |
| HR8799 b | 7 | 1.5 | 68 | 1.73 | 60 |
| HR8799 c | 10 | 1.5 | 38 | 0.96 | 60 |
| HR8799 d | 10 | 1.5 | 24 | 0.61 | 60 |
| Fomalhaut b | $<3$ | 2.06 | 115 | 14.94 | 200 |

Table 9.1: Exoplanets discovered by direct imaging

properties. As it can be seen, detection was made possible because some of the following circumstances (or all of them) hold: description

(i) the planet-star mass ratio is small (the contrast is lower);

(ii) young age (the planet is brighter);

(iii) large physical/angular separation between the planet and the star.
As already mentioned before, the concerns related to the large contrast and small separation determine the characteristics of the instrumentation required to image exoplanets. In the optical and near infrared (NIR), all but the very youngest and massive planets shine due to reflected starlight. Contrast is expected to be very large: e.g. the most luminous Solar System planets (Venus, Jupiter and Earth) have luminosities of about $10^{-9}$ that of the Sun or less. The contrast is much more favourable in the mid-IR, where thermal emission from the planets may be $10^{-4}$ (or even more, for very young and massive planets) that of the star. However, background is a serious issue at these wavelengths, making these observations of a difficulty comparable to those at shorter wavelengths.

## 9.2 PROJECTS FOR THE NEXT DECADE

Several instruments specifically designed to image extra-solar planets are under construction or in design. These new instruments will provide a wealth of new data about exoplanets, and ultimately we hope that direct imaging will allow answering fundamental questions about planetary sys-

tems. In this talk, we will review some of the expected output from these instruments, focusing on only those instruments that use single apertures; instruments based on interferometric approaches will be discussed in another talk at this meeting. Among the various projects existing, we selected for our analysis only a few of them, which appeared to us more likely to be realized in the mid-term.

1. A number of Planet Finders are already available or under construction for ground based 8m telescopes. These include Hi-Ciao at Subaru (Tamura et al. 2006), SPHERE at VLT (Beuzit et al. 2008), and GPI at Gemini South Macintosh et al. (2008), the two last being more ambitious and likely more performing. Both of them are foreseen to be operative in 2011. Designs are similar, including an Extreme AO systems, a coronagraphic module, and an Integral Field Spectrograph (IFS) working in the Y-J-H bands. SPHERE will also include IRDIS, which allows differential imaging over a wider field of view and long slit spectroscopy, and a high precision differential polarimeter (ZIMPOL). Performances of SPHERE and GPI are expected to be similar, although GPI should reach a deeper contrast (due to a further stage in the control of static aberrations), while SPHERE should allow observations of slightly fainter sources (being still limited at targets with $I < 10$).

2. JWST, which launch is expected in 2014, will provide facilities allowing to image exosolar planets in the NIR ($< 5$ $\mu$m: NIRCAM/TFI[2]) and in the mid IR ($> 5$ $\mu$m: MIRI[3]). Due to the worse control of the wavefront errors and smaller telescope size, NIRCAM will not allow higher contrasts and smaller inner field of view with respect to SPHERE and GPI; however, it will not be limited to bright targets, and will then have an important niche for nearby extreme M stars. MIRI will open a new window, outperforming by far existing ground based mid-IR imagers.

3. A third group of instruments includes 1.5 m class space coronagraphs, forerunners of the much more ambitious TPF. There are many projects proposed: PECO (Guyon et al. 2008), EPIC (Clampin et al. 2006; Lyon et al. 2008), ACCESS (Trauger et al. 2008), SEECOAST (Schneider et al. 2009). None of these projects is presently

[2]http://ircamera.as.arizona.edu/nircam/

[3]http://www.roe.ac.uk/ukatc/consortium/miri/index.html

| Instrument | Contrast | Wavelength ($\mu$m) | IWA (arcsec) | Year |
|---|---|---|---|---|
| 8 m ground-based telescopes | | | | |
| VLT-SPHERE<br>Gemini-GPI | $10^{-7}$ | 0.9-1.7 | 0.08 | 2011 |
| JWST | | | | |
| NIRCAM | $10^{-5}$ | 2.1-4.6 | 0.30 | 2014 |
| MIRI | $10^{-4}$ | 5-25 | 0.35 | |
| 1.5 m Space Coronagraphs | | | | |
| | $10^{-9} - 10^{-10}$ | 0.3-1.3 | 0.08 | ? |
| ELT's class instruments | | | | |
| E-ELT-EPICS | $10^{-8} - 10^{-9}$ | 0.9-1.7 | 0.03 | $>$ 2018 |
| E-ELT-METIS | $10^{-5}$ | 2.5-20 | 0.08 | |

Table 9.2: Instruments for direct imaging of exoplanets considered in this analysis

funded, but if approved they can likely become operative before the end of the next decade. Without entering into the details of this competition, expected performances from these various instruments are quite similar each other, defining the same science niche.

4. At last, there are three projects for extremely large telescopes that are very actively pursued by the North American (TMT and GMT) and European (E-ELT) astronomical communities. While not yet approved, these programs appear feasible in 8-10 years from now. All these projects consider instrument for direct imaging of exoplanets. Some of them are in the near-IR: EPICS at E-ELT (Kasper et al. 2008), PFI at TMT (Crampton et al. 2009), HRCAM at GMT (Johns 2008). Other in the mid-IR: METIS at E-ELT (Brandl et al. 2008), MIRES at TMT (Crampton et al. 2009), MIISE at GMT (Johns 2008). E-ELT, with its 42 m diameter is the most ambitious among these projects.

Table 9.2 lists the main properties of these projects.

## 9.3 WHICH PLANETS CAN BE OBSERVED IN THE NEXT DECADE

We used the *Prediction Mode* of MESS to analyze the discovery niches for each of the instruments considered in the previous section.

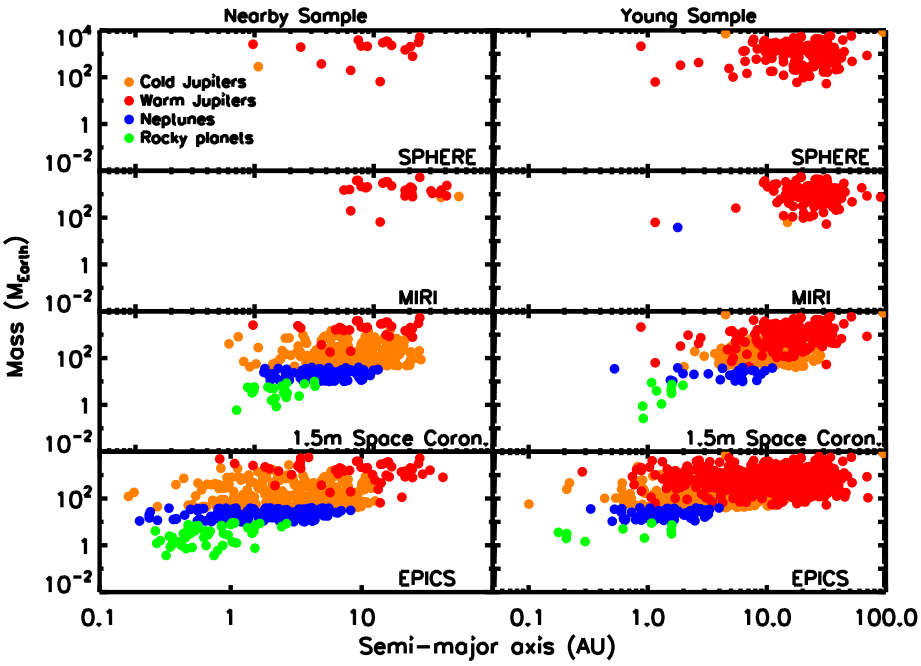


Figure 9.1: Planets expected to be discovered by SPHERE (representative of planet finders on 8m class ground-based telescopes), JWST-MIRI, 1.5m Space coronagraphs, and EPICS/E-ELT (representative of 30-40m class telescopes) in the mass vs separation plane. Different colours are used for warm giant (orange), cold giant (red), Neptune-like (blue), and rocky planets (green) respectively. Plots at left are obtained considering the nearby sample, those on the right with the young star sample

| Instrument | Year | Young Giants | Old Giants | Neptunes Planets | Rocky Planets | Habit. Planets |
|---|---|---|---|---|---|---|
| Ground based 8m | 2011 | tens | few | | | |
| JWST | 2014 | tens | few | | | |
| 1.5m Space Coro. | ? | tens | tens | tens | few | ?? |
| ELT's | $> 2018$ | hundred. | hinder. | tens | few | ?? |

Table 9.3: Summary of expected detections from imagers in the next decade

Figure 9.3 compares the planets expected to be discovered by the various instruments considered in the present review. Different colours are used for warm giant, cold giant, Neptune-like and rocky planets respectively. Table 9.3 summarizes the results. Ground based 8 m telescopes and JWST will allow for mid of the next decade to have a quite clear picture of the outer parts of the planetary systems, not explored by the indirect techniques. Not only the architecture of the systems can be determined, but also photometry and spectroscopy of these planets can be obtained, providing information about the physics of their atmospheres. Most observations will be focused on young systems, providing crucial information about the formation phases, and data about the disk-planet interactions.

At the end of the decade, 1.5 m space coronagraphs and ground based ELT will allow to enlarge considerably the range of masses and separations of the imaged planets. Some tens of Neptune-like and even a few rocky planets will become detectable. With some luck, even some planets in the habitable zone might be discovered.

## 9.4 SPECTROSCOPY AND ATMOSPHERE COMPOSITION

Imagers equipped with IFS's or long-slit spectrographs will allow obtaining low resolution spectra of exosolar planets, information that can now only be obtained for transiting systems. This allow probing the atmospheric composition. Bands of different species are accessible in the spectral ranges observed by the various instruments. CO, $O_2$, $NH_3$, $CO_2$, $CH_4$ and $H_2O$ can be observed by NIR instruments (Sphere, GPI, NIRCAM, EPICS) in the next few years for giant planets, and possibly at the end of the decade for Neptune-like and rocky planets. Additional species, including $O_3$, $H_2S$, $PH_3$, $C_2H_2$, and $H_3^+$ have prominent bands in the mid-

IR, observable with MIRI and METIS; such observations will be limited to giant planets due to the detection limits of these instruments. Finally, space coronagraphs working at visible wavelengths will also allow observations of several molecules, including life signalling $O_2$, possibly for rocky planets. However, the rocky planets discovered by such last instruments will likely be too cold for hosting life. In spite of these limitations, all these spectroscopic information, coupled with additional polarimetric observations (crucial to determine the height where haze or clouds form), will allow a much better understanding of planetary atmospheres, and will pave the road for ambitious projects like TPF.

Spectra at higher resolution than in standard set-up for planet detection will allow a more detailed characterization (for planets detected with high enough S/N). Some science goals include identification of spectral features, determination of physical parameters (temperature, gravity, chemical composition), cloud formation processes and their variation with time (e.g. for planets in eccentric orbits). Various resolution, from R=3000 to R=20000 are considered, the higher resolution modes being more suitable on ELT's (see Sec. 8.3): we expect hundreds of exoplanets observable at medium resolution, and some tens at the higher resolution. Also planet radial velocities could be determined. This will be useful to constrain the planetary orbit if only visual measurements available, and the planet-star mass ratio even based on small time baseline; or to detect binary planets, if any. Finally, planet rotational velocity could also be determined (for reference, Jupiter equatorial rotation velocity is 12.6 km/s); field T dwarfs typically rotate faster (30-50 km/s: McLean et al. 2007; Zapatero Osorio et al. 2006). 2006). R=20,000 corresponds to FWHM=15 km/s, and R=3000 to 100 km/s. There is then the possibility of measuring rotational velocity similar to that of Jupiter. This is very interesting if coupled with photometric rotational modulation, providing the planet radius independent of luminosity, or the inclination of rotational axis over the orbital plane.

## 9.5 SYNERGIES WITH OTHER TECHNIQUES

In this last section we comment on synergies of imaging with other techniques. Those with dynamical methods are interesting, because these last allow determining the planet masses, eliminating the degeneracy with age. Until mid of next decade, exoplanets discovered using ground based

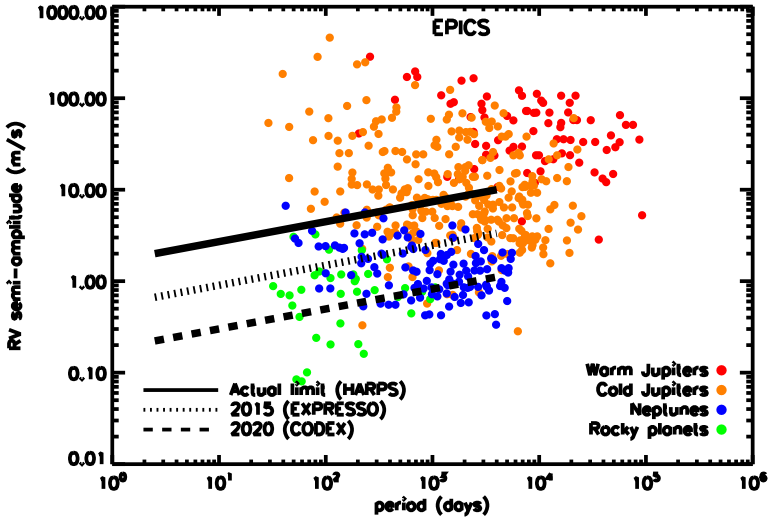


Figure 9.2: Planets expected to be detected by EPICS (nearby sample) in the RV signal vs. period plane, compared with detection limits for RV instruments (HARPS, ESPRESSO and CODEX). Colour code is the same as in Figure 9.3.

8 m telescopes or JWST will likely be at large distances from the star. Periods of these planets are long (tens of years or even more), and only limited information about them could be obtained from dynamical methods: dynamical masses will then be determined only in a few favourable cases. The situation will however change completely if 1.5 m class space coronagraphs will be available, and even more with ELT's. The discovery space for EPICS at E-ELT overlaps well with those from radial velocity (RV) instruments (HARPS at ESO 3.6m telescope, ESPRESSO at VLT, and especially CODEX at E-ELT: see Figure 9.2), so that we may expect to get both spectra and masses for a large number of targets. The discovery space of EPICS overlaps also well with that of GAIA (Casertano et al. 2008, see Figure 9.4), which will likely detect hundreds, or even thousands of giant planets from astrometric signature. GAIA is on track for launch in 2011 and data will be available before the end of the decade. However, astrometric detection of rocky planets requires dedicated observations of a limited number of targets, as it will be possible if the SIM-LITE mission (Goullioud et al. 2008) will be approved and launched.

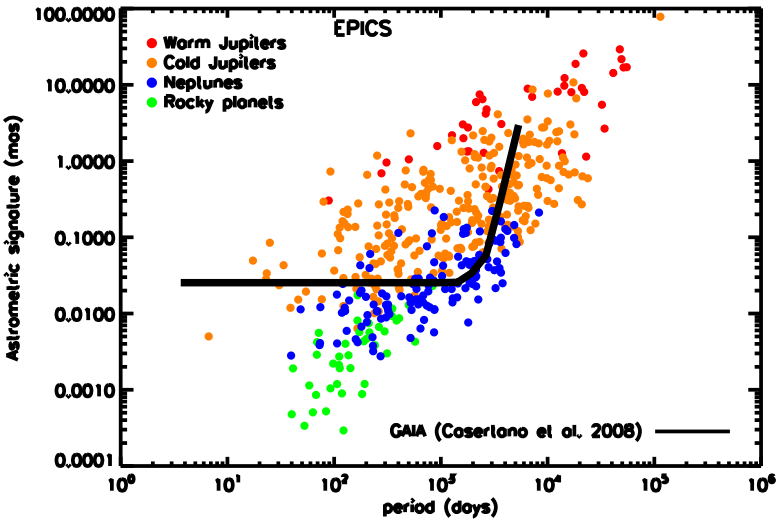


Figure 9.3: Planets expected to be detected by EPICS (nearby sample) in the astrometric signal vs. period plane, compared with detection limits for astrometric satellites GAIA and SIM-LITE. Colour code is the same as in Figure 9.3.

Finally, we already showed in the last Chapter (Sec. 8.3) that there is some potential overlap also with transit missions, like PLATO (Catala 2009). Availability of planet spectrum from EPICS and radius from PLATO will be relevant for the physical study of the planets. For G and F stars (and K and M dwarfs as well) planets at separations larger than that accessible to PLATO can be detected, allowing to study the outer planetary system of PLATO targets.

## 9.6 CONCLUSIONS

In this chapter we presented the comparison, made with MESS, of different planned instruments, aimed at figuring out which can be the expected progress in the exoplanet science, due to these facilities. The results foreseen that enormous progress can be expected in the next decade. The available measurements are already giving us indirect informations on far away planets around young stars, but only passing trough the intermediate step of next generation imagers and finally with the advantage of ELT instruments we will have a wide view on planetary systems at different stages of their evolution. ELT's instruments will in fact represent the ideal link between direct and indirect detections, covering both young, nearby systems discovered by next generation imagers and also providing the first images of planets already detected by RV. Moreover, this kind of instruments will reach for the first time the outer zones of planetary systems around stars similar to our Sun (being sensitive also at planets shining through their reflected light) and, in some favourable cases, will be able to detect rocky planets in the habitable zones of their hosts. We will then move from pure discovery of existence to characterisation of planets, in an era in which the synergy between the different techniques will be crucial for the discovery and characterization of habitable planets.

# BIBLIOGRAPHY


Antichi, J., Dohlen, K., Gratton, R. G., et al. 2009, ApJ, 695, 1042

Beuzit, J., Feldt, M., Dohlen, K., et al. 2008, in Society of Photo-Optical Instrumentation Engineers (SPIE) Conference Series, Vol. 7014, Society of Photo-Optical Instrumentation Engineers (SPIE) Conference Series

Brandl, B. R., Lenzen, R., Pantin, E., et al. 2008, in Society of Photo-Optical Instrumentation Engineers (SPIE) Conference Series, Vol. 7014, Society of Photo-Optical Instrumentation Engineers (SPIE) Conference Series

Casertano, S., Lattanzi, M. G., Sozzetti, A., et al. 2008, A&A, 482, 699

Catala, C. 2009, Communications in Asteroseismology, 158, 330

Clampin, M., Melnick, G., Lyon, R., et al. 2006, in Society of Photo-Optical Instrumentation Engineers (SPIE) Conference Series, Vol. 6265, Society of Photo-Optical Instrumentation Engineers (SPIE) Conference Series

Crampton, D., Simard, L., & Silva, D. 2009, in Science with the VLT in the ELT Era, ed. A. Moorwood, 279–+

Cumming, A., Butler, R. P., Marcy, G. W., et al. 2008, PASP, 120, 531

Fegley, Jr., B. & Lodders, K. 1996, ApJl, 472, L37+

Goullioud, R., Catanzarite, J. H., Dekens, F. G., Shao, M., & Marr, IV, J. C. 2008, in Society of Photo-Optical Instrumentation Engineers (SPIE) Conference Series, Vol. 7013, Society of Photo-Optical Instrumentation Engineers (SPIE) Conference Series

Guyon, O., Angel, J. R. P., Backman, D., et al. 2008, in Society of Photo-Optical Instrumentation Engineers (SPIE) Conference Series, Vol. 7010, Society of Photo-Optical Instrumentation Engineers (SPIE) Conference Series

Johns, M. 2008, in Society of Photo-Optical Instrumentation Engineers (SPIE) Conference Series, Vol. 6986, Society of Photo-Optical Instrumentation Engineers (SPIE) Conference Series

Jolissaint, L., Véran, J., & Conan, R. 2006, Journal of the Optical Society of America A, 23, 382

Kasper, M. E., Beuzit, J., Verinaud, C., et al. 2008, in Society of Photo-Optical Instrumentation Engineers (SPIE) Conference Series, Vol. 7015, Society of Photo-Optical Instrumentation Engineers (SPIE) Conference Series

Lyon, R. G., Clampin, M., Melnick, G., et al. 2008, in Society of Photo-Optical Instrumentation Engineers (SPIE) Conference Series, Vol. 7010, Society of Photo-Optical Instrumentation Engineers (SPIE) Conference Series

Macintosh, B. A., Graham, J. R., Palmer, D. W., et al. 2008, in Society of Photo-Optical Instrumentation Engineers (SPIE) Conference Series, Vol. 7015, Society of Photo-Optical Instrumentation Engineers (SPIE) Conference Series

McLean, I. S., Prato, L., McGovern, M. R., et al. 2007, ApJ, 658, 1217

Mohanty, S., Basri, G., Jayawardhana, R., et al. 2004, ApJ, 609, 854

Schneider, J., Boccaletti, A., Mawet, D., et al. 2009, Experimental Astronomy, 23, 357

Soummer, R., Ferrari, A., Aime, C., & Jolissaint, L. 2007, ApJ, 669, 642

Sparks, W. B. & Ford, H. C. 2002, ApJ, 578, 543

Sudarsky, D., Burrows, A., & Hubeny, I. 2003, ApJ, 588, 1121

Tamura, M., Hodapp, K., Takami, H., et al. 2006, in Society of Photo-Optical Instrumentation Engineers (SPIE) Conference Series, Vol. 6269, Society of Photo-Optical Instrumentation Engineers (SPIE) Conference Series

Thatte, N., Abuter, R., Tecza, M., et al. 2007, MNRAS, 378, 1229

Trauger, J., Stapelfeldt, K., Traub, W., et al. 2008, in Society of Photo-Optical Instrumentation Engineers (SPIE) Conference Series, Vol. 7010, Society of Photo-Optical Instrumentation Engineers (SPIE) Conference Series

Zapatero Osorio, M. R., Martín, E. L., Bouy, H., et al. 2006, ApJ, 647, 1405

# Part VI

# CONCLUSIONS

In this thesis we presented the result of our research, aimed at the creation of a Monte Carlo tool for the statistical analysis and prediction of survey results for exoplanets.

The work is divided into five parts. In the first one, we briefly summarizes the state of the art of the exoplanet science, both from the theoretical and observational side.

The second part analyzes in detail the differences in the planet frequency due to the presence of a stellar companion, presenting the results of our work on the frequency of planets in binaries.

Part three is completely dedicated to present our Multi-purpose Exoplanet Simulation System (MESS). It reviews all the assumptions and the possible operation modes.

The main strength of the code is that it is meant to be independent from the kind of instrument or techniques under test.

Moreover, for the synthetic planet population it creates, the code provides all the orbital elements, together with all the physical characteristics of the planets (temperature, radii, luminosity, etc.). Then all the observables can be easily evaluated, for a comparison with the detection limits.

The approach still has several limitations, due principally to the assumptions about the planetary distribution and to the choice of the evolutionary models used to evaluate the planet luminosity.

Beside that, being these given as inputs of the code, they can be easily changed, and this also allows testing several hypothesis and initial conditions.

Having in hands such a versatile tool, we used it for several studies. Part four and five are, in fact, dedicated to the review of the results of the application of the *Statistical Analysis Mode* and the *Prediction Mode* respectively.

In Chapter 5 we presented the results of the statistical analysis of the results a deep adaptive optics imaging survey with NACO at the VLT of 88 nearby stars of the southern hemisphere, as a result of the use of the *statistical analysis mode* of MESS (see Sec. 4.7.1). The sample was selected favouring youth ($\leq$ 100 Myr) and proximity to Earth ($\leq$ 100 pc) to optimize the detection of close planetary mass companions. Known visual binaries were excluded to avoid degrading the NACO AO and/or coronagraphic detection performances. Within our sample, 51 stars are members of young, nearby comoving groups. 32 stars are young and nearby objects currently not identified as members of any known association, and 5 stars have been reclassified as older ($\geq$ 100 Myr) systems. The

spectral types cover the sequence from B to M spectral types with 19% BAF stars, 48% GK stars and 33% M dwarfs. The separation investigated typically ranges between 0.1″ to 10″, i.e. between approximately 10 to 500 AU. We selected 65 stars of our sample that were observed in deep coronagraphic imaging, with contrast performances to $10^{-6}$ and thus sensitive to planetary mass companions down to 1 $M_{Jup}$ (at 24% of our sample) and 3 $M_{jup}$ (at 67%). For those objects, the use of the complete set of detection limits enabled us to constrain various mass, period and eccentricity distributions of giant planets extrapolated and normalized from RV surveys at large semi-major axes, from 20 to a few 100 AU,. This allowed us deriving limits on the occurrence of giant planets for a given set of physical and orbital distributions. The survey constrain significantly the population of giant planet for masses $\geq 3$ $_{Jup}$.

Chapter 6 has been dedicated to the analysis of the VLT/NACO observation of The T-Tauri star LkCa 15. This object was observed using the 4QPM coronagraph, reaching a contrast lower than 9.5 in $K_s$ band, at separations higher than 0.5″. Our goal was the detection of a low-mass companion, with a mass spanning from 0.2 $M_{\odot}$ down to 5 $M_{Jup}$, which presence has been suggested as an explanation for the large cavity, evidenced by sub-millimeter observations, in the disk surrounding the star.

We do not report any positive detection of a close companion to the star LkCa15. Based on our detection limits and Hot Start evolutionary model predictions, we ran simulations to take into account that the presence of a putative companion enable us to constrain its mass and semi-major axis given reasonable assumptions from the disk geometry. We can exclude the existence of a low mass star and brown dwarf companion with a probability of 85% and 70% resp. at more than 46 AU. The confidence level goes down 50% in both cases at 30 $AU$. The planetary mass regime is only explored at larger semi-major axis where the existence of massive ($M \geq 5$ $M_{Jup}$) planetary mass companions can be excluded with $P_{\rm D} = 70\%$ detection probability.

Limitations of our study are discussed. The LkCa15 age uncertainty does not affect much our conclusions in the case of low mass star and brown dwarf companions. Also and of the uncertainty related to the initial conditions adopted for the evolutionary model is particularly critical only in the planetary mass regime. Finally, in case of a true companion orbiting LkCa15 in the inner disk cavity, our observations would favor a planetary mass or low-mass brown dwarf companion, although more

massive companions cannot be completely excluded with high detection probability.

Further deep imaging studies at the $5 - 50$ $AU$ scale at a new epoch should provide complementary information to completely reject the existence of close stellar or brown dwarf companion to LkCa15 and pursue the search for the putative companion that would be responsible for the disk geometry and inner cavity within 46 $AU$.

In Chapter 7 we started reviewing the results of the use of the *Prediction Mode* of MESS, presenting its application aimed to evaluating the performances of the SPHERE IFS.

This analysis confirmed the potential of SPHERE IFS in the discovery of young giant planets orbiting far away from theyr host stars. This makes SPHERE, as the other next generation imagers, complementary to the traditional indirect methods, allowing us to explore a nearly undiscovered mass-period domain. Moreover, being the young stars the most favourable targets for SPHERE IFS, it will provide informations on the first stages of the planet evolution, helping in clarifying the uncertainties on the evolutionary models at such young ages. Furthermore, coupling integral field spectrographs to extreme adaptive optic modules, would allow us to perform a first order characterization of the exoplanets themselves, giving informations on their atmosphere and composition. Finally, even if only in some favourable cases, SPHERE will also allow the characterization of planets already detected by radial velocity searches.

Such an instrument is then an indispensable intermediate step that will allow us to gather informations on the behaviour of the external part of the planetary systems, preparing the path of ELT instruments that will give us a wide view on planetary systems at different stages of their evolution.

Going a step further, in Chapter 8 we discussed the application of MESS to evaluate the performances of the Exo-Planet Imaging Camera and Spectrograph (EPICS). EPICS is an instrument project for the direct imaging and characterization of extrasolar planets with the E-ELT. EPICS will have photometric, spectroscopic and polarimetric capabilities and will be optimized for observations in the visible and near-IR. This instruments has essentially three science goals: to determine frequency and mass distribution of self-luminous gas giants within star forming regions or young associations; to detect and characterize of mature planets in the solar neighbourhood and finally imaging and characterization of planets already detected with indirect techniques.

Summarizing, the most critical requirement for the first science goal of EPICS concerns the limiting contrast achievable with EPICS, which is determined by photon and calibration noise. Limiting contrast should be $10^{-9}$ (Neptunes), ideally $10^{-10}$ (Super-Earths), at a separation of 0.1 arcsec. Longer exposure times can be considered, but of course high instrument efficiency and small calibration errors are critical. For science goal 2, the Inner Working Angle is critical (0.03 arcsec, and possibly 0.02 arcsec) together with the contrast at small separation (a contrast better than $10^{-8}$ and as good as $10^{-9}$ at separation in the range 0.05-0.1 arcsec is required). With expected contrasts in the range $10^{-7} - 10^{-8}$, spectra at reasonable high S/N ($> 30$) can be obtained for several tens of these planets in a few hour of observations each with the IFS; higher resolution observations will be possible for a few of them. Coupled with the polarization information that can be derived using E-POL, a detailed characterization of the planetary atmospheres at different position angles will be possible with EPICS.

Finally, as an ideal conclusion of the work, in Chapter 9 we presented the comparison, made with MESS, of different planned instruments, aimed at figuring out which can be the expected progress in the exoplanet science, due to these facilities. The results foreseen that enormous progress can be expected in the next decade. The available measurements are already giving us indirect informations on far away planets around young stars, but only passing trough the intermediate step of next generation imagers and finally with the advantage of ELT instruments we will have a wide view on planetary systems at different stages of their evolution. ELT's instruments will in fact represent the ideal link between direct and indirect detections, covering both young, nearby systems discovered by next generation imagers and also providing the first images of planets already detected by RV. Moreover, this kind of instruments will reach for the first time the outer zones of planetary systems around stars similar to our Sun (being sensitive also at planets shining through their reflected light) and, in some favourable cases, will be able to detect rocky planets in the habitable zones of their hosts. We will then move from pure discovery of existence to characterisation of planets, in an era in which the synergy between the different techniques will be crucial for the discovery and characterization of habitable planets.

Throughout the current study we have noted many areas that still require work. Some of them are listed below, some has been discussed in detail trough the manuscript.

- On the basis of the results reported in Chap. 3, it comes out that a proper treatment of the binarity is currently missing, and must be included.
- Each planet in the generated stellar population is now considered as single. A study of the planet-planet interaction and planetary system stability needs to be implemented.
- Only the results of the application of the semi-empirical approach of MESS has been showed trough this work. More simulations using the results of the theoretical models are needed, to compare the results of the two methods.
- a sample of more than 200 stars belonging from the major deep imaging surveys is currently under construction, to extend the results of Chapter 5.
- an extensive use of the code, as the one done for EPICS, requires a complete knowledge of the instrument under test, of all the error sources and of the detection capabilities. Then, to really extend the use of MESS to other facilities one should first properly set all the needed parameters. For example the astrometric part is currently included in a simplistic way. A better treatment of the dependence of the detectability from the orbital parameters should be included. Moreover a rigorous treatment of the stellar jitter evaluation must be implemented to allow a better comparison between the imaging and radial velocity capabilities. Especially in the case of E-ELT instruments, this would allow to better define the synergies between the various channels, for a more focused observing strategy.

It can be seen from this (non exhaustive) list that many uncertainties and unknown remains on the path that leads to a perfect tool, and thus there is much work that still needs to be done. We shall certainly not be lost for things to do!

Part VII

# APPENDIX

# A

# THE UNIFORM DETECTABILITY BINARY SUB SAMPLE

## A.1 LIST OF TARGETS

Table A.1: Properties of binaries found in the UD sample: projected separation (arcsec), eccentricity and semi major-axis (when available), masses of the object and the companion, and critical semi major axis for dynamical stability of planets (Holman & Wiegert 1999). For systems for which only the projected separation was available (empty spaces in eccentricity column) the semi major axis was derived from the projected separation using the relation $a$(AU)=1.31$\rho$(arcsec)$d$(pc) (see Fischer et al. 2002; Duquennoy & Mayor 1991). The asterisk in the last column marks systems discussed individually in Appendix **??**. The mass flag indicates the source for the companion mass: **a:** $M_{comp}$ from VF06; **b:** $M_{comp}$ from Reid & Gizis (1997); Delfosse et al. (2000); **c:** $M_{comp}$ from individual papers (see Reference below).

| Star ID HD | $\rho$ (") | ecc | a (AU) | $a_{crit}$ (AU) | $M_{obj}$ ($M_\odot$) | $M_{com}$ ($M_\odot$) | Remarks |
|---|---|---|---|---|---|---|---|
| 531 | 5.30 | 0.00 | 482.30 | 76.37 | $1.64^a$ | 1.66 | S |
| 531 | 5.30 | 0.00 | 482.30 | 76.94 | $1.66^a$ | 1.64 | S |
| 3074 | 4.80 | 0.00 | 225.89 | 38.01 | $1.20^b$ | 0.99 | S |
| 3651 | 43.20 | 0.00 | 623.38 | 151.00 | $0.89^b$ | 0.06 | S (*) |
| 3770 | 0.00 | 0.00 | 0.00 | 0.00 | 1.25 | 0.00 | S, RV |
| 3795 | 0.00 | 0.00 | 0.00 | 0.00 | 1.94 | 0.00 | S, RV, $\Delta\mu$ |
| 3821 | 8.45 | 0.00 | 284.51 | 51.50 | $1.00^b$ | 0.63 | S |
| 4614 | 12.49 | 0.49 | 72.00 | 10.30 | $0.99^b$ | 0.51 | S |
| 4747 | 0.00 | 0.64 | 6.70 | 0.79 | $0.82^c$ | 0.04 | S, SB |
| 5470 | 0.00 | 0.00 | 20.50 | 4.44 | $1.13^c$ | 0.29 | S (*) |
| 6734 | 0.00 | 0.00 | 0.00 | 0.00 | 1.08 | 0.00 | S, $\Delta\mu$ |
| 6872 | 14.60 | 0.00 | 1442.48 | 271.29 | $1.91^b$ | 1.03 | S |
| 6872 | 14.60 | 0.00 | 1442.48 | 187.22 | $1.03^a$ | 1.91 | S |
| 7693 | 0.90 | 0.04 | 23.40 | 5.98 | $0.84^b$ | 0.89 | S (*) |

*(continued on next page)*

*(Table A.1 - continued from previous page)*

| Star ID HD | $\rho$ (") | ecc | a (AU) | $a_{crit}$ (AU) | $M_{obj}$ ($M_\odot$) | $M_{com}$ ($M_\odot$) | Remarks |
|---|---|---|---|---|---|---|---|
| 8765 | 0.00 | 0.00 | 5.30 | 1.31 | 1.20[c] | 0.06 | S, G, $\Delta\mu$ (*) |
| 10360 | 11.20 | 0.53 | 52.20 | 5.66 | 0.75[a] | 0.77 | S |
| 10361 | 11.20 | 0.53 | 52.20 | 5.74 | 0.77[a] | 0.75 | S |
| 11964 | 40.50 | 0.00 | 1790.10 | 325.00 | 1.13[b] | 0.67 | S (*) |
| 13043 | 79.20 | 0.00 | 3809.52 | 684.35 | 1.14[b] | 0.74 | S |
| 13507 | 0.00 | 0.14 | 4.30 | 1.57 | 1.00[c] | 0.05 | S, SB, $\Delta\mu$ (*) |
| 13531 | 0.70 | 0.00 | 23.30 | 5.21 | 0.94[c] | 0.19 | S |
| 13612 | 16.70 | 0.00 | 1000.83 | 121.14 | 1.02[c] | 2.32 | S (*) |
| 16141 | 6.20 | 0.00 | 289.35 | 62.00 | 1.15[c] | 0.31 | S (*) |
| 16160 | 3.30 | 0.75 | 15.00 | 1.04 | 0.76[c] | 0.09 | S (*) |
| 17037 | 0.00 | 0.00 | 0.00 | 0.00 | 1.23 | 0.00 | S, RV |
| 16895 | 20.50 | 0.13 | 249.50 | 76.20 | 1.24[b] | 0.43 | S |
| 18143 | 44.10 | 0.00 | 1312.86 | 222.85 | 0.90[b] | 0.72 | S (*) |
| 18445 | 0.10 | 0.56 | 1.06 | 0.14 | 0.78[c] | 0.18 | S (*) |
| 20766 | 310.00 | 0.00 | 4876.30 | 711.69 | 0.91[a] | 1.19 | S |
| 20807 | 310.00 | 0.00 | 4876.30 | 736.00 | 0.95[a] | 1.12 | S |
| 21019 | 3.90 | 0.00 | 187.08 | 36.48 | 1.11[b] | 0.51 | S |
| 23439 | 8.00 | 0.00 | 254.80 | 37.41 | 0.67[b] | 0.86 | S (*) |
| 26491 | 0.00 | 0.00 | 0.00 | 0.00 | 1.00 | 0.00 | S, $\Delta\mu$ |
| 28255 | 5.90 | 0.00 | 199.42 | 31.78 | 1.07[a] | 1.06 | S |
| 28255 | 5.90 | 0.00 | 199.42 | 31.60 | 1.06[a] | 1.07 | S |
| 29461 | 0.00 | 0.00 | 7.30 | 1.71 | 1.20[c] | 0.15 | S, RV (*) |
| 29836 | 100.00 | 0.00 | 5590.00 | 852.14 | 1.19[c] | 1.36 | S (*) |
| 30339 | 0.00 | 0.25 | 0.13 | 0.04 | 1.39[c] | 0.07 | S, SB |
| 30649 | 0.00 | 0.00 | 0.00 | 0.00 | 0.90 | 0.00 | S, RV (*) |
| 31412 | 0.20 | 0.00 | 9.36 | 1.91 | 1.17[c] | 0.43 | S, RV (*) |
| 32923 | 0.18 | 0.90 | 2.86 | 0.03 | 1.03[c] | 1.11 | S |
| 33473 | 100.00 | 0.00 | 7475.00 | 1358.02 | 1.32[c] | 0.82 | S |
| 33636 | 14.20 | 0.48 | 3.40 | 0.61 | 1.02[c] | 0.14 | S (*) |
| 35956 | 0.00 | 0.62 | 2.60 | 0.30 | 0.98[c] | 0.18 | S, SB (*) |
| 37394 | 97.50 | 0.00 | 1546.35 | 292.41 | 0.93[b] | 0.49 | S |
| 39587 | 0.00 | 0.45 | 5.90 | 1.13 | 1.05[c] | 0.14 | S, SB |
| 40397 | 4.10 | 0.00 | 123.66 | 25.62 | 0.92[b] | 0.31 | S |
| 43587 | 0.00 | 0.80 | 11.60 | 0.53 | 1.06[c] | 0.34 | S, SB (*) |
| 43834 | 3.00 | 0.00 | 39.39 | 9.14 | 0.98[c] | 0.14 | S |

*(continued on next page)*

*(Table A.1 - continued from previous page)*

| Star ID HD | $\rho$ (") | ecc | a (AU) | $a_{crit}$ (AU) | $M_{obj}$ ($M_\odot$) | $M_{com}$ ($M_\odot$) | Remarks |
|---|---|---|---|---|---|---|---|
| 44120 | 40.40 | 0.00 | 1911.73 | 330.66 | 1.23[b] | 0.92 | S |
| 45701 | 0.00 | 0.00 | 0.00 | 0.00 | 1.18 | 0.00 | S, $\Delta\mu$ |
| 45588 | 41.20 | 0.00 | 1601.44 | 325.89 | 1.21[b] | 0.45 | S |
| 47157 | 10.10 | 0.00 | 502.88 | 105.72 | 1.13[b] | 0.35 | S |
| 50281 | 58.30 | 0.00 | 659.37 | 118.04 | 0.76[b] | 0.50 | S |
| 50639 | 0.00 | 0.00 | 0.00 | 0.00 | 1.16 | 0.00 | S, RV, $\Delta\mu$ |
| 51929 | 0.00 | 0.00 | 0.00 | 0.00 | 0.86 | 0.00 | S, $\Delta\mu$ |
| 53705 | 21.00 | 0.00 | 425.88 | 69.47 | 0.97[a] | 0.89 | S (*) |
| 53706 | 21.00 | 0.00 | 425.88 | 65.90 | 0.89[a] | 0.97 | S (*) |
| 61606 | 58.10 | 0.00 | 1072.53 | 184.33 | 0.81[b] | 0.62 | S |
| 63754 | 5.60 | 0.00 | 376.38 | 71.81 | 1.50[b] | 0.76 | S |
| 64468 | 0.00 | 0.26 | 0.56 | 0.15 | 0.81[c] | 0.14 | S, SB |
| 65907 | 60.00 | 0.00 | 1263.60 | 201.45 | 0.99[c] | 0.98 | S (*) |
| 65277 | 4.10 | 0.00 | 93.27 | 18.82 | 0.72[b] | 0.28 | S, $\Delta\mu$ |
| 65430 | 0.00 | 0.32 | 4.00 | 1.05 | 0.83[c] | 0.06 | S, SB |
| 66171 | 49.00 | 0.00 | 3013.01 | 730.27 | 0.91[b] | 0.07 | S |
| 72760 | 0.90 | 0.00 | 25.51 | 5.92 | 0.91[c] | 0.13 | S, $\Delta\mu$ (*) |
| 72780 | 0.00 | 0.00 | 9.30 | 2.32 | 1.28[c] | 0.05 | S, RV (*) |
| 73668 | 0.00 | 0.00 | 8.00 | 1.85 | 1.13[c] | 0.17 | S (*) |
| 74014 | 0.00 | 0.00 | 11.60 | 2.87 | 1.04[c] | 0.05 | S (*) |
| 77407 | 1.60 | 0.00 | 50.00 | 9.65 | 1.12[c] | 0.54 | S (*) |
| 86728 | 134.00 | 0.00 | 2595.58 | 626.32 | 1.08[b] | 0.09 | S (*) |
| 88218 | 2.00 | 0.00 | 79.82 | 14.49 | 1.09[b] | 0.68 | S |
| 90839 | 122.80 | 0.00 | 2043.39 | 372.01 | 1.12[b] | 0.69 | S (*) |
| 92222 | 17.70 | 0.00 | 2070.90 | 332.90 | 1.09[c] | 1.05 | S (*) |
| 92987 | 0.00 | 0.00 | 0.00 | 0.00 | 1.15 | 0.00 | S, $\Delta\mu$ |
| 52942 | 17.60 | 0.00 | 2779.92 | 418.07 | 1.04[b] | 1.24 | S (*) |
| 52940 | 0.00 | 0.37 | 2.60 | 0.60 | 1.12[c] | 0.12 | S, SB (*) |
| 97334 | 90.00 | 0.00 | 2620.00 | 649.08 | 1.09[c] | 0.05 | S (*) |
| 99491 | 28.80 | 0.00 | 666.43 | 111.12 | 1.01[a] | 0.86 | S |
| 99492 | 28.80 | 0.00 | 666.43 | 100.71 | 0.86[a] | 1.01 | S (*) |
| 100180 | 15.40 | 0.00 | 460.46 | 82.24 | 1.10[b] | 0.73 | S |
| 100623 | 17.00 | 0.00 | 209.95 | 51.31 | 0.77[b] | 0.05 | S |
| 101177 | 9.70 | 0.00 | 293.81 | 45.85 | 0.99[c] | 1.05 | S (*) |
| 102365 | 23.00 | 0.00 | 275.08 | 65.42 | 0.86[b] | 0.09 | S |

*(continued on next page)*

*(Table A.1 - continued from previous page)*

| Star ID HD | $\rho$ (") | ecc | a (AU) | $a_{crit}$ (AU) | $M_{obj}$ ($M_\odot$) | $M_{com}$ ($M_\odot$) | Remarks |
|---|---|---|---|---|---|---|---|
| 103432 | 73.20 | 0.00 | 3520.92 | 565.26 | 0.92[b] | 0.89 | S |
| 103829 | 0.00 | 0.00 | 0.00 | 0.00 | 1.20 | 0.00 | S, RV |
| 104556 | 0.00 | 0.00 | 0.00 | 0.00 | 1.12 | 0.00 | S, $\Delta\mu$, G |
| 105113 | 6.60 | 0.00 | 440.15 | 75.43 | 1.28[b] | 0.99 | S |
| 107705 | 20.00 | 0.00 | 774.80 | 141.13 | 1.22[b] | 0.75 | S |
| 111031 | 0.00 | 0.00 | 0.00 | 0.00 | 1.14 | 0.00 | S, $\Delta\mu$ |
| 111398 | 0.00 | 0.00 | 75.00 | 17.52 | 1.06[b] | 0.14 | S |
| 111484 | 8.80 | 0.00 | 846.56 | 134.25 | 1.38[a] | 1.39 | S |
| 111484 | 8.80 | 0.00 | 846.56 | 134.84 | 1.39[a] | 1.38 | S |
| 114729 | 8.00 | 0.00 | 364.00 | 79.00 | 1.00[b] | 0.25 | S (*) |
| 116442 | 26.50 | 0.00 | 564.98 | 90.90 | 0.76[a] | 0.73 | S |
| 116443 | 26.50 | 0.00 | 564.98 | 88.68 | 0.73[a] | 0.76 | S |
| 120066 | 488.50 | 0.00 | 19432.53 | 3581.91 | 1.16[b] | 0.68 | S |
| 120237 | 11.60 | 0.00 | 426.76 | 81.04 | 1.16[b] | 0.60 | S |
| 120476 | 3.40 | 0.44 | 33.15 | 4.36 | 0.76[b] | 0.83 | S |
| 120690 | 0.00 | 0.00 | 0.00 | 0.00 | 1.02 | 0.00 | S, $\Delta\mu$ |
| 120780 | 0.00 | 0.00 | 0.00 | 0.00 | 0.74 | 0.00 | S, G, $\Delta\mu$ (*) |
| 121384 | 33.00 | 0.00 | 1634.49 | 328.24 | 1.18[b] | 0.47 | S |
| 122742 | 0.00 | 0.48 | 5.30 | 0.75 | 0.92[c] | 0.54 | S, SB |
| 125455 | 15.30 | 0.00 | 413.71 | 91.76 | 0.79[b] | 0.17 | S |
| 126614 | 41.90 | 0.00 | 3725.75 | 883.39 | 1.19[b] | 0.13 | S |
| 128428 | 0.80 | 0.00 | 54.39 | 9.99 | 1.26[b] | 0.75 | S |
| 128621 | 17.51 | 0.51 | 22.76 | 2.44 | 0.89[a] | 1.12 | S (*) |
| 128620 | 17.51 | 0.51 | 22.76 | 2.79 | 1.12[a] | 0.89 | S (*) |
| 128674 | 490.00 | 0.00 | 17453.80 | 2906.33 | 0.83[b] | 0.71 | S |
| 129814 | 0.00 | 0.00 | 0.00 | 0.00 | 1.06 | 0.00 | S, RV, $\Delta\mu$ |
| 130984 | 2.60 | 0.00 | 60.50 | 14.44 | 1.11[c] | 0.11 | S |
| 131156 | 4.90 | 0.51 | 32.80 | 3.93 | 0.92[b] | 0.79 | S (*) |
| 131511 | 0.00 | 0.51 | 0.52 | 0.07 | 0.93[c] | 0.45 | S, SB |
| 131977 | 24.90 | 0.00 | 190.98 | 28.29 | 0.76[b] | 0.95 | S (*) |
| 131923 | 0.00 | 0.00 | 0.00 | 0.00 | 1.04 | 0.00 | S, $\Delta\mu$, G |
| 133161 | 0.00 | 0.00 | 0.00 | 0.00 | 1.18 | 0.00 | S, $\Delta\mu$ |
| 134440 | 302.00 | 0.00 | 11581.70 | 1830.52 | 0.55[a] | 0.56 | S |
| 134439 | 302.00 | 0.00 | 11581.70 | 1850.83 | 0.56[a] | 0.55 | S |
| 134331 | 50.60 | 0.00 | 1993.13 | 325.83 | 1.12[a] | 1.02 | S |

*(continued on next page)*

*(Table A.1 - continued from previous page)*

| Star ID HD | $\rho$ (") | ecc | a (AU) | $a_{crit}$ (AU) | $M_{obj}$ ($M_\odot$) | $M_{com}$ ($M_\odot$) | Remarks |
|---|---|---|---|---|---|---|---|
| 134330 | 50.60 | 0.00 | 1993.13 | 307.70 | 1.02[a] | 1.12 | S |
| 135101 | 23.50 | 0.00 | 870.67 | 209.00 | 1.07[c] | 0.92 | S |
| 136580 | 0.00 | 0.00 | 0.00 | 0.00 | 1.17 | 0.00 | S, RV, $\Delta\mu$ |
| 137778 | 51.90 | 0.00 | 1403.38 | 182.11 | 0.90[c] | 1.67 | S (*) |
| 139323 | 121.90 | 0.00 | 3533.88 | 468.58 | 0.89[c] | 1.55 | S (*) |
| 139477 | 42.00 | 0.00 | 1042.86 | 221.21 | 0.75[b] | 0.22 | S |
| 140913 | 0.00 | 0.54 | 0.55 | 0.09 | 1.17[c] | 0.04 | S, SB |
| 140901 | 8.10 | 0.00 | 160.06 | 36.49 | 1.00[b] | 0.17 | S |
| 142229 | 0.00 | 0.00 | 6.90 | 1.61 | 1.09[c] | 0.15 | S, RV (*) |
| 144579 | 70.10 | 0.00 | 1312.27 | 308.93 | 0.75[b] | 0.09 | S |
| 145435 | 0.00 | 0.00 | 0.00 | 0.00 | 1.19 | 0.00 | S, $\Delta\mu$ |
| 145958 | 4.20 | 0.39 | 124.00 | 18.66 | 0.90[a] | 0.89 | S (*) |
| 145958 | 4.20 | 0.39 | 124.00 | 18.53 | 0.89[a] | 0.90 | S |
| 146362 | 6.80 | 0.76 | 130.00 | 5.03 | 1.12[c] | 2.19 | S (*) |
| 147722 | 5.40 | 0.00 | 220.43 | 33.89 | 1.16[a] | 1.29 | S |
| 147723 | 5.40 | 0.00 | 220.43 | 36.17 | 1.29[a] | 1.16 | S |
| 149806 | 5.90 | 0.00 | 154.17 | 31.20 | 0.94[b] | 0.36 | S |
| 150554 | 0.00 | 0.00 | 7.60 | 1.86 | 1.13[c] | 0.07 | S (*) |
| 150248 | 0.00 | 0.00 | 0.00 | 0.00 | 0.96 | 0.00 | S, $\Delta\mu$ |
| 151090 | 163.60 | 0.00 | 10102.30 | 1929.65 | 1.17[b] | 0.59 | S |
| 156274 | 8.65 | 0.78 | 91.65 | 4.30 | 0.79[b] | 0.47 | S |
| 157466 | 0.00 | 0.00 | 0.00 | 0.00 | 0.92 | 0.00 | S, $\Delta\mu$ |
| 159909 | 0.00 | 0.00 | 0.00 | 0.00 | 1.04[b] | 0.00 | S |
| 161797 | 0.20 | 0.32 | 22.00 | 3.90 | 1.15[c] | 1.02 | S, RV,$\Delta\mu$ (*) |
| 164595 | 88.00 | 0.00 | 3306.16 | 674.36 | 0.98[b] | 0.36 | S |
| 166553 | 1.40 | 0.00 | 77.17 | 13.83 | 1.22[b] | 0.80 | S |
| 167215 | 0.00 | 0.00 | 0.00 | 0.00 | 1.15 | 0.00 | S, G, $\Delta\mu$ (*) |
| 167665 | 0.00 | 0.33 | 5.47 | 1.44 | 1.11[c] | 0.05 | S, RV (*) |
| 169586 | 0.00 | 0.00 | 0.00 | 0.00 | 1.29 | 0.00 | S, $\Delta\mu$ |
| 169822 | 0.00 | 0.48 | 0.84 | 0.13 | 0.91[c] | 0.30 | S, SB (*) |
| 173667 | 48.20 | 0.00 | 1196.81 | 266.63 | 1.54[b] | 0.32 | S |
| 174457 | 0.00 | 0.23 | 1.90 | 0.60 | 1.07[c] | 0.06 | S, SB |
| 175345 | 5.40 | 0.00 | 348.89 | 67.43 | 1.17[b] | 0.56 | S |
| 179957 | 8.20 | 0.00 | 254.77 | 40.25 | 1.01[a] | 1.03 | S |
| 179958 | 8.20 | 0.00 | 254.77 | 40.73 | 1.03[a] | 1.01 | S |

*(continued on next page)*

*(Table A.1 - continued from previous page)*

| Star ID HD | $\rho$ (") | ecc | a (AU) | $a_{crit}$ (AU) | $M_{obj}$ ($M_\odot$) | $M_{com}$ ($M_\odot$) | Remarks |
|---|---|---|---|---|---|---|---|
| 179140 | 0.50 | 0.00 | 34.06 | 5.60 | $1.12^b$ | 1.00 | S |
| 184860 | 0.00 | 0.67 | 1.40 | 0.15 | $0.77^c$ | 0.03 | S, SB (*) |
| 185395 | 37.00 | 0.00 | 894.66 | 196.56 | $1.34^b$ | 0.31 | S |
| 187691 | 14.40 | 0.00 | 363.17 | 79.35 | $1.37^b$ | 0.33 | S (*) |
| 190360 | 188.60 | 0.00 | 3898.36 | 864.00 | $1.01^b$ | 0.20 | S (*) |
| 190406 | 0.80 | 0.00 | 18.41 | 4.52 | $1.09^c$ | 0.06 | S, RV (*) |
| 190067 | 2.86 | 0.00 | 55.00 | 12.91 | $0.80^b$ | 0.10 | S (*) |
| 190771 | 0.00 | 0.00 | 0.00 | 0.00 | 1.07 | 0.00 | S, RV, $\Delta\mu$ |
| 191785 | 103.80 | 0.00 | 2766.27 | 559.07 | $0.83^b$ | 0.32 | S |
| 191408 | 7.10 | 0.00 | 56.30 | 11.60 | $0.69^b$ | 0.24 | S |
| 192343 | 43.40 | 0.00 | 3627.81 | 577.95 | $1.28^b$ | 1.27 | S |
| 192344 | 43.40 | 0.00 | 3627.81 | 575.18 | $1.27^b$ | 1.28 | S |
| 194766 | 43.60 | 0.00 | 2635.62 | 423.63 | $1.10^b$ | 1.06 | S |
| 195564 | 2.90 | 0.00 | 91.23 | 17.39 | $1.12^b$ | 0.57 | S |
| 196201 | 2.20 | 0.00 | 109.54 | 18.72 | $0.87^b$ | 0.68 | S |
| 197076 | 125.00 | 0.00 | 3412.50 | 767.57 | $0.99^b$ | 0.19 | S (*) |
| 196068 | 17.40 | 0.00 | 882.18 | 159.88 | $1.69^b$ | 1.06 | S |
| 198387 | 0.00 | 0.00 | 0.00 | 0.00 | 1.32 | 0.00 | S, G, $\Delta\mu$ (*) |
| 199598 | 0.00 | 0.00 | 15.10 | 3.61 | $1.15^c$ | 0.11 | S, $\Delta\mu$ (*) |
| 200565 | 0.00 | 0.00 | 0.00 | 0.00 | 1.06 | 0.00 | S, RV, $\Delta\mu$ |
| 206387 | 3.70 | 0.00 | 264.07 | 48.40 | $1.20^b$ | 0.72 | S |
| 206860 | 43.20 | 0.00 | 1033.34 | 260.95 | $1.07^c$ | 0.02 | S |
| 208776 | 0.00 | 0.27 | 4.20 | 0.97 | $1.14^c$ | 0.51 | S, SB |
| 211681 | 0.00 | 0.00 | 5.30 | 1.30 | $1.31^c$ | 0.08 | S |
| 212330 | 81.10 | 0.00 | 2161.31 | 513.18 | $1.12^b$ | 0.12 | S |
| 212168 | 20.10 | 0.00 | 603.60 | 112.67 | $1.06^b$ | 0.59 | S |
| 213519 | 62.00 | 0.00 | 3481.92 | 734.00 | $1.05^b$ | 0.32 | S |
| 214953 | 7.80 | 0.00 | 239.30 | 44.82 | $1.13^b$ | 0.62 | S |
| 215578 | 0.00 | 0.00 | 10.00 | 1.92 | $1.02^c$ | 0.50 | S, RV (*) |
| 215648 | 11.80 | 0.00 | 2485.08 | 538.88 | $1.26^b$ | 0.32 | S |
| 217004 | 8.90 | 0.00 | 794.86 | 136.69 | $1.27^b$ | 0.97 | S |
| 217165 | 0.00 | 0.00 | 5.10 | 1.27 | $1.10^c$ | 0.04 | S (*) |
| 218101 | 0.00 | 0.00 | 0.00 | 0.00 | 1.26 | 0.00 | S, $\Delta\mu$ |
| 219542 | 5.28 | 0.00 | 388.00 | 71.00 | $1.08^c$ | 1.05 | S (*) |
| 219542 | 5.28 | 0.00 | 388.00 | 67.00 | $1.05^c$ | 1.08 | S (*) |

*(continued on next page)*

*(Table A.1 - continued from previous page)*

| Star ID HD | $\rho$ (") | ecc | a (AU) | $a_{crit}$ (AU) | $M_{obj}$ ($M_\odot$) | $M_{com}$ ($M_\odot$) | Remarks |
|---|---|---|---|---|---|---|---|
| 219834 | 13.00 | 0.00 | 331.24 | 48.80 | $0.74^c$ | 0.94 | S (*) |
| 220077 | 0.20 | 0.00 | 19.89 | 3.19 | $1.09^b$ | 1.06 | S |
| 221830 | 8.00 | 0.00 | 335.92 | 70.79 | $0.95^b$ | 0.29 | S |
| 223084 | 0.00 | 0.00 | 0.00 | 0.00 | 1.09 | 0.00 | S, RV, $\Delta\mu$ |

Stars with planets

| Star ID HD | $\rho$ (") | ecc | a (AU) | $a_{crit}$ (AU) | $M_{obj}$ ($M_\odot$) | $M_{com}$ ($M_\odot$) | Remarks |
|---|---|---|---|---|---|---|---|
| 142 | 4.10 | 0.00 | 136.45 | 35.00 | $1.24^b$ | 0.59 | P |
| 9826 | 55.50 | 0.00 | 974.02 | 223.00 | $1.32^b$ | 0.19 | P |
| 13445 | 1.30 | 0.40 | 18.40 | 3.10 | $0.77^b$ | 0.49 | P, $\Delta\mu$ (*) |
| 20782 | 252.20 | 0.00 | 11802.96 | 1940.00 | $1.00^c$ | 0.84 | P (*) |
| 27442 | 13.80 | 0.00 | 326.51 | 62.00 | $1.49^c$ | 0.60 | P (*) |
| 38529 | 283.02 | 0.00 | 15600.06 | 3190.00 | $1.47^b$ | 0.50 | P, G (*) |
| 40979 | 192.20 | 0.00 | 8320.34 | 1488.00 | $1.21^c$ | 1.21 | P (*) |
| 46375 | 10.00 | 0.00 | 434.20 | 80.00 | $0.92^b$ | 0.58 | P |
| 75732 | 84.90 | 0.00 | 1379.62 | 291.00 | $0.91^b$ | 0.26 | P |
| 120136 | 12.00 | 0.91 | 245.00 | 2.80 | $1.35^c$ | 0.40 | P (*) |
| 177830 | 1.60 | 0.00 | 122.72 | 28.22 | $1.47^c$ | 0.23 | P (*) |
| 178911 | 13.60 | 0.00 | 830.96 | 108.00 | $1.42^c$ | 1.89 | P (*) |
| 188015 | 13.00 | 0.00 | 888.94 | 198.00 | $1.25^b$ | 0.21 | P |
| 195019 | 4.00 | 0.00 | 194.48 | 35.00 | $1.07^b$ | 0.70 | P |
| 196050 | 10.70 | 0.00 | 652.38 | 129.79 | $1.15^b$ | 0.48 | P |
| 196885 | 0.70 | 0.40 | 17.20 | 3.40 | $1.25^c$ | 0.34 | P, $\Delta\mu$ (*) |
| 222582 | 113.30 | 0.00 | 6171.45 | 1246.00 | $0.99^b$ | 0.36 | P |

**Remarks: P:** Stars with planets as in FV05; **S:** Stars without planets as in FV05; **SB:** Spectroscopic Binaries; **RV:** Stars with RV linear trends (see Nidever et al. 2002); $\Delta\mu$**:** Stars with discrepant proper motion in Hipparcos and Thyco II (see Makarov & Kaplan 2005); **G:** Stars with accelerating proper motions in Hipparcos. (see Makarov & Kaplan 2005).

## A.2 COMMENTS ON INDIVIDUAL OBJECTS

### A.2.1 *List of included binaries*

- HD 3651: planet outside the UD limits. The companion is a cool brown dwarf.
- HD 7693: Hipparcos lists a companion at 0.9 arcsec ($\sim$ 19 AU). Furthermore, the star is listed in CCDM as the wide companion of HD 7788, with a separation of 319 arcsec ($\sim$ 6731 AU). The values of parallaxes and proper motion in right ascension would suggest a physical bounding, and the RV value reported by Nordström et al. (2004) seems to confirm this hypothesis. But the RV values for HD 7788 have a large error, and the proper motion in declination reported by Hipparcos are in disagreement. Probably this peculiarity could be explained by considering that both HD 7693 and HD 7788 are close binaries themselves. In fact Hipparcos lists a companion at 0.9 arcsec for the first star, and one at 5 arcsec = 105 AU, for the last one. Since we are interested in the effect of the binarity on the planetary formation/evolution, we will take only the closest companion to HD 7693 into account .
- HD 11964: planet outside the UD limits.
- HD 13445 (GL 86): the companion was discovered by Els et al. (2001) and it was classified as a brown dwarf, but successive work shows that the secondary is a $\sim$ 0.5 $M_{\odot}$ white dwarf (Mugrauer & Neuhäuser 2005; Lagrange et al. 2006). Desidera & Barbieri (2006) described a possible evolution of the system during the mass-loss phase of the originally more massive star. The white dwarf companion is responsible for the observed RV and astrometric trends.
- HD 13507: suspected for some time of harboring a planet, but the later measurements obtained with ELODIE invalidated this interpretation and instead revealed a classical spectroscopic binary velocity curve, caused by a low-mass ($m \sin i \sim 50 M_J$) companion (Perrier et al. 2003). Adaptive optics imaging did not directly detect the companion.
- HD 13612: triple system. AB is a CPM pair. A is an SB2 (Duquennoy & Mayor 1991) and the disagreement between spectral and photo-

metric parallaxes of A and B are probably due to its nature. An additional component at 2′.9 is optical (Worley 1967b); the component included in the UD sample is HD 13612 B and, since the mass of this star is not listed in VF05, we derive it according to the Reid & Gizis (1997) and Delfosse et al. (2000) mass-luminosity calibration.

- HD 16141: planet outside the UD limits.

- HD 16160=GL105: triple system composed of an inner pair and another wide companion ($\rho = 164.8$ arcsec = 1200 AU, mass 0.38 $M_{\odot}$). The orbit of the close pair was derived by Golimowski et al. (2000) ($a = 15$ AU $e = 0.75$). The mass of the close companion is about 0.09 $M_{\odot}$.

- HD 18143: triple system. Component B at 6.5 arcsec = 149 AU, component C at 43 arcsec = 985 AU.

- HD 18445: is a member of a quintuple system (component C). Components AB (HD 18455) form a visual binary with P=147 yr and a=1.55 arcsec = 40 AU (Worley & Heintz 1983), C is at 27.2 arcsec $\sim$ 700 AU and is a spectroscopic binary with minimum mass in the brown dwarf range ($m \sin i = 0.042$ $M_{\odot}$ according to Zucker & Mazeh 2001). Halbwachs et al. (2000) demonstrated that the pair is close to face-on and derived a mass of 0.176 $M_{\odot}$. The close companion was also visually resolved by Beuzit et al. (2004) at 0.1 arcsec = 2.6 AU. A further CPM companion (D) is at a projected separation 5.090 arcsec = 130 AU from C.

- HD 20782: listed as a binary in the CCDM catalog. The companion is HD 20781. Desidera & Barbieri (2006) suggest a physical association and consider HD 20782 and HD 20781 as a very wide CPM pair.

- HD 23439: triple system. The secondary is a spectroscopic binary (period = 49 days, masses 0.74+0.12 $M_{\odot}$).

- HD 27442 ($\epsilon$ Ret): a companion at $\sim$13 arcsec $\sim$ 237 AU is included in WDS and was confirmed by Chauvin et al. (2006). HD 27442 B is probably a white dwarf with a mass of about 0.6 $M_{\odot}$ (see Desidera & Barbieri 2006).

- HD 29836: triple system. HD 285970 is a wide companion of the star included in the UD sample. HD 285970 is also a short-period spectroscopic binary (Griffin & Gunn 1981). Another companion to HD 29836 at 100 arcsec is listed in CCDM, probably optical.

- HD 30649: CCDM lists a companion at 3.37 arcsec = 101 AU, but probably this is not the cause of the linear trend reported by Nidever et al. (2002).

- HD 31412: additional common proper motion companion (CNS3, Lépine & Bongiorno 2007) at 22 arcsec = 792 AU; it should not be responsible for the observed RV trend.

- HD 33636

- HD 35956: triple system. The primary (the star in the UD sample) is a spectroscopic and astrometric binary (Vogt et al. 2002). An additional companion ($M = 0.44\ M_{\odot}$) is at a projected separation of 99 arcsec = 2860 AU.

- HD 38529: it hosts two low-mass companions with projected masses of 0.78 $M_J$ for the inner companion and 12.70 $M_J$ for the outer companion. This star shows an astrometric motion (it is marked with G-Flag in the Hipparcos Catalogue) which is probably due to the presence of the outer companion (HD 38529 C) for which Reffert & Quirrenbach (2006) derived a mass of $37^{+36}_{-19} M_J$, clearly into the brown dwarf regime. A stellar companion at very wide separation is also present. The classification of this star as a two-planet host with a wide stellar companion or a single-planet host with a brown dwarf and another wide companion is ambiguous (Desidera & Barbieri 2006).

- HD 40979

- HD 43587: triple system. The primary (in the UD sample) is a spectroscopic binary (Vogt et al. 2002). An additional component ($M \sim 0.30\ M_{\odot}$, $\rho = 95$ arcsec = 2860 AU was shown to be physically associated (Duquennoy & Mayor 1991). Other 3 faint companions are listed, probably all optical (NLTT);

- HD 53705- HD 53706: another distant companion (K5, mass 0.69) at 185 arcsec = 3000 AU.

- HD 65907: triple system. The secondary, at a projected separation of 60 arcsec from the primary, is itself a close visual binary (projected separation 37 AU). Individual masses 0.63 and 0.35 $M_{\odot}$.
- HD 72760: Metchev (2006) reports a companion of 0.13 $M_{\odot}$ at a separation of 0.96 arcsec = 21 AU, which is probably responsible of the astrometric trend found by Makarov & Kaplan (2005).
- HD 77407: 0.30 $M_{\odot}$ companion at 1.6 arcsec = 50 AU separation imaged by Calar Alto Adaptive optic system ALFA and confirmed as physically bound to the primary by a multi-epoch, high-resolution spectrum (Mugrauer et al. 2004) that shows a long-term radial velocity trend for HD 77407 A. The companion was also confirmed by Metchev (2006).
- HD 86728: the M dwarf companion is over-luminous with an high activity level. Gizis et al. (2000) suggest it is itself a close binary.
- HD 90839: CPM pair. There is a third companion, HD 89862, but it is not physical (see Gliese & Jahreiß 1991; Duquennoy & Mayor 1991).
- HD 92222 A: it is not included in the Hipparcos Catalogue. For this reason the mass of this star is not listed in VF05. We derived a photometric distance assuming that both components are on the main sequence; and by using the isochrones by Girardi et al. (2002) we found $d = 90$ pc and $M_A$= 1.09 $M_{\odot}$, $M_B$ = 1.05 $M_{\odot}$.
- HIP 52940 - HIP 52942: triple system. The primary is a spectroscopic binary discovered by Nidever et al. (2002). Both components are in the UD sample and both masses are derived according with Reid & Gizis (1997) and Delfosse et al. (2000) mass-luminosity calibrations, because VF05 do not list any mass value for these objects.
- HD 97334: a close pair of brown dwarfs (separation 1.5 AU, total mass = 0.05 $M_{\odot}$) is at a projected separation of about 2000 AU from the primary (Burgasser et al. 2005).
- HD 99492 B: planet outside the UD limits.
- HD 101177: triple system. The secondary is a spectroscopic binary (P=23 d, masses = 0.74 and 0.31 $M_{\odot}$). Component C is optical as the other two companions listed most likely are (NLTT).

- HD 114729: planet outside the UD limits.

- HD 120136 = $\tau$ Boo: the orbital solution by Hale (1994) is very preliminary. Another L dwarf companion candidate at 42 arcsec = 664 AU has been reported by Pinfield et al. (2006). The physical association has yet to be confirmed.

- HD 120780: CCDM lists a companion at 6 arcsec = 98 AU (M=0.53 $M_{\odot}$), but probably this is not responsible for the astrometric signature reported by Makarov & Kaplan (2005).

- HD 128620-HD128621 ($\alpha$ Cen): Triple system: another low mass companion (Proxima Cen) at very wide separation (10000 AU).

- HD 131156=$\xi$ Boo: visual binary ($\rho = 4.9$ arcsec = 33 AU, $P = 152$ yr) (see Worley & Heintz 1983). The visual companion explains the long-term radial velocity trend with a significant curvature detected by Wittenmyer et al. (2006). There are two additional components listed in WDS: C ($V$=12.6, $\rho = 66.7$ arcsec = 447 AU, from CCDM), which is optical (Duquennoy & Mayor 1991), and D ($V = 9.6$, $\rho = 49$ arcsec = 328.3 AU).

- HD 131977: quadruple system. The secondary (HD 131976) is itself a binary with $a = 0.9$ AU and individual masses 0.57 and 0.38 $M_{\odot}$. The fourth component is the brown dwarf GL 570 B at a projected separation of 1500 AU (Burgasser et al. 2000).

- HD 137778: wide visual pair with a similar component. Only the secondary (HD 137778) is included in the UD sample. The primary (HD 137763) is a spectroscopic binary with extreme eccentricity ($e = 0.975$; Duquennoy et al. 1992).

- HD 139323: hierarchical triple system. The companion HD 139341 is a visual binary with $a = 18$ AU and individual masses of 0.74 and 0.81 $M_{\odot}$.

- HD 145958: another companion candidate has been reported at 0.2 arcsec = 5 AU by Tokovinin (1997) but it needs confirmation (no RV variations observed). Preliminary binary orbit of the wide pair in WDS (grade 4).

- HD 146362: member of a hierarchical multiple system. The star included in the UD sample is orbiting the nearly equal-mass double-lined spectroscopic binary HD 146361 (period 1.1 days, individual masses 1.10 and 1.09 $M_{\odot}$). Preliminary orbit of the wide pair in WDS. Another CMP companion, a faint M3V dwarf, is at 633 arcsec = 14000 AU.

- HD 161797 ($\mu$ Herculis): astrometric orbit by Heintz (1994) (period 65 years). The companion was also identified using adaptive-optics imaging by Turner et al. (2001) and Debes et al. (2002). Radial velocity monitoring revealed a long term trend with significant curvature (Nidever et al. 2002; Wittenmyer et al. 2006). The star is also listed as a $\Delta\mu$ binary in Makarov & Kaplan (2005). Another companion, $\mu^2$ Her B, lies at 34 arcsec = 285 AU and is itself a visual binary with period 43.2 yr (WDS).

- HD 167215: CCDM lists a companion with $\rho = 54''.8$ (M=1.05 $M_{\odot}$), but is not expected to be responsible of the astrometric signature reported by Makarov & Kaplan (2005).

- HD 169822: triple system. The star included in the UD sample is a spectroscopic binary detected during the Keck survey. Vogt et al. (2002) derived a combined spectroscopic and astrometric solution ($M = 0.30\ M_{\odot}$, $a = 0.84$ AU). HD 169889, at 608.4 arcsec = 16426.8 AU, is a CPM star. The revised distance of HD 169822 by Vogt et al. (2002) (32 pc), coupled with the common RVs for the two stars (Nordström et al. 2004) makes the indication of a physical association stronger.

- HD 178911: triple system (Tokovinin et al. 2000).

- HD 184860: triple system. The star included in the UD sample is a spectroscopic binary (Vogt et al. 2002). The projected mass of the companion is in the brown dwarf range (32 $M_J$). An additional companion is at 5.0 arcsec = 151 AU.

- HD 187691: three components listed in CCDM/WDS. AC is a CPM pair, B is optical, C is physical (Duquennoy & Mayor 1991).

- HD 190067: Turner et al. (2001) listed a companion at 2.86 arcsec = 55.19 AU, confirmed by Chakraborty et al. (2002) that reported $m \sim 0.08 - 0.10 M_{\odot}$.

- HD 190360: Planet outside the UD limits.

- HD 190406 (15 Sge): A brown dwarf companion ($\rho = 0.79$ arcsec = 14 AU) was found with high-resolution imaging made using adaptive optics at the Gemini-North and Keck telescopes (Liu et al. 2002). The primary shows a long-term radial velocity trend that confirms that HD 190406 B is physical, with a minimum mass of M = 48 $M_J$.

- HD 196885: Chauvin et al. (2006) identified at about 0.7 arcsec a relatively bright companion candidate: HD 196885 B, that is likely to be a late K-dwarf, with a mass of 0.6 $M_\odot$, orbiting HD 196885 A at a projected physical distance of 25 AU. HD 196885 was also classified as a $\Delta\mu$ binary by Makarov & Kaplan (2005). The astrometric signature is probably due to HD 196885 B. A planetary companion was also claimed from the Lick RV Survey [1], but it is not confirmed in the recent work by Butler et al. (2006). The companion BD+104351 B, listed in WDS and CCDM, is probably optical.

- HD 197076: the companion listed as B in WDS and CCDM ($m_v$=11.6 and $\rho = 94$ arcsec = 1974 AU) is optical, but the really bound companion is component C ($\rho = 125$ arcsec = 2625 AU) (Duquennoy & Mayor 1991).

- HD 198387: CCDM lists a companion with $\rho = 12.2$ = 511 AU, but probably this is not responsible for the astrometric signature reported by Makarov & Kaplan (2005).

- HD 215578: the mass of this star is not listed in VF05, so we derive the value listed in Table 8 according with Reid & Gizis (1997) and Delfosse et al. (2000) mass-luminosity calibration.

- HD 219542: the masses of the components of this star were taken from Desidera et al. (2004), as there is some confusion in the identification of the components in the photometry used by VF05 to derive stellar masses (for one of the components, the joint A+B magnitude is used).

- HD 219834: hierarchical triple system. The primary is a spectroscopic binary (period=6.2 yr, individual masses of 0.90 and 0.04 $M_\odot$). The secondary is the star included in the UD sample and the mass

[1] http//exoplanets.org/esp/hd196885/hd196885.shtml

was apparently derived in VF05 from the magnitude of the much brighter primary. We assumed the mass given in the on-line version of the MSC (Tokovinin 1997).

### A.2.2 *Unconfirmed binaries*

- HD 23249 ($\delta$ Eri): belongs to the group of nearest stars and is classified as a weakly active and X-ray soft source (Huensch et al. 1998). Fisher et al. (1983) tried to detect a periodic variation in the photometric data and suggest that $\delta$ Eri could be classified as an RS CVn star: that is, a F-G binary star having a period $< 14$ days, with chromospheric activity and with a period of rotation synchronized with its orbital period (Linsky 1984), giving the star high rotational velocity inducing strong activity. This contrasts with the low level of activity detected by Thévenin et al. (2005) and the lack of radial velocity variations, making this classification doubtful.

- HD 52265, HD 154857, HD 179949: first epoch observations by Chauvin et al. (2006) revealed companion candidates, but the physical association with the planet hosts has not yet been confirmed;

- HD 102158: the presence of a common proper motion companion at 1175.2 arcsec was proposed by Lépine & Bongiorno (2007). The corresponding projected separation (61000 AU) is much larger than any other companion in Table 8, so it is not considered here.

- HD 107213: Lépine & Bongiorno (2007) propose that this star form a wide (projected separation 546 arcsec) common proper motion pair with BD+28 2103 = HIP 60061. However, the discrepant RVs for the two stars (Latham et al. 2002; Nordström et al. 2004) argue against a physical association.

- HD 117176: an L dwarf companion candidate at 848 AU has been reported by Pinfield et al. (2006). The physical association has yet to be confirmed.

- HD 168443: as for HD 38529, there is an ambiguity about the physical classification of the companion as a massive planet or brown dwarf (see Desidera & Barbieri 2006).

- HD 217107: the presence of the companion listed in WDS is not confirmed by recent adaptive optics searches. See Desidera & Barbieri (2006) for discussion and references.

*References for table A.1*

**HD 3074:** Allen et al. (2000); **HD 4614:** Worley & Heintz (1983); **HD 4747:** Nidever et al. (2002); **HD 7693:** Nordström et al. (2004); **HD 10360 - HD 10361 :** Worley & Heintz (1983); **HD 11964:** Allen et al. (2000); **HD 13445:** Lagrange et al. (2006); Desidera & Barbieri (2006); **HD 13507:** Perrier et al. (2003); **HD 13531:** Metchev (2006); **HD 13612:** Worley (1967a); Duquennoy & Mayor (1991); **HD 16141:** Desidera & Barbieri (2006); Mugrauer et al. (2004); **HD 16160:** Allen et al. (2000), Golimowski et al. (2000); **HD 16895:** Worley & Heintz (1983); **HD 18445:** Duquennoy & Mayor (1991); Halbwachs et al. (2000); Zucker & Mazeh (2001); **HD 20782:** Desidera & Barbieri (2006); **HD 23439:** Allen et al. (2000); **HD 27442:** Chauvin et al. (2006); Desidera & Barbieri (2006); Mugrauer et al. (2007); **HD 29836:** Griffin & Gunn (1981); **HD 30649:** Nidever et al. (2002); Dommanget & Nys (2002); **HD 31412:** Nidever et al. (2002); Gliese & Jahreiß (1991); Patel et al. (2007); **HD 33636:** Bean et al. (2007); **HD 35956:** Vogt et al. (2002); **HD 38529:** Reffert & Quirrenbach (2006); Desidera & Barbieri (2006); **HD 39587:** Nidever et al. (2002); **HD 43587:** Vogt et al. (2002); Duquennoy & Mayor (1991); Salim & Gould (2003); **HD 40979:** Mugrauer et al. (2007); **HD 64468:** Vogt et al. (2002); **HD 65430:** Nidever et al. (2002); **HD 65907:** Tokovinin (1997); **HD 72760:** Metchev (2006); **HD 77407:** Mugrauer et al. (2004), Metchev (2006); **HD 86728:** Gizis et al. (2000); Lépine & Bongiorno (2007); **HD 90839:** Gliese & Jahreiß (1991); Duquennoy & Mayor (1991); **HIP 52940:** Nidever et al. (2002); **HD 92222:** Fabricius et al. (2002), this paper; **HD 97334:** Burgasser et al. (2005); **HD 101177:** Duquennoy & Mayor (1991); Salim & Gould (2003); **HD 111398:** Lépine & Bongiorno (2007); **HD 120066:** Allen et al. (2000); Gould & Chanamé (2004); **HD 120136:** Raghavan et al. (2006); Desidera & Barbieri (2006); **HD 120237:** Allen et al. (2000); **HD 120780:** Makarov & Kaplan (2005); **HD 122742:** Nidever et al. (2002); **HD 128620 - HD 128627**:Worley & Heintz (1983); **HD 131156:** Worley & Heintz (1983); Duquennoy & Mayor (1991); **HD 131511:** Nidever et al. (2002); **HD 134440/39:**Allen

et al. (2000); **HD 135101:** Desidera et al. (2004); **HD 139323:** Worley & Heintz (1983); **HD 139477:** Lépine & Bongiorno (2007); **HD 140913:** Nidever et al. (2002); **HD 146362 B:** Worley & Heintz (1983); Tokovinin (1997); **HD 150554:** Metchev (2006); Patel et al. (2007); **HD 156274:** Worley & Heintz (1983); **HD 161797:** Worley & Heintz (1983); Nidever et al. (2002); Wittenmyer et al. (2006); Makarov & Kaplan (2005);
**HD 167215:** Makarov & Kaplan (2005); **HD 169822:** Vogt et al. (2002); **HD 174457:** Nidever et al. (2002); **HD 178911 B:** Tokovinin et al. (2000); **HD 184860:** Vogt et al. (2002); **HD 185395:** Lépine & Bongiorno (2007); **HD 187691:** Duquennoy & Mayor (1991); **HD 190360:** Allen et al. (2000); Desidera & Barbieri (2006); **HD 190406:** Liu et al. (2002); **HD 191408:** Allen et al. (2000); **HD 195019:** Allen et al. (2000); Desidera & Barbieri (2006); **HD 197076:** Duquennoy & Mayor (1991); **HD 196885:** Chauvin et al. (2006); **HD 198387:** Makarov & Kaplan (2005); **HD 206860:** Luhman et al. (2006); **HD 208776:** Nidever et al. (2002); **HD 213519:** Lépine & Bongiorno (2007); **HD 219542:** Desidera et al. (2004); **HD 219834:** Tokovinin (1997); **HD 221830:** Allen et al. (2000).

# B

# VLT/NACO DEEP IMAGING SURVEY SAMPLE OF SOUTHERN YOUNG, NEARBY STARS

Table B.1: Sample of southern young, nearby stars observed during our VLT/NACO deep imaging survey.

| Name | $\alpha$ [J2000] | $\delta$ [J2000] | $b$ (deg) | SpT | $d$ (pc) | Age (Myr) | V (mag) | K (mag) | Mode & Filter | Stellar Multiplicity | Note |
|---|---|---|---|---|---|---|---|---|---|---|---|
| TWA22 AB | 10 17 26.9 | -53 54 28 | 2 | M5 | 18 | 8 | 13.2 | 7.69 | CI, Ks | B (N/VIS/Ph) | CCs |
| SSSPMJ1102 | 11 02 09.83 | -34 30 35 | 23 | M8 | 65 | 8 | | 11.88 | Ks | | |
| TWA3 AB | 11 10 28.8 | -37 32 04 | 21 | M3 | 42 | 8 | 12.1 | 6.77 | CI, H | B (K/VIS/Co) | |
| Twa14 | 11 13 26.3 | -45 23 43 | 14 | M0 | 63 | 8 | 13.8 | 8.50 | CI, Ks | | CCs |
| Twa12 | 11 21 05.6 | -38 45 16 | 21 | M2 | 32 | 8 | 13.6 | 8.05 | CI, Ks | | CCs |
| 2M1139 | 11 39 51.1 | -31 59 21 | 28 | M8 | 49 | 8 | | 11.50 | Ks | | |
| HIP57524 | 11 47 24.6 | -49 53 03 | 11 | G5 | 104 | 8 | 9.1 | 7.51 | CI, H | | CCs |
| Twa23 | 12 07 27.4 | -32 47 0 | 30 | M1 | 37 | 8 | 12.7 | 7.75 | CI, H | | |
| 2M1207 | 12 07 33.4 | -39 32 54 | 23 | M8 | 52 | 8 | | 11.95 | Ks | B (N/VIS/Co) | |
| Twa25 | 12 15 30.7 | -39 48 42 | 22 | M5 | 44 | 8 | 11.4 | 7.31 | CI, Ks | | |
| HR4796 A | 12 36 01.0 | -39 52 10 | 23 | A0 | 67 | 8 | 5.8 | 5.77 | CI, H | B (K/VIS/Co) | |
| Twa17 | 13 20 45.4 | -46 11 38 | 17 | K5 | 133 | 8 | 12.6 | 9.01 | CI, H | | CCs |
| $\beta$ Pictoris | | | | | | | | | | | |
| HIP27321 | 05 47 17.0 | -51 03 59 | -31 | A5 | 20 | 12 | 3.9 | 3.53 | CI, Ks | | |
| V343Nor B | 15 38 56.9 | -57 42 18 | -2 | M4 | 40.0 | 12 | 14.8 | 9.19 | CI, H | T (K/VIS+SB2/Co+Ph) | |
| HD155555 AB | 17 17 25.5 | -66 57 03 | -16 | K1 | 31.4 | 12 | 6.9 | 4.70 | CI, H | T (K/SB2+VIS/Ph+Co) | CCs |
| TYC-8742-2065 AB | 17 48 33.7 | -53 06 43 | -13 | K0 | 42 | 12 | 9.0 | 6.78 | H | B (K/SB2 and VIS/Ph) | |
| HIP88399 A | 18 03 03.4 | -51 38 56 | -14 | F5 | 46.9 | 12 | 7.0 | 5.91 | CI, Ks | B (K/VIS/Co) | CCs |
| HIP92024 | 18 45 26.9 | -64 52 16 | -24 | A7V | 29.2 | 12 | 4.8 | 4.25 | CI, Ks | | CCs |
| CD-641208 AB | 18 45 37.0 | -64 51 46 | -24 | K7 | 29.2 | 12 | 9.5 | 6.10 | CI, H | B (N/VIS) | |
| 0ES1847 | 18 50 44.5 | -31 47 47 | -14 | K5 | 50 | 12 | 10.9 | 7.46 | CI, H | | CCs |
| HIP92680 | 18 53 05.8 | -50 10 49 | -21 | K0V | 49.6 | 12 | 8.4 | 6.37 | CI, Ks | | CCs |
| HIP95270 | 19 22 58.9 | -54 32 16 | -26 | F5 | 50.6 | 12 | 7.0 | 5.91 | CI, H | | CCs |
| Tucana-Horologium | | | | | | | | | | | |
| HIP1113 | 00 13 53.01 | -74 41 17 | -42 | G6V | 43.7 | 30 | 8.7 | 6.96 | CI, Ks | | |
| HIP1481 | 00 18 26.1 | -63 28 38 | -59 | F9V | 41.0 | 30 | 8.0 | 6.15 | CI, Ks | | CCs |
| CD-7824 | 00 42 20.2 | -77 47 40 | -40 | K5 | 69 | 30 | 10.4 | 7.53 | CI, H | | |
| HIP3556 | 00 45 28.1 | -51 37 33 | -58 | M1 | 38.5 | 30 | 11.9 | 7.62 | CI, Ks | | CCs |
| HIP6485 | 01 23 21.2 | -57 28 50 | -59 | G6 | 49.3 | 30 | 8.5 | 6.85 | CI, Ks | | CCs |
| HIP6856 | 01 28 08.6 | -52 38 19 | -64 | K1 | 37.1 | 30 | 9.1 | 6.83 | CI, Ks | | CCs |
| HD13246 AB | 02 07 26.1 | -59 40 45 | -55 | F8V | 45.0 | 30 | 7.5 | 6.20 | CI, Ks | B (K/SB and VIS/Ph) | |
| GSC08056-00482 | 02 36 51.5 | -52 03 04 | -58 | M3 | 25 | 30 | 12.1 | 7.50 | CI, Ks | | |
| HIP21632 B | 04 38 45.6 | -27 02 02 | -40 | M3V | 54.7 | 30 | 7.5 | 10.41 | CI, Ks* | | CCs |
| HIP30034 | 06 19 12.9 | -58 03 15 | -30 | K2 | 45.5 | 30 | 9.1 | 6.98 | CI, H | | CCs |
| HIP100751 AB | 20 25 38.9 | -56 44 06 | -35 | B7 | 56 | 30 | 1.9 | 2.48 | CI, Ks | B (K/SB/Ph) | |
| HIP105404 ABC | 21 20 59.8 | -52 28 40 | -44 | K0V | 46.0 | 30 | 8.9 | 6.57 | CI, Ks | T (K/SB3/Ph) | CC |
| HIP107947 | 21 52 09.7 | -62 03 09 | -44 | F6 | 45 | 30 | 7.2 | 6.03 | CI, Ks | | CCs |
| HIP108195 ABC | 21 55 11.4 | -61 53 12 | -45 | F3 | 47 | 30 | 5.9 | 4.91 | CI, Ks | T (K+N/VIS/Ph+Co) | CCs |
| AB Dor | | | | | | | | | | | |
| HIP5191 A | 01 06 26.1 | -14 17 47 | -76 | K1 | 50 | 70 | 9.5 | 7.34 | CI, H | B (K/VIS/Co) | |
| HIP25283 | 05 24 30.2 | -38 58 11 | -33 | K7 | 18 | 70 | 9.2 | 5.92 | CI, H | B (K/VIS/Co) | |
| ABDor BaBb | 05 28 44.3 | -65 26 46 | -33 | M3 | 15 | 70 | 13.0 | 7.34 | CI, H | Q (K/VIS/Ph) | |
| HIP26369 | 05 36 55.1 | -47 57 48 | -32 | K7 | 24 | 70 | 9.8 | 6.61 | CI, H | B (K/VIS/Co) | |
| HIP26373 | 05 36 56.8 | -47 57 53 | -32 | K0 | 24 | 70 | 7.9 | 5.81 | CI, H | B (K/VIS/Co) | |
| HIP30314 | 06 22 30.9 | -60 13 07 | -27 | G0V | 23.5 | 70 | 6.5 | 5.04 | CI, Ks | B (K/VIS?) | CCs |
| GSC08894-00426 | 06 25 55.4 | -60 03 29 | -27 | M2 | 22 | 70 | 12.7 | 7.21 | CI, Ks | | CCs |
| HIP31878 | 06 39 50.0 | -61 28 42 | -25 | K7 | 21.9 | 70 | 9.7 | 6.50 | CI, Ks | | |
| HIP76768 AB | 15 40 28.4 | -18 41 45 | 28 | K7 | 43 | 70 | 10.2 | 6.95 | CI, Ks | B (K/VIS/Co) | CCs |
| HIP113579 | 23 00 19.2 | -26 09 13 | -65 | G1 | 32 | 70 | 7.5 | 5.94 | CI, Ks | | CCs |
| HIP118008 | 23 56 10.7 | -39 03 08 | -77 | K3 | 22.1 | 70 | 8.2 | 5.91 | CI, H | | |
| $\eta$ Cha, Near Cha, Columba and Carina | | | | | | | | | | | |
| M0838 | 08 38 51.1 | -79 16 13 | -22 | M5 | 97 | 6 | 16.5 | 10.43 | Ks | | |
| HIP58285(TCha) | 11 57 13.7 | -79 21 32 | -16 | F5 | 66.4 | 10 | 11.4 | 6.95 | CI, Ks | | CCs |
| GSC08047-00232 A | 01 52 14.6 | -52 19 33 | -62 | K3 | 85 | 30 | 10.9 | 8.41 | CI, Ks | B (K/VIS/Co) | |
| TYC-9390-0322 AB | 05 53 29.1 | -81 56 53 | -29 | K0 | 54 | 30 | 9.1 | 6.94 | H | B (N/VIS) | |

*(continued on next page)*

*(Table B.1 - continued from previous page)*

| Name | $\alpha$ [J2000] | $\delta$ [J2000] | $b$ (deg) | SpT | $d$ (pc) | Age (Myr) | V (mag) | K (mag) | Mode & Filter | Stellar Multiplicity | Note |
|---|---|---|---|---|---|---|---|---|---|---|---|

In addition to name, coordinates, galactic latitude ($b$), spectral type, distance and $V$ and $K$ photometry, the observing filter is given. All sources were observed in direct imaging, we have therefore indicated the 65 stars observed in addition in coronagraphy (CI). Finally, the multiplicity status of the primary and the presence of companion candidates (CCs) are also reported. For the multiplicity status we have flagged the following information: binary (B), triple (T) and quadruple (Q); new (N) or known/cataloged (K) multiple system; identified visual (VIS), Hipparcos astrometric (HIP) and spectroscopic (SB) binary system; and a final flag in case of a confirmed physical (Ph) or comoving (Co) system, but nothing if only an optical binary. FS stars are from a paper by Fuhrmeister & Schmitt (2003).

Table B.2: Sample of southern young, nearby stars observed during our VLT/NACO deep imaging survey.

| Name | $\alpha$ [J2000] | $\delta$ [J2000] | $b$ (deg) | SpT | $d$ (pc) | Age (Myr) | V (mag) | K (mag) | Mode & Filter | Stellar Multiplicity | Note |
|---|---|---|---|---|---|---|---|---|---|---|---|
| Additional young candidates | | | | | | | | | | | |
| BTR99 AB | 01 23 17.0 | -79 41 32 | -37 | K0 | 103 | 10 | 10.1 | 7.07 | CI, H | B (N/VIS) | |
| CD-53386 AB | 02 01 53.7 | -52 34 53 | -61 | K3 | 120 | 30 | 11.0 | 8.60 | H | B (N/VIS) | |
| FS75 | 02 04 53.2 | -53 46 16 | -60 | M4 | 30 | 100 | 15.0 | 9.6 | Ks | | |
| FS84 | 02 22 44.2 | -60 22 47 | -53 | M4 | 20 | 100 | 13.7 | 8.2 | Ks | | |
| GSC08862-00019 | 02 58 04.6 | -62 41 15 | -49 | K4 | 138 | 20 | 11.7 | 8.91 | CI, Ks | | CCs |
| TYC6461-1120 A | 04 00 03.7 | -29 02 16 | -48 | K0 | 62 | 40 | 9.6 | 7.15 | CI, Ks | B (N/VIS/Co) | CCs |
| HIP28474 AB | 06 00 41.3 | -44 53 50 | -27 | G8 | 53.7 | 100 | 9.1 | 7.32 | CI, H | B (N/VIS) | |
| FS388 ABC | 06 43 45.3 | -64 24 39 | -25 | M4 | 22 | 100 | 14.0 | 8.4 | Ks | T (N/VIS) | |
| FS465 AB | 08 17 39.4 | -82 43 30 | -24 | M4 | 10 | 100 | 12.6 | 6.6 | Ks | B (N/VIS) | |
| HIP41307 | 08 25 39.6 | -03 54 23 | 18 | A0 | 38 | 100 | 3.9 | 4.08 | CI, Ks | | |
| FS485 | 08 47 22.6 | -49 59 57 | -4 | M2 | 33 | 100 | 12.0 | 7.71 | Ks | | |
| FS488 AB | 08 54 02.4 | -30 51 36 | 9 | M5 | 15 | 100 | 13.4 | 8.10 | Ks | B (N/VIS) | |
| HIP51386 | 10 29 42.2 | +01 29 28 | 47 | F5 | 31.5 | 50 | 6.9 | 5.52 | CI, Ks | | CCs |
| FS588 | 11 20 06.1 | -10 29 47 | 46 | M3 | 20 | 100 | 12.1 | 7.0 | Ks | | |
| HIP59315 | 12 10 06.4 | -49 10 50 | 13 | G5 | 37.8 | 100 | 8.2 | 6.50 | CI, H | | CCs |
| CD-497027 | 12 21 55.6 | -49 46 12 | 13 | K0 | 89 | 20 | 10.1 | 8.01 | Ks | | |
| HIP61468 | 12 35 45.5 | -41 01 19 | 21 | A7 | 34.6 | 100 | 5.1 | 4.57 | CI, H | | |
| TYC-8992-0605 | 12 36 38.9 | -63 44 43 | 0 | K3 | 50 | 10 | 9.9 | 7.37 | CI, H | | CCs |
| TYC-09012-1005 | 13 44 42.6 | -63 47 49 | -1 | K5 | 95 | 10 | 11.0 | 7.74 | CI, H | | CCs |
| TYC-7818-0504 AB | 14 30 13.5 | -43 50 09 | 16 | K5 | 100 | 10 | 10.4 | 7.64 | H | B (N/VIS) | |
| HIP74405 | 15 12 23.4 | -75 15 15 | -15 | K0 | 50.2 | 100 | 9.4 | 7.38 | CI, H | | |
| TYC-7846-1538 | 15 53 27.3 | -42 16 02 | 9 | G1 | 48 | 30 | 7.9 | 6.34 | CI, H | | CCs |
| HIP80448 ABC | 16 25 17.5 | -49 08 52 | 0 | K1 | 45.5 | 100 | 7.1 | 5.70 | H | T (K/SB+VIS/Ph+Co) | |
| HIP84642 AB | 17 18 14.7 | -60 27 27 | -13 | K0 | 54.6 | 40 | 9.5 | 7.53 | CI, Ks | B (N/VIS) | CCs |
| FS903 | 17 37 46.5 | -13 14 47 | 9 | K7 | 45 | 100 | 10.2 | 6.835 | CI, Ks | | CCs |
| FS979 AB | 18 35 20.8 | -31 23 24 | -11 | M5 | 18 | 100 | 13.1 | 7.8 | Ks | B (N/VIS) | CCs |
| FS1017 | 19 19 20.2 | -01 33 54 | -6 | M5 | 25 | 100 | 16.6 | 9.667 | Ks | | CCs |
| FS1035 | 19 42 12.8 | -20 45 48 | -20 | M5 | 20 | 100 | 14.4 | 8.756 | Ks | | CCs |
| HIP98495 | 20 00 35.5 | -72 54 37 | -31 | A0 | 33.3 | 50 | 3.9 | 3.80 | CI, H | | |
| HIP102626 | 20 47 45.0 | -36 35 40 | -38 | K0 | 44.4 | 30 | 9.4 | 6.79 | CI, H | B (K/HIP?) | |
| FS1136 AB | 21 49 06.2 | -64 12 55 | -43 | M5 | 25 | 100 | 15.5 | 9.5 | CI, Ks | B (N/VIS) | |
| FS1174 | 22 44 08.0 | -54 13 20 | -54 | M4 | 30 | 100 | 13.4 | 8.5 | Ks | | CCs |
| Reclassified as older systems | | | | | | | | | | | |
| HIP7805 | 01 40 24.1 | -60 59 57 | -55 | F2 | 67 | $\geq$ 100 | 7.7 | 6.63 | CI, H | | |
| HIP69562 ABC | 14 14 21.3 | -15 21 21 | 42 | K5V | 26.5 | $\geq$ 100 | 10.5 | 6.60 | Ks | T (N/VIS) | |
| HIP76107 | 15 32 36.7 | -52 21 21 | 3 | M0 | 30.6 | $\geq$ 100 | 11.0 | 7.60 | CI, Ks | B (K/HIP?) | CCs |
| HIP96334 | 19 35 09.7 | -69 58 32 | -29 | G1V | 35.4 | $\geq$ 100 | 7.9 | 6.30 | CI, Ks | | CCs |
| HIP107705 AB | 21 49 05.8 | -72 06 09 | -39 | M0 | 16.1 | 200 | 9.8 | 5.65 | Ks | B (N/VIS) | |

# C

# MERIT FUNCTIONS

The scope of the merit function is to order the targets from the input catalogue according to the probability that they have detectable planets (of the type considered). To be detectable, the planet star contrast C should be larger than a threshold contrast $C_T$: $C/C_T > 1$

Based on simulations, the threshold contrast (for bright objects) can be roughly written as:

$C_T \sim 1/s \sim d/a$

Where s and a are the planet/star apparent and real separations, and d is the star distance from the Sun. The planet star contrast is:

$C = L_P/L_*$

Where $L_P$ and $L_*$ are the planet and stellar absolute luminosity, respectively. The planet luminosity might be due either to reflection or to intrinsic emission.

In the case of reflection planet we may write:

$L_P \sim A\Phi L_* R_P^2/a^2$,

Where A is the albedo, $\Phi$ a phase dependent factor which accounts for the fraction of the planet illuminated by the star and seen from the observer and RP is the planet radius. Assuming constant density (not a terribly bad approximation in this context), we have

$L_P \sim A\Phi L_* MP_{2/3}/a_2$

Combining the various equations, a planet can be detected if:

$C/C_T \sim (A\Phi MP_{2/3}/a)(L_*/d) > 1$

where the first term is a property of the planet, while the second can be considered as a property of the star. It is then quite natural to define $MF_1 = 1/d$. The probability of detecting a planet by reflecting light should increase with MF1; it should then decrease with distance.

In the case of planets shining by intrinsic emission we write:

$L_P\ M_P^2/t$

where now t is the age of the system. After some algebra, we can then write:

$C/C_T\ (M_P^2 a)/(tL * d) > 1$

Where the numerator is a property of the planet, and the denominator is a property of the star. In this case we may then define a second merit function $MF_2 = 1/(tL * d)$.

The probability of detecting a planet shining by intrinsic light should increase with $MF_2$.

Note that deriving these formulas, we assumed that the planet characteristics (mass, semi-major axis) are independent of stellar characteristics. More likely, $M_P$ is proportional to $M_*$, which on turn is proportional to $L_*1/3$; in our simulations we further assume that a is proportional to $M_*^{2/3}$, that is to $L_*^{2/9}$.

When these dependencies are taken into consideration, $MF_1$ does not change, while for $MF_2$ we have:

$MF_2 = 1/(tL_*^{2/9}d)$

# BIBLIOGRAPHY


Allen, C., Poveda, A., & Herrera, M. A. 2000, A&A, 356, 529

Bean, J. L., McArthur, B. E., Benedict, G. F., et al. 2007, ArXiv e-prints, 705

Beuzit, J.-L., Ségransan, D., Forveille, T., et al. 2004, A&A, 425, 997

Burgasser, A. J., Kirkpatrick, J. D., Cutri, R. M., et al. 2000, ApJl, 531, L57

Burgasser, A. J., Kirkpatrick, J. D., & Lowrance, P. J. 2005, AJ, 129, 2849

Butler, R. P., Wright, J. T., Marcy, G. W., et al. 2006, ApJ, 646, 505

Chakraborty, A., Ge, J., & Debes, J. H. 2002, AJ, 124, 1127

Chauvin, G., Lagrange, A.-M., Udry, S., et al. 2006, A&A, 456, 1165

Debes, J. H., Ge, J., & Chakraborty, A. 2002, ApJl, 572, L165

Delfosse, X., Forveille, T., Ségransan, D., et al. 2000, A&A, 364, 217

Desidera, S. & Barbieri, M. 2006, A&A, in press

Desidera, S., Gratton, R. G., Scuderi, S., et al. 2004, A&A, 420, 683

Dommanget, J. & Nys, O. 2002, VizieR Online Data Catalog, 1274, 0

Duquennoy, A. & Mayor, M. 1991, A&A, 248, 485

Duquennoy, A., Mayor, M., Andersen, J., Carquillat, J. M., & North, P. 1992, A&A, 254, L13+

Els, S. G., Sterzik, M. F., Marchis, F., et al. 2001, A&A, 370, L1

Fabricius, C., Høg, E., Makarov, V. V., et al. 2002, A&A, 384, 180

Fischer, D. A., Marcy, G. W., Butler, R. P., et al. 2002, , 114, 529

Fisher, G. F., Hall, D. S., Henry, G. W., et al. 1983, Informational Bulletin on Variable Stars, 2259, 1

Girardi, L., Bertelli, G., Bressan, A., et al. 2002, A&A, 391, 195

Gizis, J. E., Monet, D. G., Reid, I. N., Kirkpatrick, J. D., & Burgasser, A. J. 2000, MNRAS, 311, 385

Gliese, W. & Jahreiß, H. 1991, Preliminary Version of the Third Catalogue of Nearby Stars, Tech. rep.

Golimowski, D. A., Henry, T. J., Krist, J. E., et al. 2000, AJ, 120, 2082

Gould, A. & Chanamé, J. 2004, ApJs, 150, 455

Griffin, R. F. & Gunn, J. E. 1981, AJ, 86, 588

Halbwachs, J. L., Arenou, F., Mayor, M., Udry, S., & Queloz, D. 2000, A&A, 355, 581

Hale, A. 1994, AJ, 107, 306

Heintz, W. D. 1994, AJ, 108, 2338

Holman, M. J. & Wiegert, P. A. 1999, AJ, 117, 621

Huensch, M., Schmitt, J. H. M. M., & Voges, W. 1998, A&As, 132, 155

Lagrange, A.-M., Beust, H., Udry, S., Chauvin, G., & Mayor, M. 2006, A&A, 459, 955

Latham, D. W., Stefanik, R. P., Torres, G., et al. 2002, AJ, 124, 1144

Lépine, S. & Bongiorno, B. 2007, AJ, 133, 889

Linsky, J. L. 1984, NASA STI/Recon Technical Report N, 85, 13704

Liu, M. C., Fischer, D. A., Graham, J. R., et al. 2002, ApJ, 571, 519

Luhman, K. L., Patten, B. M., Marengo, M., et al. 2006

Makarov, V. V. & Kaplan, G. H. 2005, AJ, 129, 2420

Metchev, S. 2006, PhD Thesis

Mugrauer, M., Neuhaeuser, R., & Mazeh, T. 2007, ArXiv Astrophysics e-prints

Mugrauer, M. & Neuhäuser, R. 2005, MNRAS, 361, L15

Mugrauer, M., Neuhäuser, R., Guenther, E. W., et al. 2004, A&A, 417, 1031

Nidever, D. L., Marcy, G. W., Butler, R. P., Fischer, D. A., & Vogt, S. S. 2002, ApJs, 141, 503

Nordström, B., Mayor, M., Andersen, J., et al. 2004, A&A, 418, 989

Patel, S. G., Vogt, S. S., Marcy, G. W., et al. 2007, ArXiv e-prints, 704

Perrier, C., Sivan, J.-P., Naef, D., et al. 2003, A&A, 410, 1039

Pinfield, D. J., Jones, H. R. A., Lucas, P. W., et al. 2006, MNRAS, 368, 1281

Raghavan, D., Henry, T. J., Mason, B. D., et al. 2006, ApJ, 646, 523

Reffert, S. & Quirrenbach, A. 2006, A&A, 449, 699

Reid, I. N. & Gizis, J. E. 1997, AJ, 113, 2246

Salim, S. & Gould, A. 2003, ApJ, 582, 1011

Thévenin, F., Kervella, P., Pichon, B., et al. 2005, A&A, 436, 253

Tokovinin, A. A. 1997, A&As, 124, 75

Tokovinin, A. A., Griffin, R. F., Balega, Y. Y., Pluzhnik, E. A., & Udry, S. 2000, Astronomy Letters, 26, 116

Turner, N. H., ten Brummelaar, T. A., McAlister, H. A., et al. 2001, AJ, 121, 3254

Vogt, S. S., Butler, R. P., Marcy, G. W., et al. 2002, ApJ, 568, 352

Wittenmyer, R. A., Endl, M., Cochran, W. D., et al. 2006, AJ, 132, 177

Worley, C. E. 1967a, AJ, 72, 899

Worley, C. E. 1967b, in On the Evolution of Double Stars, ed. J. Dommanget, 221–+

Worley, C. E. & Heintz, W. D. 1983, Publications of the U.S. Naval Observatory Second Series, 24, 1

Zucker, S. & Mazeh, T. 2001, ApJ, 562, 549